Yang Tang

Atlas of Emergency Neurovascular Imaging

Springer

Atlas of Emergency Neurovascular Imaging

Yang Tang

Atlas of Emergency Neurovascular Imaging

Springer

Yang Tang
Department of Radiology
Virginia Commonwealth University Health System
Richmond, VA
USA

ISBN 978-3-030-43653-7 ISBN 978-3-030-43654-4 (eBook)
https://doi.org/10.1007/978-3-030-43654-4

© Springer Nature Switzerland AG 2020
This work is subject to copyright. All rights are reserved by the Publisher, whether the whole or part of the material is concerned, specifically the rights of translation, reprinting, reuse of illustrations, recitation, broadcasting, reproduction on microfilms or in any other physical way, and transmission or information storage and retrieval, electronic adaptation, computer software, or by similar or dissimilar methodology now known or hereafter developed.
The use of general descriptive names, registered names, trademarks, service marks, etc. in this publication does not imply, even in the absence of a specific statement, that such names are exempt from the relevant protective laws and regulations and therefore free for general use.
The publisher, the authors and the editors are safe to assume that the advice and information in this book are believed to be true and accurate at the date of publication. Neither the publisher nor the authors or the editors give a warranty, expressed or implied, with respect to the material contained herein or for any errors or omissions that may have been made. The publisher remains neutral with regard to jurisdictional claims in published maps and institutional affiliations.

This Springer imprint is published by the registered company Springer Nature Switzerland AG
The registered company address is: Gewerbestrasse 11, 6330 Cham, Switzerland

To my beloved family for their patience and support and to all the patients I have the privilege to serve.

Preface

Ischemic stroke and hemorrhage are commonly encountered in the emergency setting and are among the leading causes of morbidity and mortality worldwide. Imaging plays a central role in diagnosing and triaging these patients. The emergent utilization of computed tomography (CT) and magnetic resonance imaging (MRI)-based neurovascular imaging has increased tremendously in the recent years, mostly driven by the advance of endovascular stroke intervention and the need of screening severe trauma patients for blunt cerebrovascular injury. Neurovascular imaging has become a key element in the training and clinical practice of neuroradiologists, emergency radiologists, neurointerventionalists, stroke neurologists, and neurosurgeons.

This book aims to provide a concise but comprehensive review of the entire spectrum of emergent neurovascular imaging, with emphasis on noninvasive CT angiography (CTA), MR angiography (MRA), and perfusion techniques. It is organized into 11 chapters. The first three chapters address the topics of acute stroke imaging, including algorithms based on recent clinical trials and updated American Heart Association stroke guideline, vascular territories, and stroke mimics. These are followed by discussions of cerebral venous thrombosis, vasculopathies, aneurysms, and vascular malformations. The remaining chapters are devoted to the traumatic neurovascular injury, as well as the relatively rare albeit important topics of head and neck vascular emergencies and spinal vascular diseases. The book has an image-rich format, including more than 280 selected CT, MRI, or digital subtraction angiography (DSA) images. The readers can use the book either as a primary learning tool or a quick reference guide.

I would like to thank my colleagues at Virginia Commonwealth University for their contributions, as well as the editorial staff at Springer for inspiring me and making this book possible.

Richmond, VA, USA — Yang Tang, MD, PhD

Contents

1 Acute Stroke Imaging . . . 1
1.1 Introduction . . . 1
1.2 Core, Penumbra, and Oligemia . . . 1
1.3 Goal of Acute Stroke Imaging . . . 1
1.4 CT-Based Imaging . . . 2
1.4.1 NCCT . . . 2
1.4.2 CT Angiography . . . 4
1.4.3 Collateral Assessment . . . 5
1.4.4 CT Perfusion . . . 5
1.4.5 Limitation of CT Perfusion . . . 11
1.5 MRI-Based Imaging . . . 11
1.5.1 Strengths and Weaknesses of MRI in Acute Stroke Imaging . . . 11
1.5.2 MRI Protocol . . . 18
References . . . 19

2 Ischemic Stroke Vascular Territory . . . 21
2.1 Introduction . . . 21
2.2 Anterior Circulation . . . 21
2.2.1 Internal Carotid Artery (ICA) . . . 21
2.2.2 Middle Cerebral Artery (MCA) . . . 21
2.2.3 Anterior Cerebral Artery (ACA) . . . 23
2.3 Posterior Circulation . . . 23
2.3.1 Vertebral Artery . . . 23
2.3.2 Basilar Artery . . . 24
2.3.3 Anterior Inferior Cerebellar Artery (AICA) and Superior Cerebellar Artery (SCA) . . . 26
2.3.4 Posterior Cerebral Artery (PCA) . . . 28
2.4 Border Zone Infarction . . . 30
References . . . 32

3 Imaging of Stroke Mimics . . . 33
3.1 Introduction . . . 33
3.2 Seizure . . . 33
3.3 Migraine . . . 33
3.4 Tumor . . . 33
3.5 Infection and Inflammation . . . 33
3.6 MELAS (Mitochondrial Myopathy, Encephalopathy with Lactic Acidosis, and Stroke-Like Episodes) . . . 35
3.7 Creutzfeldt–Jakob Disease (CJD) . . . 36
3.8 Hypoxic–Ischemic Encephalopathy (HIE) . . . 41
3.9 Hypoglycemic Encephalopathy . . . 41
3.10 Hyperammonemic Encephalopathy . . . 41
3.11 Wernicke's Encephalopathy . . . 42

3.12 Osmotic Demyelination Syndrome (ODS) . . . 45
3.13 Drug Toxicity . . . 46
3.14 Cerebral Fat Embolism (CFE) . . . 46
References . . . 47

4 Cerebrovenous Thrombosis . . . 49
4.1 Introduction . . . 49
4.2 Parenchymal Changes Associated with CVT . . . 49
4.3 Identification of Venous Thrombosis . . . 49
4.3.1 Non-contrast CT (NCCT) . . . 49
4.3.2 CT Venogram . . . 54
4.3.3 MRI . . . 54
4.3.4 MR Venogram . . . 57
4.4 Treatment . . . 57
References . . . 57

5 Cerebral Vasculopathy: CNS Vasculitis, RCVS, and PRES . . . 59
5.1 Introduction . . . 59
5.2 CNS Vasculitis . . . 59
5.2.1 Secondary CNS Vasculitis . . . 59
5.2.2 Imaging Modality of CNS Vasculitis . . . 60
5.2.3 Primary Angiitis of CNS (PACNS) . . . 61
5.3 RCVS . . . 63
5.3.1 Definition of RCVS . . . 63
5.3.2 Clinical Presentation . . . 63
5.3.3 Conventional Imaging . . . 63
5.3.4 MRI Vessel Wall Imaging of Cerebral Vasculopathy . . . 65
5.3.5 Treatment . . . 65
5.4 PRES . . . 65
References . . . 67

6 Miscellaneous Cerebral Vasculopathy . . . 69
6.1 Moyamoya Vasculopathy . . . 69
6.2 Radiation-Induced Vasculopathy . . . 70
6.3 Drug-Induced Cerebral Vasculopathy . . . 72
6.4 Childhood Stroke and Arteriopathy . . . 72
6.5 CADASIL . . . 74
6.6 Cerebral Amyloid Angiopathy . . . 74
References . . . 77

7 Traumatic Neurovascular Injury . . . 79
7.1 Mechanism and Pathophysiology . . . 79
7.2 Screening Criteria . . . 79
7.3 Screening Modality . . . 80
7.4 BCVI Grading . . . 80
7.5 Differential Diagnosis . . . 83
7.6 Treatment and Follow-Up Imaging . . . 88
7.7 Spontaneous Dissection . . . 89
7.8 Traumatic Dural Sinus Injury . . . 89
References . . . 92

8 Cerebral Aneurysm . . . 93
8.1 Pathophysiology . . . 93
8.2 Classification . . . 93
8.2.1 Saccular Aneurysms . . . 93
8.2.2 Fusiform and Dissecting Aneurysms . . . 95
8.2.3 Dolichoectasia . . . 95
8.2.4 Blood-Blister Aneurysm . . . 101

8.2.5 Infectious Aneurysms. . . . 101
8.2.6 Size. . . . 101
8.3 Clinical Manifestations 101
8.4 Imaging Modality of Intracranial Aneurysms 104
8.5 Management. . . . 104
8.5.1 Ruptured Aneurysms 104
8.5.2 Unruptured Aneurysms 106
8.6 Follow-Up After Treatment 107
References. . . . 108

9 Cerebral Vascular Malformations. . . . 111
9.1 Arteriovenous Malformation (AVM) 111
9.1.1 Definition 111
9.1.2 Feeding Artery and Draining Vein 111
9.1.3 Associated Aneurysms. . . . 111
9.1.4 Grading 111
9.1.5 Imaging Evaluation 111
9.1.6 Treatment 113
9.1.7 Differential Diagnosis 116
9.2 Dural Arteriovenous Fistula (DAVF) 116
9.2.1 Definition 116
9.2.2 Classifications 117
9.2.3 Imaging 117
9.2.4 Treatment 117
9.3 Vein of Galen Aneurysmal Malformation (VGAM) 121
9.4 Cavernous Malformation (CM) 121
9.5 Developmental Venous Anomaly (DVA) 121
References. . . . 125

10 Vascular Emergency of the Head and Neck 127
10.1 Traumatic Injury to External Carotid Artery 127
10.2 Iatrogenic Vascular Injury 127
10.3 Vascular Complication of Head and Neck Infections 129
10.4 Vascular Complications of Head and Neck Tumors 129
10.5 Vascular Malformation. . . . 135
10.5.1 Carotid-Cavernous Fistula 135
10.5.2 Low-Flow Orbital Vascular Lesions 135
10.5.3 Mandibular AVM 135
10.6 Carotidynia. . . . 136
References. . . . 140

11 Spinal Vascular Diseases. . . . 143
11.1 Vascular Anatomy 143
11.1.1 Arterial System 143
11.1.2 Venous System. . . . 143
11.2 Diagnostic Modality. . . . 143
11.3 Cord Infarction. . . . 144
11.4 Spinal Vascular Malformation 144
11.4.1 Type I Spinal Dural AV Fistula (SDAVF) 144
11.4.2 Type II Intramedullary AVM 147
11.4.3 Type III Intradural and Extradural AVM 148
11.4.4 Type IV Intradural Perimedullary AVF 148
11.5 Spinal Cavernous Malformation 148
11.6 Spinal Hemangioblastoma 148
References. . . . 151

Index. . . . 153

Contributors

Xinli Du, MD, PhD Department of Neurology, Virginia Commonwealth University Health System and Hunter Homes McGuire Veterans Affair Medical Center, Richmond, VA, USA

Seyed Mohammad Gharavi, MD Department of Radiology, Virginia Commonwealth University Health System, Richmond, VA, USA

Christopher Ovanez, MD, MPH, MS Department of Radiology, Virginia Commonwealth University Health System, Richmond, VA, USA

Yang Tang, MD, PhD Department of Radiology, Virginia Commonwealth University Health System, Richmond, VA, USA

Acute Stroke Imaging

1

Yang Tang

1.1 Introduction

Acute ischemic stroke (AIS) is commonly due to cardioembolism, large vessel atherosclerosis, or lacunar infarctions. Other rare etiologies including dissection, vasculopathy, and cerebrovenous thrombosis will be discussed in other chapters. Anterior circulation large vessel occlusion (LVO) involving the intracranial ICA and middle cerebral artery (MCA) M1 segment is a very common stroke subtype and is associated with significant morbidity and mortality.

There has been a major paradigm shift in the AIS treatment in the past several years. Until 2015, intravenous administration of tissue plasminogen activator (IV tPA) has been the mainstay of treatment, which can be given up to 4.5 hours after symptom onset [1]. In 2015, a total of six randomized clinical trials established the significant benefit of emergent endovascular treatment (EVT) in treating patients with anterior circulation LVO within 6 hours of symptom onset compared to the best medical treatment [2–7]. In 2018, two late-window trials including DAWN [8] and DEFUSE 3 [9] have demonstrated similarly overwhelming benefit of EVT, leading to new guidelines that recommend endovascular treatment of anterior circulation LVO up to 24 hours of stroke onset or last known well [10]. Most recently, investigators have been able to extend the IV tPA treatment window from 4.5 to 9 hours in patients with salvageable tissue identified by CT perfusion or DWI/MR perfusion [11] and in patients of unknown stroke onset with DWI/FLAIR mismatch on MRI [12]. Advanced neuroimaging plays a critical role in triaging patients for endovascular and thrombolytic treatments, and its application has continued to evolve.

1.2 Core, Penumbra, and Oligemia

The concepts of ischemic core and penumbra are essential to understanding the current role of acute stroke imaging and intervention.

In cases of LVO, the brain tissue in close proximity to the occluded vessel undergoing irreversible cell death regardless of subsequent reperfusion status is defined as the infarction "core."

The functionally impaired yet still viable and salvageable tissue surrounding the core is commonly termed as "penumbra" or "tissue at risk." The penumbra will progress to infarction if timely reperfusion does not occur. The fate of penumbra largely depends on the quality of pial collateral flow and on the severity/duration of ischemia.

Further away from the ischemic core, there is tissue of "benign oligemia," which is hypoperfused yet functionally intact due to adequate collateral flow. This tissue will survive even if reperfusion does not occur. It is important to distinguish benign oligemia from true penumbra to avoid the overestimation of tissue at risk, although this is frequently difficult on perfusion imaging, especially in cases complicated by underlying chronic vascular stenosis.

1.3 Goal of Acute Stroke Imaging

The goal of acute stroke imaging includes:

1. Exclude acute intracranial hemorrhage.
2. Evaluate the patency of intracranial and cervical vasculature.
3. Assess the quality of collateral circulation in cases of LVO.
4. Estimate the volume of core infarct and penumbra.

Both CT- and MRI-based techniques have been used to achieve the above goals. The currently recommended imaging algorithm varies for patients who present within the early window (<6 hours from symptom onset or last known well) and late window (6–24 hours from symptom onset or last known well).

For early-window patients, non-contrast CT (NCCT) and CT angiography (CTA) can usually provide sufficient

© Springer Nature Switzerland AG 2020

Y. Tang, *Atlas of Emergency Neurovascular Imaging*, https://doi.org/10.1007/978-3-030-43654-4_1

information for EVT selection. Patients with anterior circulation LVO and absence of a large infarction on NCCT are considered safe candidates for EVT. Perfusion imaging may not be necessary in these patients, as it can potentially cause delay of treatment and inappropriate exclusion of patients who may otherwise benefit from EVT [13].

For late-window patients with anterior circulation LVO confirmed by vascular imaging, a perfusion study, either CT perfusion (CTP) or MRI with diffusion-weighted imaging (DWI) with or without MR perfusion (MRP), is recommended to select the subgroup of patients meeting the eligibility criteria of DAWN and DEFUSE 3 [13].

1.4 CT-Based Imaging

Owing to its widespread availability and rapid acquisition, CT is the modality of choice in the vast majority of stroke centers. A multimodal stroke CT consists of NCCT, CTA, and CTP, which can be performed within a few minutes by current multidetector scanners.

1.4.1 NCCT

NCCT is typically the first imaging modality performed to exclude intracranial hemorrhage, as well as other acute pathologies such as mass or hydrocephalus that can mimic AIS clinically. It is recommended that initial brain imaging should be performed within 20 minutes of arrival in the emergency department in at least 50% of patients who may be candidates for thrombolysis or thrombectomy [14].

Initial interpretation can be made on the CT console to facilitate the clinical decision-making regarding IV tPA. Axial, coronal, and sagittal reconstructed images should be carefully reviewed on the PACS workstation immediately afterward. Subtle hemorrhages can be missed on the axial images and more easily detectable on the sagittal and coronal reformations (Fig. 1.1).

Although not sensitive, NCCT can detect early ischemic changes including subtle loss of gray–white matter differentiation, sulcal effacement, parenchymal hypodensity, or hyperdense vessels.

Loss of gray–white differentiation is the hallmark of acute infarction at NCCT. Special attention should be directed to insula and basal ganglia, which are most commonly affected by MCA occlusion (Fig. 1.2). It is helpful to use a narrow "stroke window" on PACS station to detect early ischemia. Hypodensity > 1/3 of MCA territory used to be considered as a relative contraindication for IV tPA, although the recent guideline states that the extent and severity of acute hypoattenuation or early ischemic changes should not be used as a criterion to withhold therapy due to insufficient evidence [14].

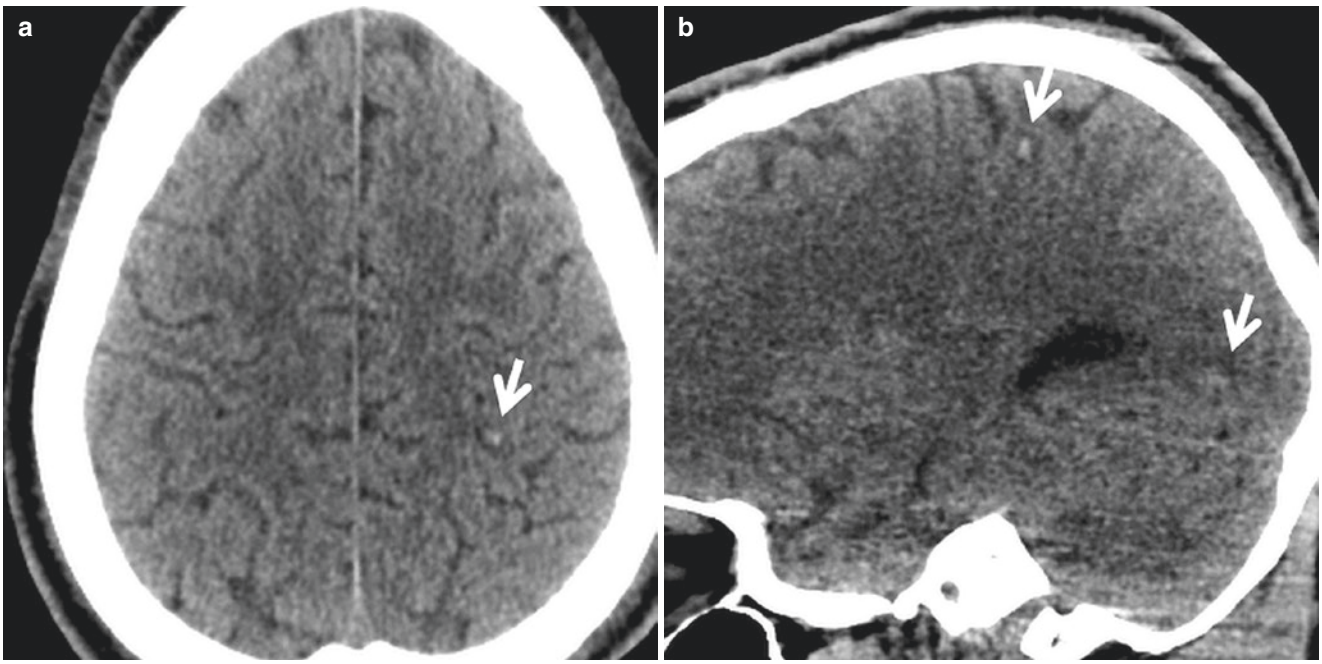

Fig. 1.1 Subtle intracranial hemorrhage in NCCT for patients with stroke alert. (**a** and **b**), Axial and sagittal CT demonstrate a small focus on intraparenchymal hemorrhage in the left parietal lobe (*arrow*). An additional focus of hemorrhage is seen in the left occipital lobe on the sagittal image (*arrow*). (**c** and **d**), Axial and coronal CT show sulcal subarachnoid hemorrhage in the right occipital lobe (*arrow*). (**e** and **f**), Axial and coronal CT demonstrate small amount of subdural hemorrhage along the right cerebral convexity, nearly isodense to the brain parenchyma. It is critical to evaluate the NCCT for subtle hemorrhage in stroke patient before administering tPA

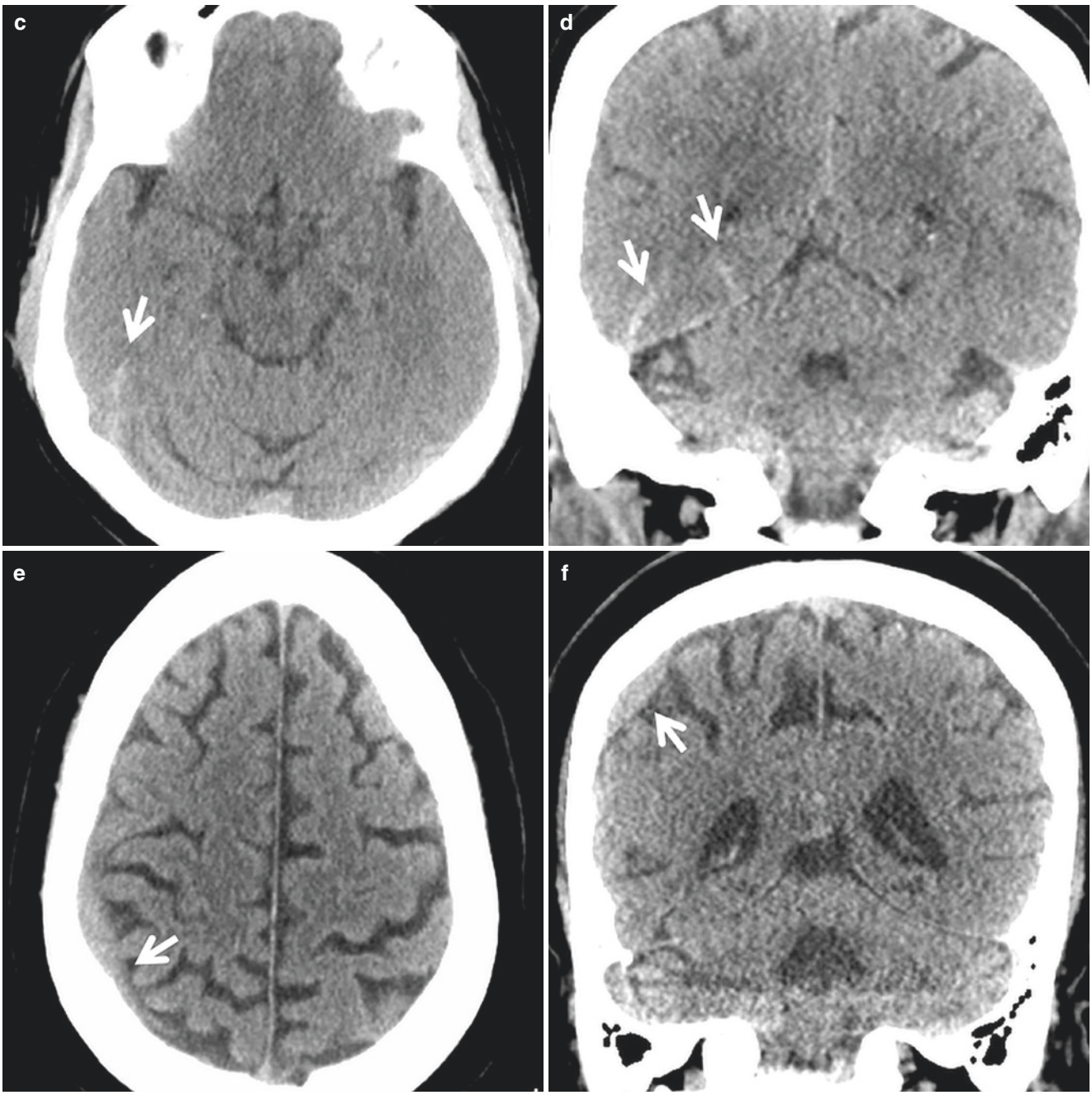

Fig. 1.1 (continued)

The hyperdense vessel sign corresponds to acute luminal thrombosis, which can be seen in intracranial ICA, MCA, ACA, and vertebral and basilar artery. A hyperdense MCA > 8 mm in length is an indicator that IV tPA alone is unlikely to achieve successful recanalization although this should not be used as a criterion to withhold IV tPA from patients who otherwise qualify [14].

Alberta Stroke Program Early CT Score (ASPECTS) has been developed as a system to quantify the early ischemic changes from MCA stroke (http://www.aspectsinstroke.com). The MCA territory is divided into 10 segments at ganglionic and supraganglionic levels [15]. With a score of 10 indicating a normal CT, the score is decreased by 1 point for each segment of the brain affected by ischemic change. Patients with ASPECTS of 7 or less have been shown to have poor outcome [16]. Despite its successful application in several clinical trials, ASPECTS has only moderate interobserver reliability even among the experienced neuroradiologists, which limits its routine use in EVT selection [17]. A recent study showed that ASPECTS by using automated software had better agreement than did experienced neuroradiologists [18].

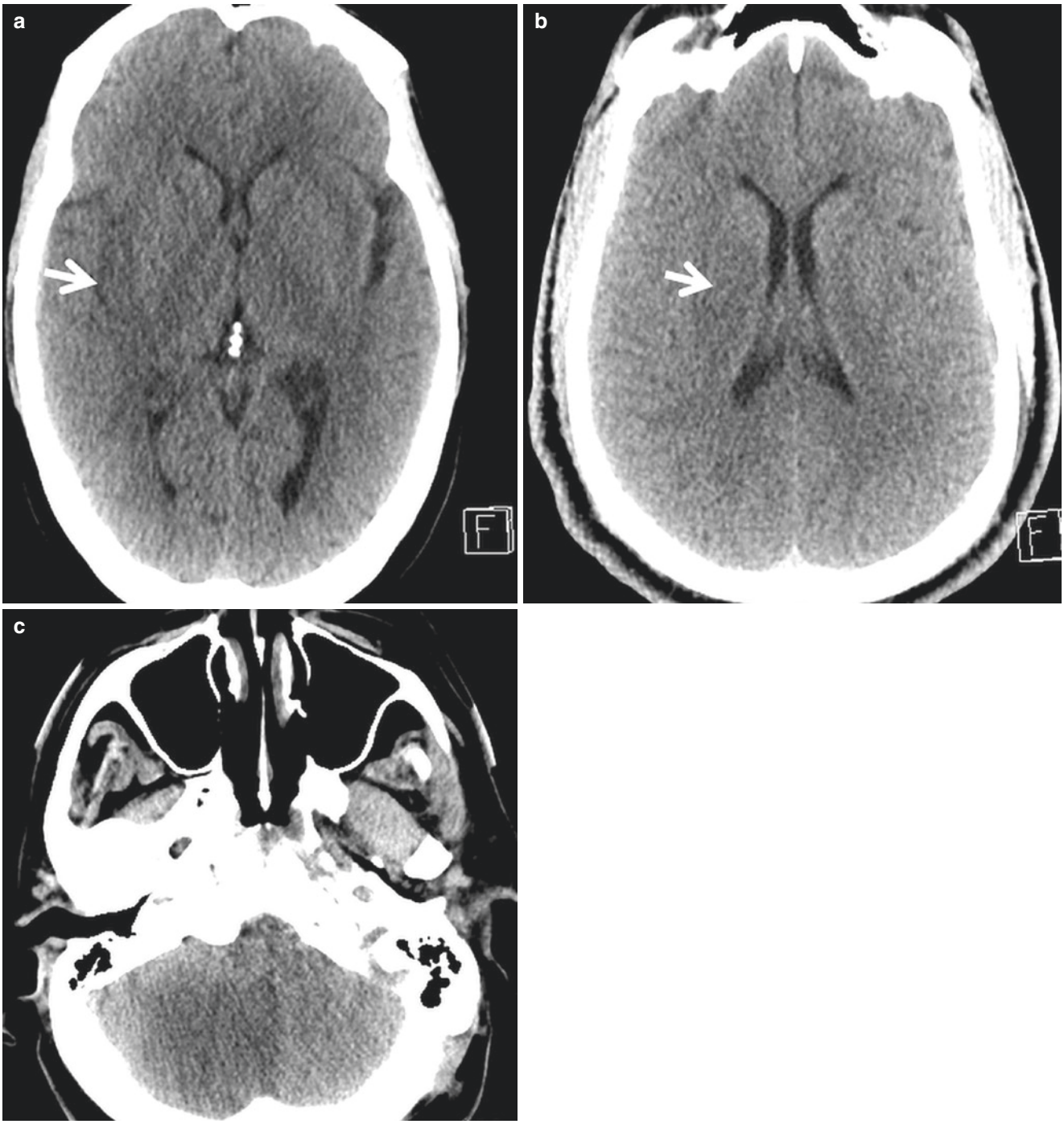

Fig. 1.2 CT findings of acute ischemic stroke. (**a**), NCCT shows loss of gray–white matter differentiation of right insula. (**b**), NCCT in a different stroke patient shows hypodensity in the right lentiform nucleus. (**c**), NCCT shows hypodensity of right cerebellum

1.4.2 CT Angiography

CTA from arch to vertex is the preferred modality to evaluate intracranial and cervical large vessel occlusion. In addition, CTA can provide useful information for EVT planning, such as variant anatomy of the aortic arch, tortuosity of supra-aortic branches, and extracranial vascular stenoses, occlusions, and dissections.

CTA should be performed immediately after NCCT without removing the patient from the scanner. Administration of iodinated contrast without first testing renal function in AIS patients without known history of renal impairment is an

accepted practice, as the benefit of salvaging brain from potentially devastating ischemic injury outweighs the risk of contrast-induced nephropathy [19]. It should be noted that performing CTA should not delay the administration of IV tPA. If NCCT is negative for acute hemorrhage and the patient has no other contraindications, tPA should be reconstituted and given as a parallel process to the CTA.

CTA source data should be immediately post-processed into thick slab (typically 30 mm slice thickness with 5 mm overlapping interval) axial, coronal, and sagittal maximum intensity projection (MIP) images to facilitate the identification of LVO. Coronal images are best to evaluate ICA terminus and M1 and A1 segments, while sagittal images are best to depict M2/M3 and A2/A3 occlusion/stenosis.

In addition to the vascular evaluation, CTA source images can be used to detect brain parenchymal ischemic changes, which correlate with low cerebral blood volume (CBV). It is more sensitive than NCCT for this purpose but can potentially overestimate core infarct volume in regions of poor but not critical hypoperfusion [20, 21].

1.4.3 Collateral Assessment

The quality of collateral flow is an important determinant of infarct progression in cases of LVO. Infarct core progresses more slowly for patients with good collaterals (slow progressors), who are more likely to tolerate the ischemic insults and benefit from thrombectomy. For patients with poor collaterals, infarct core grows more rapidly (fast progressors), and there is a relatively lower probability of penumbral salvage unless thrombectomy can be performed very rapidly [22].

CTA can provide valuable information regarding the status of collateral circulation that can be used to select candidates for thrombectomy. It can be performed as a single phase or a multiphasic study. The multiphasic study consists of arterial, peak venous, and late venous phases.

Several systems have been developed to define collateral flow based on CTA findings. For example, a commonly used system compares the collateral vessels in the region of the Sylvian fissure and cerebral convexity of the symptomatic hemisphere to the contralateral normal hemisphere with the following grading: 1, absent; 2, less than normal side; 3, equal to normal side; 4, greater than normal side; and 5, exuberant [23]. In a different system, the collaterals are graded by the degree of filling of the occluded vascular territory: 0, absent collaterals; 1, collaterals filling 50% of the territory; 2, collaterals filling > 50% but < 100% territory; and 3, collaterals filling 100% of the occluded territory [24]. A good collateral pattern can be defined as a symmetric or nearly symmetric leptomeningeal flow when comparing to the contralateral hemisphere, which can be used to select thrombectomy candidates [22].

1.4.4 CT Perfusion

CTP has become the primary modality to assess the size of core infarction and penumbra and select patients for mechanical thrombectomy in many stroke centers.

CTP is a functional technique that allows quantitative assessment of brain perfusion by acquiring serial images during the passage of a small volume of contrast (typically 30–40 ml with an injection rate of at least 4 mL/min) through the region of interest. A scan duration of 60–70 seconds is usually adequate to cover both wash-in and wash-out phases. Low peak tube potential of 80 kVp and tube current of 100–200 mAs are typically used to minimize the radiation dose.

Multiple perfusion parameters can be derived for each voxel by using various software packages, for example:

- T_{max} (time to maximum) measures the time from the start of bolus to the maximum contrast density.
- MTT (mean transit time) measures the average time for contrast bolus to pass through the voxel.
- CBF (cerebral blood flow) represents the volume of blood traversing a given amount of brain tissue per unit of time, measured in mL/100 g/min.
- CBV (cerebral blood volume) represents the volume of blood in a given amount of brain tissue measured in mL/100 g.
- CBF, MTT, and CBV are mathematically related by the central volume principle: CBF = CBV/MTT.

Analysis of CT perfusion can be made by qualitative visual assessment of parametric color maps (Figs. 1.3, 1.4, and 1.5). In cases of LVO, MTT and T_{max} are prolonged in the corresponding vascular territory, but the extent of prolongation is different for oligemia, penumbra, and core infarction. Area with severe CBV reduction usually corresponds to core infarction. Area with prolonged MTT/T_{max}, reduced CBF, but normal CBV is considered tissue at ischemic risk or penumbra (Table 1.1).

The manual post-processing and visual color map assessment require active user involvement and are subjected to great interobserver and inter-platform variability. Automated quantitative CTP analysis has been developed to address this issue and utilized in large clinical trials [8, 9]. The RAPID software uses a predefined relative CBF < 30% of normal as threshold for core infarction and T_{max} > 6 seconds for penumbra. In DEFUSE 3 trial, inclusion criteria for EVT include ischemic core infarction < 70 mL, penumbra–core mismatch volume > 15 mL, and mismatch ratio ≥ 1.8 [9].

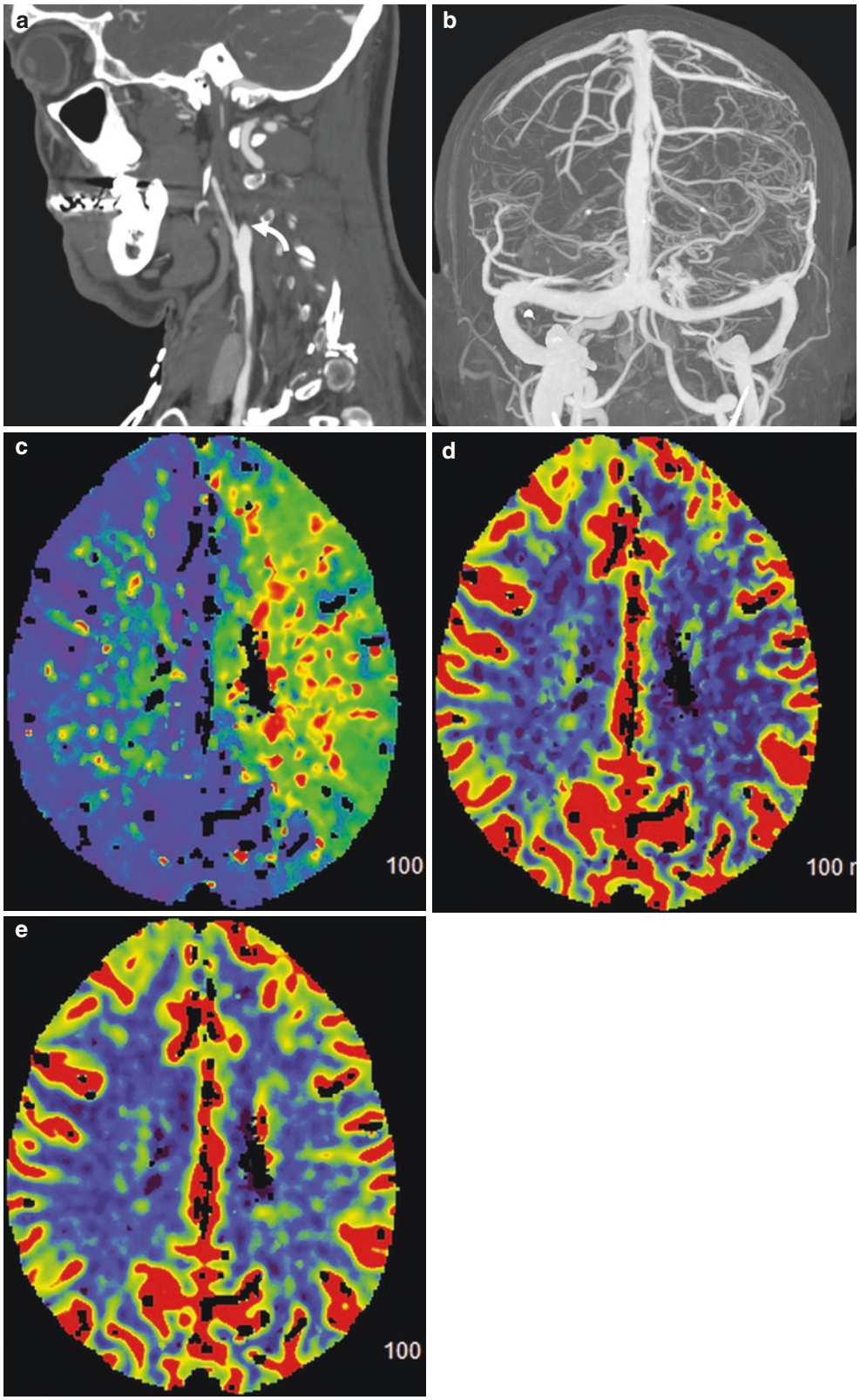

Fig. 1.3 Pattern of compensated oligemia. Young patient with recent minor injury to the neck presents with transient right-sided weakness. (**a**), CTA neck demonstrates tapered occlusion of left cervical ICA consistent with a dissection (*curved arrow*). (**b**), 3D reconstructed image of head CTA shows reconstitution of left MCA with increased vascularity compared to the right due to pial collaterals. CT perfusion demonstrates prolongation of TTD (**c**) in the left MCA and ACA territory and normal CBF (**d**) and CBV (**e**), compatible with compensated oligemia. The patient is treated with anticoagulation with no further intervention

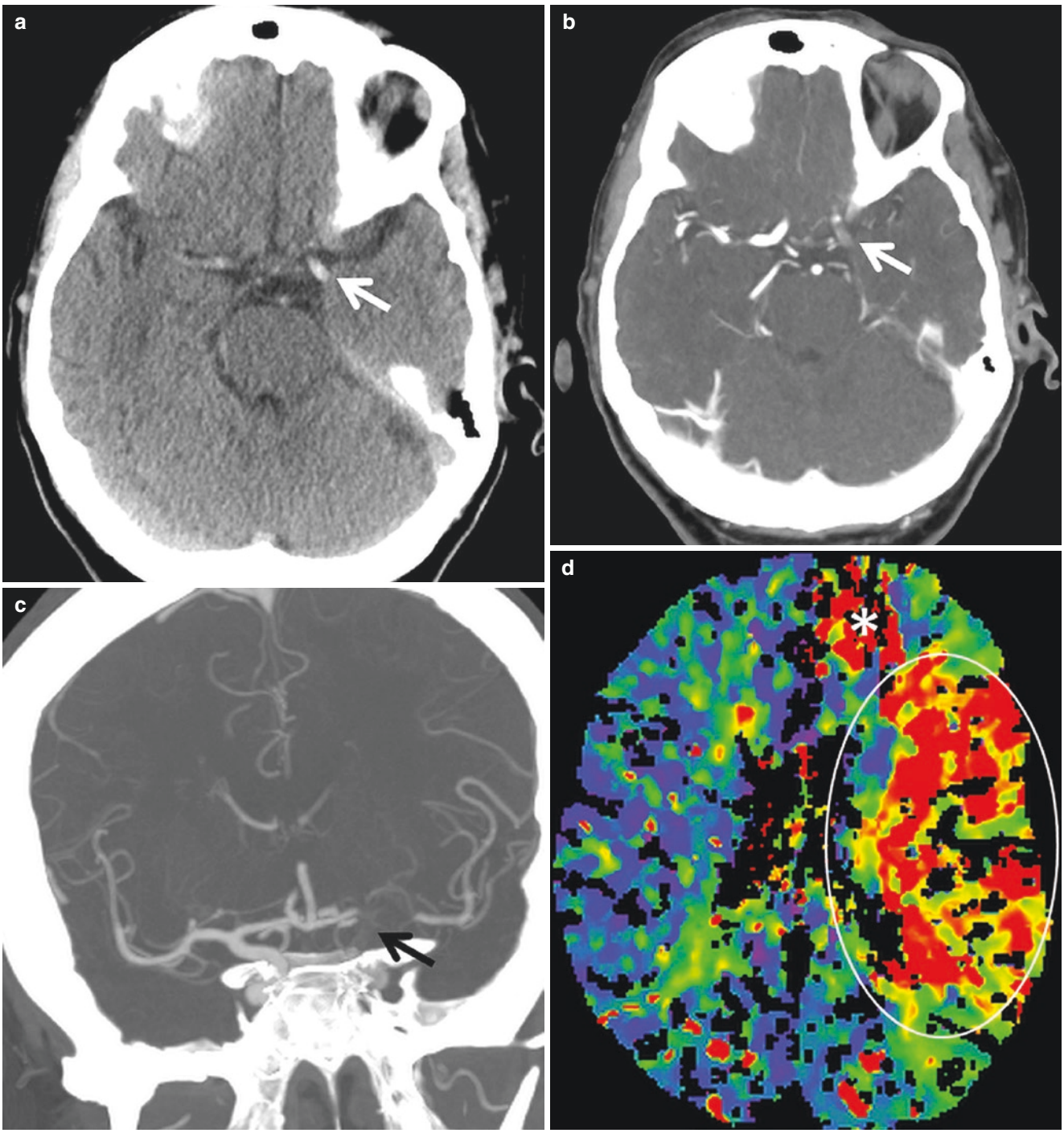

Fig. 1.4 Pattern of small infarction and large penumbra. Patient with sudden-onset right-sided weakness and aphasia. (**a**), NCCT demonstrates hyperdense left supraclinoid ICA (*arrow*). (**b**), Axial CTA demonstrates acute occlusion of left supraclinoid ICA (*arrow*). (**c**), CTA coronal MIP shows occlusion of left supraclinoid ICA, proximal M1 and A1 segment (*arrow*) with distal reconstitution through leptomeningeal collaterals. Perfusion images show prolonged TTD (**d**), decreased CBF (**e**), and preserved CBV (**f**) in the left MCA territory (*circle*), consistent with tissue at ischemic risk (penumbra). A small area in the left frontal pole (∗) shows decreased CBF and CBV, consistent with core infarction, secondary to a distal embolus in the left ACA frontopolar branch. The quantitative RAPID analysis (**g**) shows core infarction of 19 ml in the left frontal pole defined by rCBF < 30% and a large penumbra in the MCA territory of 187 ml mismatch volume defined by Tmax > 6 seconds. The patient is treated with mechanical thrombectomy. (**h**), Pre-thrombectomy AP DSA of left ICA injection shows a "T" occlusion of supraclinoid ICA, proximal M1, and origin of A1 segment. (**i**), Post-thrombectomy AP DSA shows TICI3 recanalization

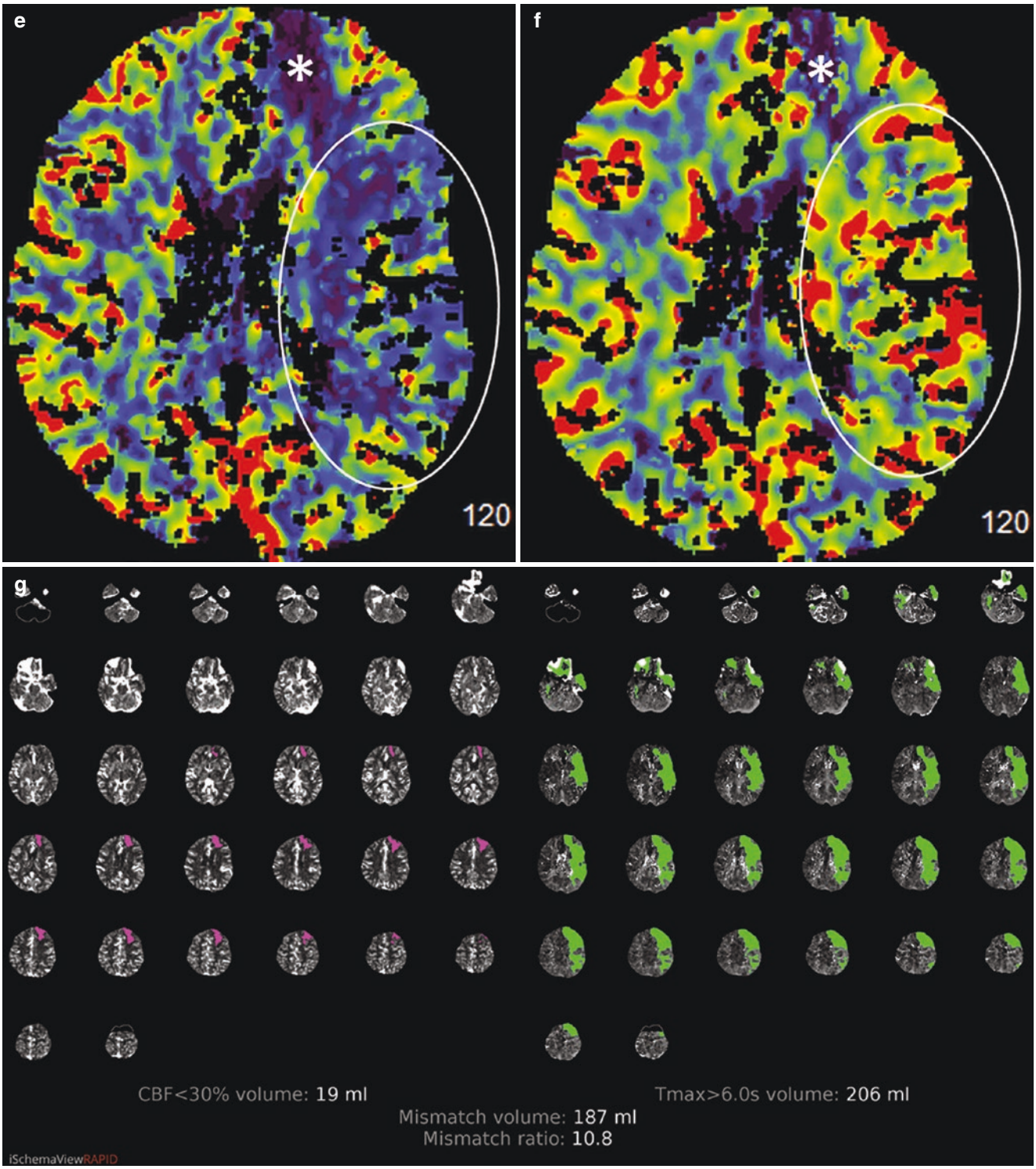

Fig. 1.4 (continued)

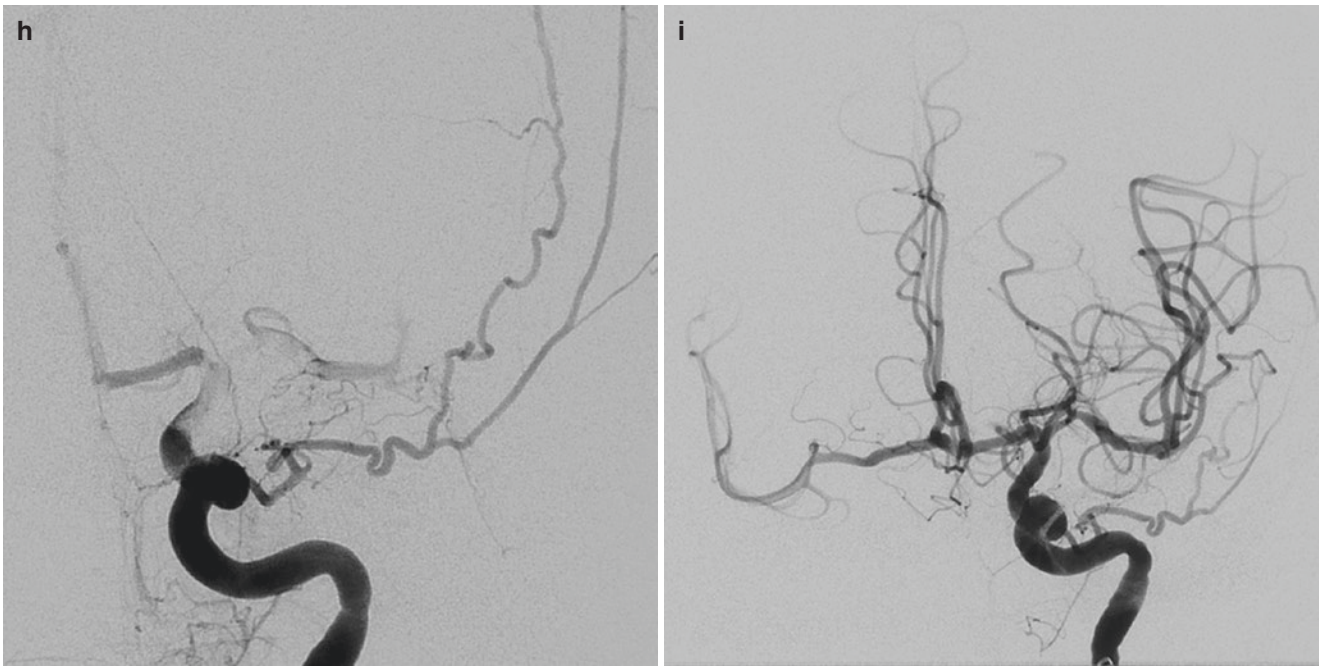

Fig. 1.4 (continued)

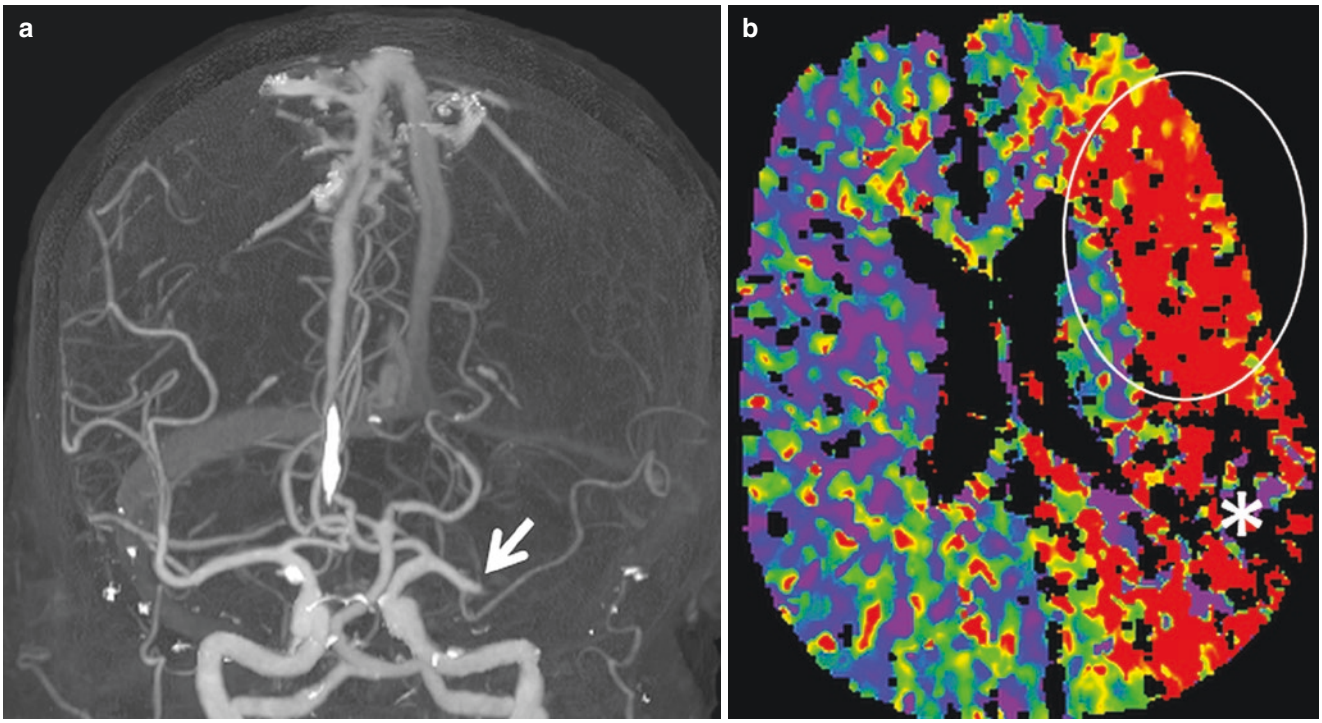

Fig. 1.5 Pattern of large core infarction. Patient with sudden-onset right-sided weakness. NCCT is unremarkable (not shown). (**a**), 3D CTA MIP image demonstrates acute occlusion of proximal left MCA just distal to the origin of anterior temporal artery (*arrow*). Note there is no reconstitution of distal MCA branches reflecting poor leptomeningeal collaterals. Perfusion images demonstrate marked prolongation of TTD (**b**), decreased CBF (**c**), and CBV (**d**) in the parietal/temporal lobes of the posterior MCA territory (∗), consistent with core infarction. The more anterior MCA territory (circle) shows relatively preserved CBV suggestive of penumbra tissue. The quantitative RAPID analysis (**e**) reveals core infarction volume of 67 ml defined by rCBF < 30% and penumbra of 177 ml mismatch volume defined by Tmax > 6 seconds. This patient received IV tPA and developed an intraparenchymal hematoma in the region of infarction on the following NCCT (**f**)

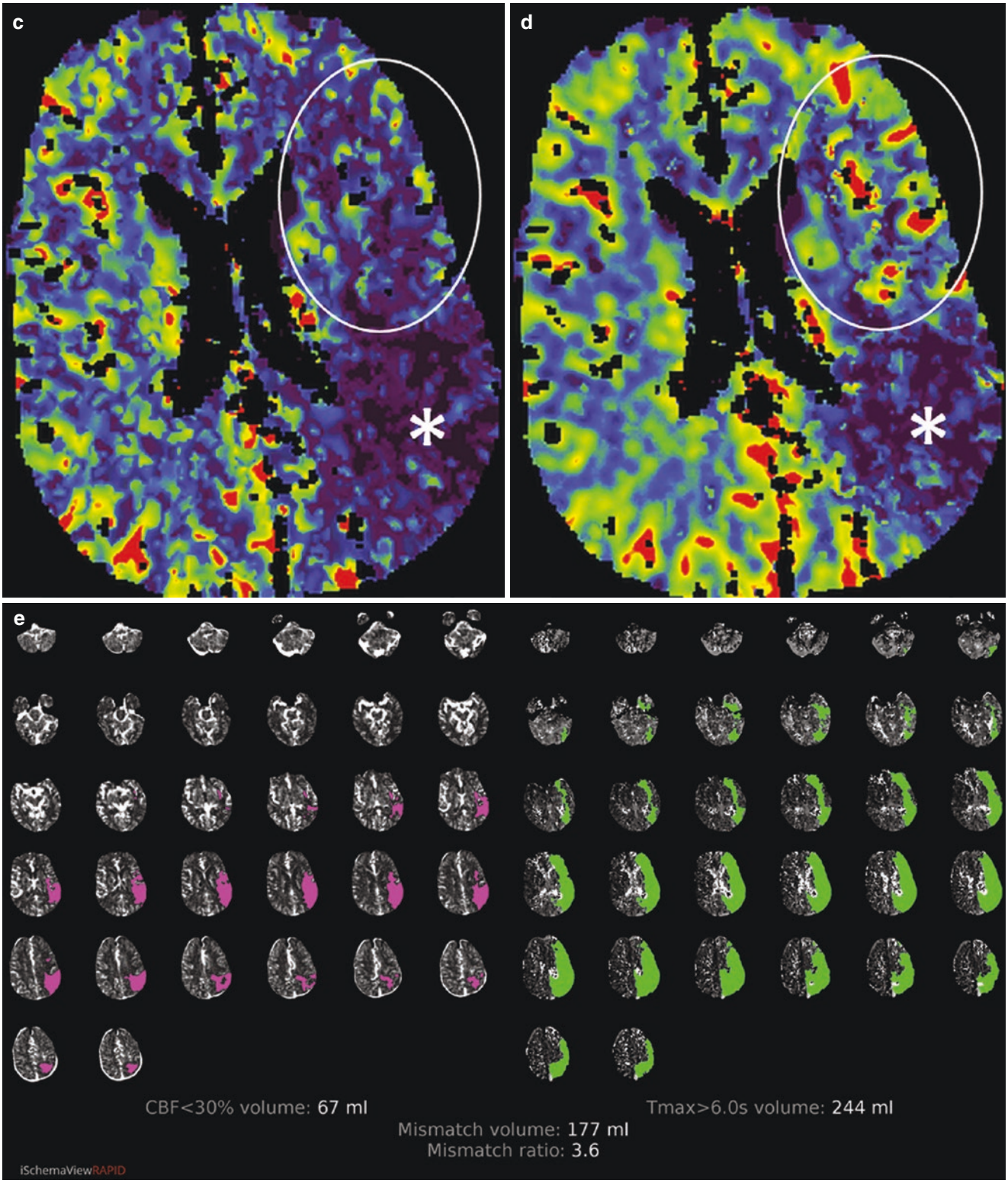

Fig. 1.5 (continued)

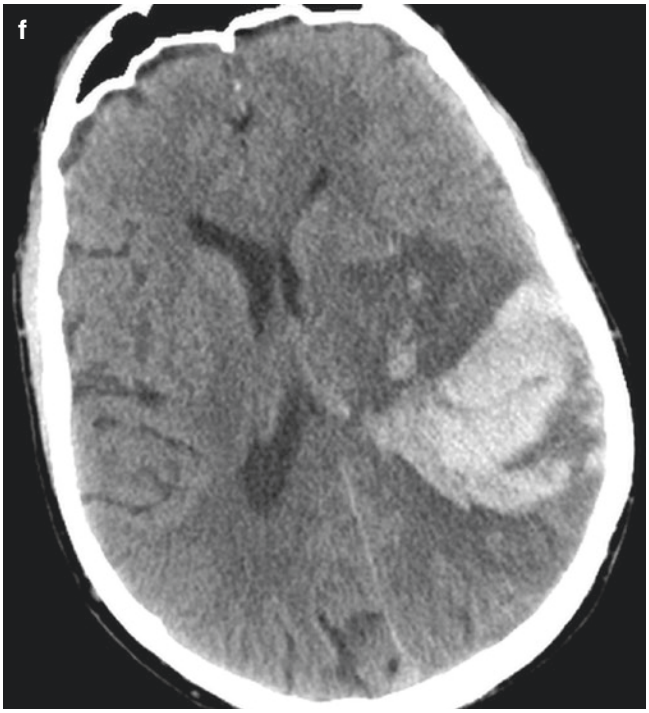

Fig. 1.5 (continued)

Table 1.1 Qualitative assessment of CT perfusion

	MTT/T_{max}	CBF	CBV
Benign oligemia	↑	Normal	Normal or ↑
Penumbra	↑↑	↓	Normal or ↓
Core	↑↑↑	↓↓	↓↓

CBF cerebral blood flow, *CBV* cerebral blood volume, *CT* computed tomography, *MMT* mean transit time

1.4.5 Limitation of CT Perfusion

Numerous technical factors can affect the quality of CTP. Motion is the most common and frequently difficult to correct. Beam hardening artifact from skull base and calvarium can affect the frontal lobes, temporal lobes, and posterior fossa, leading to erroneous interpretation. It is important to correct any head tilt and asymmetry before the scan to minimize these artifacts. Other factors such as poor contrast bolus, low cardiac output, arrhythmia, carotid stenosis, and shortened acquisition time can affect dynamic profile of contrast. These can usually be recognized by inspecting the time–density curve [25].

It is important to recognize that predefined thresholds used in clinical trials were derived from large data sets and the prediction in individual patient may not be as accurate. Although rCBF < 30% has been determined as the optimal threshold for core infarction, it can overestimate the size of infarction for patients with very early revascularization (Fig. 1.6). It has been shown that for patients who achieve rapid reperfusion through thrombectomy, a stricter rCBF threshold (<20%) better correlates with the final infarct volume [26]. On the other hand, rCBF < 30% threshold can underestimate the infarction if reperfusion is not promptly achieved (Fig. 1.7). A higher rCBF threshold < 38% corresponded best with the final DWI infarction volumes, although rCBF < 30% has greater specificity and less overcalls of core volume [27].

In subacute infarction when there is reperfusion either due to recanalization of occluded artery or leptomeningeal collaterals, since the CBF is no longer severely reduced, CTP can grossly underestimate the size of infarction [28]. In these patients, the infarct core estimated by perfusion may appear smaller than what is detected as hypodensity on NCCT or CTP source image. It is critical to evaluate all available imaging data to avoid such pitfalls (Fig. 1.8).

1.5 MRI-Based Imaging

1.5.1 Strengths and Weaknesses of MRI in Acute Stroke Imaging

MRI-based imaging protocols are being used in some stroke centers that allow immediate access to MRI scanners. In other centers, logistical challenges may delay the workflow and limit its routine use in acute stroke imaging. Patients must be screened for retained ferromagnetic metal before entering the scanner. For patients who cannot provide reliable history for the questionnaire, scout radiographs should be acquired promptly to speed up the MRI clearance. All the life support and monitoring devices need to be MRI compatible. Some stroke patients are too unstable to undergo MRI, and motion artifact can greatly degrade the diagnostic quality.

The major advantage of MRI over CT is the precise assessment of core infarction volume, which leads to better individual patient selection for EVT. Diffusion-weighted imaging (DWI) is highly sensitive and specific for the detection of core infarction. Although partial DWI reversal can occur in patients with very early reperfusion, for most patients, the initial DWI lesion represents irreversible cell death and closely correlates with the final infarct volume if there is successful recanalization [29]. The infarction volume can be calculated manually by using A∗B∗C/2 method (anteroposterior × transverse × superoinferior distance/2) or with automated software using predefined quantitative ADC

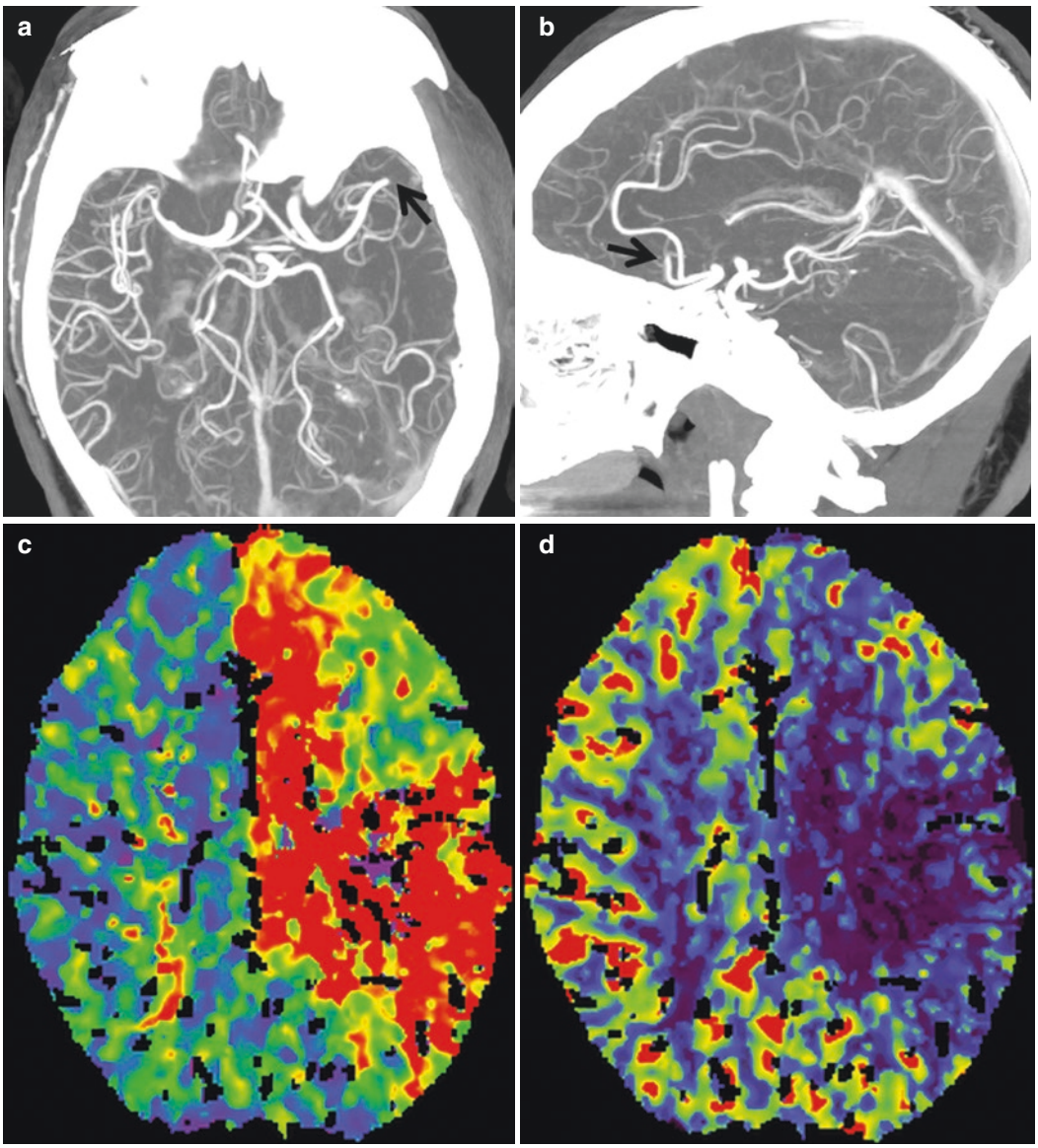

Fig. 1.6 CTP overestimation of core infarction volume in patient with early reperfusion. Patient with history of atrial fibrillation presents with sudden-onset right-sided weakness. NCCT is unremarkable (not shown). (**a**), Axial CTA MIP shows occlusion of proximal M2 segment of left MCA. This is a "M1 like" M2 occlusion since both anterior and posterior division are involved. (**b**), Sagittal CTA MIP shows additional occlusion of left ACA A2 segment. CTP color images show prolongation of TTD (**c**) and decreased CBF (**d**) in the left MCA and ACA territories. (**e**), The corona radiata in the ACA/MCA border zone and lateral frontal cortex demonstrate decreased CBV (**e**) (circle) suspicious for infarction, while the remainder areas have maintained CBV consistent with penumbra. (**f**), This is confirmed by the quantitative RAPID analysis, which shows core infarction of 31 ml by rCBF < 30% and penumbra of 190 ml by Tmax > 6 seconds threshold. (**g**), Patient is taken to angiography suite immediately. Pre-thrombectomy AP DSA of left ICA injection shows occlusion of left proximal M2 (*black arrow*) and A2 (*white arrow*) segments. (**h**), 24 hours after successful thrombectomy with TICI3 recanalization, MRI DWI shows no acute infarction. In cases of rapid reperfusion, CTP can overestimate infarction volume

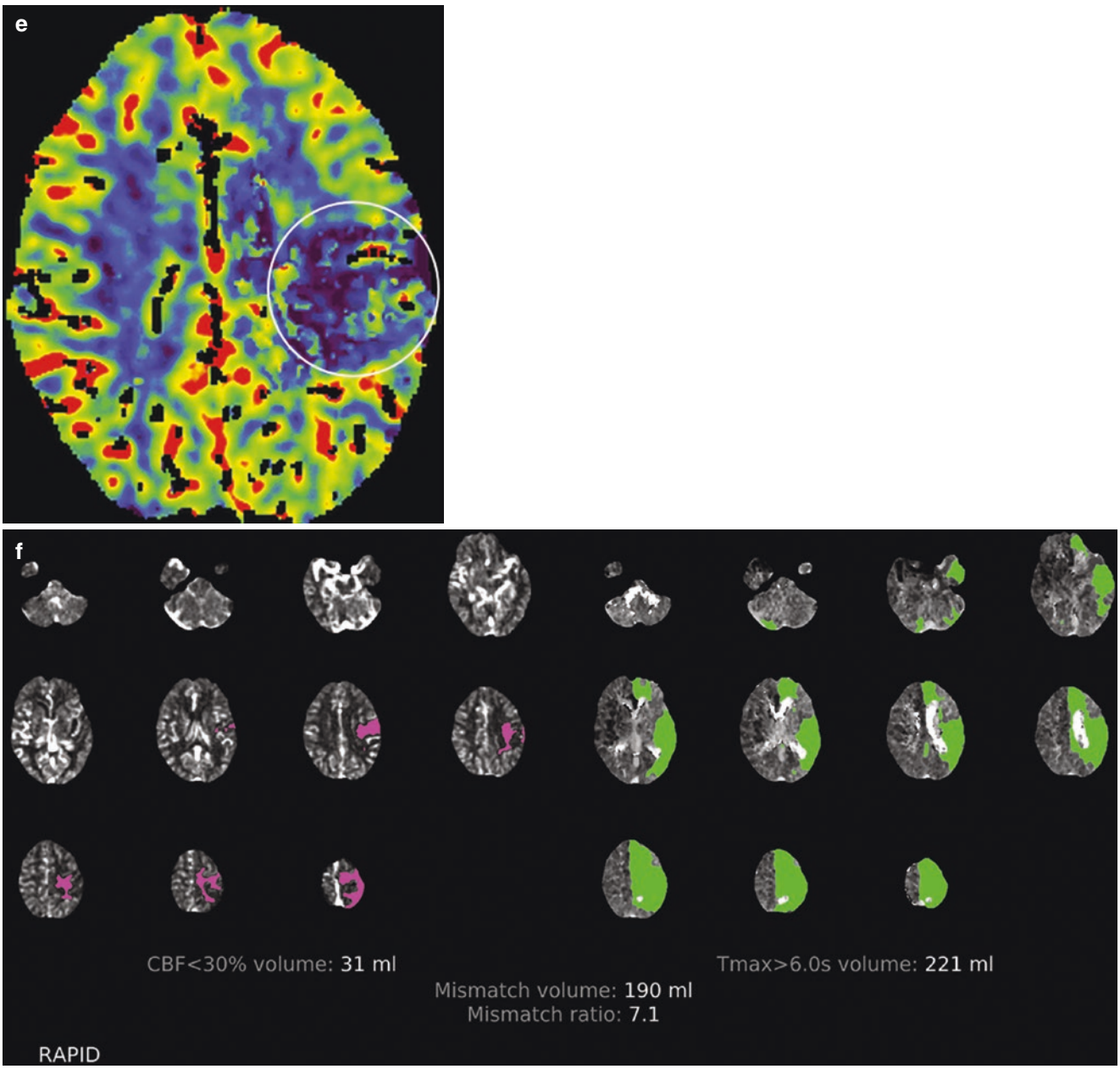

Fig. 1.6 (continued)

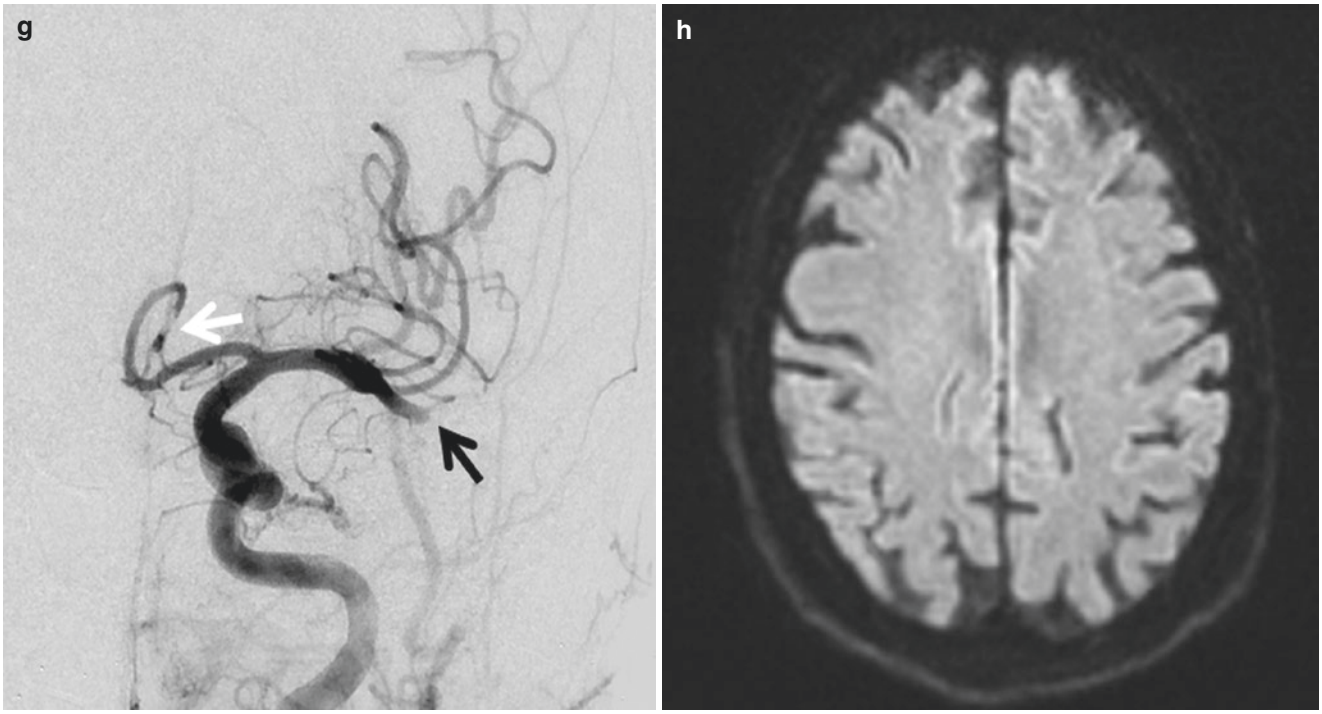

Fig. 1.6 (continued)

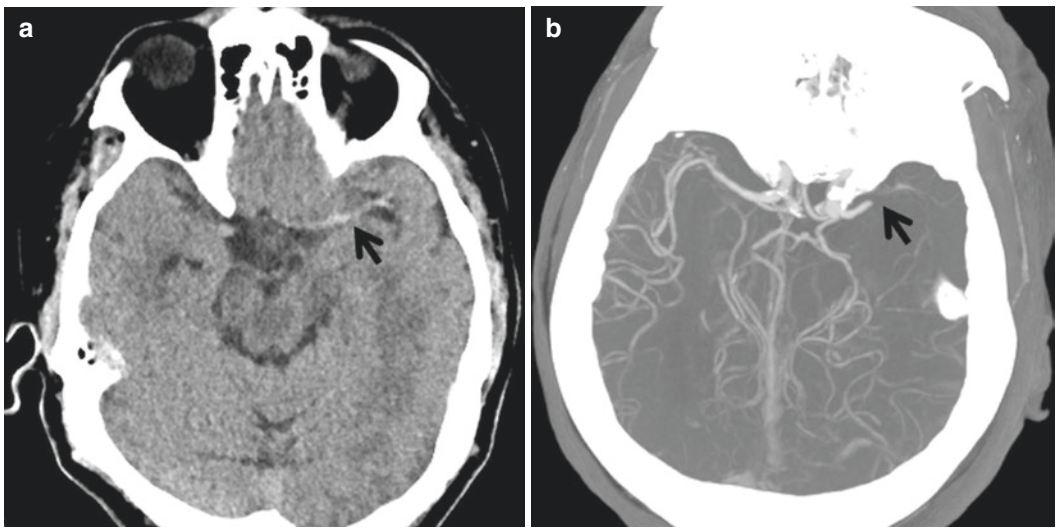

Fig. 1.7 CTP underestimation of core infarction. Patient presents with acute left MCA syndrome. (**a**), NCCT demonstrates hyperdense left MCA (*arrow*). No definite acute infarction is seen with ASPECTS of 10. (**b**), Axial CTA demonstrates proximal left M1 occlusion (arrow). Note poor leptomeningeal collaterals in the left MCA territory compared to the right side. CT perfusion shows marked prolongation of TTD (**c**), decreased CBF (**d**), but slightly elevated CBV (**e**) in the left MCA territory, mostly consistent with penumbra. (**f**), Quantitative RAPID analysis demonstrates a small infarction at the left insula and operculum of 8 ml by rCBF < 30% and large penumbra mismatch volume of 142 ml. The patient is taken into angiography, although the revascularization is delayed due to difficult groin access and tortuous arch anatomy. (**g**), Pre-thrombectomy AP angiogram from left ICA injection confirms left MCA occlusion at the origin. (**h**), Post-thrombectomy AP angiogram demonstrates TICI-3 revascularization of left MCA. (**i**), However, the subsequent DWI MRI at 24 hours shows acute infarction of the entire MCA territory. This case highlights the difficulty in accurately estimating the core infarction by CT perfusion in certain cases. In this case, the lack of leptomeningeal collaterals is a clue that the infarction will likely progress rapidly

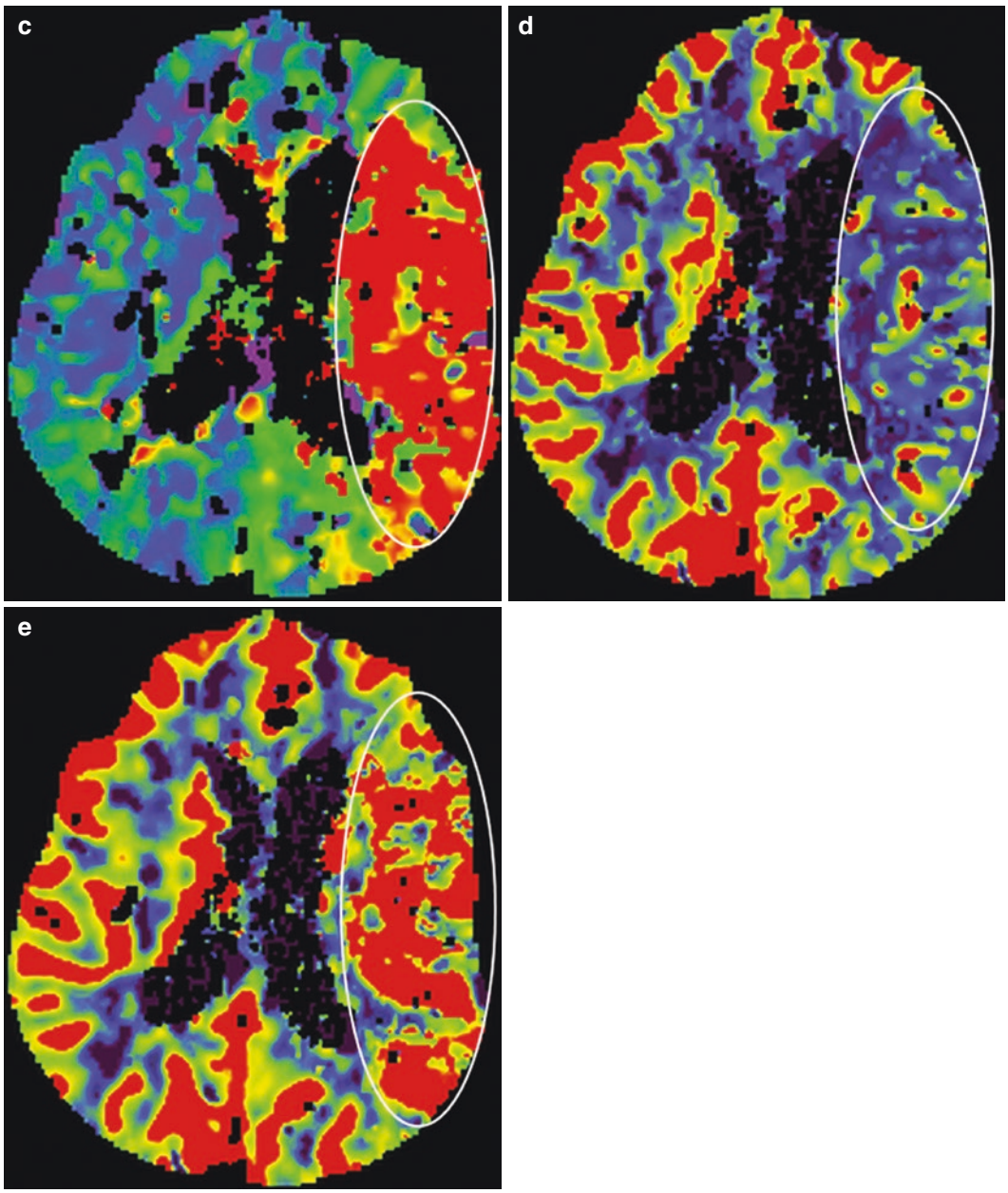

Fig. 1.7 (continued)

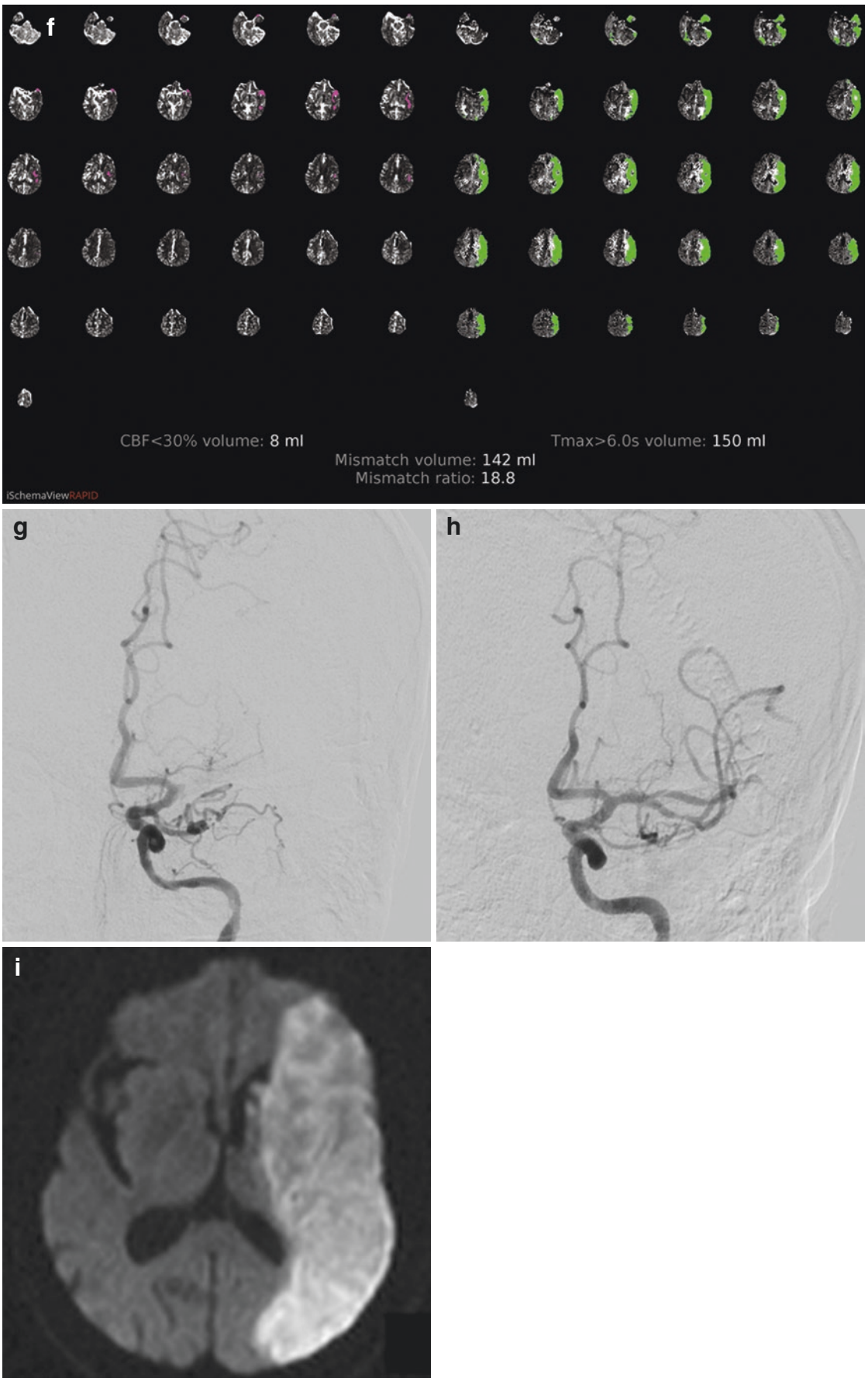

Fig. 1.7 (continued)

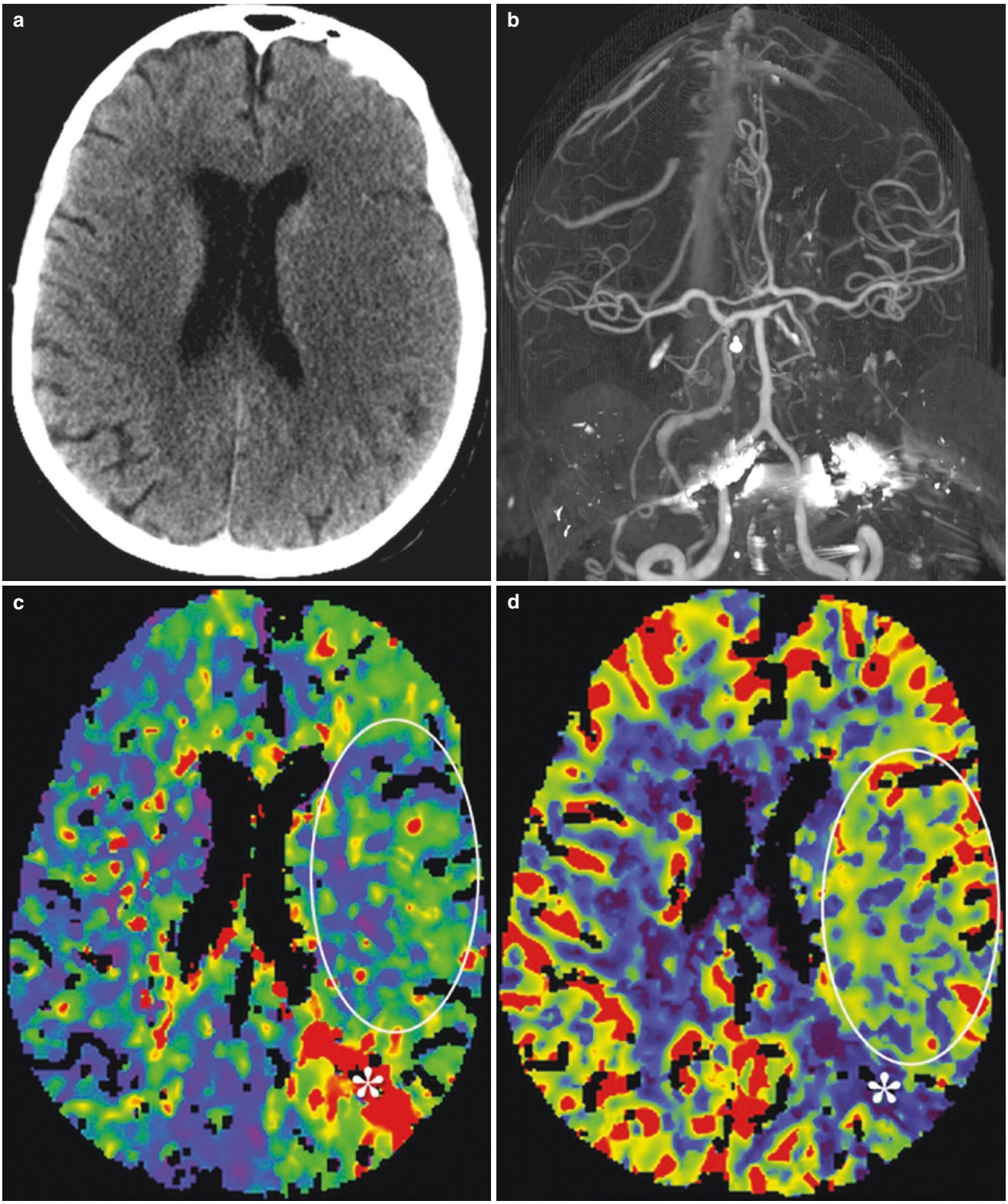

Fig. 1.8 Reperfusion of infarction on CTP. Patient presents with right-sided weakness and aphasia. (**a**), NCCT shows a large area of low attenuation in the left MCA territory consistent with acute infarctions. (**b**), Coronal CTA 3D image demonstrates occlusion of left cervical ICA with reconstitution of left MCA and ACA. CTP perfusion images show a small area of infarction (∗) in the left parietal/occipital posterior border zone with prolonged TTD (**c**), decreased CBF (**d**), and CBV (**e**), while the remainder of MCA territory (circle) has normal to slightly elevated CBF and CBV. In this case, the CTP gives inaccurate estimate of infarction volume since most of the infarction has been reperfused. It is crucial to analyze the CTP in conjunction with NCCT and CTA source images to avoid this pitfall

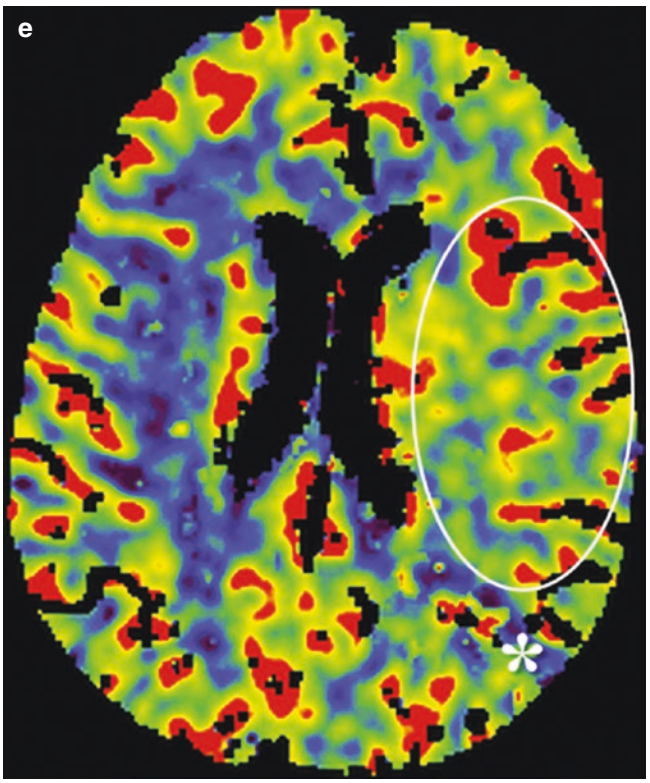

Fig. 1.8 (continued)

threshold of $< 600 \times 10^{-3}$ mm^2/sec. Patients with initial DWI lesion volume $\leq$ 70 ml and LVO on MRA are selected for EVT (Fig. 1.9) [30]. Variation of interrater measurement is much lower for DWI compared with CTP.

1.5.2 MRI Protocol

MRI protocol should be optimized for different clinical scenarios. For patients who have had a NCCT negative for acute hemorrhage and CTA positive for LVO, only the DWI sequence is essential for EVT selection. On the other hand, for patients without NCCT and CTA, MRI protocol should be comprehensive and typically includes DWI/ADC to estimate core infarction, gradient recall echo (GRE), and fluid-attenuated inversion-recovery (FLAIR) sequences to exclude intracranial hemorrhage and other acute non-ischemic pathologies, MR angiography to evaluate vascular patency, and an optional perfusion MRI sequence to assess penumbra [30]. A comprehensive stroke MRI protocol using combination of echo-planar imaging (EPI) and parallel acquisition technique can be performed within 6 minutes [31], comparable to multimodal CTs.

Elliptical centric contrast-enhanced MRA (ceMRA) is the preferred MRA technique in AIS. It can be performed

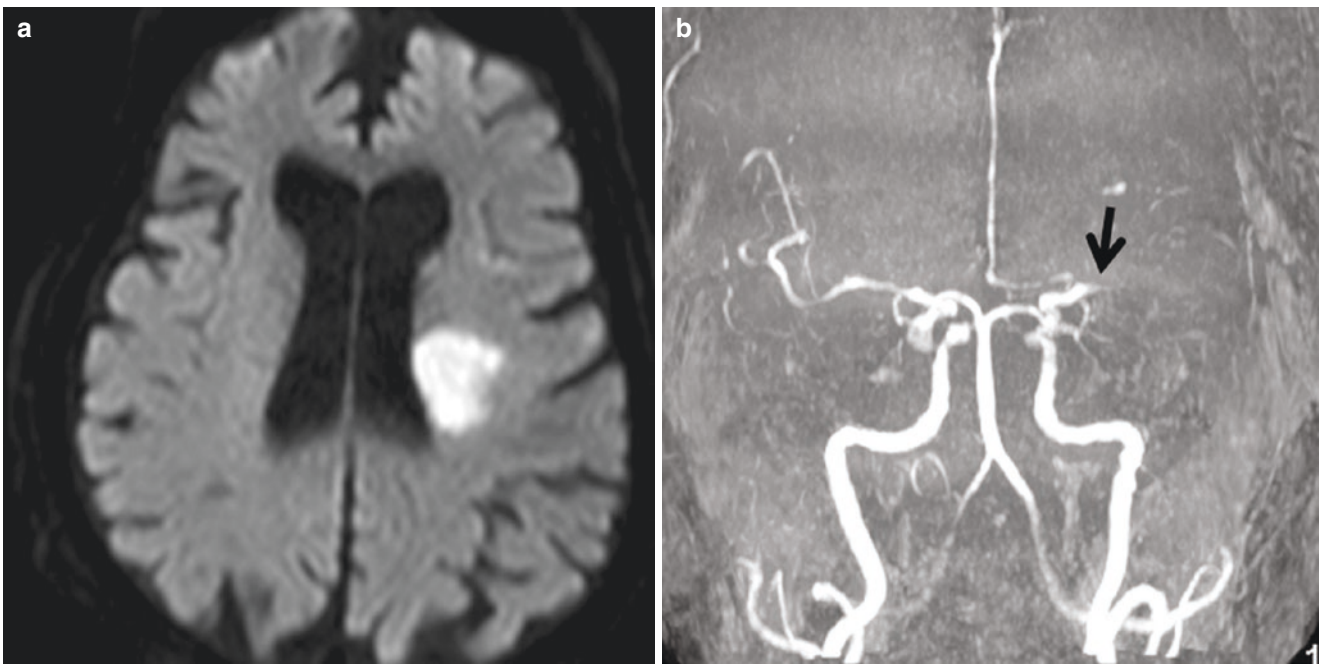

Fig. 1.9 MRI in EVT selection. (**a**), DWI shows acute infarction of left basal ganglia with the estimated core volume of 20 ml by A∗B∗C/2 method. (**b**), 3D TOF MRA shows left MCA occlusion at the origin

rapidly and covers a large field of view. Although the spatial resolution is less robust compared to CTA, ceMRA is adequate to detect LVO and assess the quality of pial collaterals. Similar to CTA, ceMRA can also provide useful information on the aortic arch and supra-aortic branch anatomy to facilitate EVT planning.

In patients with compromised renal function (eGFR < 30), time-of-flight (TOF) MRA is an alternative technique that does not require intravenous administration of gadolinium. Compared to 3D TOF, 2D TOF sequence allows for more rapid image acquisition and is more resistant to motion, since images are acquired serially and rapidly. Since TOF MRA mainly detects antegrade flow, this technique only provides limited information on the collateral status. Additional drawback of TOF MRA is the frequent poor imaging quality for the cervical arteries [30].

The use of MRI perfusion is optional. Some centers use dynamic susceptibility contrast (DSC) perfusion to assess penumbra with the same predefined threshold of Tmax > 6 seconds. However, DAWN trial uses "clinical penumbra" without MR perfusion, that is, the presence of a neurologic deficit not completely explained by the small core infarction visualized on DWI, which is indicative of a large penumbra to proceed with thrombectomy [8].

With the recent positive results of the WAKE-UP trial [12], which used DWI–FLAIR imaging mismatch to select patients with unknown time of stroke onset for intravenous thrombolysis, the indication of MRI in acute stroke imaging will likely continue to expand.

References

1. Lees KR, Bluhmki E, von Kummer R, et al. Time to treatment with intravenous alteplase and outcome in stroke: an updated pooled analysis of ECASS, ATLANTIS, NINDS, and EPITHET trials. Lancet. 2010;375:1695–703.
2. Berkhemer OA, Fransen PSS, Beumer D, et al. A randomized trial of intraarterial treatment for acute ischemic stroke. N Engl J Med. 2015;372:11–20.
3. Jovin TG, Chamorro A, Cobo E, et al. Thrombectomy within 8 hours after symptom onset in ischemic stroke. N Engl J Med. 2015;372:2296–306.
4. Goyal M, Demchuk AM, Menon BK, et al. Randomized assessment of rapid endovascular treatment of ischemic stroke. N Engl J Med. 2015;372:1019–30.
5. Campbell BCV, Mitchell PJ, EXTEND-IA Investigators. Endovascular therapy for ischemic stroke. N Engl J Med. 2015;372:2363–6.
6. Saver JL, Goyal M, Diener H-C, SWIFT PRIME Investigators. Stent-retriever thrombectomy for stroke. N Engl J Med. 2015;373:1076–8.
7. Bracard S, Ducrocq X, Mas JL, Soudant M, Oppenheim C, Moulin T, Guillemin F. Mechanical thrombectomy after intravenous alteplase versus alteplase alone after stroke (THRACE): a randomised controlled trial. Lancet Neurol. 2016;15:1138–47.
8. Nogueira RG, Jadhav AP, Haussen DC, et al. Thrombectomy 6 to 24 hours after stroke with a mismatch between deficit and infarct. N Engl J Med. 2018;378:11–21.
9. Albers GW, Marks MP, Kemp S, et al. Thrombectomy for stroke at 6 to 16 hours with selection by perfusion imaging. N Engl J Med. 2018;378:708–18.
10. Powers WJ, Rabinstein AA, Ackerson T, et al. 2018 guidelines for the early management of patients with acute ischemic stroke: a guideline for healthcare professionals from the American Heart Association/American Stroke Association. Stroke. 2018. https://doi.org/10.1161/STR.0000000000000158.
11. Ma H, Campbell BCV, Parsons MW, et al. Thrombolysis guided by perfusion imaging up to 9 hours after onset of stroke. N Engl J Med. 2019;380:1795–803.
12. Thomalla G, Simonsen CZ, Boutitie F, et al. MRI-guided thrombolysis for stroke with unknown time of onset. N Engl J Med. 2018;379:611–22.
13. Guidelines for the early management of patients with acute ischemic stroke: 2019 update to the 2018 guidelines for the early management of acute is... - PubMed - NCBI. https://www.ncbi.nlm.nih.gov/pubmed/31662037. Accessed 9 Jan 2020.
14. Powers WJ, Rabinstein AA, Ackerson T, et al. 2018 guidelines for the early management of patients with acute ischemic stroke: a guideline for healthcare professionals from the American Heart Association/American Stroke Association. Stroke. 2018;49:e46–e110.
15. Barber PA, Demchuk AM, Zhang J, Buchan AM. Validity and reliability of a quantitative computed tomography score in predicting outcome of hyperacute stroke before thrombolytic therapy. ASPECTS Study Group. Alberta Stroke Programme Early CT Score. Lancet (London, England). 2000;355:1670–4.
16. Pexman JHW, Barber PA, Hill MD, Sevick RJ, Demchuk AM, Hudon ME, Hu WY, Buchan AM. Use of the Alberta Stroke Program Early CT Score (ASPECTS) for assessing CT scans in patients with acute stroke. Am J Neuroradiol. 2001;22:1534–42.
17. Gupta AC, Schaefer PW, Chaudhry ZA, Leslie-Mazwi TM, Chandra RV, González RG, Hirsch JA, Yoo AJ. Interobserver reliability of baseline noncontrast CT Alberta stroke program early CT score for intra-arterial stroke treatment selection. Am J Neuroradiol. 2012;33:1046–9.
18. Maegerlein C, Fischer J, Mönch S, Berndt M, Wunderlich S, Seifert CL, Lehm M, Boeckh-Behrens T, Zimmer C, Friedrich B. Automated calculation of the Alberta Stroke Program Early CT Score: feasibility and reliability. Radiology. 2019;291:141–8.
19. Hopyan JJ, Gladstone DJ, Mallia G, Schiff J, Fox AJ, Symons SP, Buck BH, Black SE, Aviv RI. Renal safety of CT angiography and perfusion imaging in the emergency evaluation of acute stroke. Am J Neuroradiol. 2008;29:1826–30.
20. Camargo ECS, Furie KL, Singhal AB, et al. Acute brain infarct: detection and delineation with CT angiographic source images versus nonenhanced CT scans. Radiology. 2007;244:541–8.
21. Pulli B, Schaefer PW, Hakimelahi R, Chaudhry ZA, Lev MH, Hirsch JA, González RG, Yoo AJ. Acute ischemic stroke: infarct core estimation on CT angiography source images depends on CT angiography protocol. Radiology. 2012;262:593–604.

22. Nael K, Sakai Y, Khatri P, Prestigiacomo CJ, Puig J, Vagal A. Imaging-based selection for endovascular treatment in stroke. Radiographics. 2019;39:1696–713.
23. Maas MB, Lev MH, Ay H, et al. Collateral vessels on CT angiography predict outcome in acute ischemic stroke. Stroke. 2009;40:3001–5.
24. Tan JC, Dillon WP, Liu S, Adler F, Smith WS, Wintermark M. Systematic comparison of perfusion-CT and CT-angiography in acute stroke patients. Ann Neurol. 2007;61:533–43.
25. Vagal A, Wintermark M, Nael K, Bivard A, Parsons M, Grossman AW, Khatri P. Automated CT perfusion imaging for acute ischemic stroke: pearls and pitfalls for real-world use. Neurology. 2019;93:888–98.
26. Bivard A, Kleinig T, Miteff F, Butcher K, Lin L, Levi C, Parsons M. Ischemic core thresholds change with time to reperfusion: a case control study. Ann Neurol. 2017;82:995–1003.
27. Cereda CW, Christensen S, Campbell BCV, et al. A benchmarking tool to evaluate computer tomography perfusion infarct core predictions against a DWI standard. J Cereb Blood Flow Metab. 2016;36:1780–9.
28. Albers GW. Use of imaging to select patients for late window endovascular therapy. Stroke. 2018;49:2256–60.
29. Campbell BCV, Purushotham A, Christensen S, et al. The infarct core is well represented by the acute diffusion lesion: sustained reversal is infrequent. J Cereb Blood Flow Metab. 2012;32:50–6.
30. Leslie-Mazwi TM, Lev MH, Schaefer PW, Hirsch JA, González RG MR imaging selection of acute stroke patients with emergent large vessel occlusions for thrombectomy. Neuroimaging Clin. 2018. https://doi.org/10.1016/j.nic.2018.06.003.
31. Nael K, Khan R, Choudhary G, Meshksar A, Villablanca P, Tay J, Drake K, Coull BM, Kidwell CS. Six-minute magnetic resonance imaging protocol for evaluation of acute ischemic stroke: pushing the boundaries. Stroke. 2014;45:1985–91.

Ischemic Stroke Vascular Territory

2

Yang Tang

2.1 Introduction

One of the main goals of cross-sectional stroke imaging is to determine the affected vascular territory. Knowledge of this will allow the correlation between anatomic disease localization and patients' clinical symptomology and facilitate the identification of diseased vessels on the CTA, MRA, or catheter angiogram for treatment planning. In addition, knowing the pattern and distribution of disease may help determine underlying stroke etiologies. For example, infarctions involving multiple arterial territories usually suggest embolic disease or vasculopathy. It can also help differentiate arterial from venous infarctions as well as various stroke mimics that will be discussed in other chapters.

The intracranial circulation can be divided into anterior and posterior circulation.

2.2 Anterior Circulation

2.2.1 Internal Carotid Artery (ICA)

A number of ICA classification systems are available. A commonly used system divides the ICA into seven segments: cervical (C1), petrous (C2), lacerum (C3), cavernous (C4), clinoid (C5), ophthalmic (C6), and communicating (C7) segment. The supraclinoid segments (C6 and C7) are subarachnoid in location. Ophthalmic artery and superior hypophyseal artery originate from the C6 segment, while posterior communicating artery and anterior choroidal artery arise from C7 segment [1].

Anterior choroidal artery: the anterior choroidal artery (AChA) arises from the posterior wall of the ICA distal to the origin of the P-comm. Although a small artery, its occlusion can lead to infarction of important brain territories including posterior limb of the internal capsule, globus pallidus, optic tract, lateral geniculate body, origin of optic radiation, and mesial temporal lobe including amygdala and hippocampal head (Fig. 2.1) [2].

2.2.2 Middle Cerebral Artery (MCA)

MCA supplies most of the lateral cerebral convexity with the exception of the occipital lobe and posterior inferior parietal lobe that are supplied by PCAs. It is the most common territory affected by ischemic stroke. MCA can be divided into the following four segments [1].

M1 segment arises at the ICA terminus, extends horizontally in the Sylvian cistern, and terminates at the limen insulae before the bifurcation/trifurcation. Lateral lenticulostriate arteries and anterior temporal artery arise from the M1 segment. Lateral lenticulostriate arteries supply the superior part of the head and body of the caudate nucleus and putamen, while anterior temporal artery supplies the anterior tip of the temporal lobe.

M2 (insular) segment runs along the surface of the insula within the Sylvian fissure. It has superior and inferior divisions, or occasionally superior, middle, and inferior divisions if M1 trifurcates. The superior division supplies the frontal and anterior parietal lobes. The inferior division supplies the lateral temporal and inferior parietal lobes. In the dominant hemisphere, the superior division supplies the Broca's area in the pars opercularis and pars triangularis of inferior frontal gyrus (Fig. 2.2), while the inferior division supplies the Wernicke's area in the posterior superior temporal gyrus (Fig. 2.3).

At the top of the insula, MCA courses laterally under the frontal, parietal, and temporal opercula, forming the M3 opercular segment.

M4 (cortical) segment includes distal cortical branches that exit the Sylvian fissure and irrigates the lateral cerebral convexity. In a typical bifurcation pattern, the orbitofrontal,

© Springer Nature Switzerland AG 2020

Y. Tang, *Atlas of Emergency Neurovascular Imaging*, https://doi.org/10.1007/978-3-030-43654-4_2

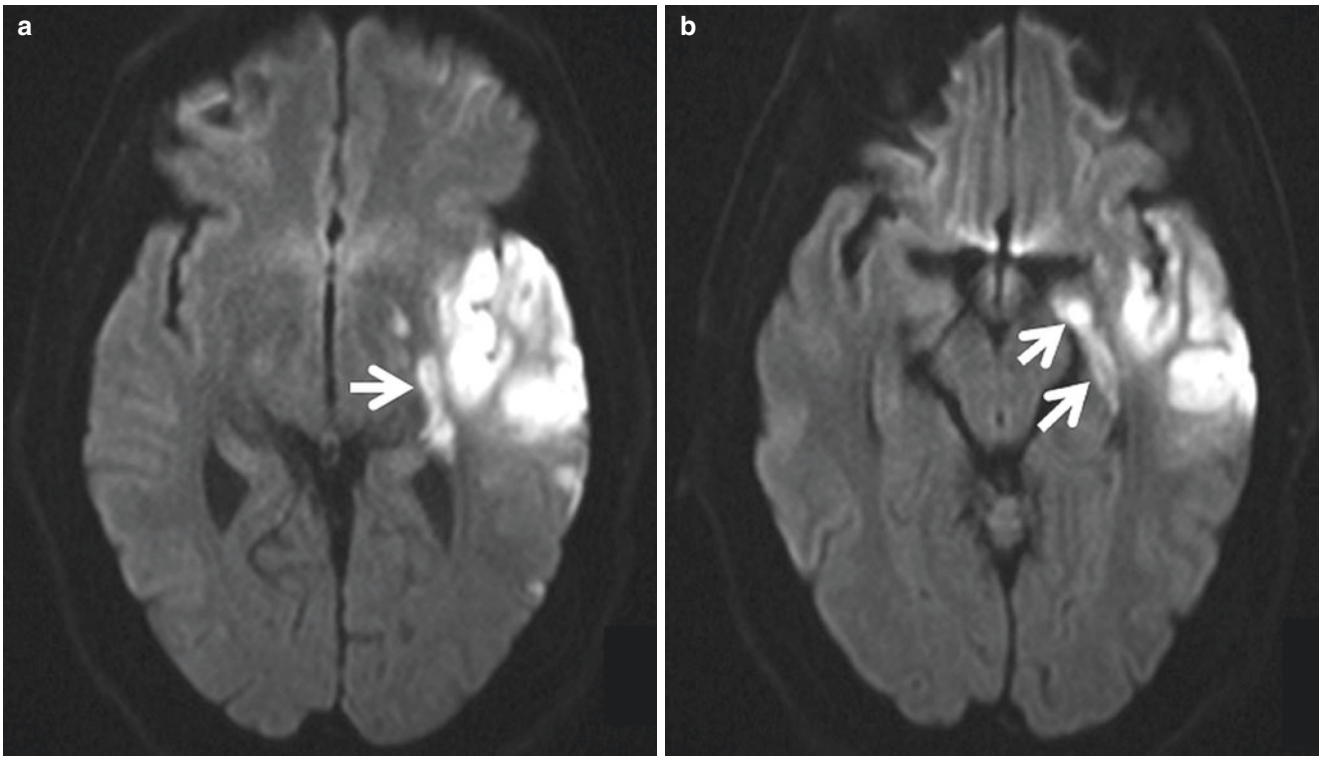

Fig. 2.1 Anterior choroidal artery infarction. Patient presents with acute left ICA occlusion. DWI images demonstrate acute infarction in the left MCA territory. In addition, there are infarctions involving the posterior limb of the internal capsule (*arrow*) (**a**), amygdala, and hippocampus (*arrow*) (**b**) in the territory of anterior choroidal artery

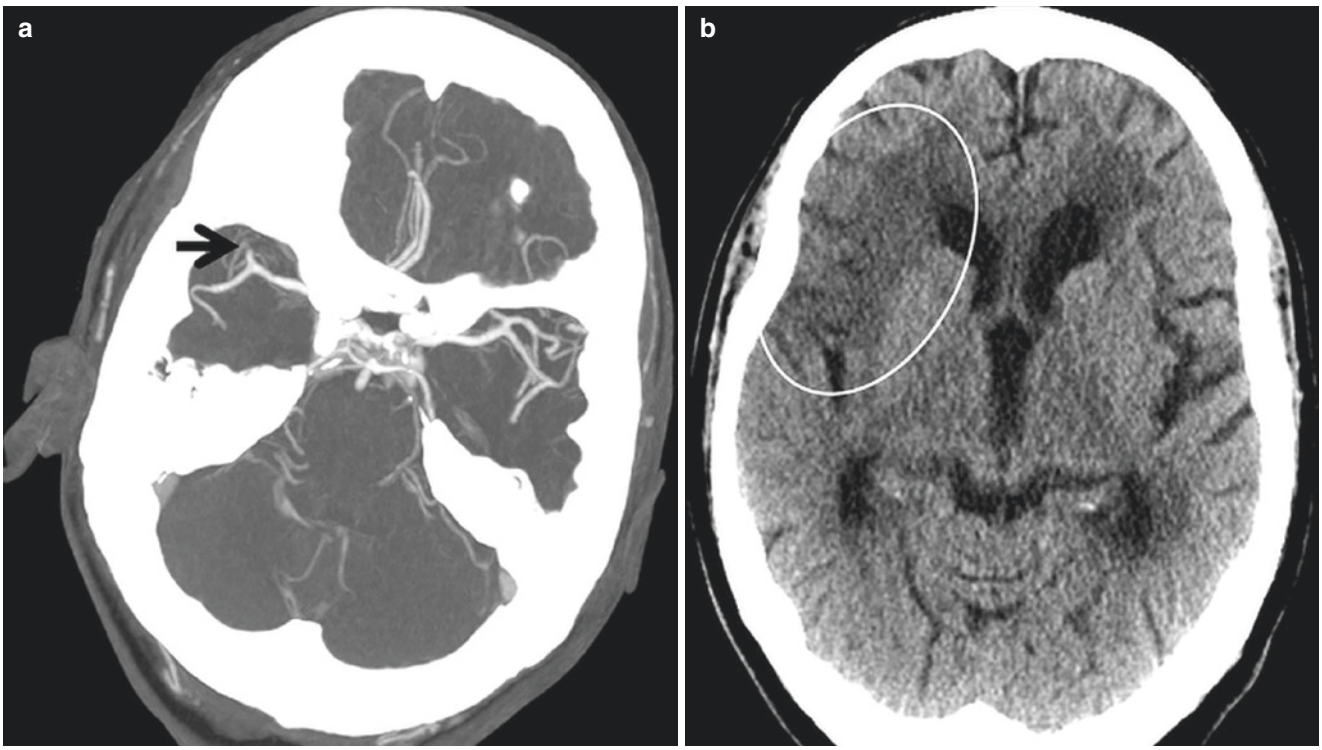

Fig. 2.2 MCA superior division infarction. Axial CTA MIP (**a**) shows occlusion of superior/anterior M2 division of the right MCA at the origin (*arrow*). (**b**), Subsequent NCCT demonstrates acute infarction in the right anterior insula and frontal operculum (*circle*)

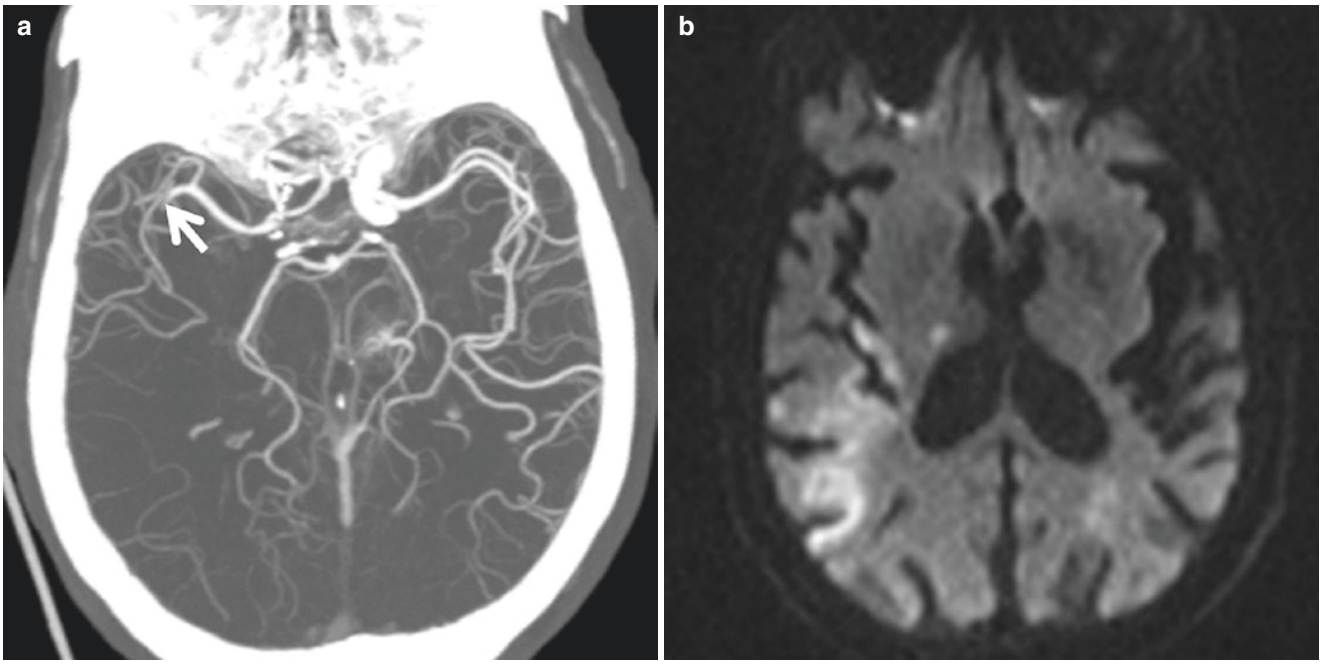

Fig. 2.3 MCA inferior division infarction. (**a**), Axial CTA MIP demonstrates occlusion of right MCA inferior/posterior division at the origin. (**b**), MRI DWI shows acute infarction in the posterior insula, inferior parietal, and posterior temporal region

operculofrontal, and central arteries arise from superior M2 division, while the remainder branches including the anterior and posterior parietal, angular, and temporal arteries arise from the inferior M2 division.

2.2.3 Anterior Cerebral Artery (ACA)

The ACA has three segments: horizontal (A1), vertical (A2), and callosal (A3) segments [1].

A1 (horizontal) segment extends from ICA terminus to the junction with anterior communicating artery (A-comm).

A2 (vertical) segment runs along the anterior interhemispheric fissure to the genu of the corpus callosum. It gives off orbitofrontal and frontopolar branches, supplying the basal frontal region and anterior medial part of the superior frontal gyrus.

The recurrent artery of Heubner (RAH) is the largest medial lenticulostriate branch that arises from the proximal A2 or less frequently the distal A1 segment. Occlusion of RAH results in characteristic infarction pattern involving the inferior part of caudate head, the inferior part of the anterior limb of the internal capsule, and adjacent part of the lentiform nucleus (Fig. 2.4) [3].

The A3 segment curves around the corpus callosum and further divides into the pericallosal and callosomarginal arteries. The pericallosal artery runs along the superior surface of the corpus callosum in the pericallosal cistern, while the callosomarginal artery courses above the cingulate gyrus within the cingulate sulcus. The distal branches supply the medial surface of the fontal and parietal lobes, a thin strip of lateral frontoparietal convexity adjacent to the interhemispheric fissure, and the majority of corpus callosum (Fig. 2.5). Occasionally, A2 segment of one ACA branches across the midline, while the contralateral A2 segment either is hypoplastic or terminates early in its course. This variant anatomy accounts for the scenario in which the occlusion of one A2 segment leads to infarctions of bilateral ACA territories (Fig. 2.6) [4].

2.3 Posterior Circulation

2.3.1 Vertebral Artery

Vertebral artery is divided into four (V1–V4) segments. The V4 segment is intradural and gives rise to the anterior and posterior spinal arteries, the medullary perforating branches, and the posterior inferior cerebellar artery (PICA). Occlusions of the anterior spinal artery results in characteristic infarction of the medullary pyramid leading to Dejerine syndrome (Fig. 2.7) [5]. The much more common PICA territory infarction involves the lateral medulla, cerebellar tonsil, and inferior cerebellar hemisphere and leads to lateral medullary or Wallenberg syndrome (Fig. 2.8).

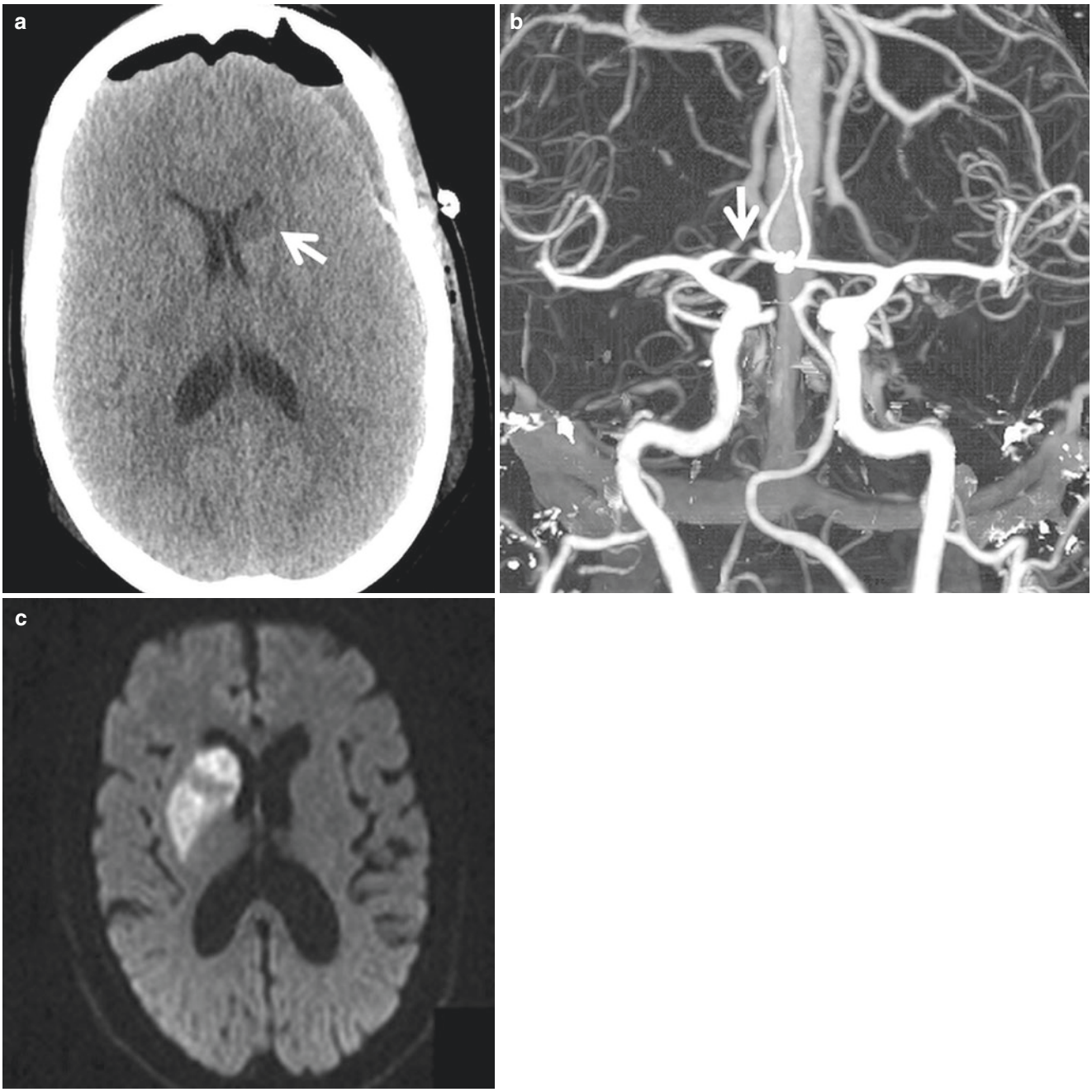

Fig. 2.4 Recurrent artery of Heubner infarction. (**a**), Patient after clipping a complex A-comm aneurysm. NCCT shows infarction in the anterior part of left caudate (*arrow*) presumably due to inadvertent occlusion of RAH. (**b**), A different patient with stroke. CTA coronal MIP shows severe stenosis versus near-occlusive thrombus in the right ACA A1 segment. (**c**), DWI shows acute infarction of the right caudate and putamen due to occlusion of RAH

2.3.2 Basilar Artery

The basilar artery is formed by two vertebral arteries near the pontomedullary junction. It courses within the prepontine cistern and terminates within the interpeduncular fossa into the posterior cerebral arteries (PCA) and superior cerebellar arteries (SCA).

"Top of the basilar syndrome" refers to thromboembolic occlusion of distal basilar artery and its terminal branches including PCAs and SCAs, leading to ischemic infarction of

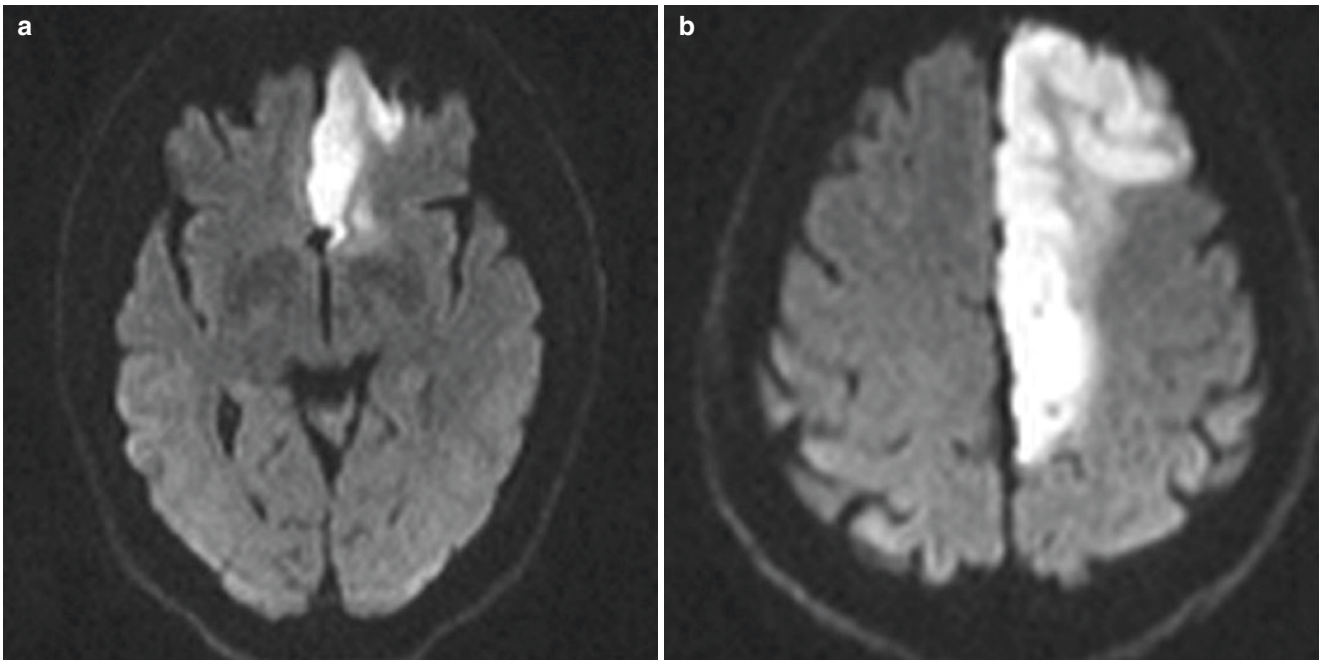

Fig. 2.5 ACA infarction. DWI shows acute infarction of the left ACA territory including anterior medial surface of the frontal lobe (**a**), extending from the frontal pole to the parieto-occipital sulcus (**b**)

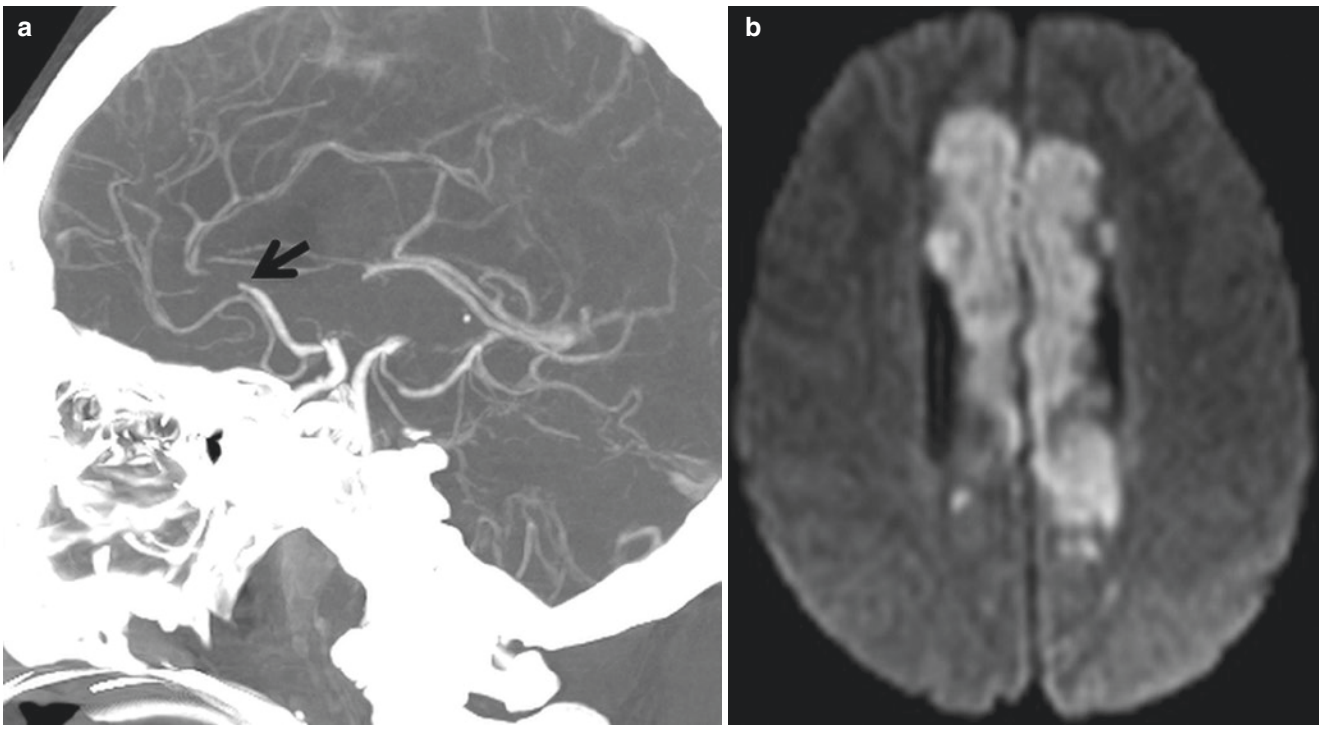

Fig. 2.6 Bihemispheric ACA infarction. (**a**), Sagittal CTA shows the occlusion of a dominant distal left ACA A2 segment (*arrow*). (**b**), DWI demonstrates infarction of bilateral ACA territories. Note the right ACA is diminutive and terminates as the callosomarginal branch. The infarction spares the orbitofrontal and frontopolar territories, which typically branch off more proximally from the A2 segment

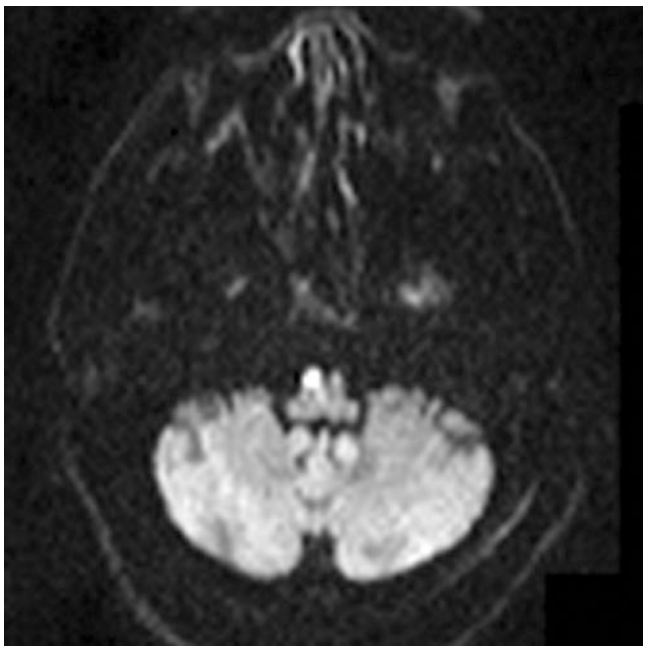

Fig. 2.7 Medial medullary infarction. DWI shows acute infarction of right medullary pyramid in a patient with right vertebral dissection. The infarction is presumably due to occlusion of the anterior spinal artery, which arises from the distal V4 segment

thalami, rostral midbrain, occipital lobes, and superior cerebellum (Fig. 2.9) [6]. Without prompt mechanical thrombectomy, it frequently results in devastating outcome including lock-in syndrome and death. Clinically, it can be challenging to make the diagnosis since patients frequently present with acute visual, oculomotor, and behavioral symptoms, while motor symptoms may not be obvious.

Paramedian perforating arteries arise from the dorsal surface of the basilar artery and supply the pons. Occlusion of these perforators leads to paramedian pontine infarction of basis pontis without or with involvement of tegmen (Fig. 2.10) [7].

2.3.3 Anterior Inferior Cerebellar Artery (AICA) and Superior Cerebellar Artery (SCA)

AICA arises from the proximal or midportion of basilar artery. It supplies a strip of the cerebellar hemisphere behind the petrous temporal bone and cranial nerves VII and VIII through the labyrinthine artery.

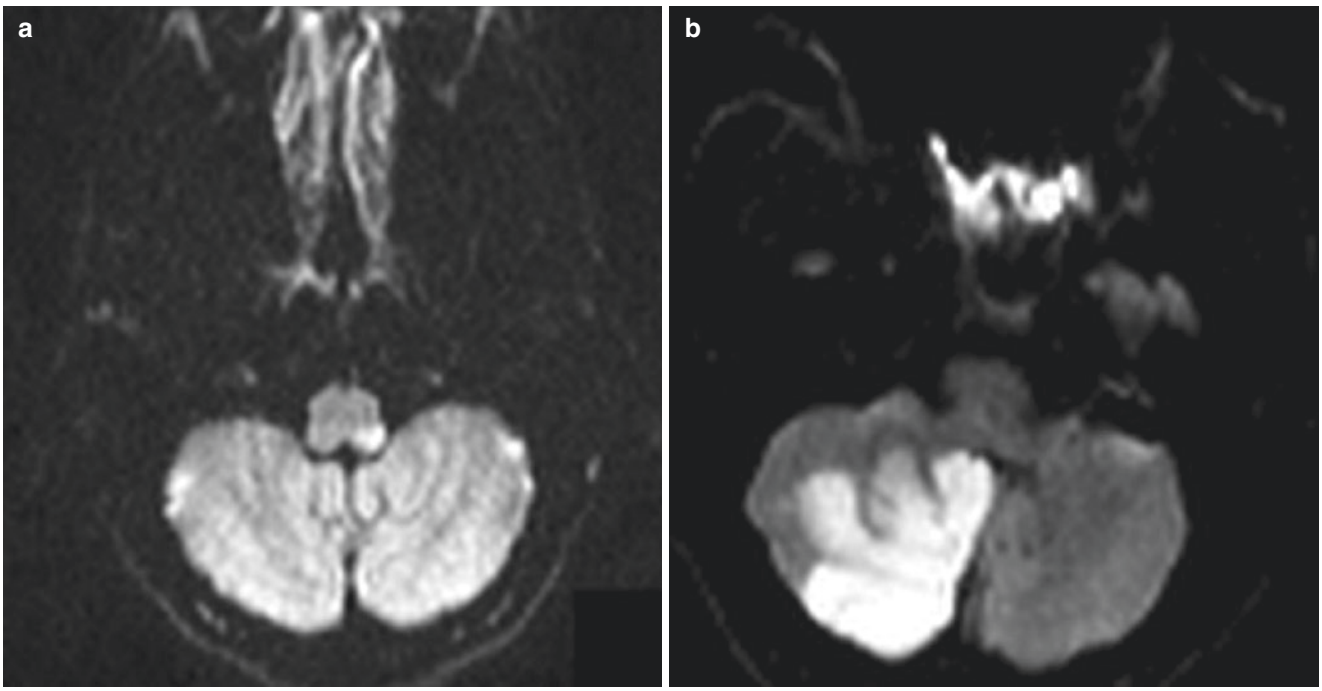

Fig. 2.8 Lateral medullary/PICA infarction. (**a**), DWI shows acute infarction of left lateral medullary pyramid. (**b**), In a different patient, DWI shows a large infarction of the right inferior cerebellar hemisphere and vermis. Both patients have vertebral occlusion on MRA

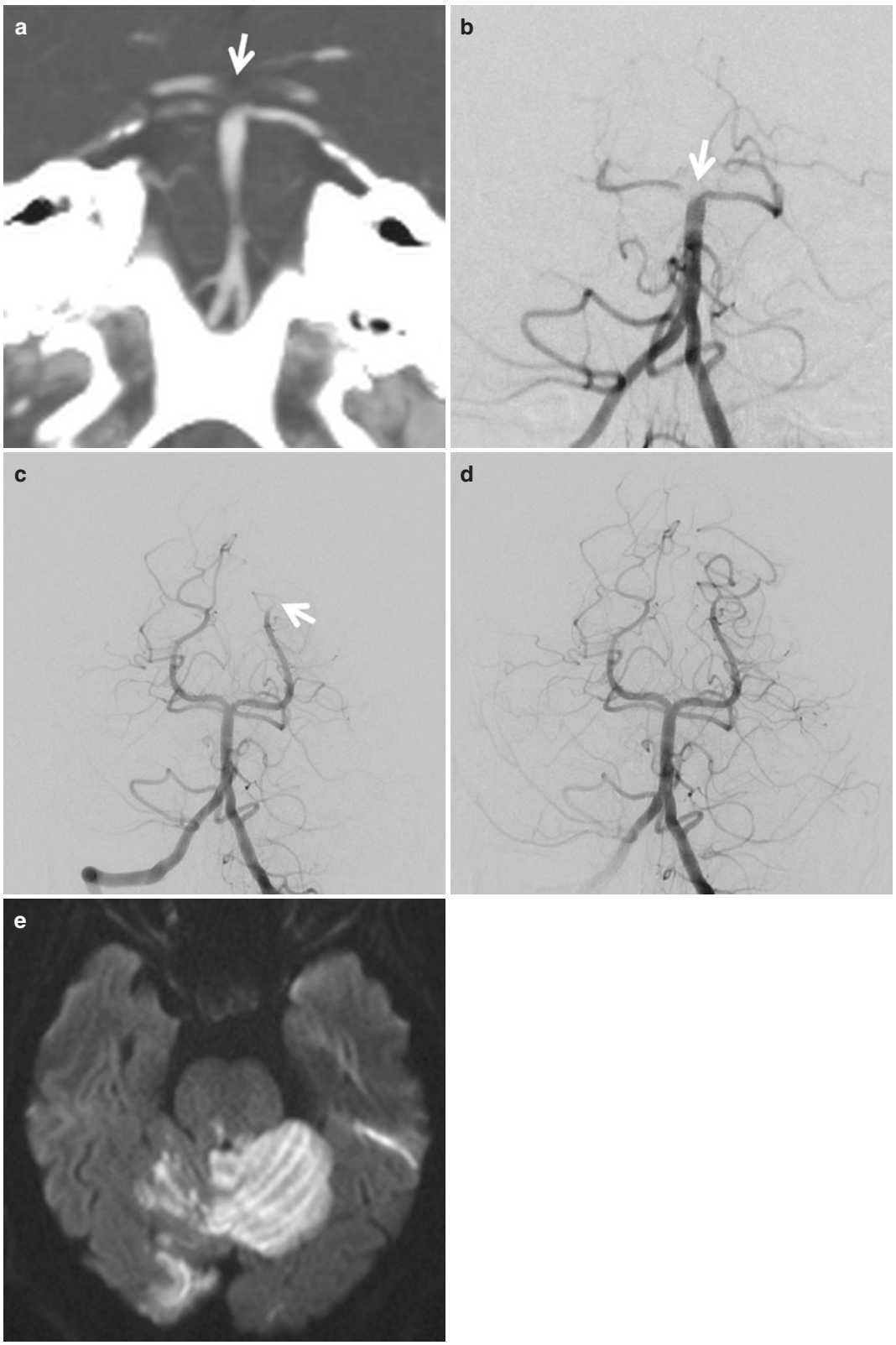

Fig. 2.9 Basilar tip thrombosis. (**a**), Coronal CTA MIP demonstrates a thrombus at the tip of basilar artery extending to the origins of bilateral PCAs and right SCA (*arrow*). (**b**), Catheter angiography confirms the basilar tip thrombosis (*arrow*) involving bilateral PCA origins and occlusion of the bilateral SCAs. (**c**), Mechanical thrombectomy is performed, and post-thrombectomy angiogram demonstrates resolution of basilar thrombosis and patent bilateral SCAs and right PCA. There is a thrombus in the left PCA P3 segment causing persistent occlusion of distal branches (*arrow*). (**d**), Angiogram after thrombectomy of distal left PCA demonstrates patency of calcarine and parieto-occipital branches. (**e**), Despite prompt thrombectomy, MRI 24 hours later demonstrates acute infarctions in the superior cerebellum and occipital lobe in the territory of distal basilar artery

SCA arises from the distal basilar artery and supplies the superior cerebellar hemisphere, superior vermis, and dentate nuclei (Fig. 2.11).

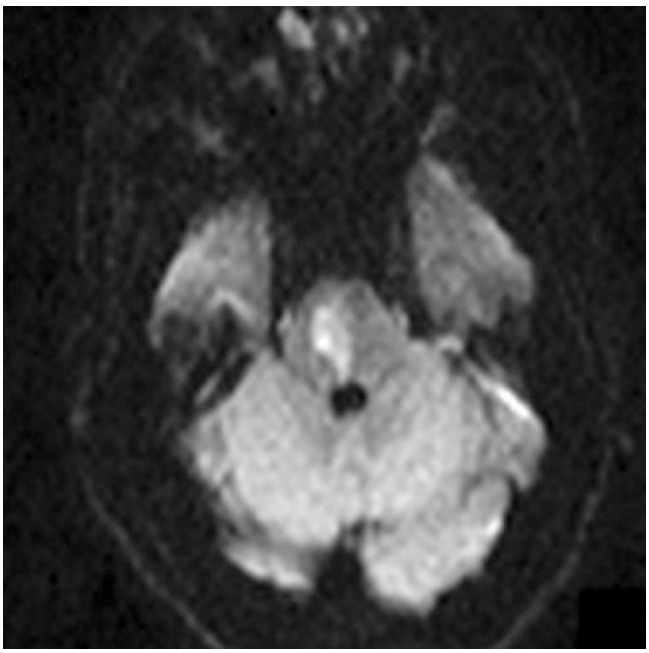

Fig. 2.10 Paramedian pontine infarction. DWI shows acute infarction of right pons in the basis pontis extending to the tegmentum and floor of fourth ventricle. The infarction does not cross the midline and lateral pons is spared, presumably due to occlusion of the paramedian pontine perforating artery

2.3.4 Posterior Cerebral Artery (PCA)

PCA can be divided into four segments. The P1 segment extends from the basilar tip to the junction with the P-comm. The P2 segment curves around midbrain in the ambient cistern. The P3 is a short segment along the surface of quadrigeminal plate. The P4 segment divides into terminal branches including parieto-occipital artery, calcarine artery, and splenial artery [1].

A number of perforating branches arise from P1 or proximal P2 segment including posterior thalamoperforating arteries, thalamogeniculate arteries, and peduncular perforating arteries and supply the thalami, subthalamic nuclei, and midbrain. The anterior thalamoperforating artery (tuberothalamic artery) arises from the P-comm.

The medial and lateral posterior choroidal arteries most frequently arise from the P2 segment, course into the lateral ventricle and choroid plexus, and anastomose with the anterior choroidal artery.

The temporal cortical branches from P2 segment supply the inferior surface of temporal lobe, hippocampus, and part of the inferior surface of the occipital lobe.

The terminal branches from P4 segment supply the nearly entire occipital lobe and medial inferior parietal lobes. It also supplies posterior one-fifth of the corpus callosum and anastomoses with the distal branch of ACA pericallosal artery.

Proximal PCA occlusion results in infarcts in the thalamus and/or midbrain as well as in the cortex, while distal PCA occlusion involves only cortical structures (Fig. 2.12).

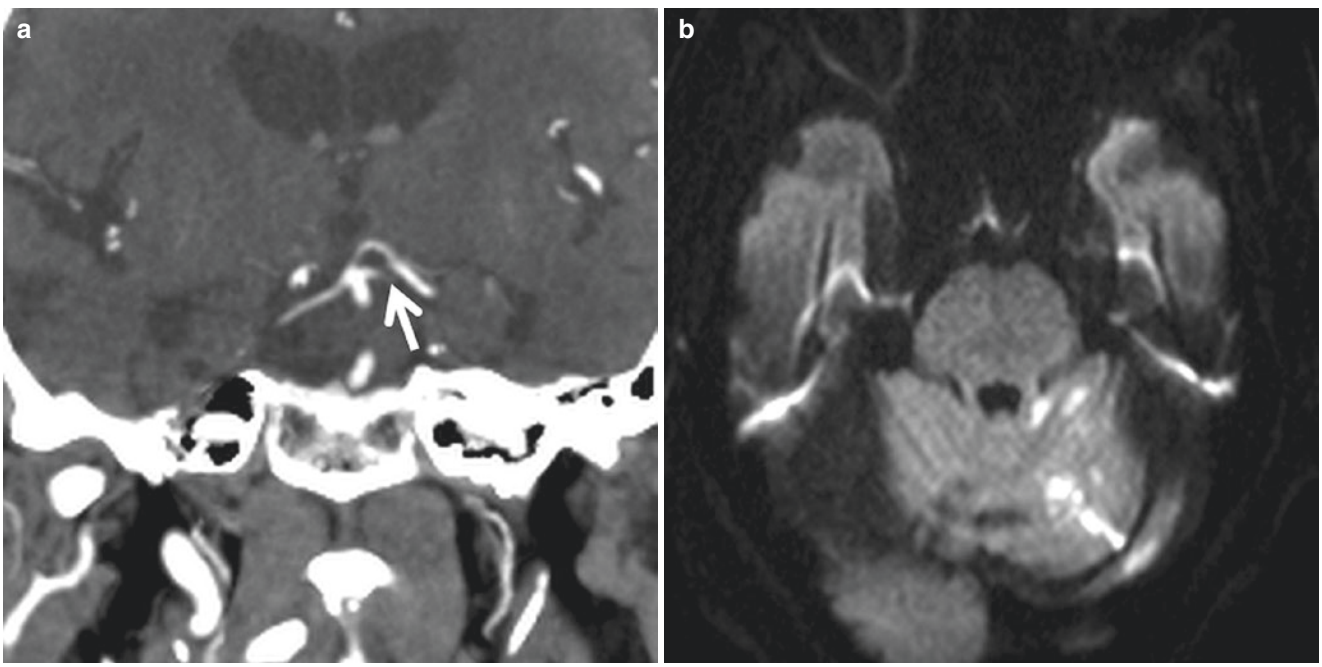

Fig. 2.11 Superior cerebellar artery infarction. (**a**), Coronal CTA MIP demonstrates occlusion of the left SCA at the origin (*arrow*). (**b**), DWI shows acute infarction in the left superior cerebellum

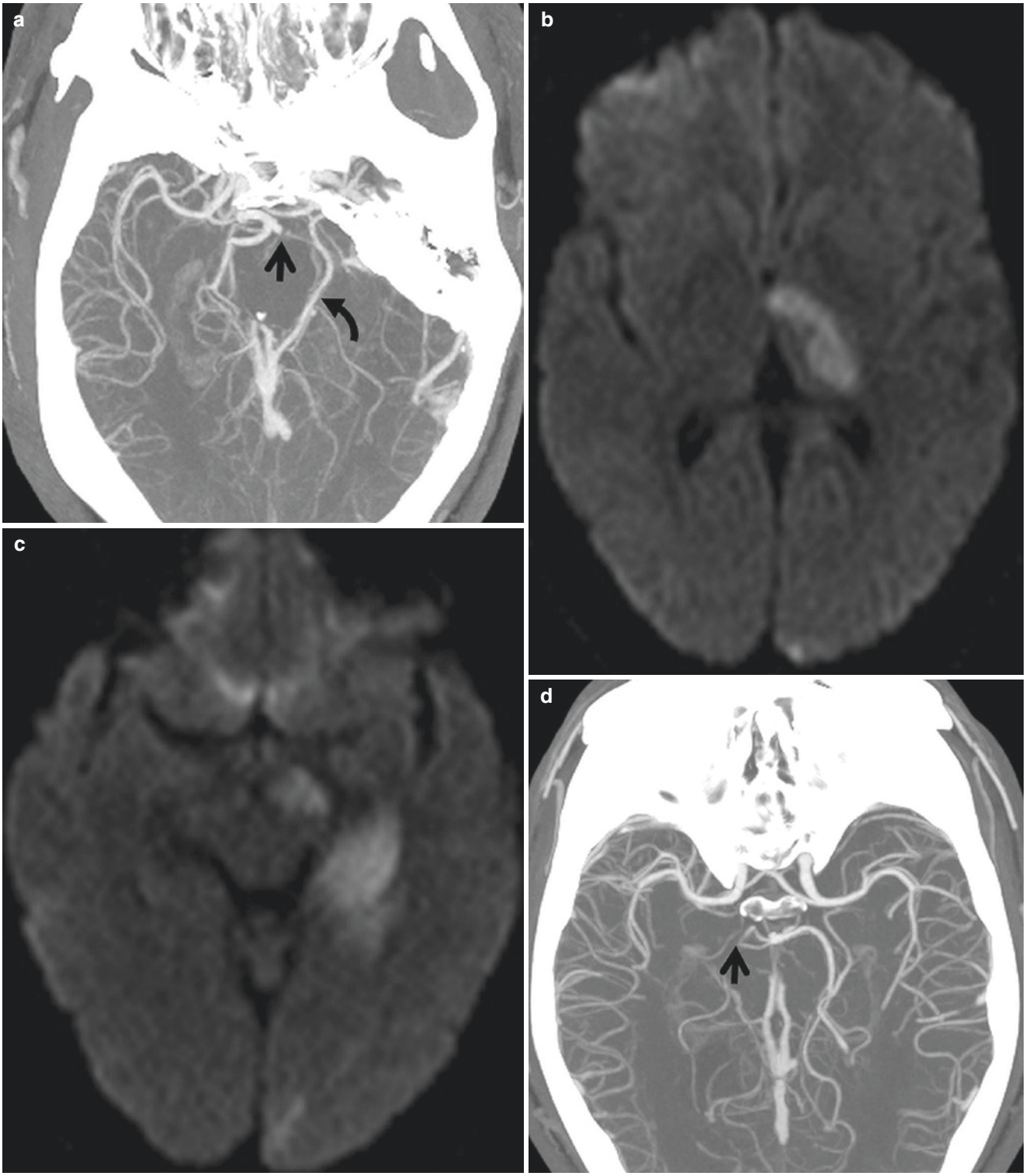

Fig. 2.12 PCA infarction. (**a**), Axial CTA MIP shows occlusion of left PCA P1 segment at the origin (*arrow*). Note the basal vein of Rosenthal (*curved arrow*), which can be mistaken for a patent PCA. (**b** and **c**), DWI images show acute infarctions in the left thalamus (**b**) and midbrain (**c**) supplied by the thalamoperforators. Additional infarctions in the medial left temporal lobe and occipital lobe. (**d**), Another patient with right PCA P2 segment occlusion on axial CTA (*arrow*). (**e**), DWI demonstrates acute infarction of the right temporal lobe supplied by temporal branches and occipital lobe supplied by calcarine and parieto-occipital arteries

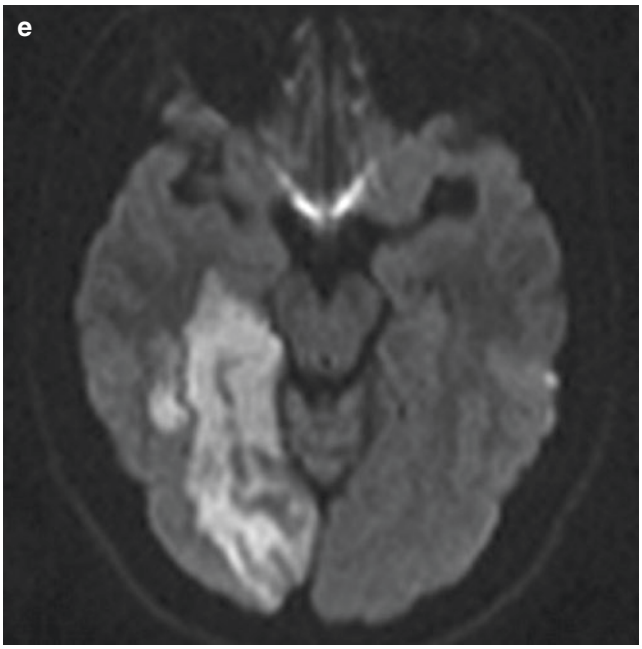

Fig. 2.12 (continued)

Artery of Percheron is a rare albeit important anatomic variant, in which a single thalamoperforator arises from P1 segment supplying the bilateral paramedian thalamic–mesencephalic junctions. Occlusion of this artery results in bilateral paramedian thalamic infarctions, with or without anterior thalamic or rostral midbrain involvement. V-shaped hyperintense signal abnormality on axial FLAIR images along the pial surface of the midbrain in the interpeduncular fossa can be seen in some patients (Fig. 2.13) [8].

2.4 Border Zone Infarction

Border zone or watershed infarctions occur at the junction between two neighboring arterial territories. Two types of border zone have been recognized including external (cortical) and internal (subcortical).

External border zone is located at the frontoparietal region between ACA and MCA territories (anterior border zone) or parieto-occipital region between MCA and PCA territories (posterior border zone). External border zone infarcts are frequently embolic in nature and may not be associated with

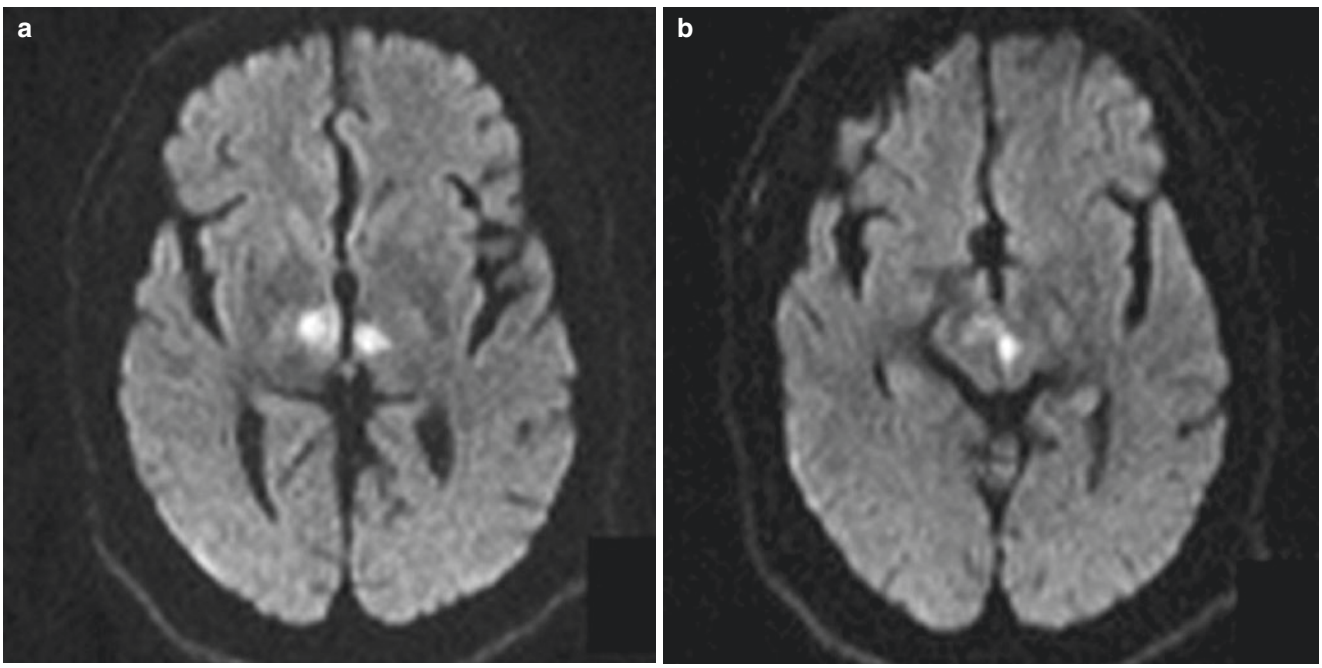

Fig. 2.13 Artery of Percheron infarction. DWI images show acute infarction of bilateral median thalami (**a**) and rostral midbrain (**b**) in the territory of artery of Percheron

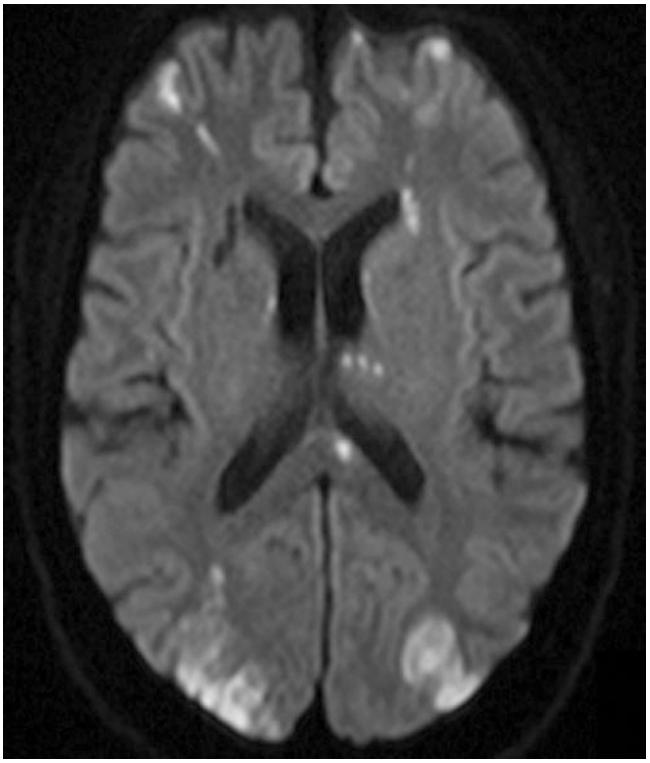

Fig. 2.14 External cortical borderzone infarction. DWI shows acute infarctions in the bilateral frontal lobes at the ACA/MCA borderzone and bilateral parieto-occipital lobes at the MCA/PCA borderzone. MRA of the head and neck demonstrates no large vessel occlusion or stenosis (not shown). These are likely due to embolic phenomenon, which are further supported by the small infarctions in the basal ganglia, thalamus, and splenium of corpus callosum

cerebral hypoperfusion. This is supported by the fact that many of these patients have concomitant smaller cortical embolic infarcts (Fig. 2.14).

On the other hand, internal border zone is located at the junctional territory between the major pial arteries (MCA, ACA, or PCA) and lenticulostriate/perforating arteries. Subcortical areas at the junction supplied by the MCA medullary perforators and the end branches of lenticulostriate arteries are the most involved. These infarctions are typically arranged in linear fashion in the centrum semiovale or corona radiata parallel to the lateral ventricular margin (Fig. 2.15). In comparison to external border zone infarcts, internal border zone infarcts are associated with arterial occlusion/stenosis and/or systemic hypoperfusion and frequently predictive of impending larger infarctions [9].

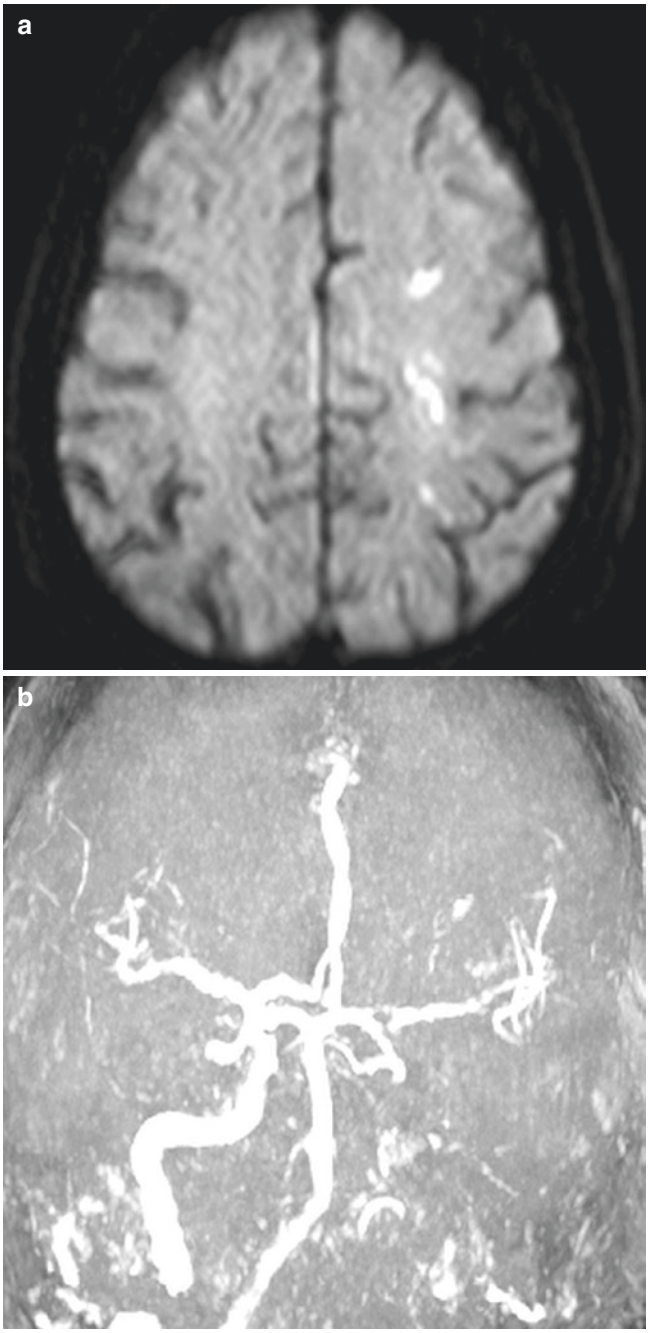

Fig. 2.15 Internal subcortical border zone infarction. (**a**), DWI shows a string of small infarctions in the centrum semiovale in the internal border zone of lenticulostriate and deep perforating medullary artery of left MCA. (**b**), MRA MIP image shows occlusion of the left ICA

References

1. Osborn AG. Diagnostic cerebral angiography. 2nd ed. Philadelphia: Lippincott Williams and Wilkins; 2001.
2. Helgason C, Caplan LR, Goodwin J, Hedges T. Anterior choroidal artery-territory infarction: report of cases and review. Arch Neurol. 1986;43:681–6.
3. Loukas M, Louis RG, Childs RS. Anatomical examination of the recurrent artery of Heubner. Clin Anat. 2005;19:25–31.
4. Kumar K, Strbian D, Sundararajan S. Acute cerebral infarction presenting with weakness in both legs and one arm. Stroke. 2015;46:e134–6.
5. Bassetti C, Bogousslavsky J, Mattle H, Bernasconi A. Medial medullary stroke: report of seven patients and review of the literature. Neurology. 1997;48:882–90.
6. Sato M, Tanaka S, Kohama A. "Top of the basilar" syndrome: clinico-radiological evaluation. Neuroradiology. 1987;29:354–9.
7. Kataoka S, Hori A, Shirakawa T, Hirose G. Paramedian pontine infarction: neurological/topographical correlation. Stroke. 1997;28:809–15.
8. Lazzaro NA, Wright B, Castillo M, Fischbein NJ, Glastonbury CM, Hildenbrand PG, Wiggins RH, Quigley EP, Osborn AG. Artery of percheron infarction: imaging patterns and clinical spectrum. Am J Neuroradiol. 2010;31:1283–9.
9. Mangla R, Kolar B, Almast J, Ekholm SE. Border zone infarcts: pathophysiologic and imaging characteristics. Radiographics. 2011;31:1201–14.

Imaging of Stroke Mimics

3

Yang Tang and Xinli Du

3.1 Introduction

Stroke is a clinical diagnosis; however the diagnosis is not always straightforward as there are many nonvascular disorders, so-called stroke mimics, that can present with acute neurological deficits and resemble ischemic syndromes. Although the frequency is variable, it is estimated that up to 25% of stroke alerts initiated in the emergency department are due to stroke mimics [1, 2]. Some of these conditions such as conversion disorder can be diagnosed by careful history taking and physical exams and confirmed by negative neuroimaging. However, many other conditions can have imaging findings that imitate acute ischemia, especially with diffusion restriction on the brain MRI. Common stroke mimics include seizure, migraine, tumor, CNS infection/inflammation, metabolic/toxic encephalopathy, etc. [3, 4]. It is critical to carefully analyze the imaging pattern and correlate with clinical history and other diagnostic tests to reach the correct diagnosis.

3.2 Seizure

Seizure or postictal Todd paralysis is one of the most common stroke mimics, both clinically and on imaging. Seizure can cause diffusion restriction, edema, and leptomeningeal enhancement on brain MRI (Fig. 3.1) [5]. It can also be associated with variable abnormalities on CT or MR perfusion [6], depending on ictal versus postictal stage. The ictal stage is often associated with hyperperfusion in the affected brain region, with decreased time to drain (TTD)/mean transit time and increased cerebral blood flow (CBF) or cerebral blood volume (CBV) (Fig. 3.2). In postictal phase, there is often a hypoperfusion pattern that resembles ischemic stroke (Fig. 3.3). Seizure-related changes commonly occur in the cortex, hippocampus, splenium of corpus callosum, etc., usually transient, and in a nonvascular distribution. These features help distinguish it from acute ischemia.

3.3 Migraine

A subset of migraine patients can present with acute neurologic symptoms (i.e., aura). Migraines with predominant motor symptoms are referred to as hemiplegic migraine, which can be difficult to differentiate from arterial ischemic stroke or TIA on the initial presentation. Initial cerebral hypoperfusion can be detected in the affected hemisphere in migraine patients with aura presumably due to vasoconstriction, followed by a rebound hyperperfusion [7]. Asymmetric prominence of cortical veins can be seen on susceptibility-weighted imaging due to hypoperfusion and susceptibility of deoxygenated blood (Fig. 3.4). MRA may show vasoconstriction of distal arterial branches. In contrary to ischemic stroke, migraine attack is not associated with DWI changes. Signal changes on MRI are reversible and not limited to a single vascular territory.

3.4 Tumor

Patients with brain tumor may present with acute neurological deficits and occasionally be confused with ischemic strokes on imaging [8], especially when there is diffusion restriction due to high tumor cellularity or when the area of tumor involvement is in a vascular distribution (Fig. 3.5). On the other hand, subacute ischemia can mimic tumors when there is vasogenic edema and enhancement (Fig. 3.6). Advanced techniques such as CT/MR perfusion or MR spectroscopy can be helpful for making the distinction. In cases of diagnostic uncertainty, short-term MRI follow-up would be beneficial to monitor the evolution of the signal changes.

3.5 Infection and Inflammation

Infectious or autoimmune encephalitis and cerebritis can mimic stroke on imaging. Herpes encephalitis is the most common viral encephalitis that present with acute

© Springer Nature Switzerland AG 2020

Y. Tang, *Atlas of Emergency Neurovascular Imaging*, https://doi.org/10.1007/978-3-030-43654-4_3

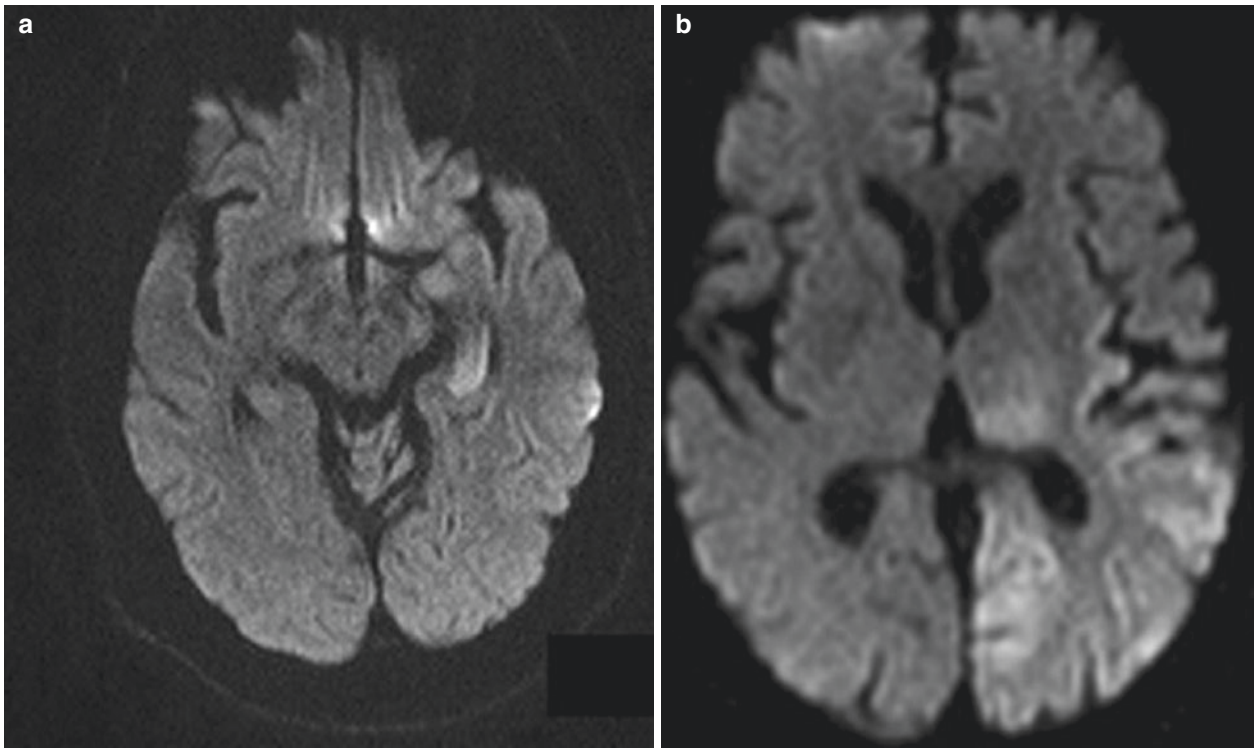

Fig. 3.1 Seizure-related MRI diffusion abnormality. (**a**), Patient with postictal Todd paralysis. DWI shows diffusion restriction in the left hippocampus. (**b**), A different patient presents with stroke alert. Axial DWI shows diffusion restriction in the left temporo-occipital lobes, insula, and thalamus, which does not conform into an arterial distribution and is compatible with seizure-related changes. Patient is later diagnosed with non-convulsive status epilepticus

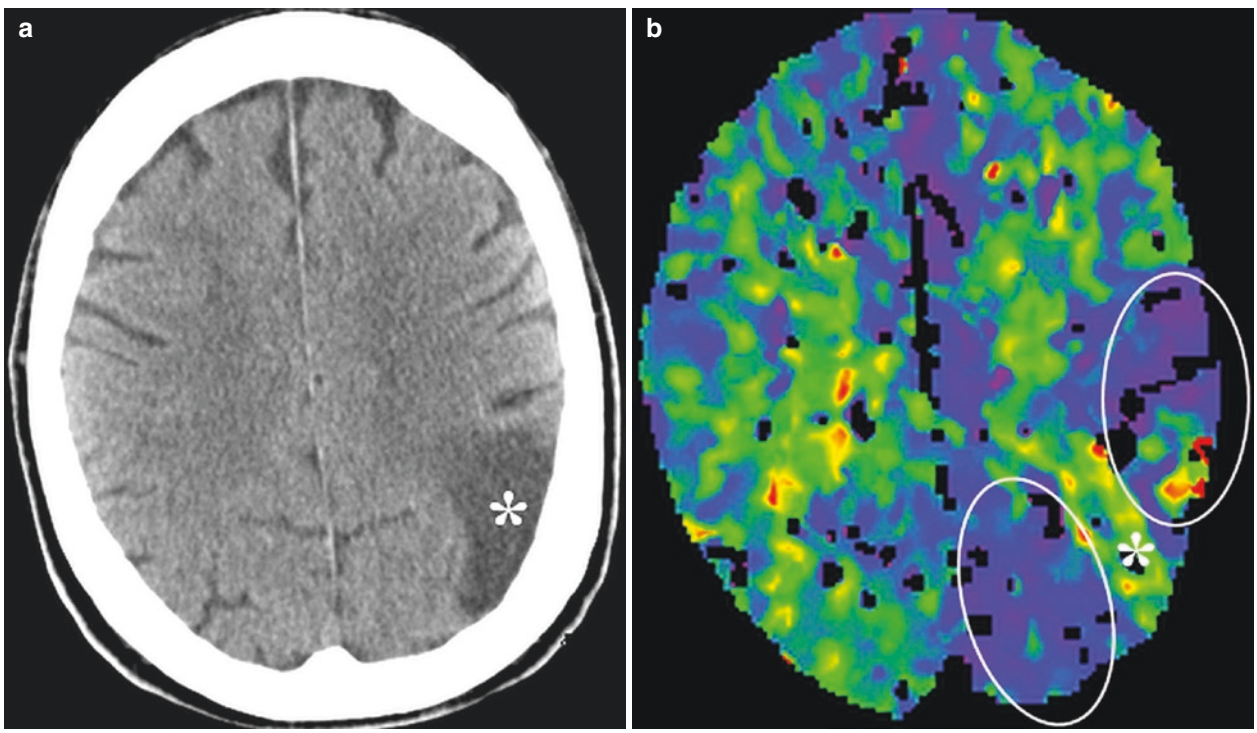

Fig. 3.2 Seizure-related hyperperfusion (ictal phase). Patient presents with right-sided weakness after a witnessed seizure. (**a**), NCCT shows encephalomalacia in the left parietal lobe (∗) and no other acute findings. (**b** and **c**), CT perfusion images with time to drain (TTD) (**b**) and cerebral blood flow (CBF) (**c**) maps. Note the area of encephalomalacia with prolonged TTD and decreased CBF (∗). However, the adjacent left frontal and parietal lobes (*circles*) show hyperperfusion with decreased TTD (**b**) and increased CBF (**c**), reflecting ongoing seizure activity due to the gliosis

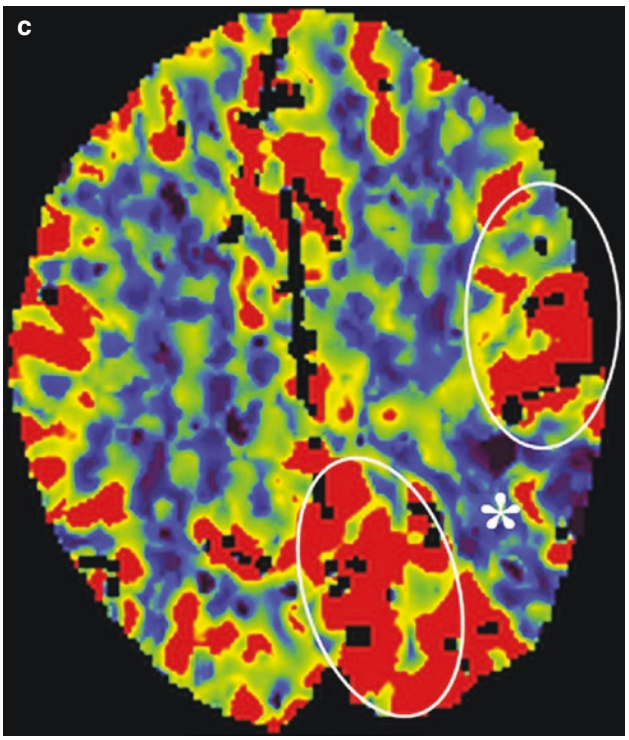

Fig. 3.2 (continued)

neurological symptoms such as hemiparesis, dysphasia, seizure, or altered level of consciousness. It typically causes asymmetric involvement of the limbic system including mesial temporal and inferior frontal lobes and insular and cingulate cortices. MRI may demonstrate edema with T2/FLAIR hyperintensity, patchy areas of diffusion restriction, hemorrhage, as well as cortical and/or leptomeningeal enhancement [9]. The involvement of temporal lobe can simulate MCA stroke on CT. MRI is critical for making the diagnosis; however early HSV encephalitis may be unilateral and mimic subacute MCA infarction (Fig. 3.7). The key is to recognize the involvement of the limbic system, which does not entirely conform to the MCA territory.

3.6 MELAS (Mitochondrial Myopathy, Encephalopathy with Lactic Acidosis, and Stroke-Like Episodes)

MELAS is a rare inherited metabolic disorder due to mitochondrial defect in the respiratory chain and oxidative phosphorylation, typically affecting young patients. It frequently

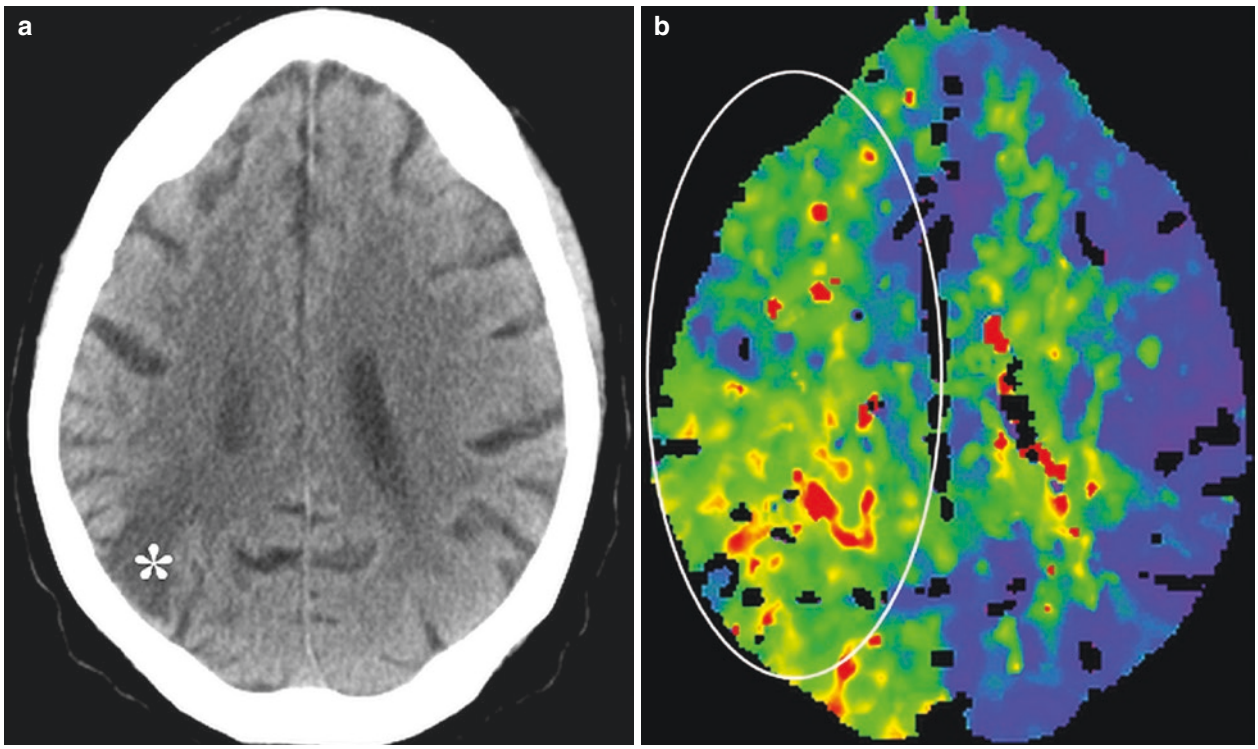

Fig. 3.3 Seizure-related hypoperfusion (postictal phase). Patient presents with left-sided weakness after a convulsion. (**a**), NCCT demonstrates focal right parietal encephalomalacia (∗). (**b** and **c**), CT perfusion images demonstrate hypoperfusion of nearly the entire right hemisphere (*circle*) with prolonged TTD (**b**) and decreased CBF (**c**) in a nonvascular distribution, consistent with postictal changes rather than ischemia. No vascular occlusion is seen on the CTA

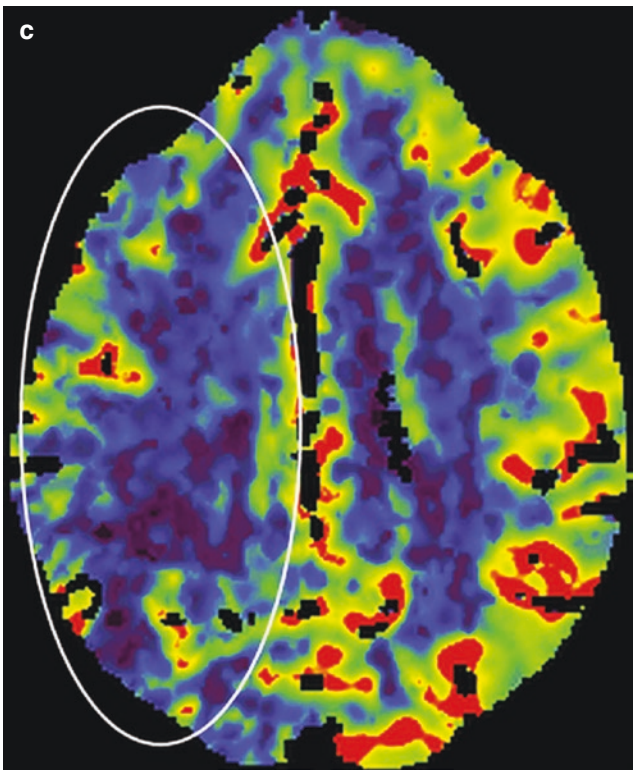

Fig. 3.3 (continued)

presents with stroke-like episodes that could confound the diagnosis with ischemic infarction, although the symptoms of MELAS are usually less intense and with more gradual onset. Imaging may reveal CT hypodensities or MRI DWI and T2 hyperintense lesions in the cerebral cortex with sparing of underlying white matter [10]. These lesions are not limited to a particular arterial territory and have a tendency to migrate over time, thus allowing differentiation from ischemic strokes (Fig. 3.8). MR spectroscopy demonstrates decrease in N-acetylaspartate and increase in lactate peak although these changes are not entirely specific and could also be found in other metabolic disorders.

3.7 Creutzfeldt–Jakob Disease (CJD)

CJD is a rare transmissible neurodegenerative disease caused by prion. The vast majority of CJD cases are sporadic, while the remainders belong to genetic, iatrogenic, or variant subtypes. Clinical features include rapidly progressive dementia, ataxia, myoclonus, visual disturbance, cerebellar dysfunction, pyramidal, or extrapyramidal features, akinetic mutism, etc. The most distinctive EEG pattern is characterized by periodic sharp waves. CSF markers include 14-3-3 and tau proteins. Brain MRI typically shows focal or diffuse

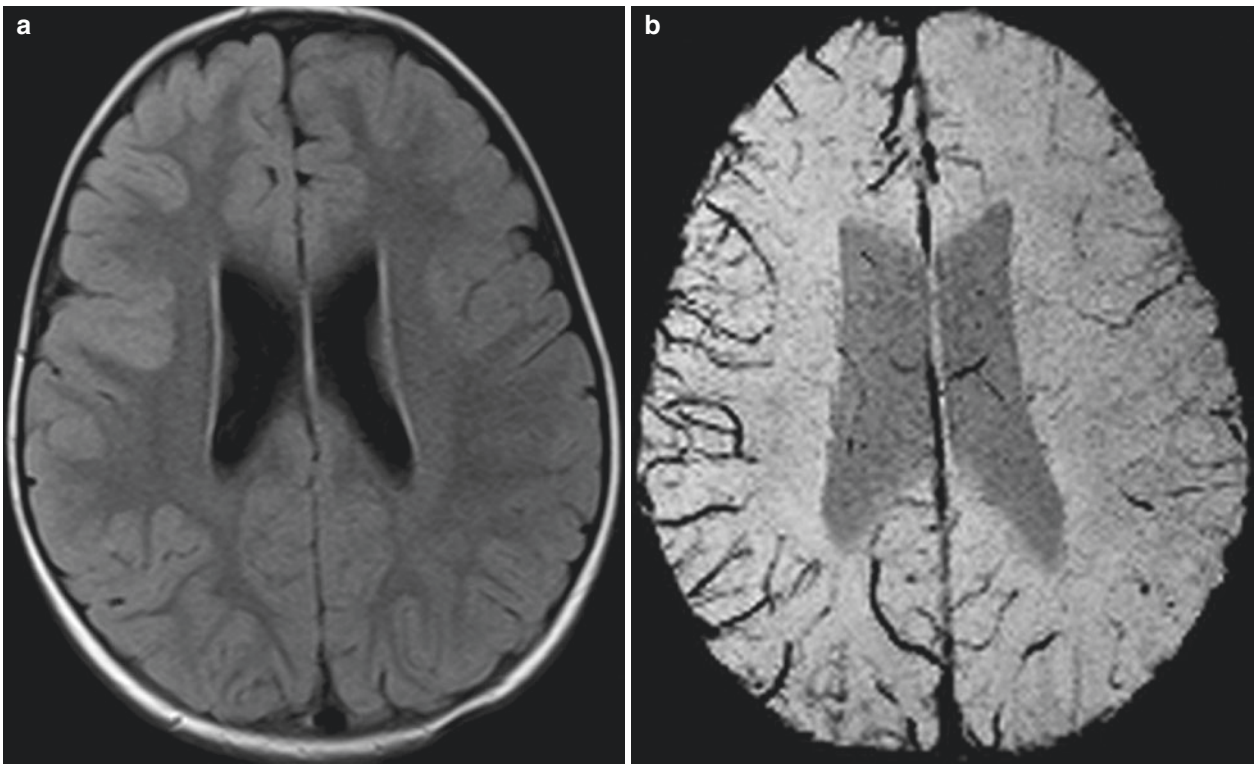

Fig. 3.4 MRI signal changes of hemiplegic migraine. 8-year-old with headache and transient left-sided hemiparesis. (**a**), Axial FLAIR shows cortical swelling of the right hemisphere. (**b**), SWI demonstrates prominence of cortical veins in the right hemisphere reflecting the presence of deoxyhemoglobin. MR perfusion demonstrates hypoperfusion of the right hemisphere associated with prolonged time to drain (**c**) and decreased CBF (**d**). No diffusion restriction is seen (not shown). MRA demonstrates no arterial occlusion or significant stenosis. Above findings resolved on the follow-up study a few months later

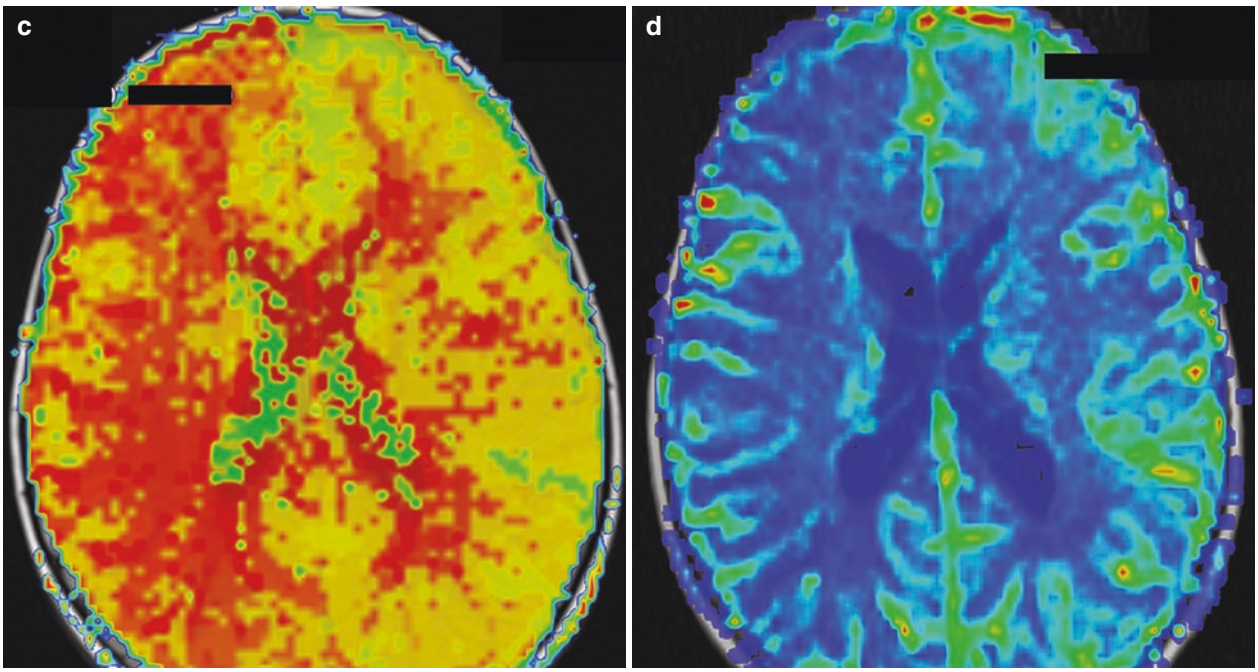

Fig. 3.4 (continued)

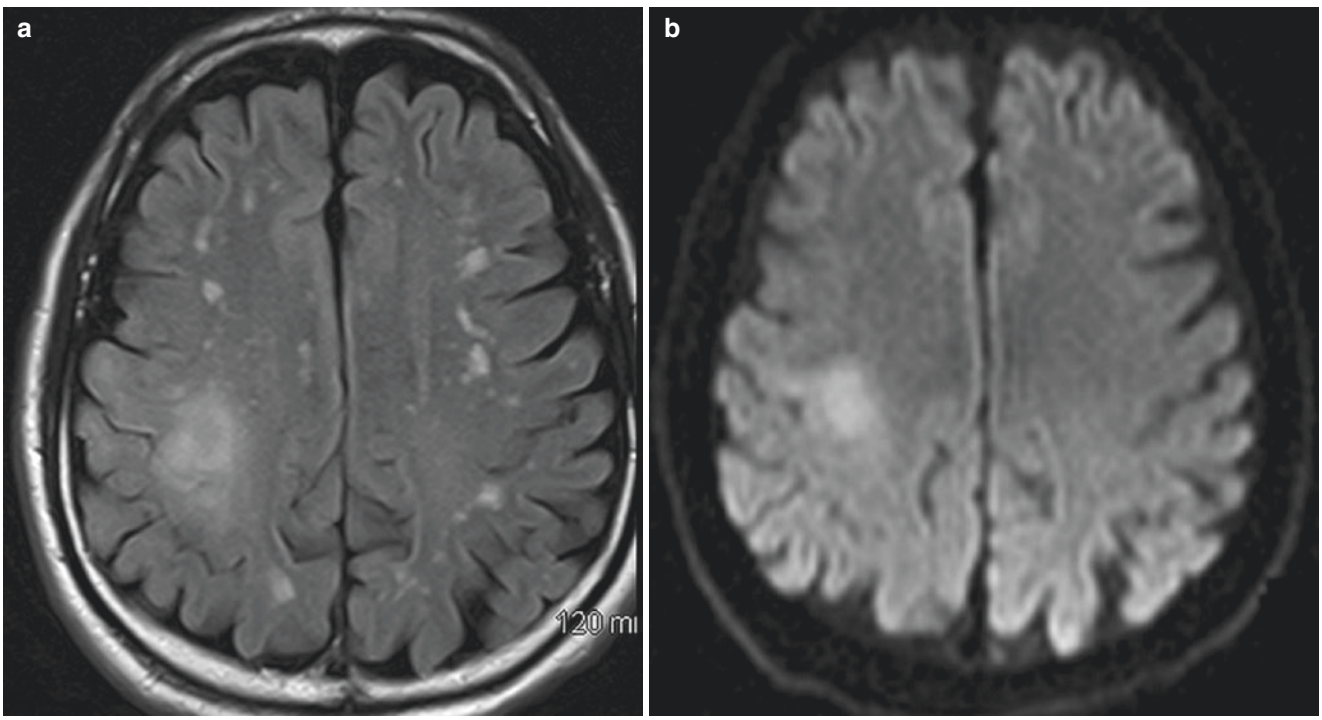

Fig. 3.5 Tumor mimicking infarction. 55-year-old with left-sided weakness. NCCT is normal (not shown). MRI brain shows FLAIR hyperintensity (**a**) and diffusion restriction (**b**) in the right peri-rolandic region, initially suspicious for acute or subacute stroke. No enhancement is seen. CTA demonstrates no large vessel occlusion or stenosis. CT perfusion shows shortened mean transit time (**c**) and increased CBF (**d**) in this region suggestive of hyperperfusion. Follow-up MRI in 1 month shows progression of the signal abnormality, proven to be high-grade glioma by biopsy

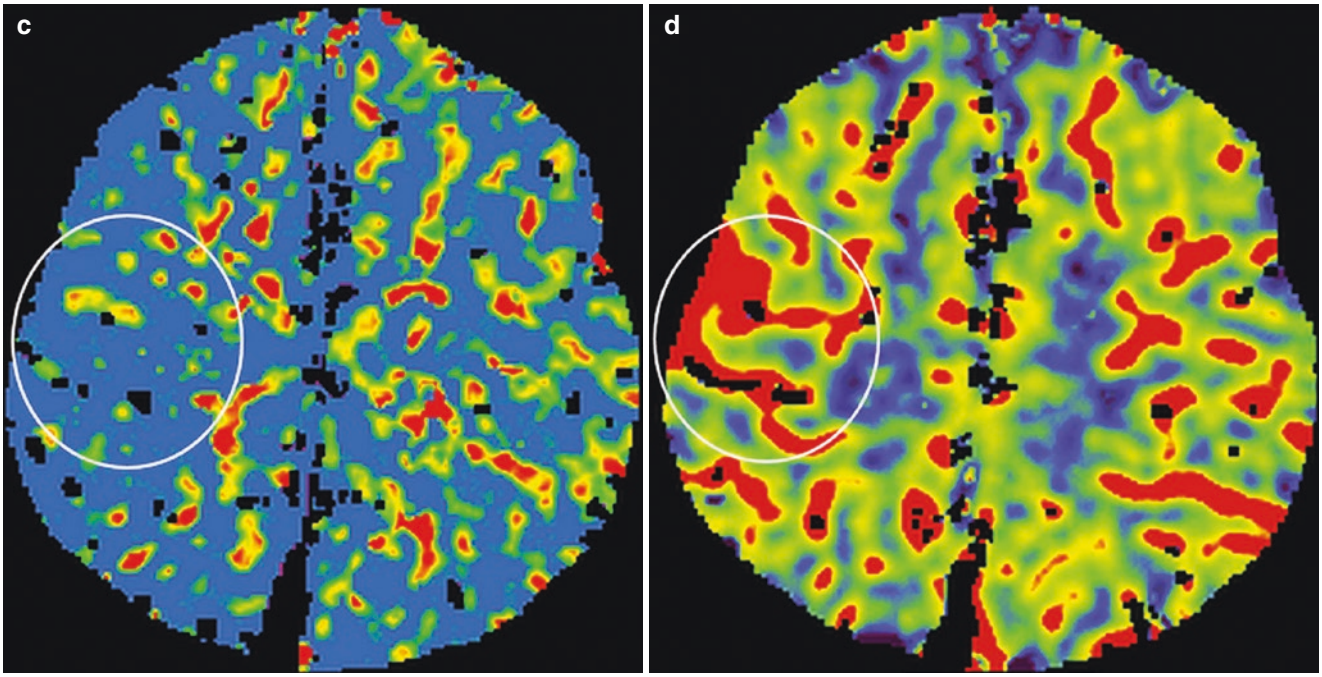

Fig. 3.5 (continued)

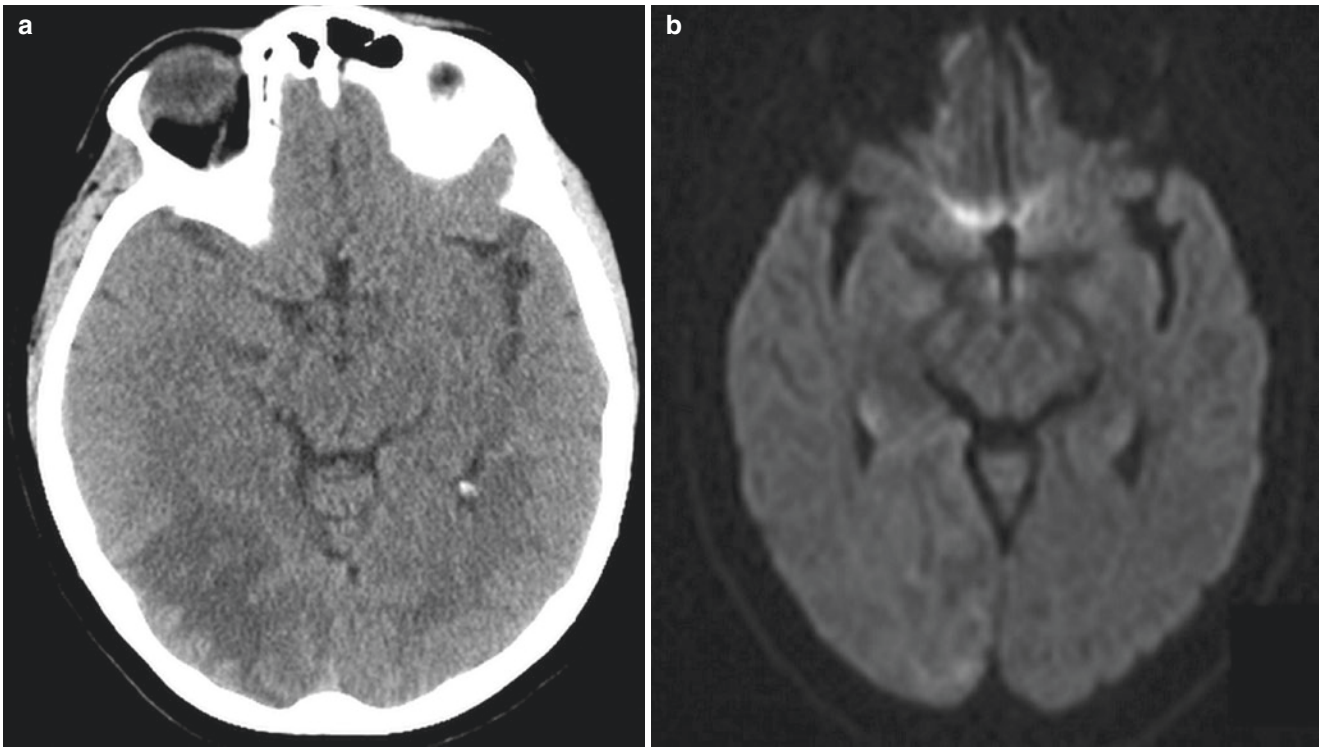

Fig. 3.6 Subacute infarction mimicking tumor. Patient presents with visual disturbance. (**a**), NCCT shows vasogenic edema in the right occipital lobe. MRI brain demonstrates minimally increased diffusion signal (**b**), FLAIR hyperintensity (**c**), and gyriform enhancement (**d**) in the right occipital lobe. CT perfusion shows hypoperfusion in this region with prolonged time to drain (**e**) and decreased cerebral blood flow (**f**). The presence of gyriform enhancement, minimal mass effect, and hypoperfusion is suggestive of subacute infarction rather than neoplasm

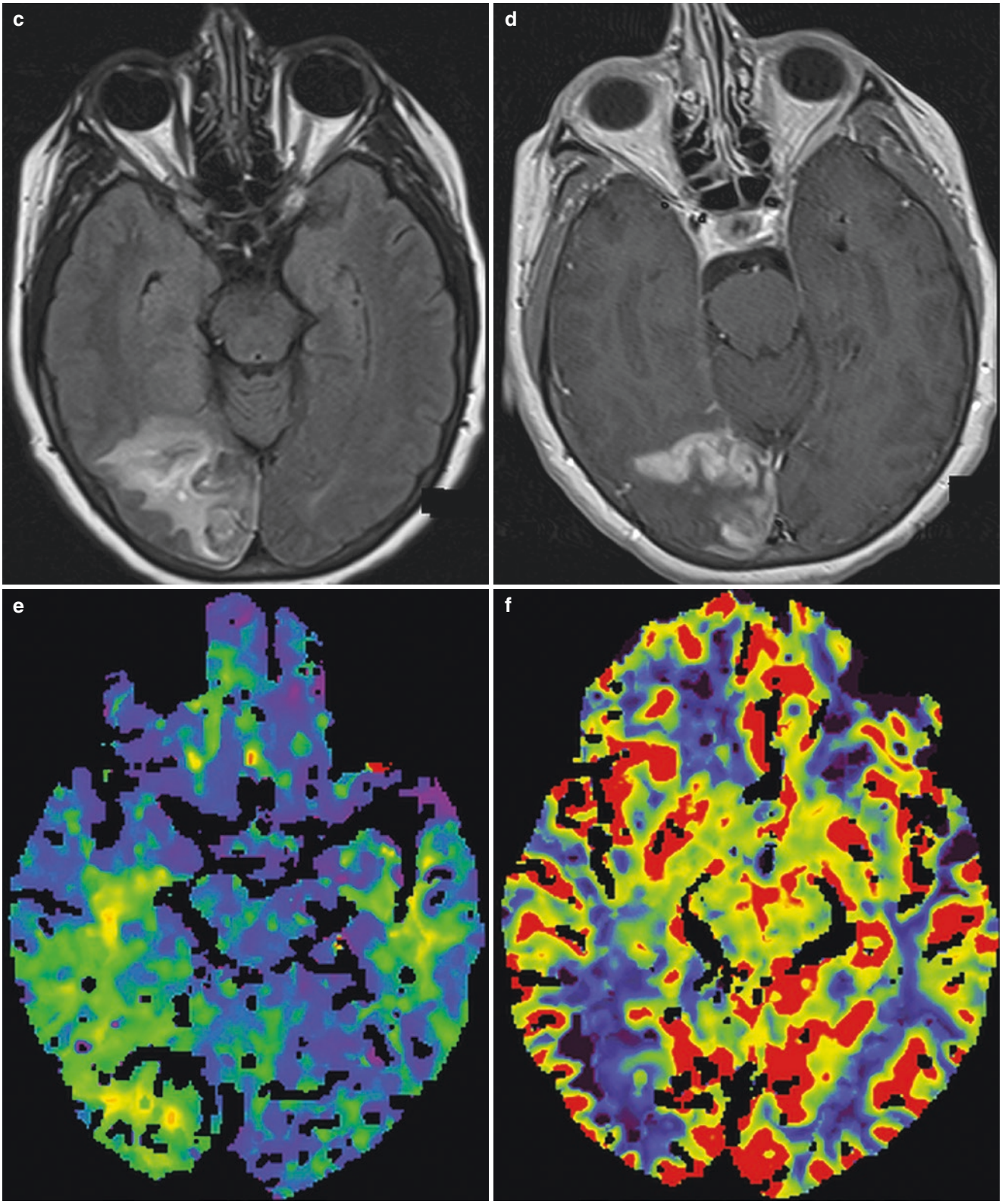

Fig. 3.6 (continued)

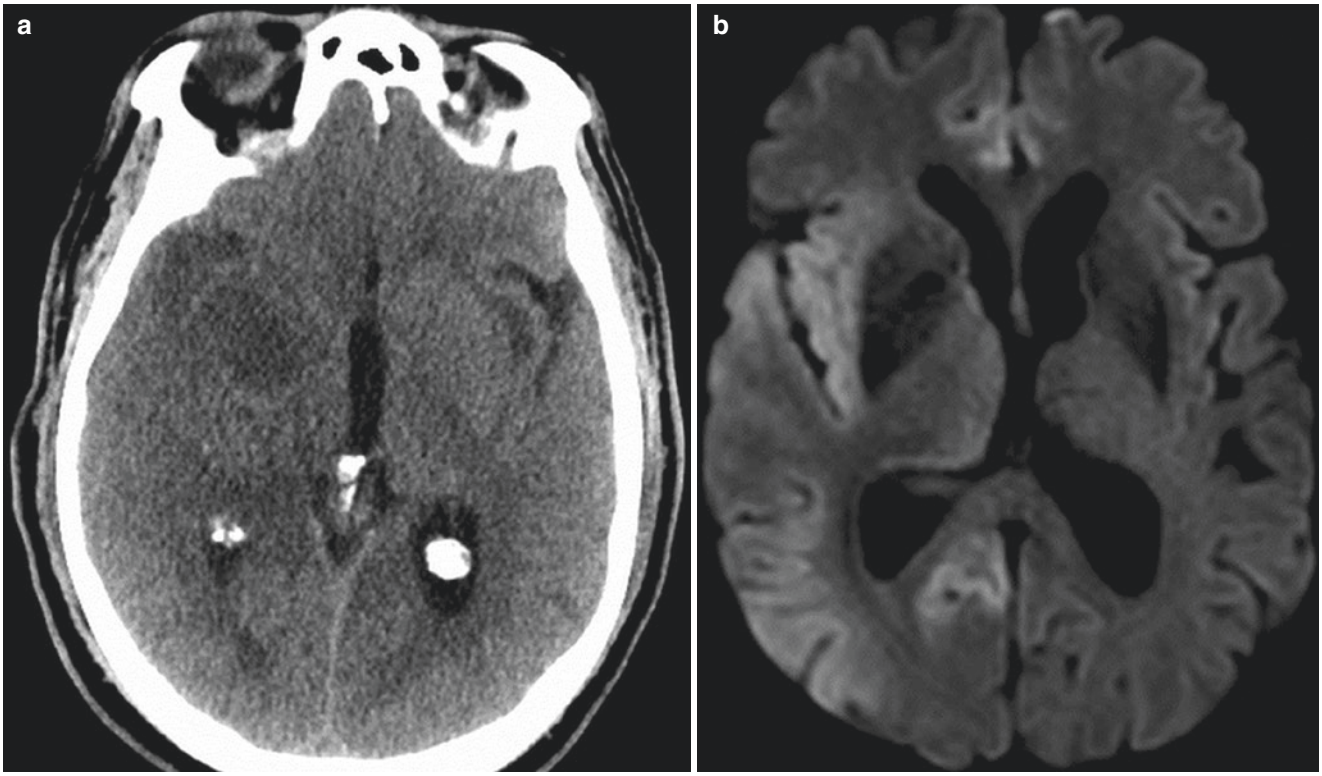

Fig. 3.7 Herpes encephalitis. Patient with headache, fever, and altered mental status. (**a**), NCCT shows hypodensity in the right temporal lobe and basal ganglia, suspicious for a subacute MCA infarction. (**b**), DWI shows diffusion restriction in the right temporal and occipital lobes, insula and cingulate gyrus, as well as left insula. The involvement of cingulate gyrus does not conform to the MCA territory. This is proven to be HSV encephalitis by CSF analysis

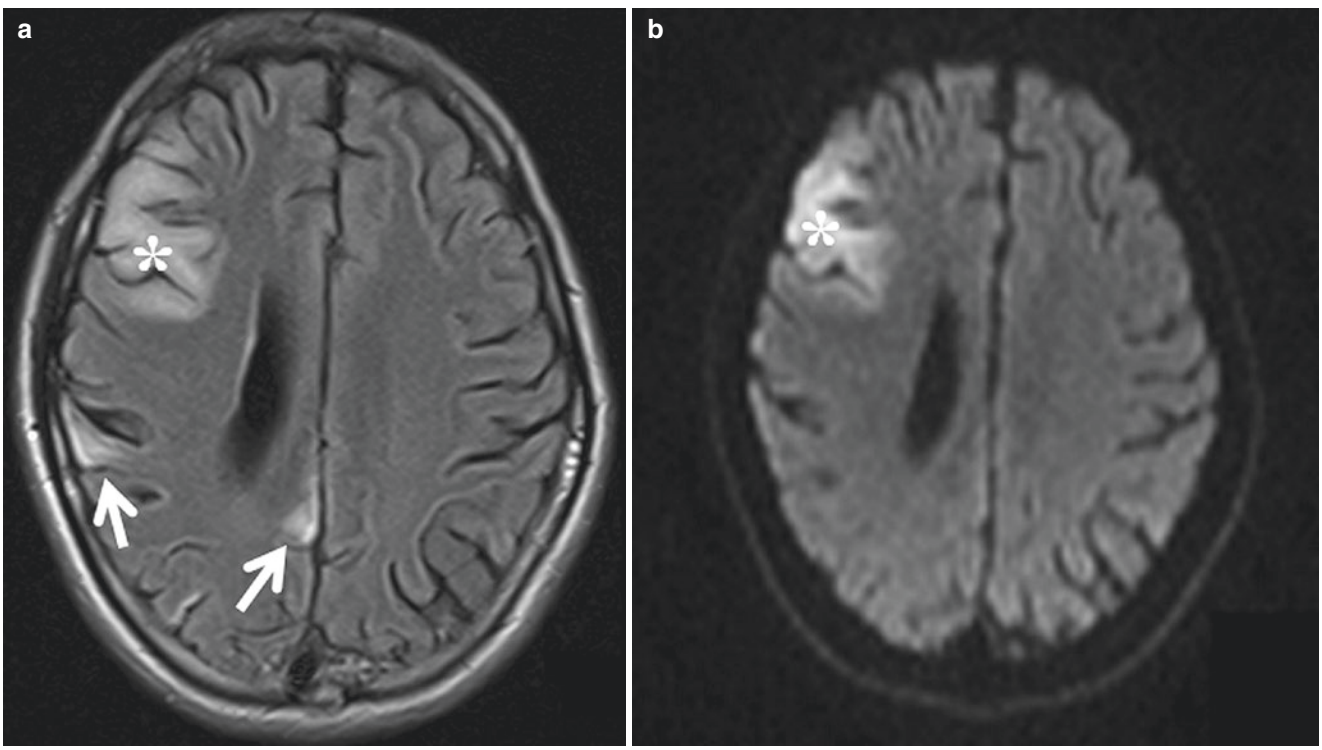

Fig. 3.8 Mitochondrial myopathy, encephalopathy, lactic acidosis, stroke-like episodes (MELAS). Ten-year old presents with recurrent strokes and seizures. (**a**), Axial FLAIR image shows multiple cortical FLAIR hyperintense lesions. (**b**), The right frontal lesion shows diffusion restriction (∗) mimicking acute infarction, while other lesions (*arrow*) are chronic without corresponding diffusion abnormality

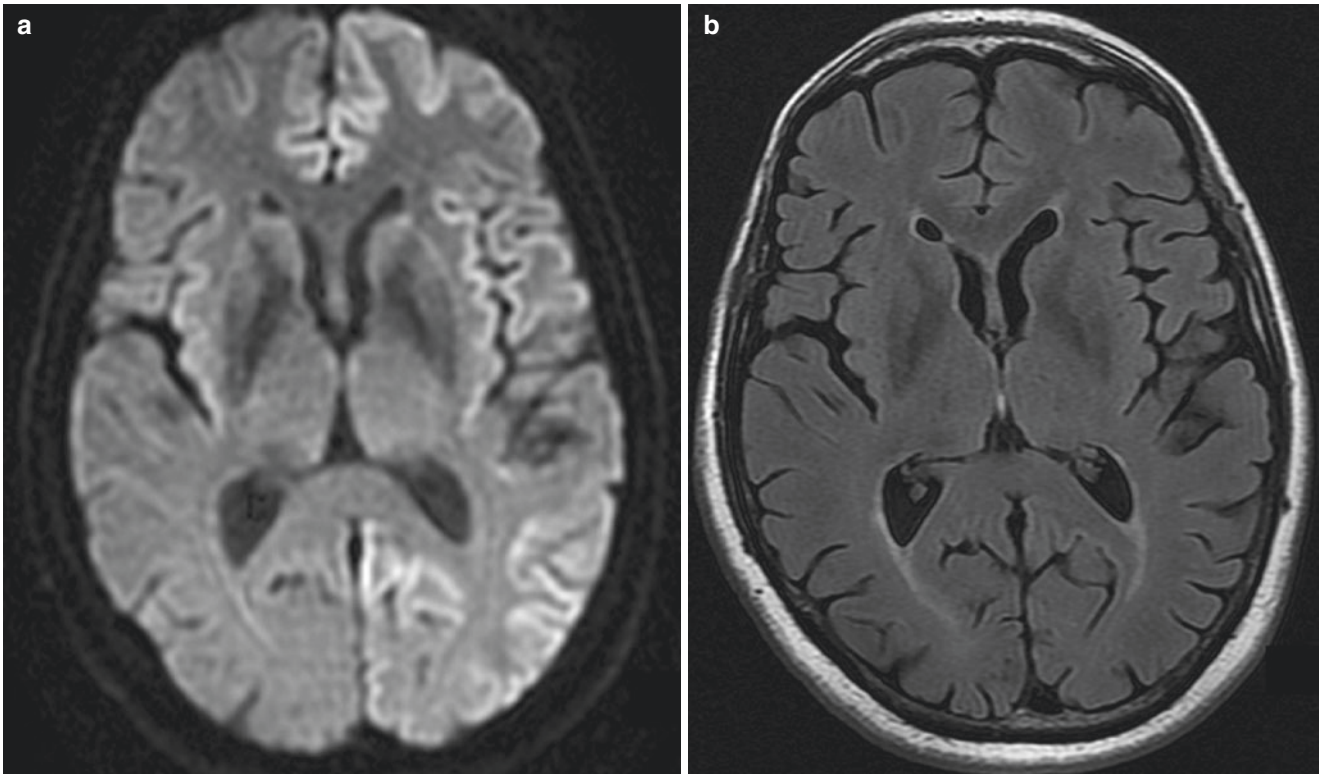

Fig. 3.9 Sporadic Creutzfeldt–Jakob disease. (**a**), Axial DWI shows cortical diffusion restriction in the bilateral insular and cingulate gyri as well as left frontal and occipital lobes. (**b**), No FLAIR signal abnormality is evident. The lack of cortical swelling helps differentiate CJD from cytotoxic or inflammatory processes

or symmetric or asymmetric involvement of the cerebral cortices (cortical ribboning) and basal ganglia with diffusion restriction, which may resemble ischemic lesions (Fig. 3.9). Peri-rolandic region is usually spared. DWI or FLAIR signal abnormality in the posterior thalami (pulvinar sign) and dorsomedial thalami (hockey stick sign) has been reported as the most sensitive markers for variant CJD, although it is not pathognomonic and has been reported in sporadic CJD cases as well [11].

3.8 Hypoxic–Ischemic Encephalopathy (HIE)

HIE in adults usually results from cardiac arrest or respiratory failure. MRI typically shows symmetric diffusion restriction, subsequent T2/FLAIR hyperintensity, and cortical swelling in regions with high metabolic demand, such as the basal ganglia, thalamus, hippocampus, cerebral cortex, and cerebellum (Fig. 3.10). CT is not sensitive but may show diffuse loss of gray–white differentiation, cerebral edema, and sulcal effacement in advanced cases.

White matter is usually spared from hypoxic–ischemic injury due to its relatively low metabolic activity, although delayed post-hypoxic leukoencephalopathy (DPHL) has been reported in patients with respiratory arrest due to drug overdose or carbon monoxide intoxication. This condition is clinically characterized by neurologic relapse following a period of stability or improvement after an episode of hypoxia. MRI usually shows diffusion restriction and high T2/FLAIR intensity with bilateral and symmetric involvement of subcortical and deep white matter [12] (Fig. 3.11).

3.9 Hypoglycemic Encephalopathy

Hypoglycemic encephalopathy typically affects diabetic patients who accidentally overuse insulin or oral hypoglycemic agents, or rarely patients with undiagnosed insulinoma. MRI shows diffusion restriction of the cortex, basal ganglia, hippocampi, and occasionally white matter and splenium of the corpus callosum, very similar to HIE.

3.10 Hyperammonemic Encephalopathy

Patients with acute hyperammonemic or hepatic encephalopathy present with progressive drowsiness, seizures, and coma. MRI may show diffuse cortical/subcortical edema and

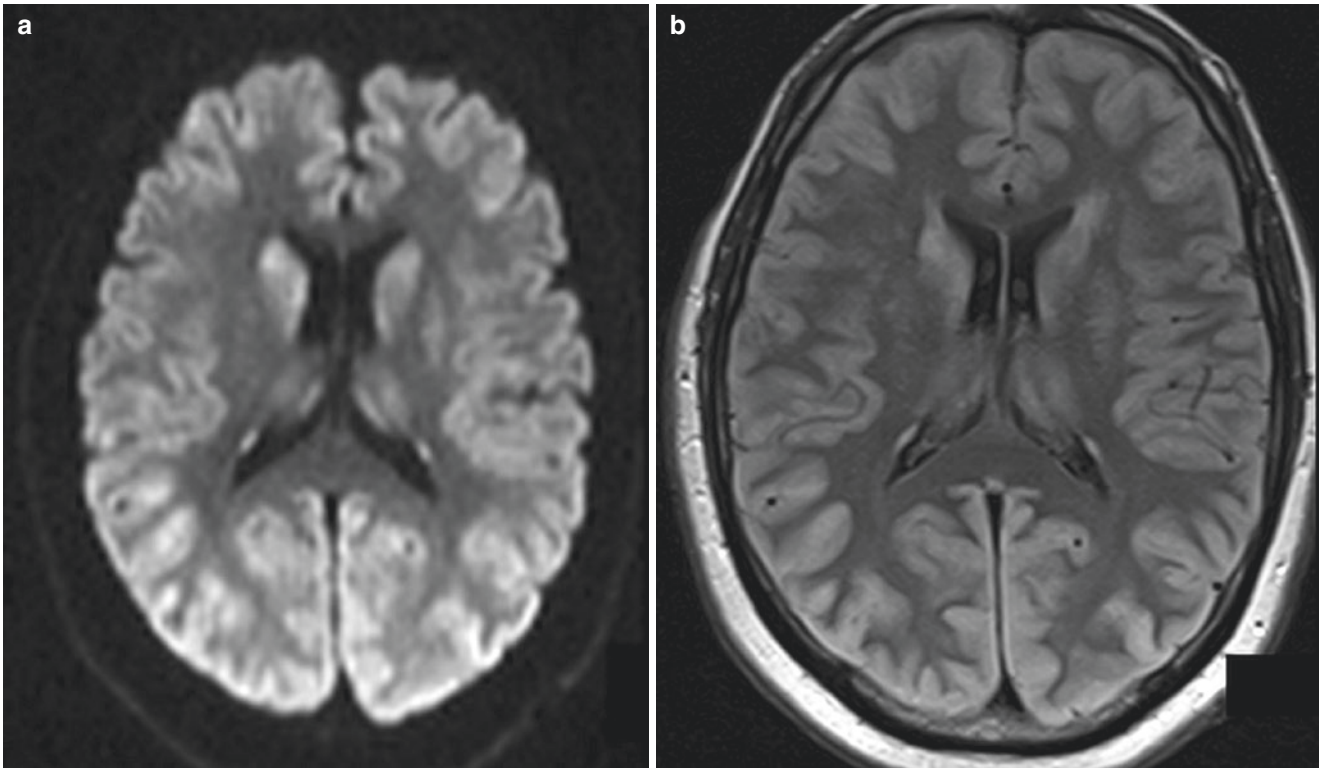

Fig. 3.10 Hypoxic–ischemic encephalopathy. MRI shows diffusion restriction (**a**) and FLAIR hyperintensity and cortical swelling (**b**) of bilateral cerebral hemispheres and basal ganglia, consistent with cytotoxic injury

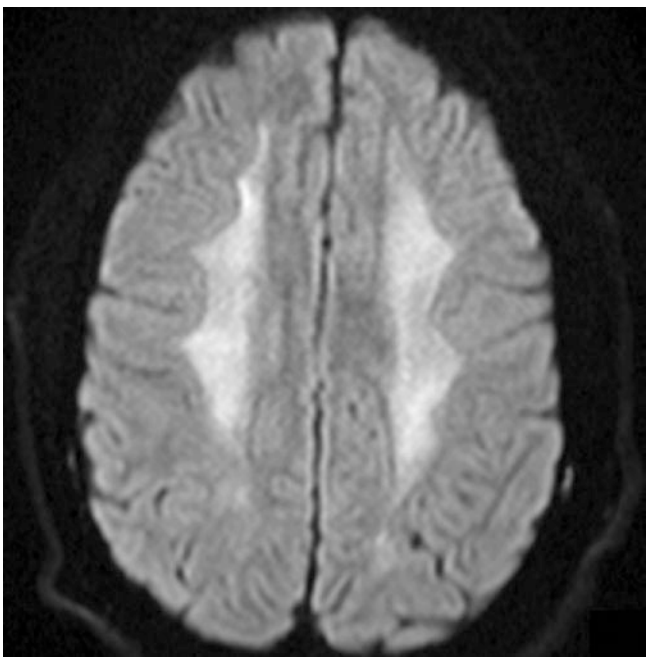

Fig. 3.11 Delayed post-hypoxic leukoencephalopathy. Patient with respiratory failure due to heroin overdose presents with progressive mental status decline. The axial DWI image shows confluent diffusion restriction in the bilateral cerebral white matter

restricted diffusion (Fig. 3.12). It has been reported that symmetric involvement of the cingulate gyrus and insular cortex are more specific imaging features for acute hepatic encephalopathy [13] . CT is less sensitive but may reveal generalized edema in severe cases.

3.11 Wernicke's Encephalopathy

Wernicke's encephalopathy is a potentially lethal neurological emergency caused by thiamine deficiency. It is most frequently seen with chronic alcohol abuse, although it has also been described in nonalcoholic patients with malnutrition. Clinical presentations are variable, and only a minority of patients present with the classic triad of ataxia, altered mentation, and oculomotor dysfunction. MRI is critical for diagnosis and typically shows symmetric T2/FLAIR hyperintensity and diffusion restriction in the mammillary bodies, hypothalami, medial thalami, tectal plate, and periaqueductal area (Fig. 3.13) [14]. This pattern may mimic infarctions due to artery of Percheron occlusion or basilar tip thrombosis.

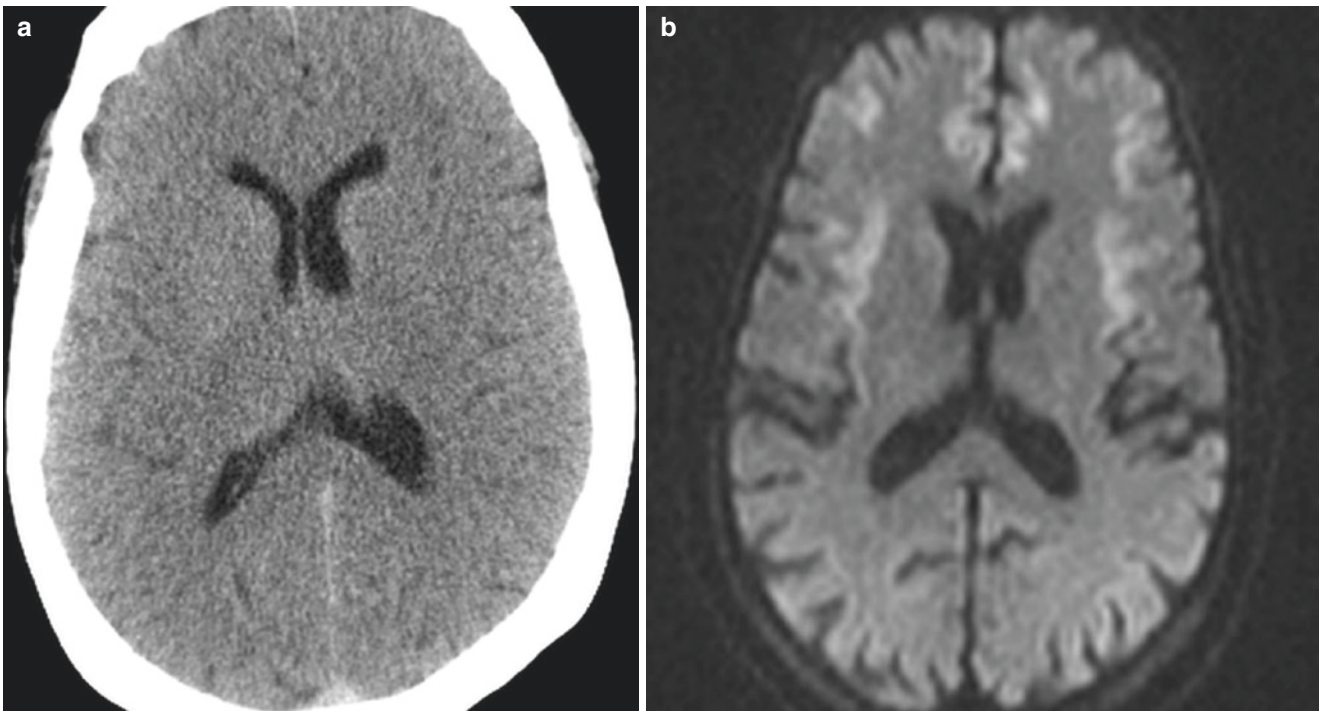

Fig. 3.12 Hyperammonemic encephalopathy. (**a**), Patient with liver failure and altered mental status. NCCT shows diffuse cerebral edema, sulcal effacement, and loss of gray–white differentiation. (**b**), DWI MRI of a different patient shows symmetric diffusion restriction of bilateral insular and cingulate cortices. The appearance can mimic hypoxic ischemic injury, and clinical history is critical for the diagnosis

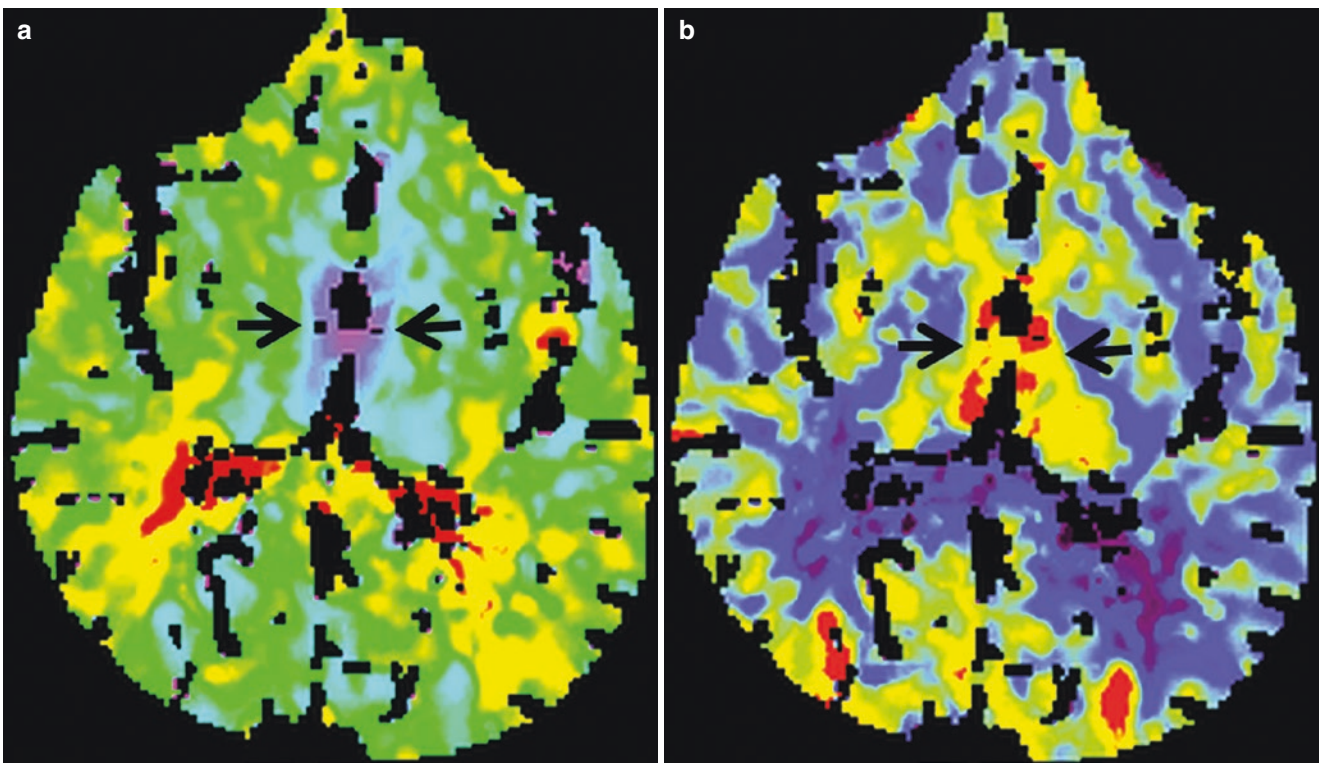

Fig. 3.13 Wernicke's encephalopathy. Alcoholic with acute mental status change. CTA demonstrate no large vessel occlusion or stenosis. CT perfusion demonstrates decreased time to drain (**a**) and increased CBF (**b**) in the bilateral medial thalami (*arrow*) suggestive of hyperperfusion. MRI shows FLAIR hyperintensity involving the bilateral medial thalami (**c**), hypothalami including the mammillary bodies and periaqueductal gray matter (**d**). (**e**) DWI shows corresponding area of diffusion restriction (*arrow*)

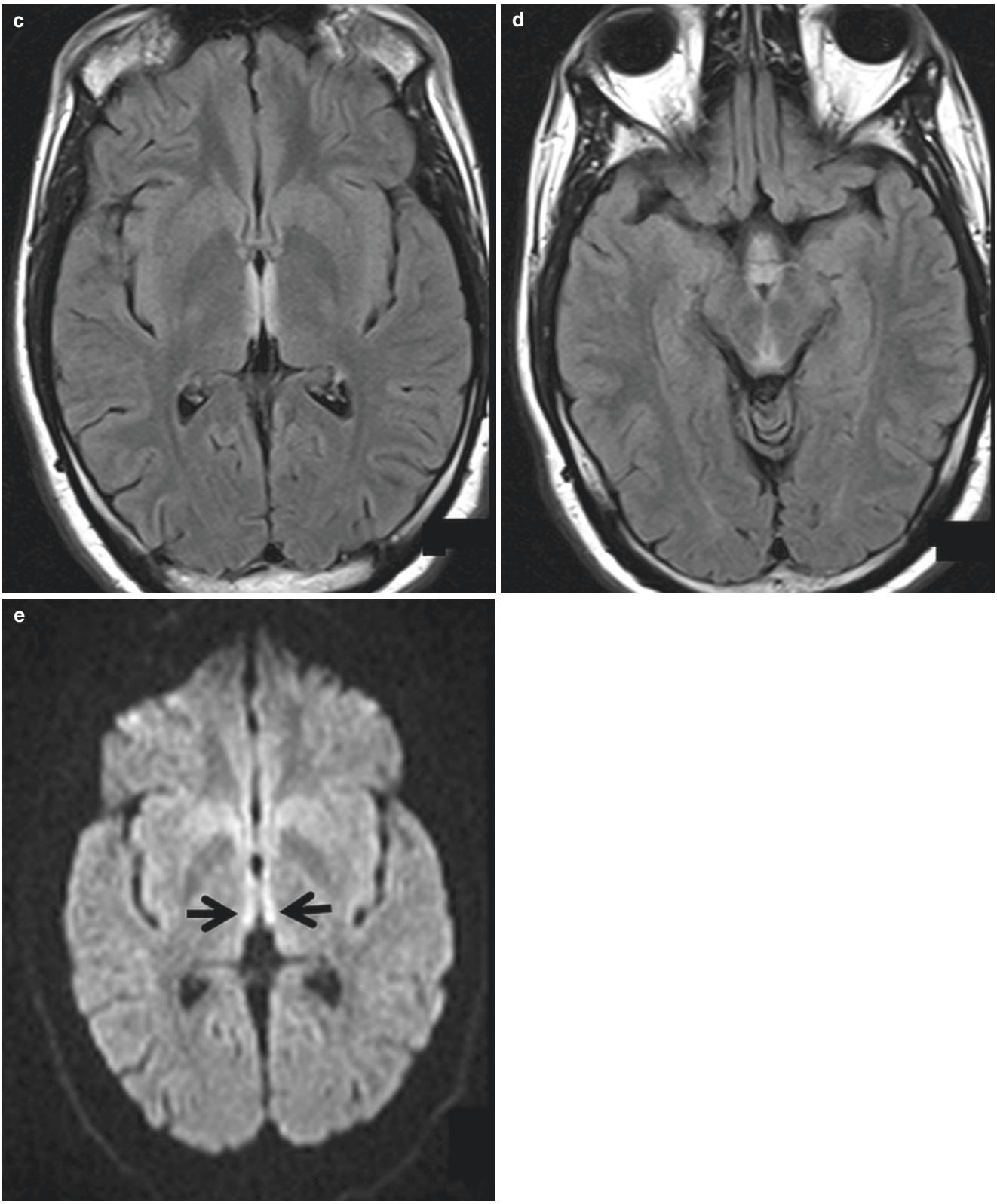

Fig. 3.13 (continued)

3.12 Osmotic Demyelination Syndrome (ODS)

ODS is a neurological disorder caused by rapid correction of hyponatremia, but it can also occur in alcoholics, malnourished, or chronically debilitated patients. Clinical presentations include altered mental status, pseudobulbar paralysis, and spastic tetraparesis. It can present with central pontine and/or extrapontine myelinolysis. In central pontine myelinolysis, confluent T2/FLAIR hyperintensity involves the central pons, typically sparing the peripheral aspect of pons and corticospinal tracts. Sometimes, a trident-shaped central signal abnormality is seen. Diffusion restriction can be present in the acute setting that can mimic acute stroke, although the pattern of involvement allows differentiation from the pontine perforator infarction, which is typically unilateral and respects the midline. Extrapontine myelinolysis can be seen symmetrically involving the thalami, basal ganglia, midbrain, and cerebral white matter (Fig. 3.14) [15].

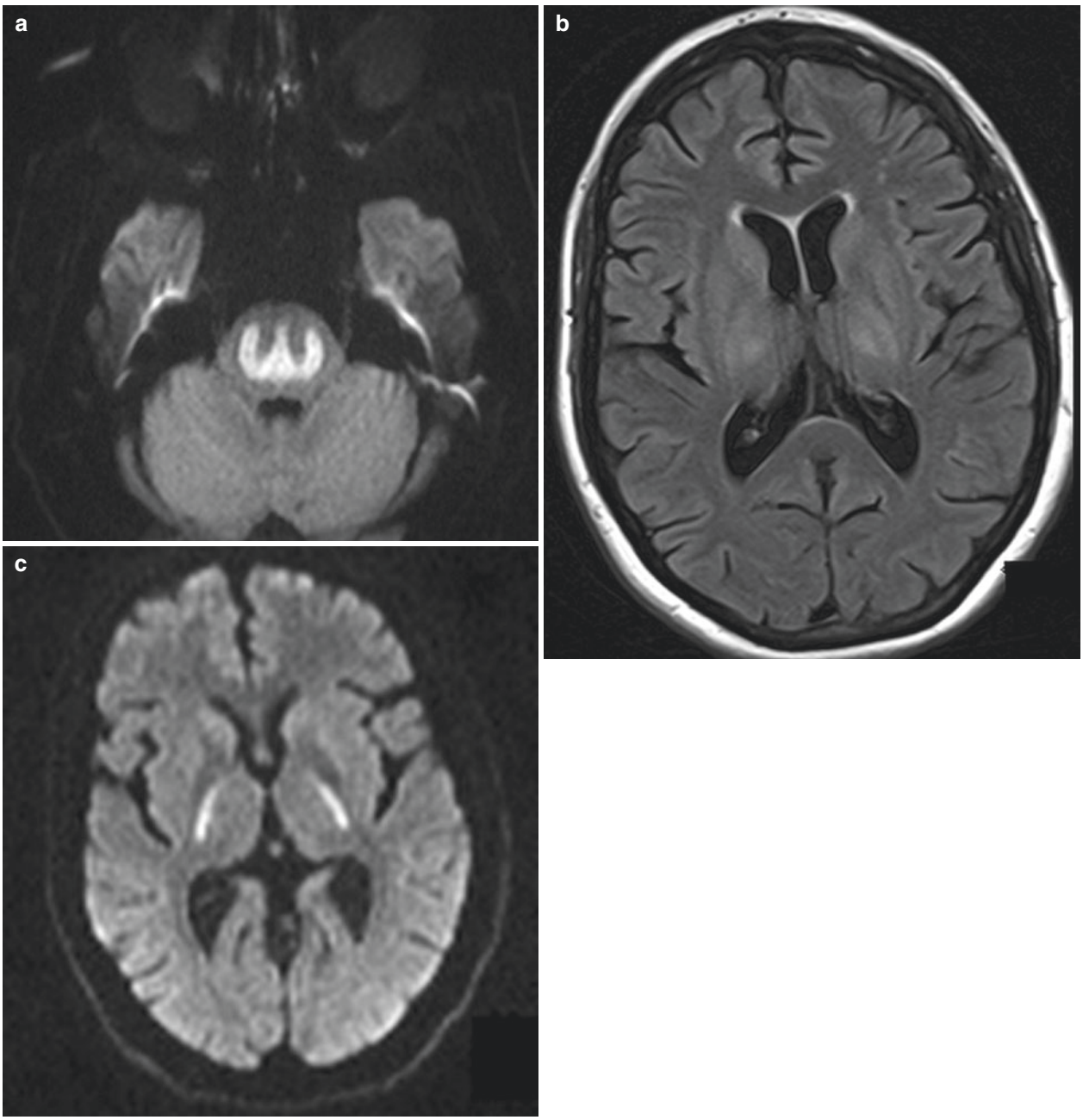

Fig. 3.14 Osmotic demyelination syndrome. (**a**), patient with acute central pontine myelinolysis. Axial DWI shows diffusion restriction of the pons sparing of the peripheral fibers and corticospinal tracts with a classic "trident" pattern. (**b**), A different patient with pontine and extrapontine myelinolysis. FLAIR image at the ventricular level shows hyperintensity of bilateral basal ganglia and thalami. (**c**), Symmetric diffusion restriction in the posterior limbs of bilateral internal capsules. FLAIR hyperintensity and enhancement are also seen in the central pons (not shown)

3.13 Drug Toxicity

A number of therapeutic or recreational drugs can cause neurotoxicity that simulate acute stroke syndrome. For example, patients with acute methotrexate-related leukoencephalopathy can present with headache, confusion, seizure, or focal neurological deficits. MRI may show transient diffusion restriction and high T2/FLAIR signal in the centrum semiovale unilaterally or bilaterally that may mimic acute stroke (Fig. 3.15) [16].

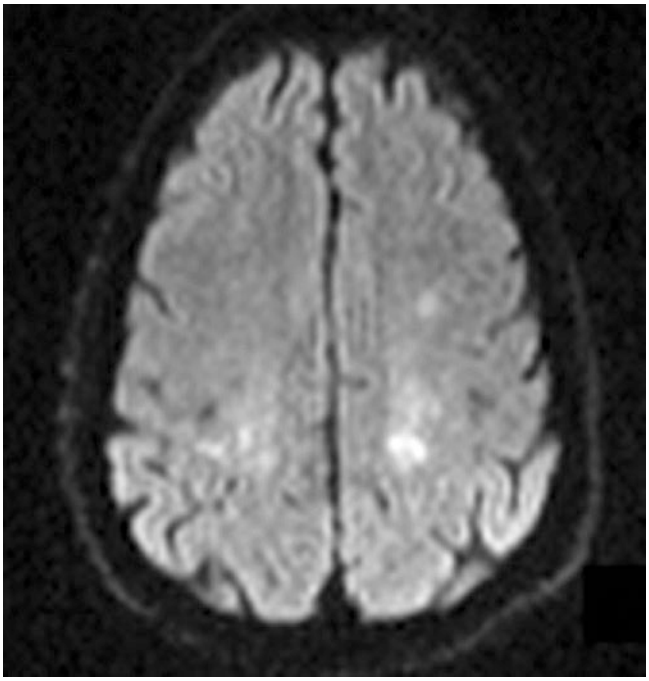

Fig. 3.15 Acute methotrexate neurotoxicity. Patient with recent intrathecal methotrexate for leukemia presents with right-sided weakness and slurred speech. DWI shows diffusion restriction of bilateral centrum semiovale on the left more than on right

3.14 Cerebral Fat Embolism (CFE)

CFE is an uncommon, but potentially life-threatening complication of long bone fractures or orthopedic procedures typically seen between 12 and 72 hours after the injury. The clinical triad of fat embolism syndrome consists of respiratory distress, altered mental status, and petechial rash. Cerebral manifestations of fat embolism syndrome are nonspecific and include headache, lethargy, delirium, seizure, coma, etc. CT is insensitive in the acute stage. MRI will demonstrate multiple scattered foci of diffusion restriction in a "star field" pattern, which can later evolve into confluent cytotoxic or vasogenic edema in the subacute stage (Fig. 3.16). Gradient recalled echo sequence demonstrates scatter foci of microhemorrhages [17]. It may mimic cardiogenic microinfarcts or diffuse axonal injury on imaging.

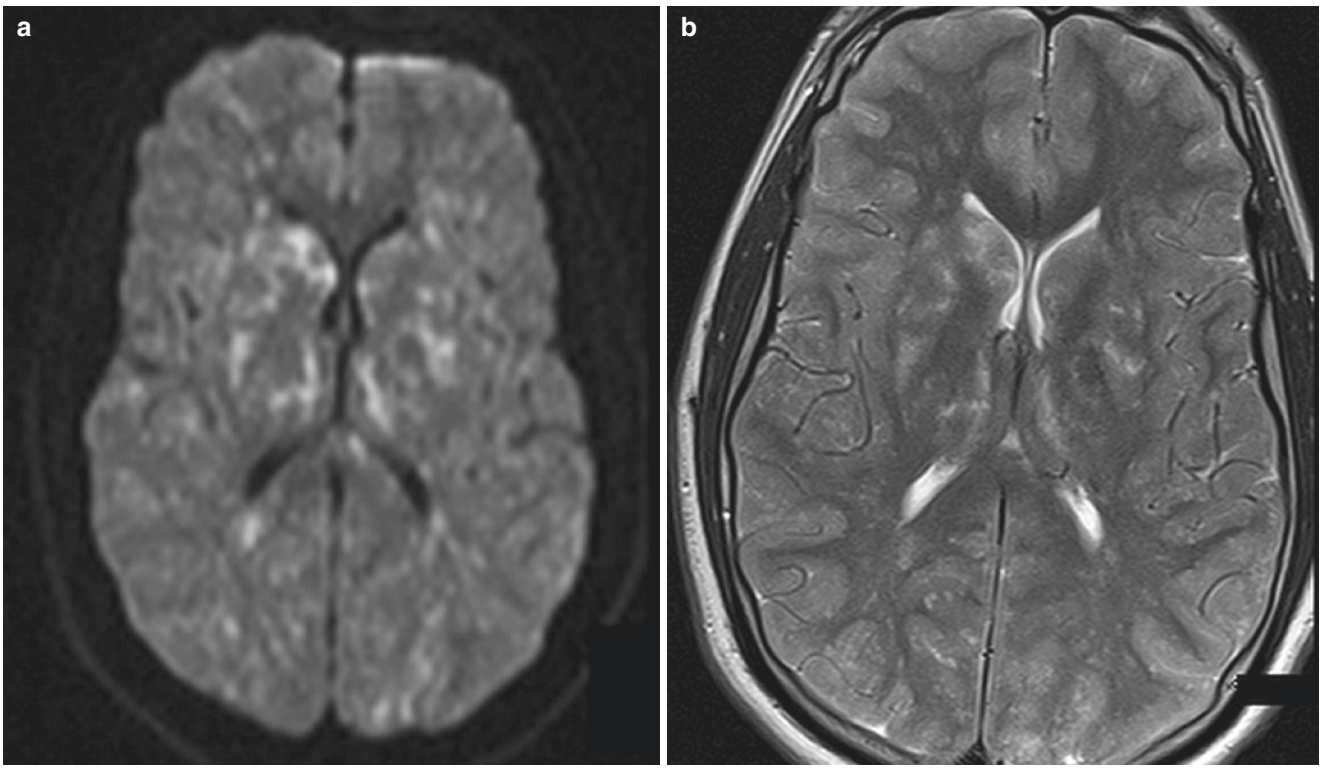

Fig. 3.16 Cerebral fat embolism. Trauma patient with femur fracture and mental status decline. (**a**), Axial DWI shows numerous foci of diffusion restriction in the bilateral basal ganglia and cortices with a "star field" pattern. (**b**), Axial T2 demonstrates corresponding areas of hyperintensity and cortical swelling

References

1. Libman RB, Wirkowski E, Alvir J, Rao TH. Conditions that mimic stroke in the emergency department. Arch Neurol. 1995;52:1119.
2. Hemmen TM, Meyer BC, McClean TL, Lyden PD. Identification of nonischemic stroke mimics among 411 code strokes at the University of California, San Diego, Stroke Center. J Stroke Cerebrovasc Dis. 2008;17:23–5.
3. Adam G, Ferrier M, Patsoura S, Gramada R, Meluchova Z, Cazzola V, Darcourt J, Cognard C, Viguier A, Bonneville F. Magnetic resonance imaging of arterial stroke mimics: a pictorial review. Insights Imaging. 2018;9:815–31.
4. Vilela P. Acute stroke differential diagnosis: stroke mimics. Eur J Radiol. 2017;96:133–44.
5. Cianfoni A, Caulo M, Cerase A, Della Marca G, Falcone C, Di Lella GM, Gaudino S, Edwards J, Colosimo C. Seizure-induced brain lesions: a wide spectrum of variably reversible MRI abnormalities. Eur J Radiol. 2013;82:1964–72.
6. Strambo D, Rey V, Rossetti AO, Maeder P, Dunet V, Browaeys P, Michel P. Perfusion-CT imaging in epileptic seizures. J Neurol. 2018;265:2972–9.
7. Cobb-Pitstick KM, Munjal N, Safier R, Cummings DD, Zuccoli G. Time course of cerebral perfusion changes in children with migraine with aura mimicking stroke. AJNR Am J Neuroradiol. 2018;39:1751–5.
8. Morgenstern LB, Frankowski RF. Brain tumor masquerading as stroke. J Neurooncol. 1999;44:47–52.
9. Soares BP, Provenzale JM. Imaging of herpesvirus infections of the CNS. Am J Roentgenol. 2016;206:39–48.
10. Malhotra K, Liebeskind DS. Imaging of MELAS. Curr Pain Headache Rep. 2016. https://doi.org/10.1007/s11916-016-0583-7.
11. Fragoso DC, Gonçalves Filho ALDM, Pacheco FT, Barros BR, Aguiar Littig I, Nunes RH, Maia Júnior ACM, da Rocha AJ. Imaging of Creutzfeldt-Jakob disease: imaging patterns and their differential diagnosis. Radiographics. 2017;37:234–57.
12. Beeskow AB, Oberstadt M, Saur D, Hoffmann KT, Lobsien D. Delayed post-hypoxic leukoencephalopathy (DPHL)-an uncommon variant of hypoxic brain damage in adults. Front Neurol. 2018. https://doi.org/10.3389/fneur.2018.00708.
13. U-King-Im JM, Yu E, Bartlett E, Soobrah R, Kucharczyk W. Acute hyperammonemic encephalopathy in adults: imaging findings. Am J Neuroradiol. 2011;32:413–8.
14. Zuccoli G, Gallucci M, Capellades J, Regnicolo L, Tumiati B, Cabada Giadás T, Bottari W, Mandrioli J, Bertolini M. Wernicke encephalopathy: MR findings at clinical presentation in twenty-six alcoholic and nonalcoholic patients. Am J Neuroradiol. 2007;28:1328–31.
15. Howard SA, Barletta JA, Klufas RA, Saad A, De Girolami U. Osmotic demyelination syndrome. Radiographics. 2009;29:933–8.
16. Sandoval C, Kutscher M, Jayabose S, Tenner M. Neurotoxicity of intrathecal methotrexate: MR imaging findings. AJNR Am J Neuroradiol. 2003;24:1887–90.
17. Kuo KH, Pan YJ, Lai YJ, Cheung WK, Chang FC, Jarosz J. Dynamic MR imaging patterns of cerebral fat embolism: a systematic review with illustrative cases. Am J Neuroradiol. 2014;35:1052–7.

Cerebrovenous Thrombosis

4

Yang Tang

4.1 Introduction

Cerebrovenous thrombosis (CVT) is a relatively uncommon disorder, with the annual incidence estimated at 2–7 cases per a population of one million and accounting for 0.5–1% of all strokes in the adult population. Compared to arterial strokes, CVT tends to affect a younger patient population and has a female predominance [1].

A number of regional and systemic risk factors are associated with CVT [2]. Regional causes include mastoiditis or meningitis, traumatic head and neck injury, surgery, tumor compression, etc. Many systemic factors may lead to hypercoagulable states such as pregnancy and postpartum status, oral contraceptive use, hormonal replacement therapy, genetic prothrombotic conditions such as protein C and S deficiency, factor V Leiden mutation, as well as systemic infections or inflammatory diseases, malignancy, dehydration, sickle cell anemia, etc.

CVT poses a considerable diagnostic challenge to the clinicians and radiologists since the clinical presentations are variable and often unspecific. Symptoms related to intracranial hypertension such as headache, nausea and vomiting, papilledema, and visual changes are common. Other presentations include seizure, focal neurological deficits, encephalopathy, etc.

Neuroimaging plays a critical role in the diagnosis of CVT. Imaging diagnosis of CVT primarily relies on the identification of the venous thrombus by variable modalities including NCCT, contrast-enhanced CT/CT venography, MRI, and MR venography. Catheter angiography, once the reference standard, is now used mostly for the purpose of endovascular intervention and rarely as a diagnostic modality.

4.2 Parenchymal Changes Associated with CVT

Approximately 50% of CVT cases have associated parenchymal changes visible on CT and MRI.

Venous occlusion and increased venous pressure lead to parenchymal changes including cerebral edema and hemorrhage, particularly if there is involvement of cortical veins and lack of adequate venous collaterals. Edema can be vasogenic, cytotoxic, or a combination of both. Vasogenic edema is much more common and often reversible with treatment. Hemorrhage is mostly intraparenchymal and occasionally subarachnoid limited to the cortical sulci. Contrast-enhanced MRI or CT may demonstrate gyriform enhancement of the affected parenchyma, venous collaterals, and meningeal thickening from venous hypertension.

Compared to the infarction and hemorrhagic transformation from arterial infarction, parenchymal lesions from CVT do not conform to typical arterial distributions and predominantly involve the subcortical regions with relative sparing of the cortices. Thrombosis of the transverse sinus or vein of Labbé can lead to changes in the temporal lobes (Fig. 4.1). Superior sagittal sinus thrombosis may cause edema/hemorrhage in the frontal and parietal parasagittal regions (Fig. 4.2). Deep venous occlusions typically involve the thalami, basal ganglia, and periventricular white matter (Fig. 4.3). Parenchymal changes in above distribution should raise high suspicion for CVT [2].

4.3 Identification of Venous Thrombosis

4.3.1 Non-contrast CT (NCCT)

NCCT is usually the first modality acquired in emergency setting. The classic finding of venous thrombosis on NCCT is increased density in the dural sinuses and/or cortical veins due to acute clot formation and retraction leading to increased red blood cells and hemoglobin concentration (dense sinus sign or cord sign). The major confounding factor is hemoconcentration from other causes such as dehydration or polycythemia, which can also cause high density in dural sinuses and lead to false-positive interpretation in

© Springer Nature Switzerland AG 2020

Y. Tang, *Atlas of Emergency Neurovascular Imaging*, https://doi.org/10.1007/978-3-030-43654-4_4

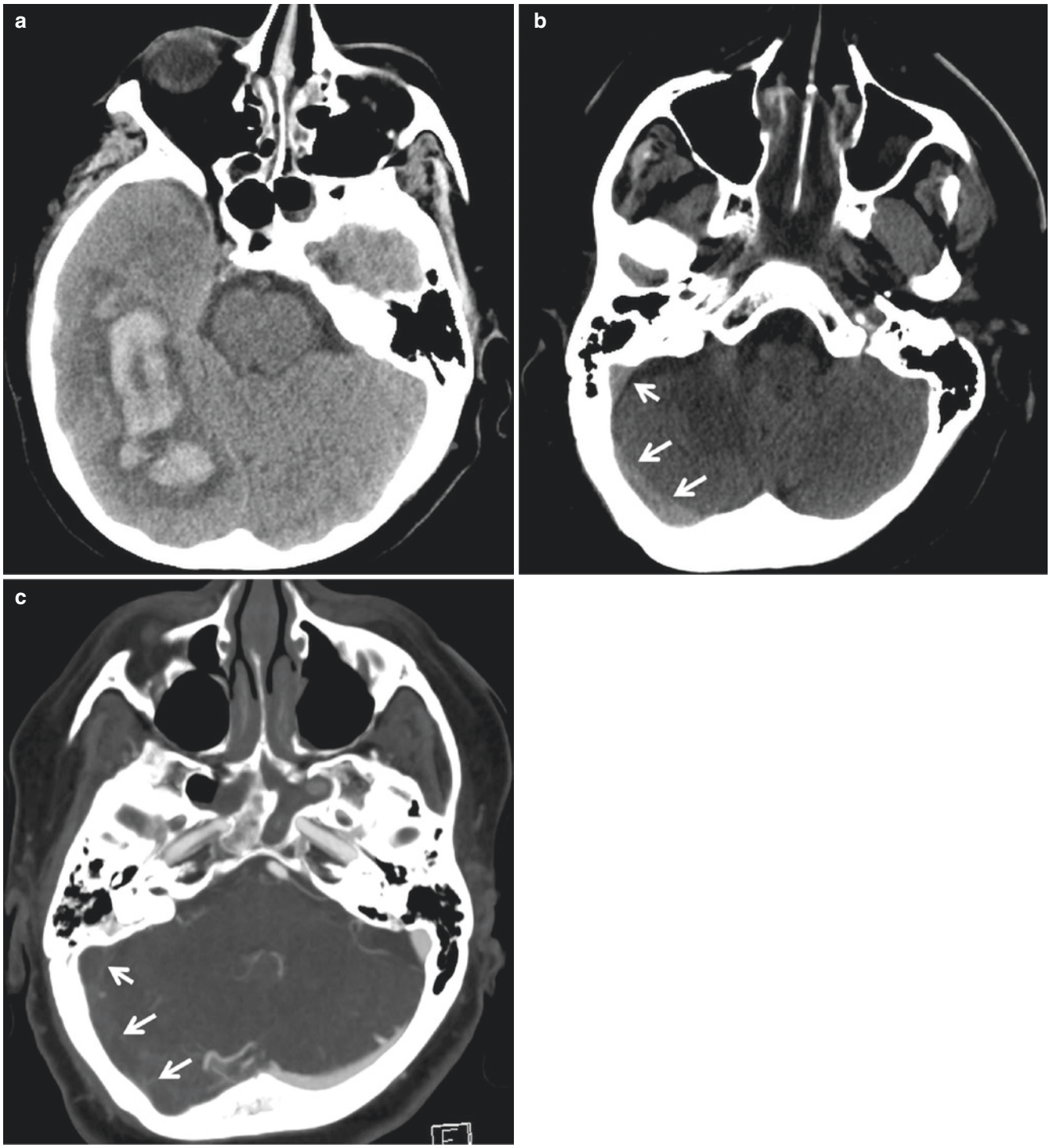

Fig. 4.1 Right transverse/sigmoid sinus thrombosis. A 65-year-old patient with severe headache and vomiting. (**a**) Axial NCCT demonstrates an irregular flame-shaped intraparenchymal hemorrhage in the right temporal subcortical region with surrounding edema. (**b**) More caudal NCCT image demonstrates asymmetric hyperdensity in the right transverse and sigmoid sinuses. (**c**) CT venogram demonstrates filling defect within the right transverse and sigmoid sinuses consistent with thrombosis, compared to the normal enhancing left transverse and sigmoid sinuses

patients without CVT. Occasionally, dense dural sinus can be confused with subdural or subarachnoid hemorrhages. Careful inspection on multiplanar CT images would help with the distinction.

Several studies have explored the utility of using quantitative Hounsfield measurement of dural sinuses and Hounsfield unit to hematocrit (H:H) ratio to diagnose acute CVT on NCCT. For example, Black et al. found that seven

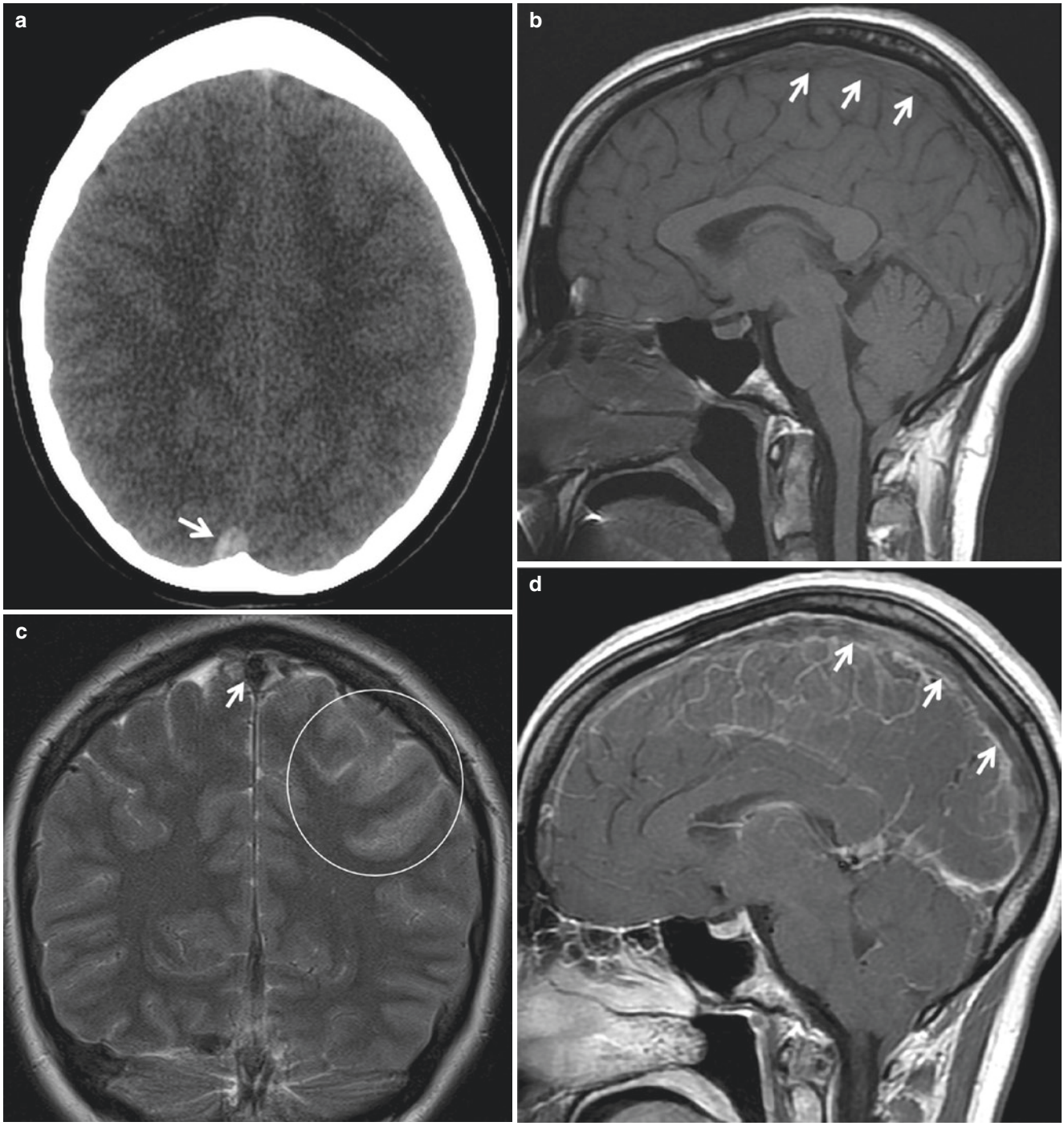

Fig. 4.2 Acute dural sinus thrombosis. A 26-year-old woman with headache for a few days and seizure. (**a**) Axial NCCT demonstrates hyperdensity of the superior sagittal sinus (SSS) suggestive of thrombosis. There is diffuse cerebral sulcal effacement but without hemorrhage or large infarction. (**b**–**e**) MRI of the brain shows isointensity on sagittal T1 (**b**) and hypointensity on coronal T2 (**c**) in the SSS, reflecting deoxyhemoglobin in the acute stage of thrombosis (*arrows*). There is mild cortical/subcortical edema in the left frontoparietal junction on the coronal T2 image (*circle* in **c**). (**d**) Sagittal postcontrast T1 demonstrates extensive filling defects of SSS (*arrows*). (**e**) Postcontrast axial T1 shows "empty delta" sign in the SSS and extensive leptomeningeal vascular enhancement due to venous congestion. (**f**) 3D contrast-enhanced first-pass MRV shows filling defect within SSS (*arrows*). (**g**) 3-D MRV MIP demonstrates absent filling of SSS, right transverse/sigmoid sinuses, and left transverse sinus. Left vein of Labbé drains into the left sigmoid sinus (*curved arrows*), which remain patent

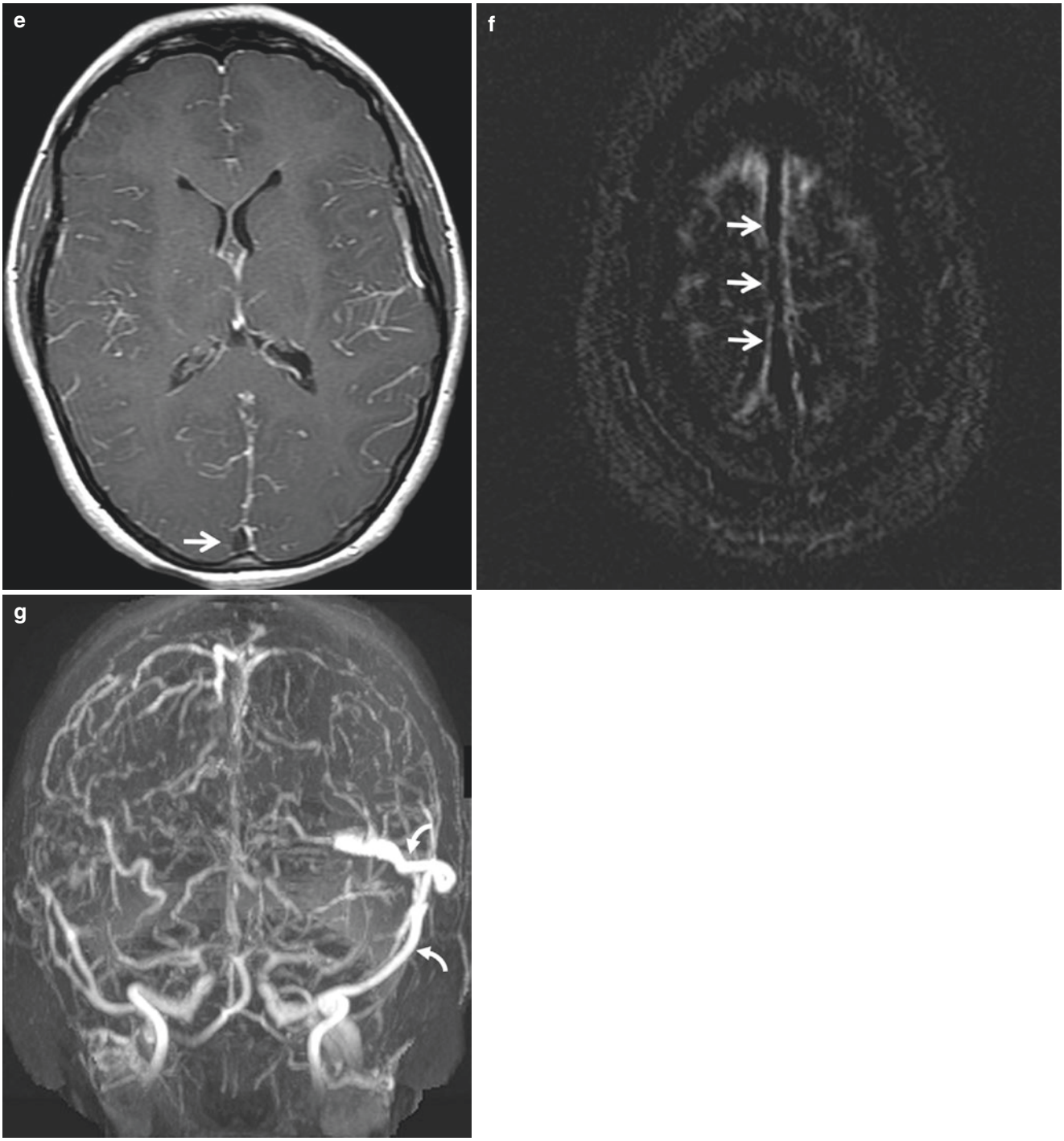

Fig. 4.2 (continued)

of the eight CVT patients had dural sinus Hounsfield unit (Hu) >70, but none of the normal subjects had Hu >70, suggesting Hu of 70 as a threshold for suspected DVT [3]. Besachio et al. reported that a majority of DVT cases can be diagnosed on NCCT by using Hu > 65, H:H ratio > 1.7, and venoarterial difference values greater than 15 [4]. Buyck et al. reported Hounsfield unit threshold of ≥62 HU and H:H ratio of ≥1.52 as optimal threshold for detecting CVT on NCCT [5].

It should be noted that the density of the venous thrombi gradually decreases as the red blood cells and hemoglobin degrade over time and eventually cannot be differentiated from normal blood or may even appear hypodense compared to the blood pool. This will cause false-negative interpretation, especially in subacute or chronic stages.

The sensitivity of NCCT in detecting CVT is variable in the literature. According to a recent multicenter retrospective study, sensitivity of visual inspection ranged from 41% to

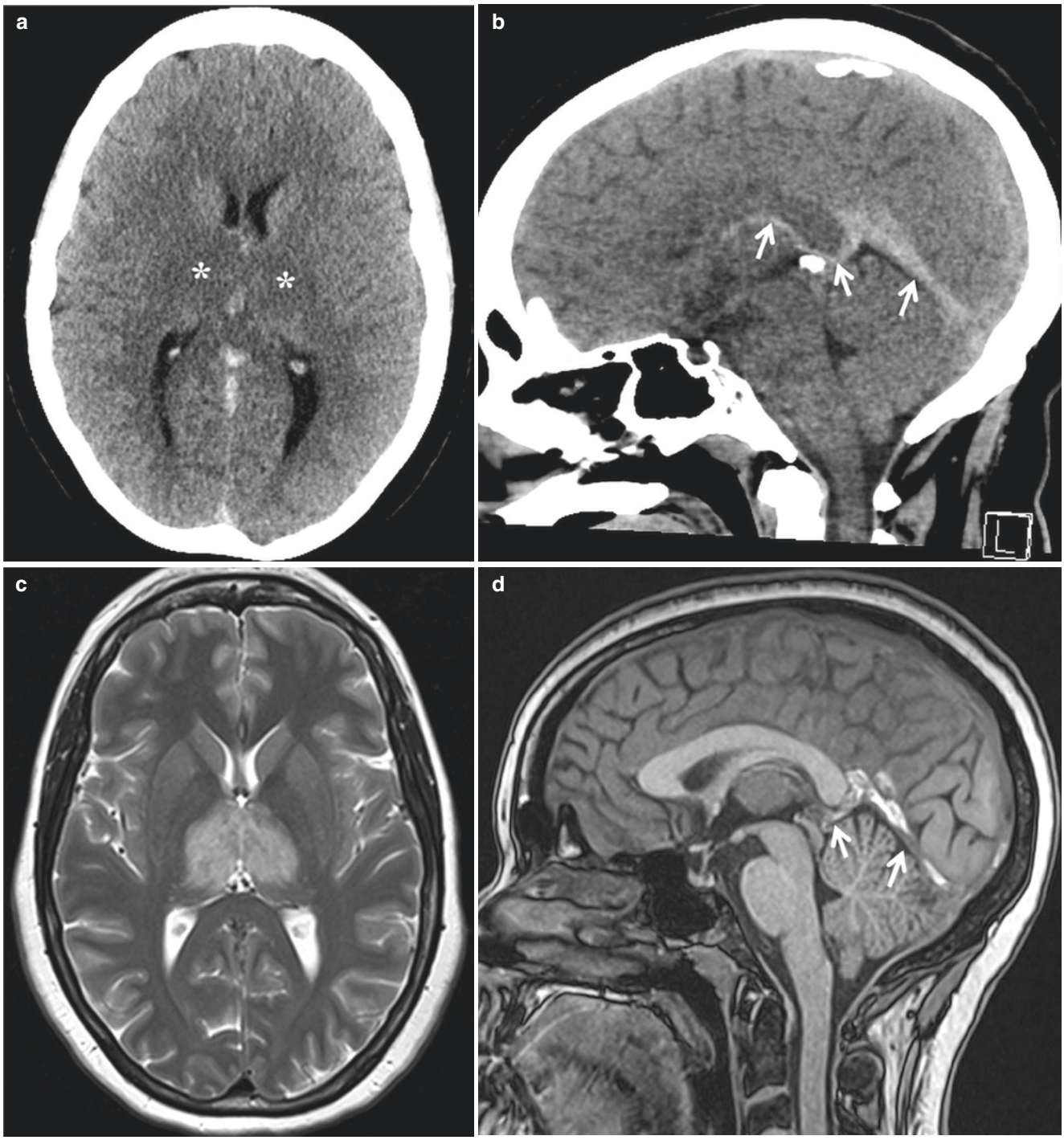

Fig. 4.3 Subacute deep venous thrombosis. A 31-year-old woman with severe headache and altered mentation for a week. (**a**, **b**) Axial (**a**) and sagittal (**b**) NCCT demonstrates hyperdensity involving the deep venous structures (*arrow*) including internal cerebral veins, vein of Galen, and straight sinus extending to the torcula, consistent with deep venous thrombosis. Note subtle bilateral thalamic edema (∗ in **a**). (**c**) Axial T2 MRI shows symmetric bilateral thalamic edema. (**d**) Non-contrast sagittal T1 MPRAGE sequence demonstrates hyperintensity in the thrombosed veins, consistent with methemoglobin in the subacute stage. There is also partial thrombosis of the superior sagittal sinus. (**e**) axial SWI image shows susceptibility within thrombosed deep veins. Small amount of petechial hemorrhage is also noted in the bilateral thalami

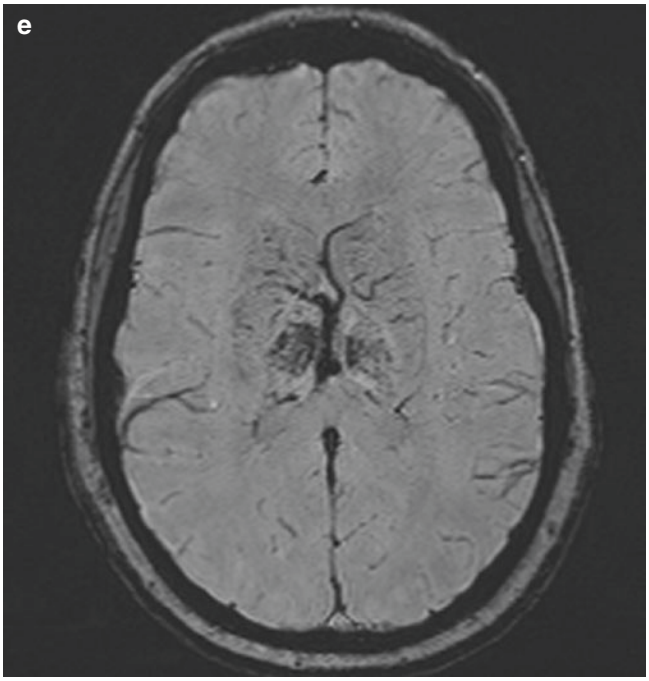

Fig. 4.3 (continued)

73%. Adding quantitative measurements improves the detection; however it still failed to identify one out of the four cases, in order to maintain a high specificity [6].

4.3.2 CT Venogram

Venous thrombi manifests as filling defects on the contrast enhanced CT or CT venogram (empty delta sign) (Fig. 4.1). Compared to MRI/MRV, CTV is more widely available in the emergency setting, allowing more rapid acquisition and less prone to motion artifacts. It can be used in patients with ferromagnetic devices when MRI is contraindicated. CTV has been shown to have similar accuracy as MRV.

With the widespread use of emergent CT angiography in evaluating acute stroke patients, it is critical for the radiologists to pay close attention to the venous structures as CVT can be a hidden cause for patients' neurological deficits. A cautionary note is that venous structures are frequently not adequately opacified during the arterial phase CTA acquired at 20–25 seconds after starting the contrast bolus, which can lead to missed diagnosis. Suboptimal venous opacification can also lead to false-positive results, as transverse and sigmoid sinuses (especially on the left) can have delayed filling due to compression of innominate vein at the thoracic inlet. Image acquisition at 40–45 seconds is frequently required to optimize the venous opacification and clarify the findings seen on arterial phase CTA. Some institutions have routinely integrated delayed postcontrast CT or CT venogram into the stroke CTA protocol to exclude CVTs, although this approach would result in increased radiation.

One of the potential drawbacks of CTV is that maximum intensity projection (MIP) image generation can be problematic due to inadvertent sinus exclusion from bone subtraction; however, this can be improved with specific software for mask bone elimination or using dual-energy CT.

4.3.3 MRI

MRI/MRV is the preferred modality to evaluate CVTs. Compared to CTV, MRI has no risk of ionizing radiation and less incidence of adverse contrast reactions by using gadolinium. Postcontrast images can be obtained in multiple phases to differentiate sinus thrombosis from delayed filling. Non-contrast MRI and time-of-flight MRV can be used in patients with gadolinium allergy, severe renal insufficiency, and during pregnancy beyond first trimester. MRI is more sensitive in detecting brain parenchymal changes than CT. In addition, the evolutionary signal changes of hemoglobin on MRI allow for the estimation of the age of thrombus.

The overall sensitivity of routine MRI without dedicated MRV sequence in identifying the venous thrombosis is over 80%. Findings include abnormal dural sinus signal or lack of normal flow voids and filling defects on the postcontrast T1 sequence.

Th T1 and T2/FLAIR signal of thrombosed dural sinus is highly variable depending on the age of thrombi [7].

In the acute stage (0–5 days), the thrombi are usually isointense on T1 and hypointense on T2 images because of deoxyhemoglobin, which can mimic normal or turbulent flow and lead to missed diagnosis (Fig. 4.2). MR or CT venography is usually necessary for the diagnosis at this stage.

In the subacute stage (6–15 days), the thrombi are predominantly hyperintense on both T1- and T2-weighted images because of methemoglobin (Fig. 4.3). This is the stage when venous thrombi are most conspicuous on routine MRI.

In the chronic stage (weeks), the thrombi usually become isointense on T1 and hyperintense on T2, which can resemble slow flow. On the postcontrast T1 sequence, chronic thrombi can enhance due to partial clot recanalization and capillary channels. It is important to remember that sinus enhancement on postcontrast T1 does not necessarily confirm its patency and CT/MR venography is necessary for a definitive diagnosis (Fig. 4.4).

T2∗ gradient-echo (GRE) and susceptibility-weighted (SWI) sequences can identify dural sinus thrombosis by the blooming from blood products contained within the thrombi. This is particularly useful in the acute stage when the thrombi may be missed by other sequences, although it can be obscured by susceptibility artifact from the adjacent calvarium. Isolated cortical vein thrombosis is responsible for approximately 6% of CVT, and it is also best identified on SWI or GRE sequence (Fig. 4.5).

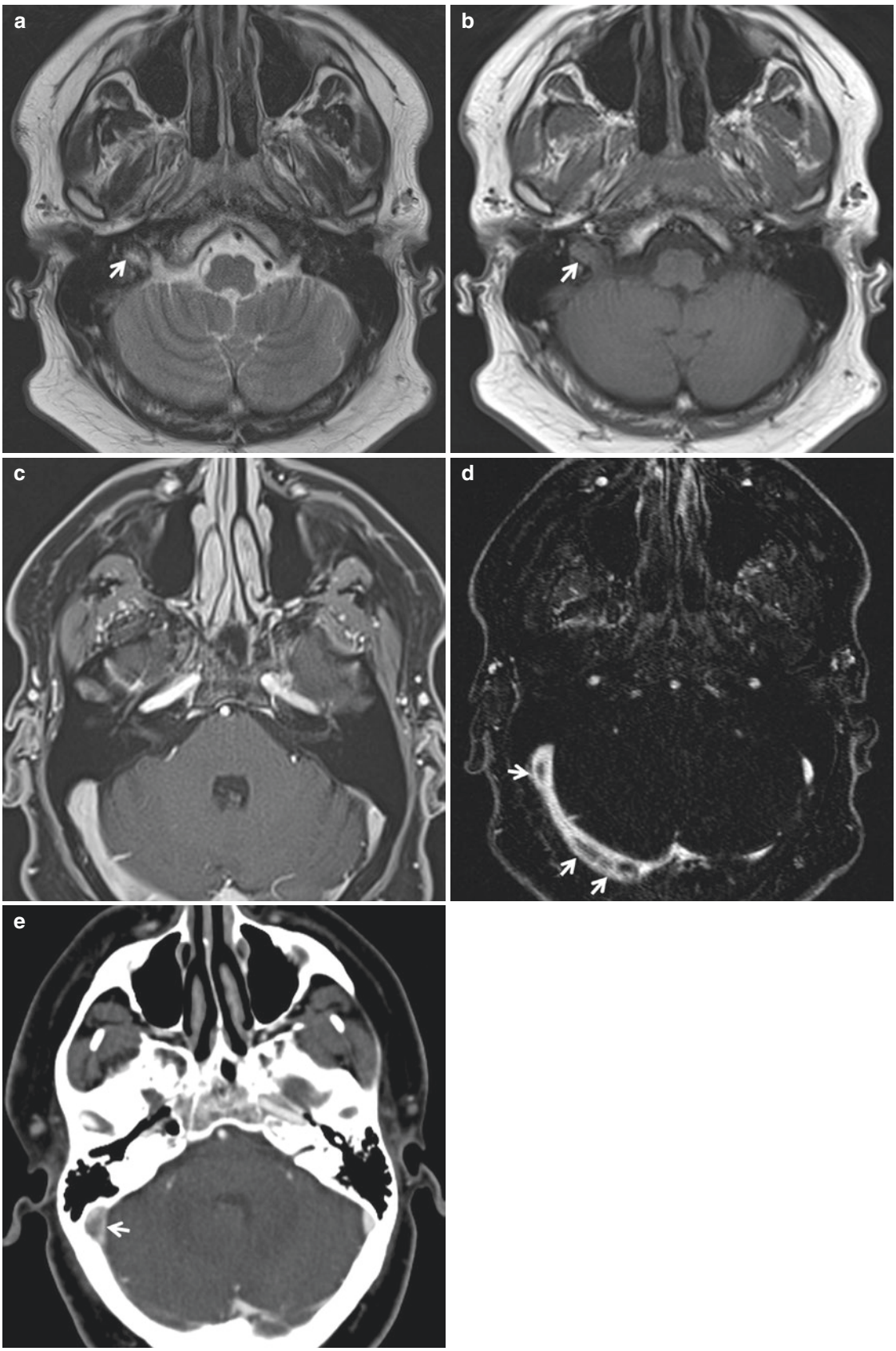

Fig. 4.4 Chronic dural sinus thrombosis. A 37-year-old with headache and blurred vision for a few months. (**a**, **b**) MRI of the brain. The right sigmoid sinus shows slight T2 hyperintense (**a**) and T1 isointense (**b**) signal (*arrow*). (**c**) Postcontrast 3D MPRAGE image demonstrates normal enhancement of the transverse sinuses. (**d**) Elliptical centric contrast-enhanced MRV demonstrates filling defect within the right transverse and sigmoid sinuses consistent with chronic thrombosis (*arrow*), which was confirmed by CTV (*arrow*) (**e**)

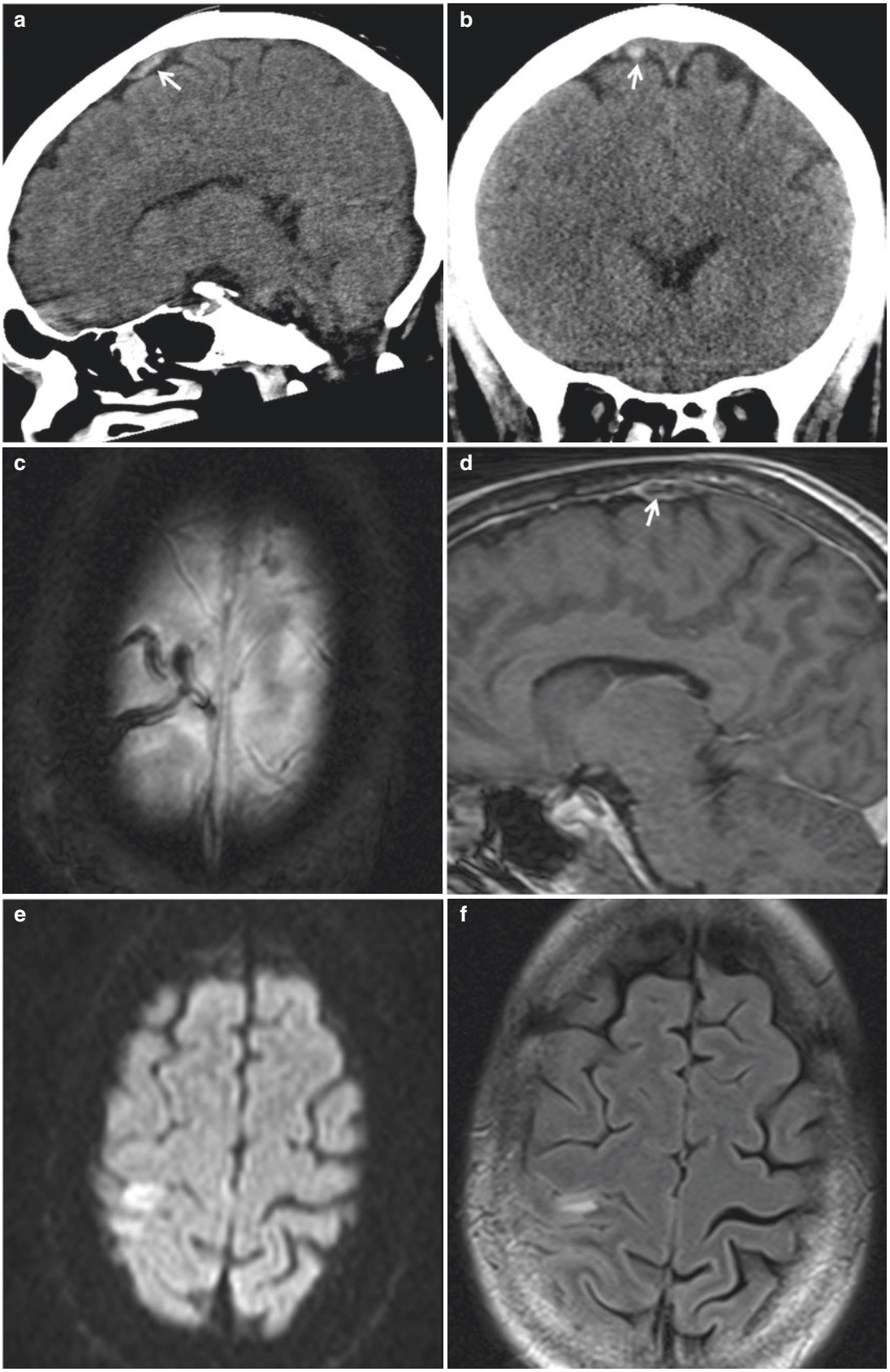

Fig. 4.5 Isolated cortical vein thrombosis. A 54-year-old with history of lymphoma presents with seizure. Sagittal (**a**) and coronal (**b**) NCCT images show a cord-like hyperdense structure in the right superior frontal subarachnoid space (*arrow*). This was initially misinterpreted as sulcal subarachnoid hemorrhage. (**c**) Axial MRI gradient recall echo sequence demonstrates blooming artifacts from the thrombosed right frontal cortical veins. (**d**) Postcontrast sagittal MPRAGE demonstrates a venous filling defect (*arrow*). The adjacent brain parenchyma shows diffusion restriction (**e**) and FLAIR hyperintensity (**f**), consistent with cytotoxic edema

Diffusion restriction can be seen in the thrombosed sinuses, although this almost always occur with concomitant signal changes on T1 and/or FLAIR sequences and may not provide additional diagnostic value.

4.3.4 MR Venogram

MRV can be performed using multiple techniques including time-of-flight (TOF), phase-contrast, volumetric T1 postcontrast MPRAGE, elliptic centric contrast-enhanced, and time-resolved contrast-enhanced MRV.

2D time-of-flight (2D TOF) MRV of the head is the most commonly used technique because it is easy to perform and does not require the use of gadolinium. It is superior to 3D TOF due to relative lack of saturation effects and better sensitivity to detect slow flow. There are several limitations of this technique. For example, it is prone to signal nulling in portions of dural sinuses that are parallel to the image acquisition plane (in plane artifact); therefore acquisition using multiple planes (axial, coronal, and oblique) is needed to mitigate this artifact. In addition, subacute thrombi may mimic patent flow on the TOF MRV due to intrinsic T1 hyperintensity from extracellular methemoglobin, leading to false-negative interpretation.

Contrast-enhanced MRV is more accurate and less prone to artifact compared to TOF. High-resolution postgadolinium 3D T1 volumetric sequence, which is now part of routine MRI brain in many practices, has been reported to be 83% sensitive and almost 100% specific to identify CVT [8].

So far, the best technique to evaluate intracranial venous structures is dynamic first-pass bolus contrast-enhanced MR venography. It avoids the pitfalls of TOF and long-acquisition contrast-enhanced MRV sequences and has shown the highest diagnostic accuracy for dural sinus thrombosis as compared with T2-weighted, GRE, and TOF MRV sequences.

It is important to be familiar with variant venous anatomy to avoid mistaking it for thrombotic occlusion. These include developmentally hypoplasia or atresia, high bifurcation, intrasinus septum, arachnoid granulations, etc.

4.4 Treatment

Anticoagulation is the standard of treatment for CVT. In contrast with arterial ischemic infarcts, many parenchymal abnormalities secondary to venous occlusion are reversible if treated early. The presence of intraparenchymal or isolated subarachnoid hemorrhage is not a contraindication for anticoagulation.

For patients who are refractory to adequate anticoagulation and develop progressive neurologic deterioration, endovascular treatment including intrasinus thrombolysis or mechanical thrombectomy may be treatment options [9].

References

1. Stam J. Current concepts: thrombosis of the cerebral veins and sinuses. N Engl J Med. 2005;352:1791–8.
2. Leach JL, Fortuna RB, Jones BV, Gaskill-Shipley MF. Imaging of cerebral venous thrombosis: current techniques, spectrum of findings, and diagnostic pitfalls. Radiographics. 2006;26:S19. https://doi.org/10.1148/rg.26si055174.
3. Black DF, Rad AE, Gray LA, Campeau NG, Kallmes DF. Cerebral venous sinus density on noncontrast CT correlates with hematocrit. Am J Neuroradiol. 2011;32:1354–7.
4. Besachio DA, Quigley EP, Shah LM, Salzman KL. Noncontrast computed tomographic Hounsfield unit evaluation of cerebral venous thrombosis: a quantitative evaluation. Neuroradiology. 2013;55:941–5.
5. Buyck PJ, De Keyzer F, Vanneste D, Wilms G, Thijs V, Demaerel P. CT density measurement and H:H ratio are useful in diagnosing acute cerebral venous sinus thrombosis. Am J Neuroradiol. 2013;34:1568–72.
6. Buyck PJ, Zuurbier SM, Garcia-Esperon C, et al. Diagnostic accuracy of noncontrast CT imaging markers in cerebral venous thrombosis. Neurology. 2019;92:E841–51.
7. Patel D, Machnowska M, Symons S, Yeung R, Fox AJ, Aviv RI, Maralani PJ. Diagnostic performance of routine brain MRI sequences for dural venous sinus thrombosis. Am J Neuroradiol. American Society of Neuroradiology. 2016;37:2026–32.
8. Liang L, Korogi Y, Sugahara T, et al. Evaluation of the intracranial dural sinuses with a 3D contrast-enhanced MP-RAGE sequence: prospective comparison with 2D-TOF MR venography and digital subtraction angiography. Am J Neuroradiol. 2001;22:481–92.
9. Lee SK, Mokin M, Hetts SW, Fifi JT, Bousser MG, Fraser JF. Current endovascular strategies for cerebral venous thrombosis: report of the SNIS standards and guidelines committee. J Neurointerv Surg. 2018;10:803–10.

Cerebral Vasculopathy: CNS Vasculitis, RCVS, and PRES

5

Yang Tang and Xinli Du

5.1 Introduction

Cerebral vasculopathy is a heterogeneous group of diseases associated with intracranial arterial contour irregularity, luminal stenosis, and wall thickening. Collectively, cerebral vasculopathies are the most common causes of stroke in children and young adults [1, 2]. Despite different etiologies and treatment options, these diseases can have rather similar findings on brain parenchymal and vascular luminal imaging, therefore posing great diagnostic and therapeutic challenges. The differential considerations for cerebral vasculopathy include:

- Primary angiitis of CNS (PACNS)
- CNS vasculitis secondary to intracranial infections, systemic vasculitis, or connective tissue diseases
- Intracranial atherosclerotic disease (ICAD)
- Reversible cerebral vasoconstriction syndrome (RCVS)
- Posterior reversible encephalopathy syndrome (PRES)
- Moyamoya disease/syndrome
- Radiation- or drug-related vasculopathy
- Focal cerebral arteriopathy in pediatric patients
- Amyloid angiopathy in elderly patients
- Genetic diseases such as CADASIL

This chapter will focus on CNS vasculitis, RCVS, and PRES. Other cerebral vasculopathies will be discussed in the next chapter.

5.2 CNS Vasculitis

CNS vasculitis refers to a group of diseases that result in inflammation and destruction of the blood vessels of the brain, spinal cord, and meninges. It can be classified into primary and secondary types.

5.2.1 Secondary CNS Vasculitis

Secondary CNS vasculitis is more common than the primary type and can occur following CNS infection, systemic vasculitis, or connective tissue disease.

Many infectious processes can cause intracranial vasculitides, including septic meningitis, mycobacterium tuberculosis, and spirochetal (neurosyphilis, neuroborreliosis), viral (varicella-zoster, HIV, hepatitis C, etc.), fungal (aspergillosis, mucormycosis), and parasitic (cysticercosis) CNS infections (Fig. 5.1).

Systemic connective tissue diseases such as systemic lupus erythematosus, Sjögren syndrome, rheumatoid arthritis, and scleroderma can also have intracranial manifestations.

Systemic vasculitides can have intracranial involvement and have been classified based on the size of the involved vessels according to Chapel Hill classification and American College of Rheumatology [3, 4]. Large vessel vasculitis includes Takayasu and giant cell arteritis; medium vessel vasculitis includes polyarteritis nodosa and Kawasaki disease; and small vessel vasculitis includes IgA vasculitis, microscopic polyangiitis, granulomatosis with polyangiitis (Wegener's granulomatosis), and eosinophilic granulomatosis with polyangiitis (Churg–Strauss). Behcet disease and Cogan syndrome can affect vessels of variable sizes.

Patients of secondary vasculitis usually have clinical presentations involving multiple organs. Systemic manifestations such as fever, malaise, weight loss, and arthralgia are common and are frequently accompanied by elevated inflammatory markers such as erythrocyte sedimentation rate (ESR) and C-reactive protein (CRP) and positive serological tests such as antinuclear antibody (ANA), antineutrophil cytoplasmic antibody (ANCA), etc. Diagnoses are usually made before patients develop intracranial diseases.

© Springer Nature Switzerland AG 2020

Y. Tang, *Atlas of Emergency Neurovascular Imaging*, https://doi.org/10.1007/978-3-030-43654-4_5

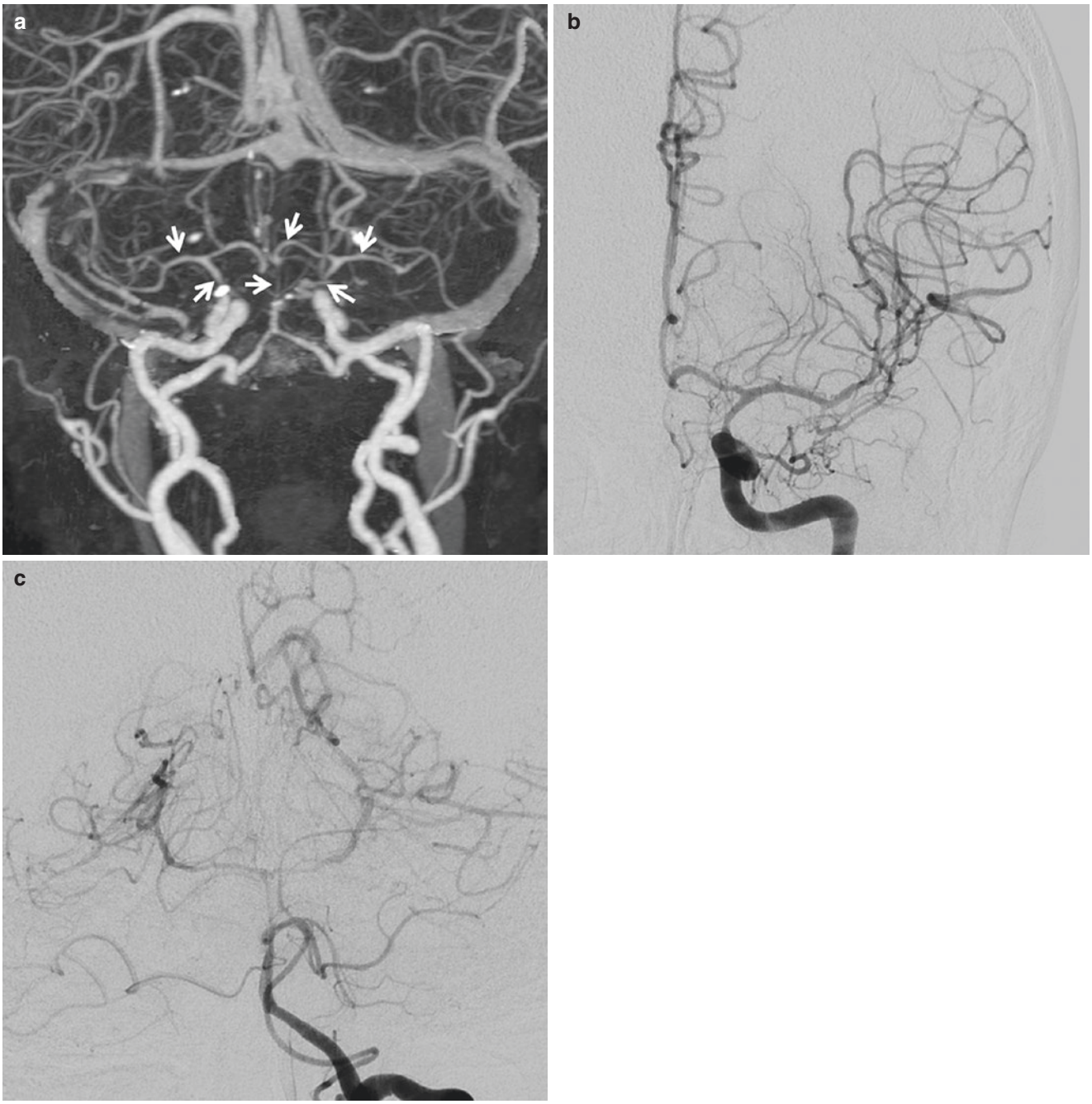

Fig. 5.1 Vasculitis or vasospasm secondary to meningitis. Patient with pneumococcal meningitis develops sudden onset of left-sided weakness. MRI shows acute left parietal lobe infarction (not shown). (**a**) CTA 3D reconstruction shows diffuse narrowing of the basilar artery and bilateral supraclinoid ICA, MCA, and ACA (*arrows*) compared to the normal caliber of extracranial arteries. The PCAs are not opacified. (**b**) DSA of left ICA injection shows diffuse narrowing/vasospasm of the left supraclinoid ICA, MCA, and ACA. (**c**) DSA of left vertebral injection shows diffuse narrowing/vasospasm of the basilar artery and bilateral PCAs

5.2.2 Imaging Modality of CNS Vasculitis

It is worth noting that all the intracranial arteries are classified as medium or small vessels based on the above classification schemes that are designed for systemic vasculitis, but this is different from the conventions used in radiology literature. For example, supraclinoid ICAs, intracranial vertebral arteries, basilar artery, and M1, A1, and P1 segments are generally considered as large intracranial vessels by radiologists, while these are classified as systemic medium vessels by the rheumatology classifications. Vessels distal to the MCA bifurcations and anterior and posterior communicating arteries are considered as medium-sized vessels by both radiology and rheumatology classifications.

The large intracranial arteries and proximal medium-sized vessels (M2, A2, P2 segments) can usually be well evaluated by a high-quality CT angiography using 64-slice or greater CT, or 3-T time-of-flight MR angiography. MRA using 1.5 T magnet is adequate for large intracranial arteries but limited for medium-sized arteries due to flow artifacts and tortuosity of the vessels. With superb spatial (up to 0.2 mm) and temporal (0.25 second) resolution, catheter angiography remains the reference standard angiographic technique for vasculitis evaluation. The overall sensitivity of angiography in detecting CNS vasculitis has been estimated at between 50% and 90% [5]. The smallest arteries and arterioles in the brain parenchyma as well as the capillaries and proximal venules are considered small vessels that are beneath the resolution of angiography, thus requiring tissue biopsy to diagnose vasculitic involvement.

5.2.3 Primary Angiitis of CNS (PACNS)

PACNS is confined to the CNS with no involvement of other organs or systems. Despite increased awareness, it remains a very rare disorder with the incidence of 2.4 cases per one million population each year [6]. Most patients suspected of having PACNS based on cerebral angiography will actually have different diagnosis. The mean age of onset is 50 years, and men are affected twice as often as women.

The clinical presentations of PACNS are nonspecific. Many patients present with subacute onset progressive headache, cognitive impairment, and encephalopathy. Thirty to fifty percent of the patients have recurrent strokes and transient ischemic attacks [6]. Compared to secondary vasculitis, systemic symptoms are lacking.

MRI brain is the imaging modality of choice for the parenchymal changes of PACNS. Abnormal findings are present in nearly 100% of patients, although these findings are mostly nonspecific. MRIs may be abnormal even when catheter angiograms are normal, given many cases are due to small vessel vasculitis. In patients of PACNS, T2/FLAIR hyperintense lesions are commonly seen in the subcortical and deep white matter, central gray matter, and cerebral cortex, which are rather nondescript and difficult to distinguish from the garden variety small vessel ischemic diseases from chronic hypertension, diabetes, etc. Sometimes the white matter involvement is confluent and can mimic demyelinating process. Ischemic infarctions are common, often multiple, bilateral, involving different vascular territories, and in various ages. Mass-like lesions, parenchymal/leptomeningeal enhancement, and intracranial hemorrhages can be seen in a minority of patients.

Multifocal, alternating areas of arterial stenosis and dilatation, commonly referred to as "beading," involving multiple vessels in different vascular territories, are the hallmark for CNS vasculitis (Fig. 5.2). Abrupt vascular truncation,

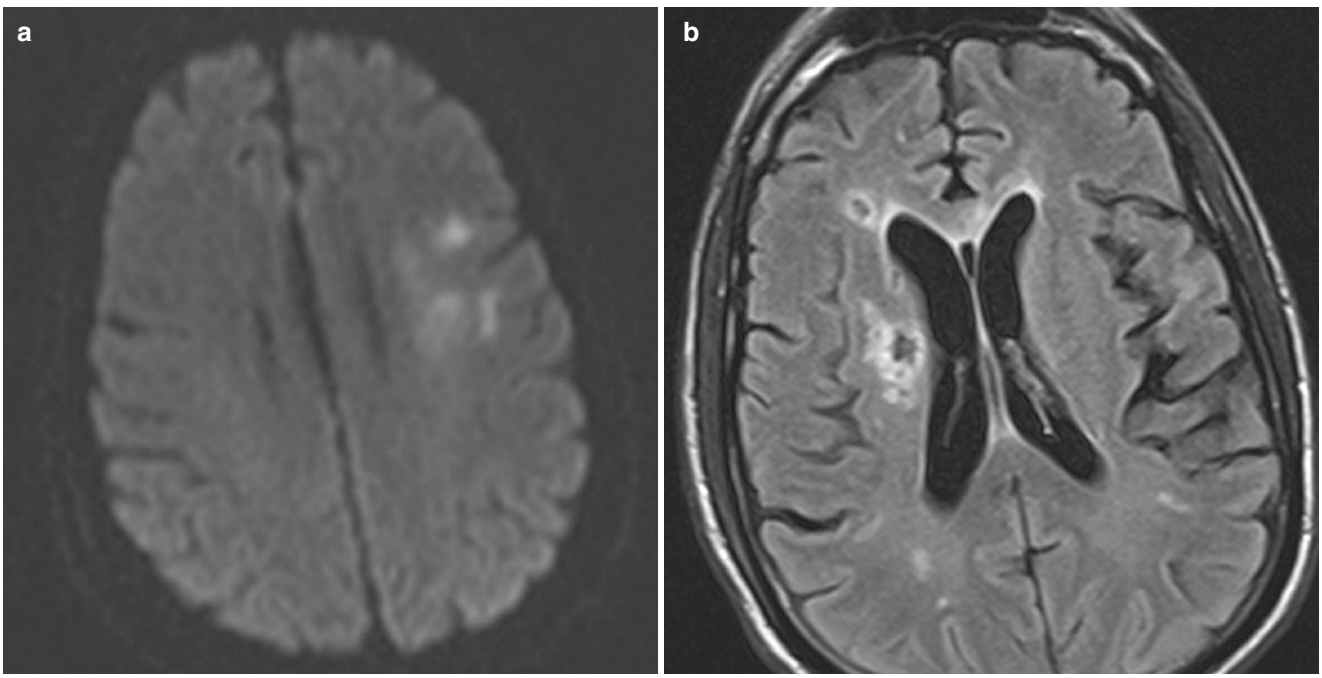

Fig. 5.2 Primary angiitis of CNS. A 35-year-old with progressive weakness and mental status decline. (**a**) DWI shows an acute to subacute infarction in the left corona radiata. (**b**) Axial FLAIR shows several additional chronic lacunar infarctions most prominent in the right basal ganglia. (**c**, **d**) 3D TOF MRA axial (**c**) and sagittal (**d**) reformations show multi-segmental stenosis of bilateral distal MCAs and PCAs with beaded appearance, compatible with medium vessel vasculopathy. (**e, f**) Catheter angiograms of left ICA injection (**e**) and vertebral injection (**f**) confirm the findings of MRA. This case is proven to be vasculitis by brain biopsy

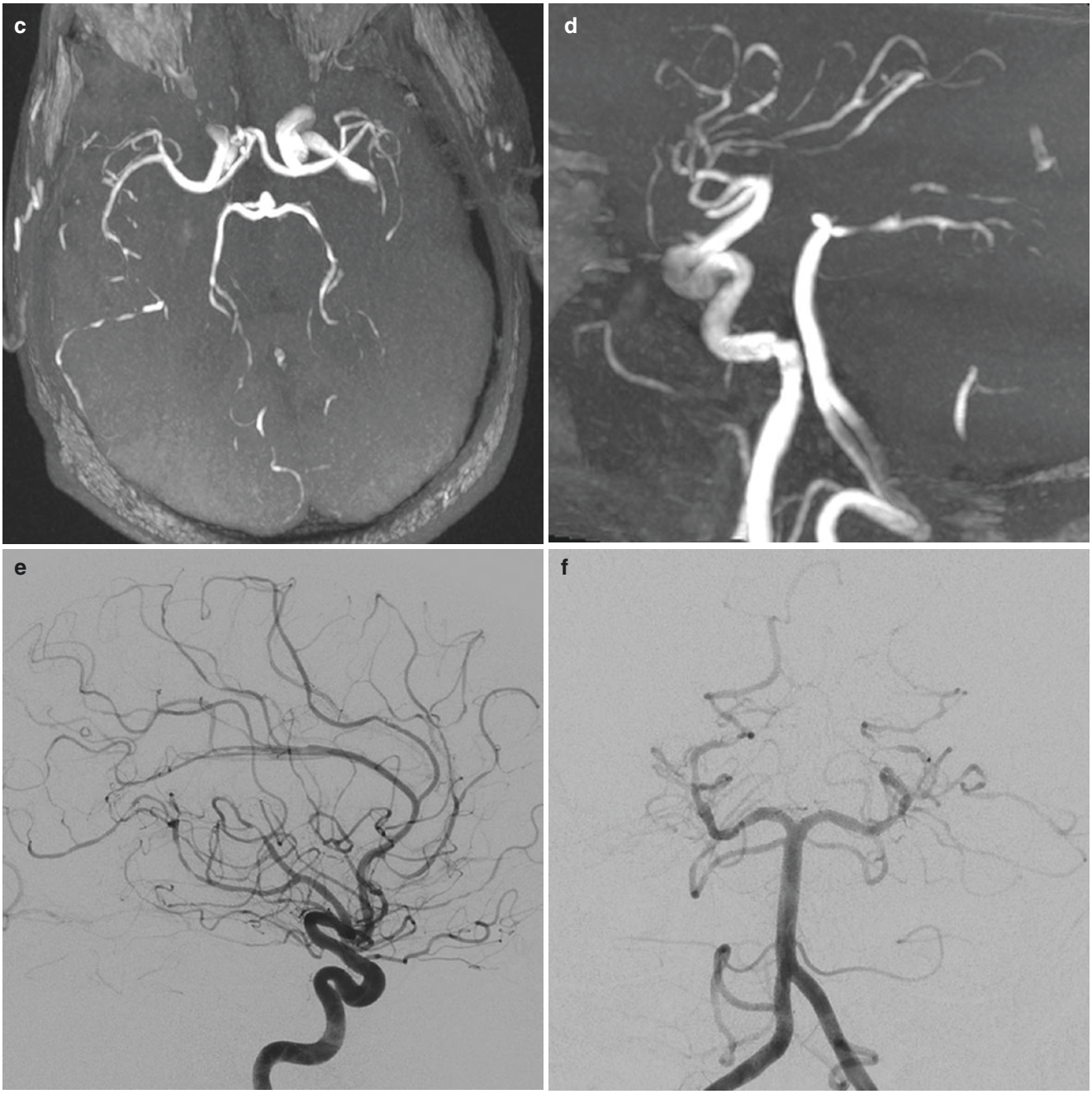

Fig. 5.2 (continued)

occlusion, and microaneurysms are more commonly seen in secondary vasculitis than PACNS. Compared to vasculitis, atherosclerosis typically involves regions of high shear stress and laminar flow disruption especially at vascular branch points such as carotid bifurcations and cavernous segments and is frequently associated with calcifications, although luminal angiography has low specificity to distinguish vasculitis, atherosclerosis, RCVS, or other cerebral vasculopathies.

Cerebrospinal fluid analysis should be performed on all patients suspected to have PACNS, which typically shows mild lymphocytic pleocytosis, elevated protein, and normal glucose level. Cultures and serologies should be performed to exclude infections and systemic vasculitis.

Brain parenchymal and leptomeningeal biopsy should be performed in suspected PACNS cases to confirm the diagnosis and exclude alternative diagnoses. Given the skipping and segmental nature of these vasculitic lesions, false-negative

biopsies can occur due to sampling error. The diagnostic yield improves if the biopsy is targeted at the affected areas on MRI, especially the areas with abnormal leptomeningeal enhancement.

Birnbaum et al. proposed the revised diagnostic criteria for PACNS based on the level of diagnostic certainty [7]:

1. Definite diagnosis, if confirmed by tissue diagnosis
2. Probable diagnosis, if there are high-probability findings on an angiogram and abnormal findings on MRI and CSF profile is consistent with PACNS but in the absence of tissue confirmation

Treatment of PACNS consists of long-term steroid and cytotoxic immunosuppressant such as cyclophosphamide.

5.3 RCVS

5.3.1 Definition of RCVS

The reversible vasoconstriction syndrome (RCVS) is a distinct clinical and radiological entity characterized by severe thunderclap headache and vasoconstriction of cerebral arteries, which resolves spontaneously within 3 months [8]. It has been described in the literature since the early 1970s under various names such as Call–Fleming syndrome, benign angiopathy of CNS, postpartum angiopathy, migrainous vasospasm, drug-induced angiopathy, sexual headache, etc. Once considered rare, it has become increasingly recognized due to better awareness of this condition and routine use of noninvasive vascular imaging.

5.3.2 Clinical Presentation

RCVS mainly affects young and middle-aged adults aged 20–50 years and more commonly women [8]. The most common clinical feature is sudden onset of severe headache (thunderclap headache, TCH), which reaches peak intensity in seconds to 1 min and usually abates over 1–3 hours. Many patients suffer from recurrent TCH over 1–4 weeks. Other presentations include seizure or focal neurological deficits including visual disturbance, sensory symptoms, hemiplegia, ataxia, aphasia, etc. These deficits are mostly transient, although a small percentage of patients can have unfavorable outcomes and permanent neurological deficits due to infarction and intracranial hemorrhage. A small percentage of patients do not present with headaches and are only diagnosed based on reversible angiographic findings and exclusion of PACNS.

In more than 50% of patients, a precipitating or triggering event can be identified [8]. These include various vasoactive or sympathomimetic medications such as selective serotonin reuptake inhibitors, recreational substance (cannabis, cocaine), binge alcohol drinking, postpartum status, traumatic cervical vascular injury, physical exertion, sexual activity, etc.

In most cases of RCVS, CSF analysis will be unremarkable or with mildly elevated cell count and protein. Serum inflammatory markers such as erythrocyte sedimentation rate and C-reactive protein are usually within normal limits in patients with RCVS.

Recently, Rocha et al. developed a simple quantitative scoring system (RCVS2) to distinguish RCVS from PACNS and other arteriopathies in the acute setting. The score ranged from −2 to +10. It was shown that a score ≥ 5 diagnosed RCVS with 90% sensitivity and 99% specificity and a score ≤ 2 excluded RCVS with 85% sensitivity and 100% specificity [9]. The score includes R (recurrent or single thunderclap headaches +5), C (intracranial carotid artery involvement scores −2), V (vasoconstrictive trigger +3), S (female sex +3), and S (convexity subarachnoid hemorrhage +1).

5.3.3 Conventional Imaging

CT and CTA are often the first diagnostic modalities obtained in emergency departments to exclude aneurysmal subarachnoid hemorrhage (SAH) in patients presenting with thunderclap headaches. MRI/MRA are occasionally performed.

Many RCVS patients have normal findings on brain parenchymal imaging. Small SAH can occur in RCVS, but with a characteristic sulcal/cortical distribution along the high cerebral convexity. This is distinguished from the diffuse cisternal SAH along the base of the brain, which typically occurs following aneurysm rupture. Other causes for the cortical/sulcal SAH include trauma, PRES, cerebral venous thrombosis, and in elderly patients amyloid angiopathy. RCVS can occasionally cause intraparenchymal hemorrhage, cerebral edema, infarctions, or PRES-like appearance. Infarctions are usually multifocal, bilateral, and in watershed distribution, due to severe vasoconstriction and diminished blood flow.

Hyperintense vessels on FLAIR sequence have been reported and can precede the detection of vasoconstriction in RCVS [10]. This finding is nonspecific and likely reflects abnormal flow in the distal cortical or leptomeningeal arteries. It can also be seen in cases of proximal arterial stenosis from atherosclerosis and moyamoya disease and needs to be distinguished from subarachnoid hemorrhage or meningitis.

Vascular imaging (CTA, MRA, DSA) can demonstrate cerebral vasoconstriction of large to medium arteries in different vascular territories, with multi-segmental narrowing interspersed with normal caliber vessels resulting in a beaded appearance, frequently indistinguishable from vasculitis (Fig. 5.3). CTA and MRA have sensitivity of 80% in diagnosing RCVS [11]. It is worth noting that the initial vascular evaluation in RCVS may be unremarkable in the first few days after symptom onset. In fact, some patients with suspected RCVS may never have evidence of vasoconstriction

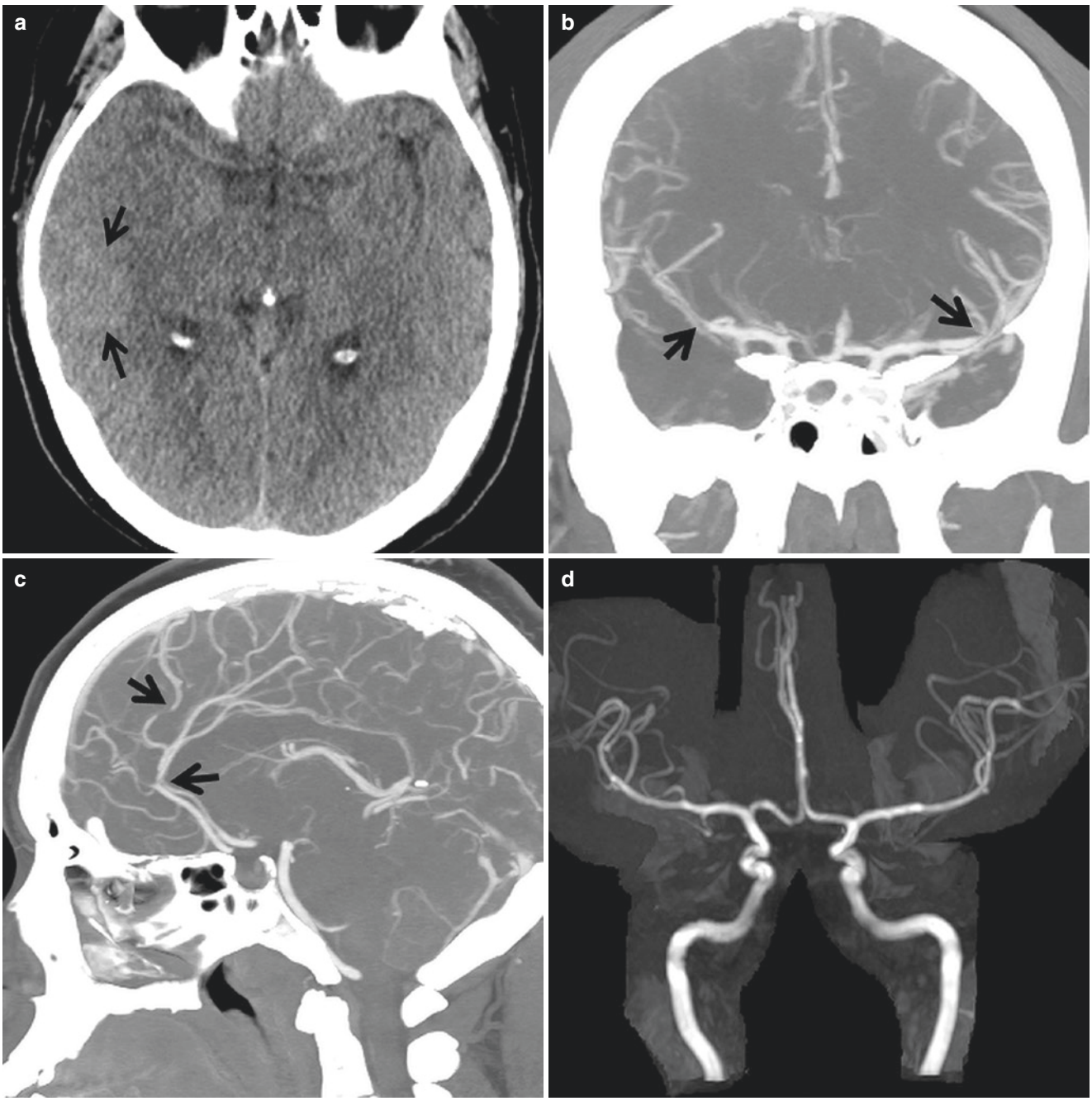

Fig. 5.3 Reversible cerebral vasoconstriction syndrome. A 24-year-old presents with thunderclap headache. (**a**) NCCT shows small subarachnoid hemorrhage in the right temporal sulci. (**b**) CTA coronal MIP shows narrowing the bilateral MCA M2 segments (*arrows*). (**c**) CTA sagittal MIP shows narrowing of bilateral ACA A3 segments. (**d**) TOF MRA 3 months later demonstrates interval resolution of previously seen multifocal vasospasm

on neuroimaging. This may reflect the fact that vasoconstriction may start in the peripheral small vessels beneath the resolution of angiogram and subsequently migrate centripetally to involve medium and large cerebral arteries and become more visible on neurovascular imaging [12].

Catheter angiography has superior spatial and temporal resolution when evaluating distal intracranial medium-sized vessels and remains the reference standard. It is especially valuable in cases when clinical diagnosis is equivocal and noninvasive vascular imaging is negative. In addition, intra-arterial administration of calcium channel blocker during catheter angiography may help confirm the reversibility of vasoconstriction, thus providing additional diagnostic information and being therapeutic as well [13, 14].

Besides indirect and direct angiography, transcranial Doppler (TCD) provides an alternative noninvasive way to monitor for response to pharmacological therapies and resolution of vasoconstriction by measuring mean and peak blood flow velocities in proximal cerebral arteries around the circle of Willis in RCVS patients [10].

5.3.4 MRI Vessel Wall Imaging of Cerebral Vasculopathy

High-resolution MRI vessel wall imaging (VWI) is an emerging technique for the evaluation of intracranial arterial wall pathology. Complementary to the conventional luminal imaging modalities, VWI has been used as a clinical tool to differentiate various cerebral vasculopathies including vasculitis, RCVS, and intracranial atherosclerosis (ICAD). VWI requires multiplanar 2D or 3D acquisitions, high spatial resolution, and suppression of CSF and intraluminal blood signal [15].

Both T1- and T2-weighted sequences have been used in characterization of vessel wall pathology. Vasculitis is associated with circumferential wall thickening and intense wall enhancement on the postcontrast T1 sequence. ICAD cases typically show eccentric wall thickening and enhancement. RCVS is characterized by mild diffuse circumferential wall thickening with negligible-to-mild wall enhancement [16]. It is worth noting that overlaps do occur among different vasculopathies. For example, vasculitis can show eccentric enhancement and ICAD can be circumferential in some cases [16]. On T2 sequence, atherosclerotic plaques are characterized by the presence of juxtaluminal T2 hyperintensity, representing the fibrous cap, and a deeper T2 hypointense component representing the lipid-rich necrotic core, while vasculitis and RCVS lesions do not have vessel wall T2 signal abnormality [17]. Recently, contrast-enhanced, high-resolution 3D VWI has been used to direct biopsies of intracranial vascular lesions with higher accuracy over the standard approach [18].

5.3.5 Treatment

Since the majority of RCVS cases are self-limiting, treatment mostly consists of removal of precipitating factors and symptomatic relief of headaches. Empiric treatment with calcium channel blockers can be used. Steroids are potentially harmful and should be avoided in RCVS [19].

5.4 PRES

Posterior reversible encephalopathy syndrome (PRES) is a neurological syndrome characterized by posterior dominant, relatively symmetric, and reversible cortical/subcortical vasogenic edema on imaging. Patients usually present with headache, altered mental status, seizures, and visual symptoms. It is associated with a number of clinical conditions including hypertension, preeclampsia/eclampsia, sepsis, chemotherapy, autoimmune diseases/immunosuppression, organ transplantation, etc. [20].

Although the exact mechanism is uncertain, PRES is likely related to disruption of cerebral autoregulation resulting in breakthrough of blood–brain barrier and leakage of fluid. The basic PRES edema pattern follows cerebral vascular border zones and most commonly involves the parieto-occipital areas, followed by the frontal and temporal lobes and cerebellum [21]. PRES can occasionally involve basal ganglia, thalami, and brain stem with sparing of cortex/subcortex, the so-called central variant [21]. Unilateral hemispheric and spinal cord involvement also rarely occurs. Though most patients present with reversible vasogenic edema, atypical imaging features are frequently encountered, including diffusion restriction indicating ischemic injury, parenchymal/subarachnoid hemorrhage, and postcontrast parenchymal/leptomeningeal enhancement.

RCVS and PRES share many clinical-radiologic features and pathophysiological elements. RCVS can present with PRES type of edema pattern. Many PRES patients have angiographic findings of vasoconstriction interspersed with normal vessels or vasodilation and even a string-of-beads appearance resembling RCVS or vasculitis (Fig. 5.4) [20].

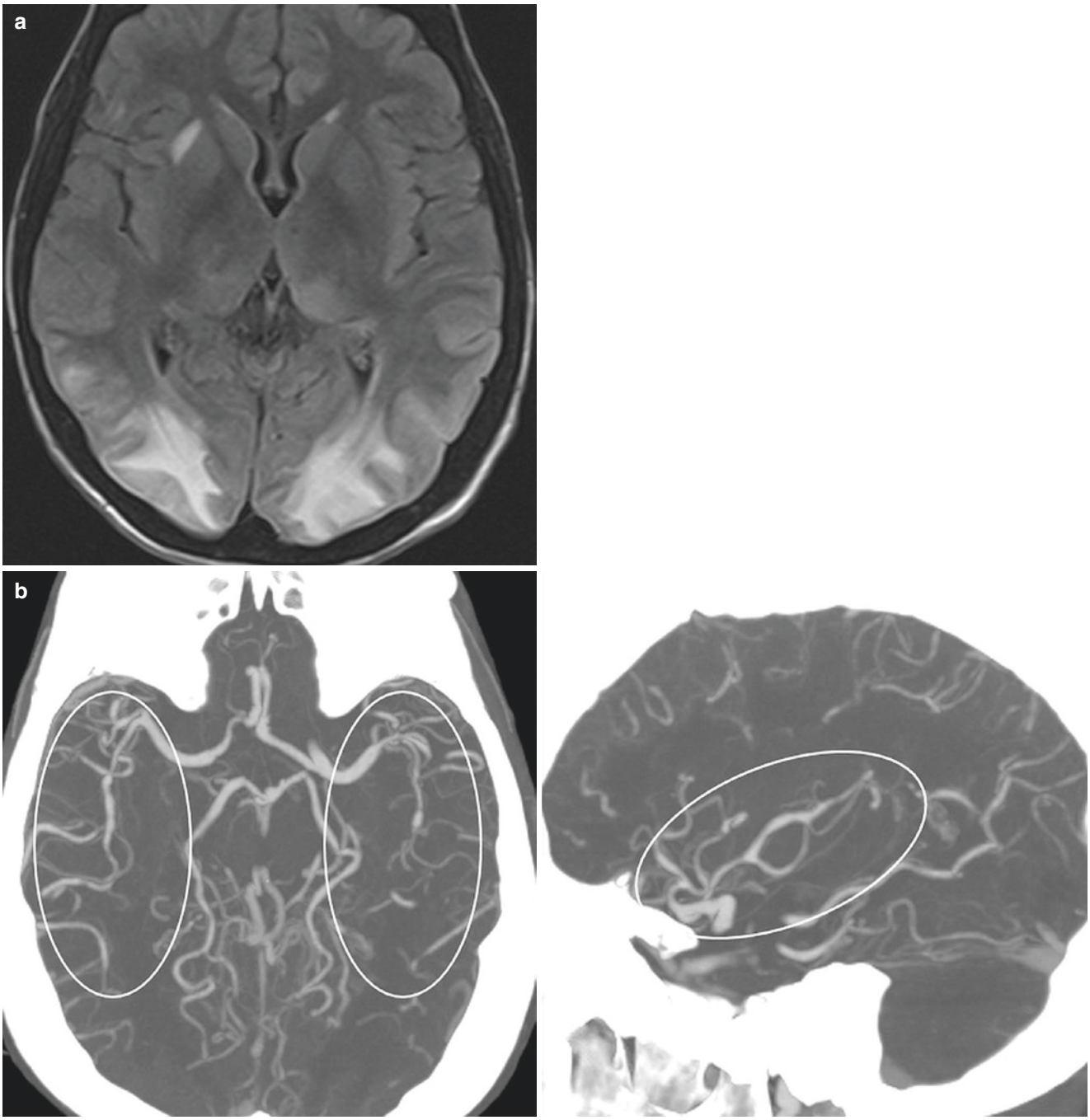

Fig. 5.4 Posterior reversible encephalopathy syndrome. Patient with seizure and altered mental status. (**a**) Axial FLAIR shows symmetric vasogenic edema most prominent in the bilateral occipital lobes compatible with PRES type of pattern. (**b**) CTA head axial and sagittal reformations demonstrate multifocal contour irregularity and beaded appearance of bilateral MCAs (*circle*). (**c**) DSA confirms multifocal arterial irregularity involving both anterior and posterior circulation. (**d**) Repeat CTA in 3 months shows resolution of vascular irregularity as compared to (**b**)

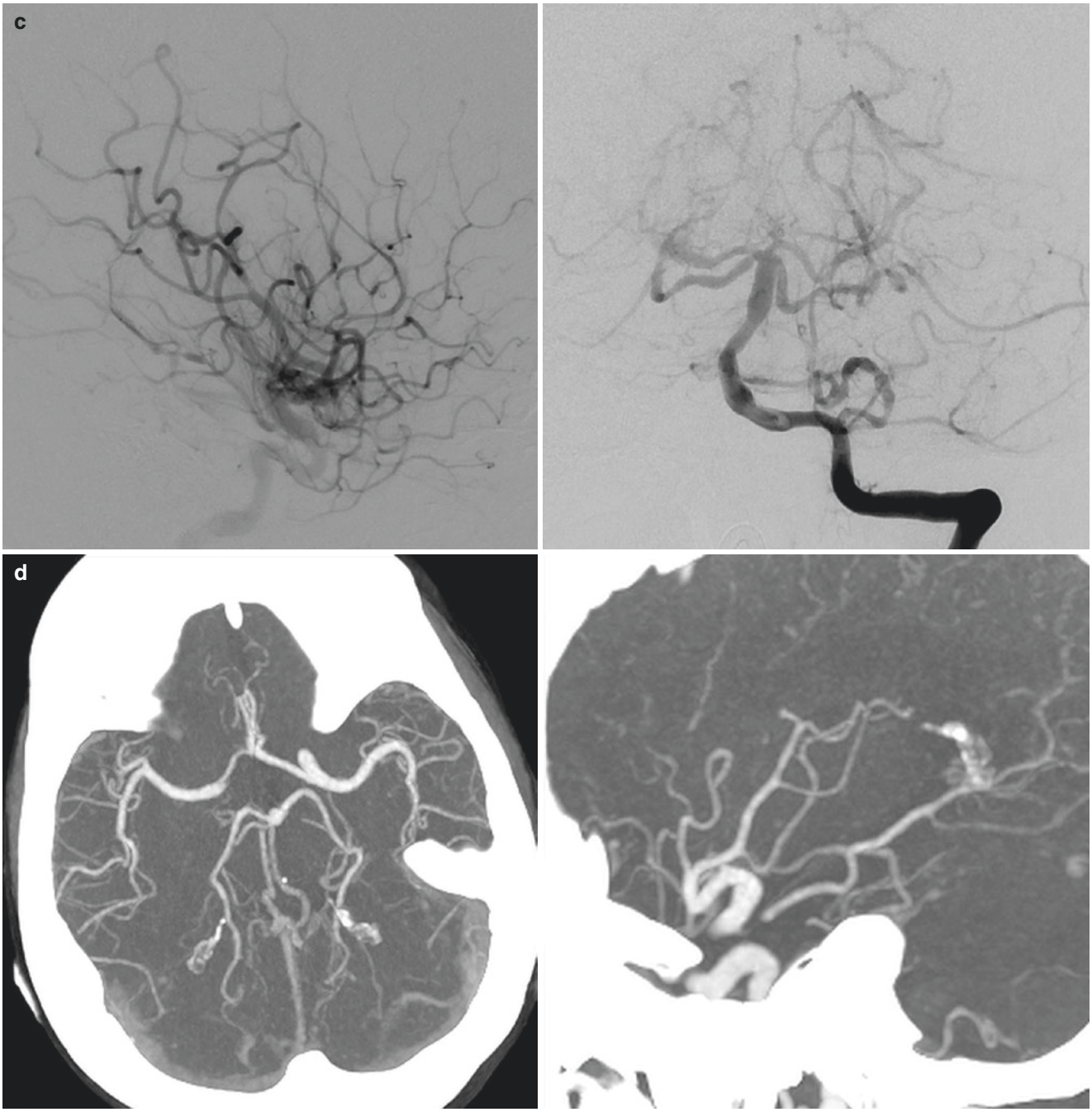

Fig. 5.4 (continued)

References

1. Kittner SJ, Stern BJ, Wozniak M, et al. Cerebral infarction in young adults: the Baltimore-Washington Cooperative Young Stroke Study. Neurology. 1998;50:890–4.
2. Mackay MT, Wiznitzer M, Benedict SL, Lee KJ, Deveber GA, Ganesan V, International Pediatric Stroke Study Group. Arterial ischemic stroke risk factors: the international pediatric stroke study. Ann Neurol. 2011;69:130–40.
3. Hunder GG, Arend WP, Bloch DA, et al. The American College of Rheumatology 1990 criteria for the classification of vasculitis: introduction. Arthritis Rheum. 1990;33:1065–7.
4. Porter RT. Nomenclature of systemic vasculitides: proposal of an international consensus conference. Radiology. 1995;194:750–750.
5. Birnbaum J, Hellmann DB. Primary angiitis of the central nervous system. Arch Neurol. 2009;66:704–9.
6. Salvarani C, Brown RD, Calamia KT, Christianson TJH, Weigand SD, Miller DV, Giannini C, Meschia JF, Huston J, Hunder GG. Primary central nervous system vasculitis: analysis of 101 patients. Ann Neurol. 2007;62:442–51.
7. Hajj-Ali RA, Calabrese LH. Diagnosis and classification of central nervous system vasculitis. J Autoimmun. 2014;48–49:149–52.
8. Calabrese LH, Dodick DW, Schwedt TJ, Singhal AB. Narrative review: reversible cerebral vasoconstriction syndromes. Ann Intern Med. 2007;146:34–44.

9. Rocha EA, Topcuoglu MA, Silva GS, Singhal AB. RCVS2 score and diagnostic approach for reversible cerebral vasoconstriction syndrome. Neurology. 2019;92:E639–47.
10. Chen S-P, Wang S-J. Hyperintense vessels: an early MRI marker of reversible cerebral vasoconstriction syndrome? Cephalalgia. 2014;34:1038–9.
11. Ducros A, Bousser MG. Reversible cerebral vasoconstriction syndrome. Pract Neurol. 2009;9:256–67.
12. Shimoda M, Oda S, Hirayama A, Imai M, Komatsu F, Hoshikawa K, Shigematsu H, Nishiyama J, Osada T. Centripetal propagation of vasoconstriction at the time of headache resolution in patients with reversible cerebral vasoconstriction syndrome. Am J Neuroradiol. 2016;37:1594–8.
13. Farid H, Tatum JK, Wong C, Halbach VV, Hetts SW. Reversible cerebral vasoconstriction syndrome: treatment with combined intra-arterial verapamil infusion and intracranial angioplasty. AJNR Am J Neuroradiol. 2011;32:E184–7.
14. Ioannidis I, Nasis N, Agianniotaki A, Katsouda E, Andreou A. Reversible cerebral vasoconstriction syndrome: treatment with multiple sessions of intra-arterial nimodipine and angioplasty. Interv Neuroradiol. 2012;18:297–302.
15. Mandell DM, Mossa-Basha M, Qiao Y, et al. Intracranial vessel wall MRI: principles and expert consensus recommendations of the American society of neuroradiology. Am J Neuroradiol. 2017;38:218–29.
16. Obusez EC, Hui F, Hajj-ali RA, Cerejo R, Calabrese LH, Hammad T, Jones SE. High-resolution MRI vessel wall imaging: spatial and temporal patterns of reversible cerebral vasoconstriction syndrome and central nervous system vasculitis. Am J Neuroradiol. 2014;35:1527–32.
17. Mahmud Mossa-Basha, William D. Hwang, Adam De Havenon M, Daniel Hippe, Niranjan Balu, Kyra J. Becker, David T. Tirschwell, Thomas Hatsukami, Yoshimi Anzai, Chun Yuan P. Multicontrast high-resolution vessel wall magnetic resonance imaging and its value in differentiating intracranial vasculopathic processes. No Title. https://doi.org/10.1161/STROKEAHA.115.009037;WGROUP:STRING:AHA.
18. Zeiler SR, Qiao Y, Pardo CA, Lim M, Wasserman BA. Vessel wall MRI for targeting biopsies of intracranial vasculitis. Am J Neuroradiol. 2018;39:2034–6.
19. Cappelen-Smith C, Fracp M, Calic Z, Cordato D. Reversible cerebral vasoconstriction syndrome: recognition and treatment. Curr Treat Options Neurol. 1940;19:21.
20. Bartynski WS. Posterior reversible encephalopathy syndrome, part 1: fundamental imaging and clinical features. Am J Neuroradiol. 2008;29:1036–42.
21. Bartynski WS, Boardman JF. Distinct imaging patterns and lesion distribution in posterior reversible encephalopathy syndrome. Am J Neuroradiol. 2007;28:1320–7.

Miscellaneous Cerebral Vasculopathy

6

Yang Tang

6.1 Moyamoya Vasculopathy

Moyamoya vasculopathy refers to a characteristic angiographic pattern of progressive stenosis/occlusion of distal intracranial ICAs and proximal circle of Willis vessels, with compensatory development of lenticulostriate, leptomeningeal, and dural collaterals. It can affect posterior circulation including the distal basilar artery and proximal posterior cerebral arteries in rare cases. *Moyamoya* means "puff of smoke" in Japanese, which has been used to describe the appearance of the collateral network seen on catheter angiography.

Moyamoya disease was first described in 1957. It has been observed in people of various ethnic backgrounds throughout the world although with a higher incidence in eastern Asian population and likely has a genetic predisposition. It has a bimodal age distribution, with peak incidence at approximately 5 years of age in children and then in adults of mid-40s and with nearly twice as many female patients as male patients [1]. Pathological analysis of the affected vessels reveals a non-inflammatory and non-atherosclerotic arteriopathy from a combination of hyperplasia of smooth muscle cells and luminal thrombosis [2].

Moyamoya syndrome refers to similar angiographic findings that are associated with many other medical conditions, including sickle cell disease, neurofibromatosis type I, Down syndrome, cranial radiation, intracranial infections, atherosclerosis, etc.

Most moyamoya patients present with ischemic symptoms (stroke or TIAs) secondary to vascular stenosis/occlusion, typically in the MCA territory or MCA/ACA border zones. Hemorrhage is more common in adults than children and can be intraventricular, intraparenchymal, or subarachnoid due to rupture of fragile collateral vessels. Other less common presentations include seizure, headache, choreiform movement, cognitive or psychiatric changes, etc.

CT can demonstrate infarction or hemorrhage although findings may be normal or very subtle in early stage of disease. MRI is the modality of choice, which demonstrates diminished flow voids in the distal ICAs and proximal MCAs and ACAs, as well as prominent flow voids of lenticulostriate collaterals within the basal cisterns and deep gray nuclei. It is more accurate than CT in determining the age and vascular distribution of the infarctions. FLAIR sequence can show bright signal within the sulci due to slow flow of engorged leptomeningeal collaterals ("ivy" sign). CTA/MRA/DSA demonstrate stenosis/occlusion of distal ICAs and proximal circle of Willis vessels with collateral formation (Fig. 6.1). Moyamoya disease can be classified into six progressive stages based on angiographic findings [3].

No effective treatment can reverse the primary disease process. Medical treatments including antiplatelet/anticoagulation and vasodilators can slow the progression of the disease. Selected patients with recurrent or progressive cerebral ischemic events and reduced cerebral perfusion reserve can be treated surgically by using the external carotid artery to revascularize the ischemic hemisphere through either direct or indirect approach. The direct approach is through the anastomosis of the external carotid artery (usually the superficial temporal artery [STA]) to a cortical branch of the middle cerebral artery (direct EC–IC bypass). Indirect type consists of the placement of STA or vascularized tissue supplied by STA in direct contact with the brain, leading to ingrowth of new blood vessels into the underlying cerebral cortex. There are multiple variations of the indirect anastomosis, such as encephaloduroarteriosynangiosis (EDAS), encephalomyoarteriosynangiosis (EMAS), and pial synangiosis [4].

Perfusion studies (SPECT, CT, or MRI perfusion) coupled with acetazolamide challenge may help identify patients with inadequate cerebral blood flow reserve and monitor the improvement after the surgery.

© Springer Nature Switzerland AG 2020
Y. Tang, *Atlas of Emergency Neurovascular Imaging*, https://doi.org/10.1007/978-3-030-43654-4_6

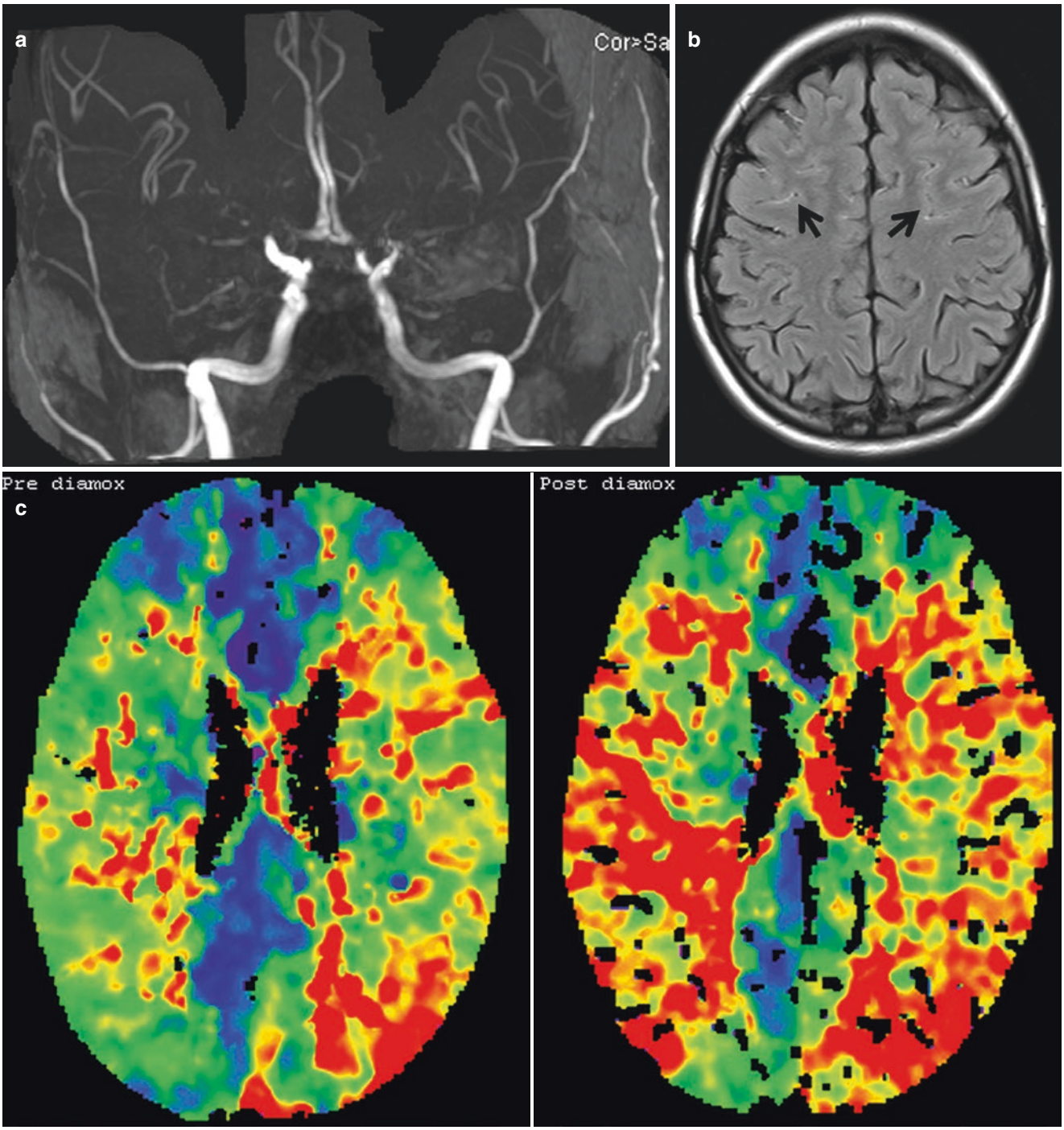

Fig. 6.1 Moyamoya vasculopathy. A 15-year-old with transient right-sided weakness. (**a**) 3D TOF MRA shows occlusion of bilateral ICA termini and M1 and A1 segments, consistent with moyamoya vasculopathy. (**b**) MRI FLAIR image shows hyperintense signals within the cortical sulci (arrows) representing leptomeningeal collaterals (ivy sign). (**c**) CT perfusion before Diamox challenge (left panel) shows prolongation of time to drain in the bilateral cerebral hemisphere suggestive of tissue at ischemic risk. After IV injection of Diamox (right panel), there is further prolongation of time to drain reflecting decreased cerebrovascular reserve

6.2 Radiation-Induced Vasculopathy

Complications from cranial radiation include radiation necrosis; leukoencephalopathy; vasculopathy; vascular malformations such as cavernous malformation, capillary telangiectasia, and aneurysm; as well as radiation-induced tumors. Cerebral vasculopathy is usually a late complication of cranial radiation. Patients may present with cerebral

ischemia or hemorrhage several months to many years after the radiation. The exact incidence is unknown, and the risk of developing vasculopathy is related to the dose and location of radiation as well as the patients' age when receiving radiation.

Radiation-induced vascular injury is a complex pathological process [5]. It starts with endothelial damage and disruption of blood–brain barrier, followed by thrombi formation and hemorrhage. Long-term changes include endothelial proliferation, thickening of basal membrane, adventitial fibrosis, and vascular remodeling [5]. In addition to inflammation, non-inflammatory mineralizing microangiopathy can also occur in pediatric patients, manifested as dystrophic calcifications on head CT.

Three angiographic patterns of radiation-induced vasculopathy have been reported including large vessel steno-occlusive disease involving intracranial ICAs and its proximal branches (Fig. 6.2), moyamoya collateral pattern accompanying the proximal occlusive vasculopathy, and diffuse multifocal stenosis of medium or small arteries mimicking vasculitis (Fig. 6.3) [6].

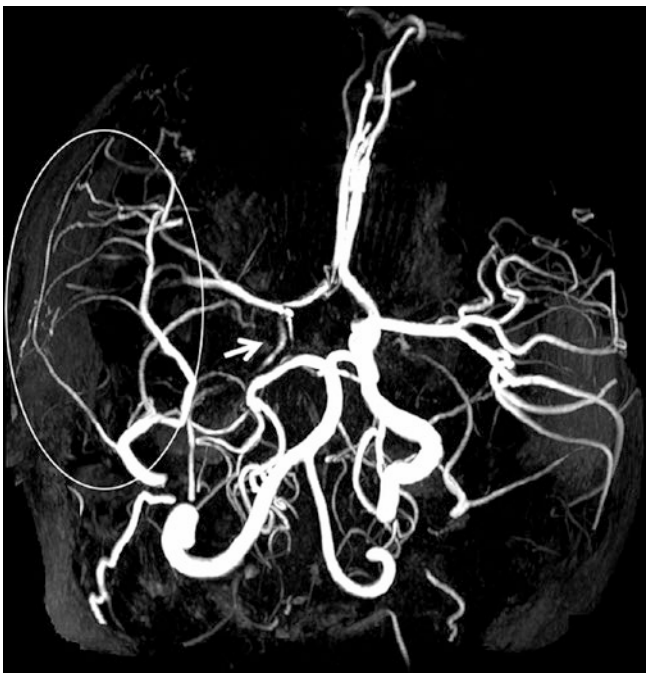

Fig. 6.2 Radiation-induced ICA occlusion. A 9-year-old with history of craniopharyngioma post-radiation presents with left-sided weakness. 3D TOF MRA demonstrates occlusion of right ICA at skull base (*arrow*). Note prominent meningeal collaterals reconstituting right MCA (*circle*)

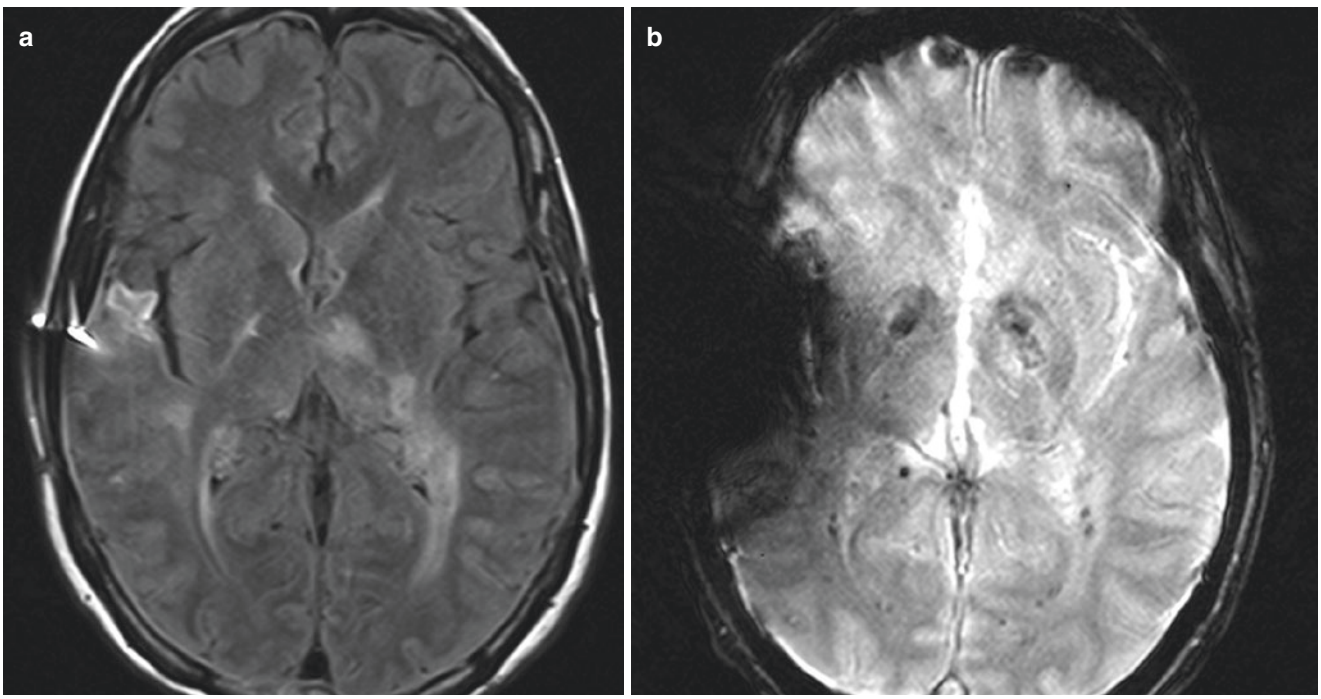

Fig. 6.3 Radiation-induced vasculopathy. A 31-year-old with history of medulloblastoma during childhood status post surgery and radiation presents with recurrent strokes. (**a**) Axial FLAIR shows infarction of left thalamus and periventricular white matter ischemic changes. (**b**) Axial GRE demonstrates multiple punctate foci of hemosiderin deposition likely reflecting microhemorrhages or cavernous malformations from remote cranial radiation. (**c**) Axial CTA MIP shows multifocal stenosis of bilateral MCA and PCA branches (*arrow*). (**d**) Coronal CTA MIP shows multifocal stenosis of left PICA

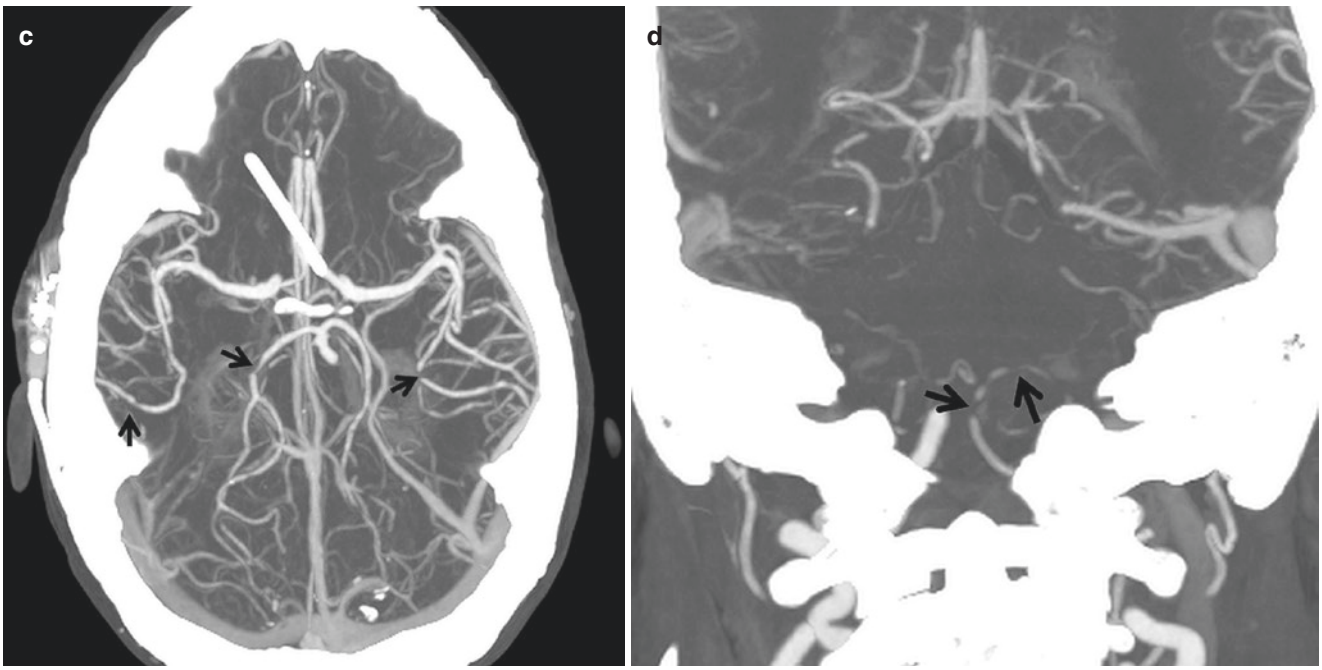

Fig. 6.3 (continued)

6.3 Drug-Induced Cerebral Vasculopathy

Neurological complications from illicit drug abuse (cocaine, heroin, etc.) are very common and mostly include hemorrhage, ischemia, and leukoencephalopathy.

Hemorrhage can be intraparenchymal or subarachnoid. Contrary to historic beliefs, approximately 40–50% of patients with cocaine-induced brain hemorrhage have an underlying vascular pathology, such as ruptured aneurysm or AVM [7], likely precipitated by the sympathomimetic effect of the drug. Angiography is important to identify these vascular malformations.

Drug-related cerebral ischemia are associated with multiple mechanisms, including reversible vasoconstriction/vasospasm, inflammatory vasculitis from immune-related response, direct procoagulant effects from cocaine, accelerated atherosclerosis, embolic events from impure additives, or septic emboli from infectious endocarditis [8]. Ischemic infarction can happen anywhere in the brain but most commonly in the MCA territory. It has been reported that mesencephalic infarction occurs more frequently when there is concurrent use of cocaine and amphetamine [8]. Angiographic studies reveal multifocal narrowing or occlusion of cerebral arteries (Fig. 6.4).

Confluent, symmetric, subcortical, and periventricular white matter T2 hyperintensity can be seen in cocaine users, reflecting chronic ischemic leukoencephalopathy. Heroin-induced leukoencephalopathy occurs exclusively following inhalation ("chasing the dragon"). Generalized cerebral edema can be seen in the acute phase, while the chronic or subacute heroin encephalopathy can result in a characteristic symmetric spongiform white matter degeneration predominantly affecting the white matter of the cerebellar hemispheres, posterior limb of the internal capsule, and the posterior cerebral white matter [8].

6.4 Childhood Stroke and Arteriopathy

Although relatively rare, stroke is an important cause of morbidity and mortality for children. The incidence is estimated at 2–13 per 100,000 person-year, slightly more common than brain tumors in this age group [9]. The risk factors for childhood acute ischemic stroke (AIS) are different from those of adults, as atherosclerosis is rare in pediatric population. Instead, childhood arteriopathy is increasingly recognized as an important cause of childhood AIS and a strong predictor of recurrence and of poor short-term outcome. It is defined as an in situ arterial abnormality on vascular imaging, not attributable to cardioembolism or congenital variant [10].

Differentiating arteriopathy from embolic strokes can be challenging. History of underlying congenital or acquired heart disease and infarctions involving multiple arterial territories are strong predictors for cardioembolism or artery-to-artery embolization. On vascular imaging, the most common abnormality in cardioembolic stroke is arterial occlusion, although this can also be seen in cases of arteri-

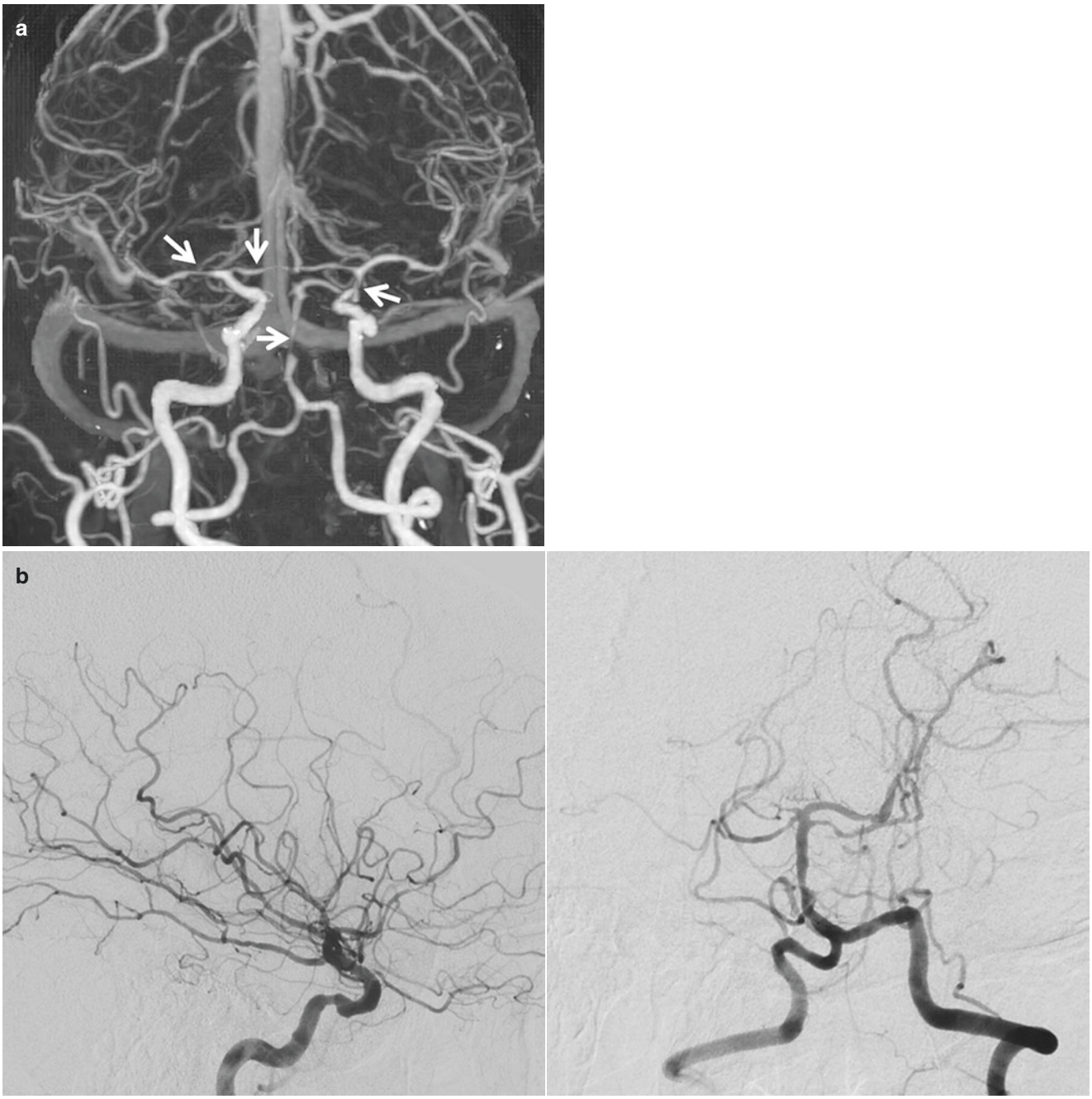

Fig. 6.4 Cocaine-induced vasculopathy. Patient with history of cocaine abuse presents with subarachnoid hemorrhage. (**a**) 3D CTA MIP image shows multifocal stenosis involving anterior and posterior circulation (*arrows*). There is severe stenosis of basilar artery. (**b**) Catheter angiograms with ICA and vertebral artery injections confirm multifocal stenosis. No aneurysm or AVM is identified

opathy. Arterial irregularity and stenosis are in favor of arteriopathy, although can also been in embolic stroke, due to partial recanalization of thrombi [10].

The definition of focal cerebral arteriopathy has evolved over the years, and many terms have been used interchangeably in the past including transient cerebral arteriopathy, post-varicella arteriopathy, childhood nonprogressive CNS angiitis, etc. The updated definition refers to unilateral stenosis/irregularity of intracranial anterior circulation including intracranial ICA and proximal MCA and ACA, which can be further classified into inflammatory type (FCA-i) and dissection type (FCA-d) [10]. Unilateral moyamoya disease is an important differential diagnosis for this pattern, which however typically progresses into bilateral cerebral arteriopathy over time and is accompanied with vascular collaterals.

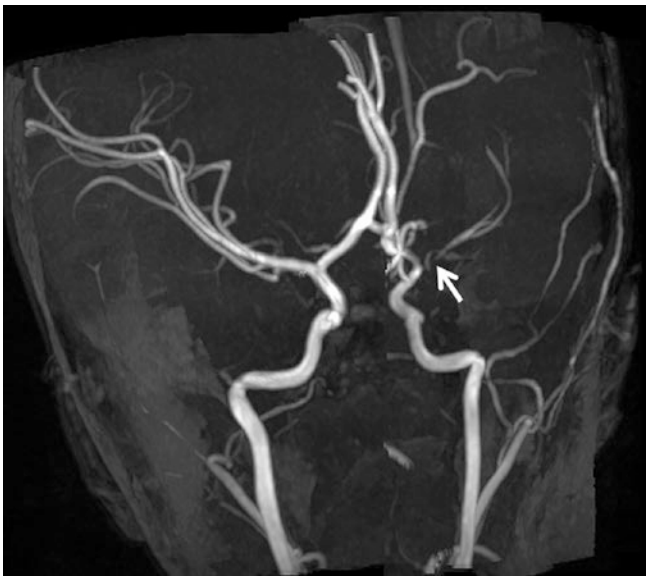

Fig. 6.5 Focal cerebral arteriopathy. A 2-year-old with left MCA stroke. 3D TOF MRA MIP demonstrates severe stenosis at the left MCA origin, suggestive of focal cerebral arteriopathy. Unilateral moyamoya vasculopathy and intracranial dissection are the main differential considerations

Although the exact pathogenesis is unknown, FCA-i is likely a focal inflammatory vasculitis and many patients have clinical history or serological evidence of recent viral exposure especially varicella-zoster. On imaging, it is associated with a small infarction volume < 25 cm^3 in the lenticulostriate territory [10]. Angiography shows narrowing of supraclinoid ICA and proximal MCA and ACA (Fig. 6.5). The banding pattern is considered pathognomonic, although was uncommon and only seen in 24% of patients with FCA-i [10]. Vessel wall imaging may show wall thickening and concentric enhancement [11]. FCA-i typically follows monophasic course, with progression of stenosis in some cases during the first 3–6 months followed by stabilization or less often normalization [12].

Intracranial dissection (FCA-d) is an important cause for pediatric AIS. Unlike adults, childhood anterior circulation dissections are more commonly intracranial and frequently without a preceding history of trauma. Compared to FCA-i, dissections tend to involve both supraclinoid ICA and M1 segment, are associated with a large infarction volume, and can involve the posterior circulation [10].

6.5 CADASIL

Chronic small vessel ischemic disease or leukoaraiosis is extremely common and in most cases is related to age and hypertension. However, the differential diagnosis is very broad, including but not limited to demyelinating disease, CNS vasculitis, infections such as Lyme disease or HIV encephalitis, neurosarcoidosis, toxic encephalopathy from radiation, chemotherapy or illicit drug use, adult-onset leukoencephalopathy, etc.

A minority of these patients have identifiable genetic causes, among which the most common and best known is cerebral autosomal dominant arteriopathy with subcortical infarcts and leukoencephalopathy (CADASIL). CADASIL is caused by mutations of the *NOTCH3* gene, which is predominantly expressed by vascular smooth muscle cells in small caliber arteries and by pericytes [13]. The clinical presentations include migraine with aura in early adulthood, recurrent subcortical infarctions leading to progressive cognitive impairment, depression, and other psychiatric disturbances.

MRI brain shows diffuse confluent white matter FLAIR/T2 hyperintensity and lacunar infarcts. The involvement of anterior temporal lobe and external capsule is more characteristic for CADASIL and allows differentiation from sporadic small vessel ischemic disease [14, 15]. Microbleeds occur frequently in CADASIL patients and can be identified by GRE or SWI sequence, but the pattern shows a significant overlap with other types of small vessel disease [16].

CADASIL patients rarely present with large territory ischemic infarctions. Angiography is mostly normal but occasionally shows multifocal segmental intracranial stenosis similar to vasculitis (Fig. 6.6) [13].

6.6 Cerebral Amyloid Angiopathy

Cerebral amyloid angiopathy (CAA) is a progressive vasculopathy caused by the deposition of amyloid in the brain parenchymal and leptomeningeal blood vessels.

According to Boston criteria [17, 18], the definitive diagnosis of CAA requires a postmortem examination. "Probable CAA with supporting pathology" can be made by histological examination of evacuated hematoma or cortical biopsy. The advances in neuroimaging have allowed the clinical diagnosis of CAA without brain biopsies. For example, in the absence of biopsy or autopsy, "probable CAA" can be diagnosed if multiple lobar hemorrhages are seen on MRI, and "possible CAA" can be diagnosed if there is single lobar hemorrhage on MRI, assuming there are no other identifiable causes of lobar hemorrhage or superficial siderosis.

There is a wide spectrum of imaging findings related to CAA, including intraparenchymal hematoma, microhemorrhages, convexity subarachnoid hemorrhage/superficial siderosis, white matter ischemic changes, and CAA-related inflammation.

CAA is a common cause of recurrent, spontaneous intraparenchymal hemorrhage in elderly patients. The hemorrhage

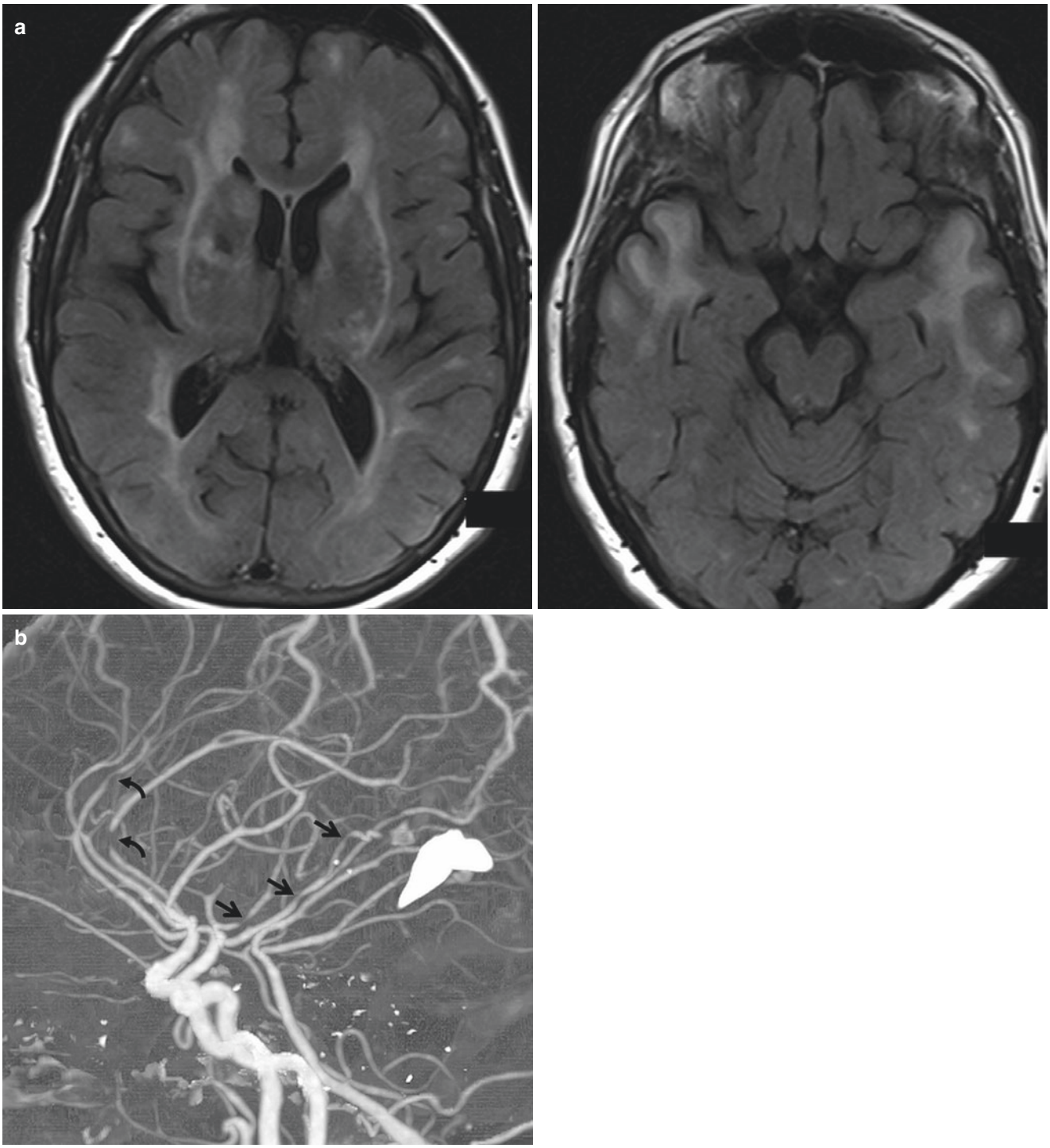

Fig. 6.6 CADASIL. Patient with recurrent strokes and mental decline. (**a**) Axial FLAIR images show confluent white matter disease with symmetric involvement of external capsules and anterior temporal lobe characteristic of CADASIL. (**b**) Sagittal MIP CTA shows multifocal stenosis of MCA and ACA branches (*arrows*)

is usually superficial, lobar, cortical, or subcortical in location, with irregular borders and surrounding edema (Fig. 6.7a). CAA-related hemorrhage can also occur in the cerebellum but not in the basal ganglia, thalami, and brain stem. MRI may show multiple hematomas in different ages with variable T1 and T2 signal intensities. SWI and GRE sequences typically show additional widespread asymptomatic foci of microhemorrhages in a similar lobar distribution.

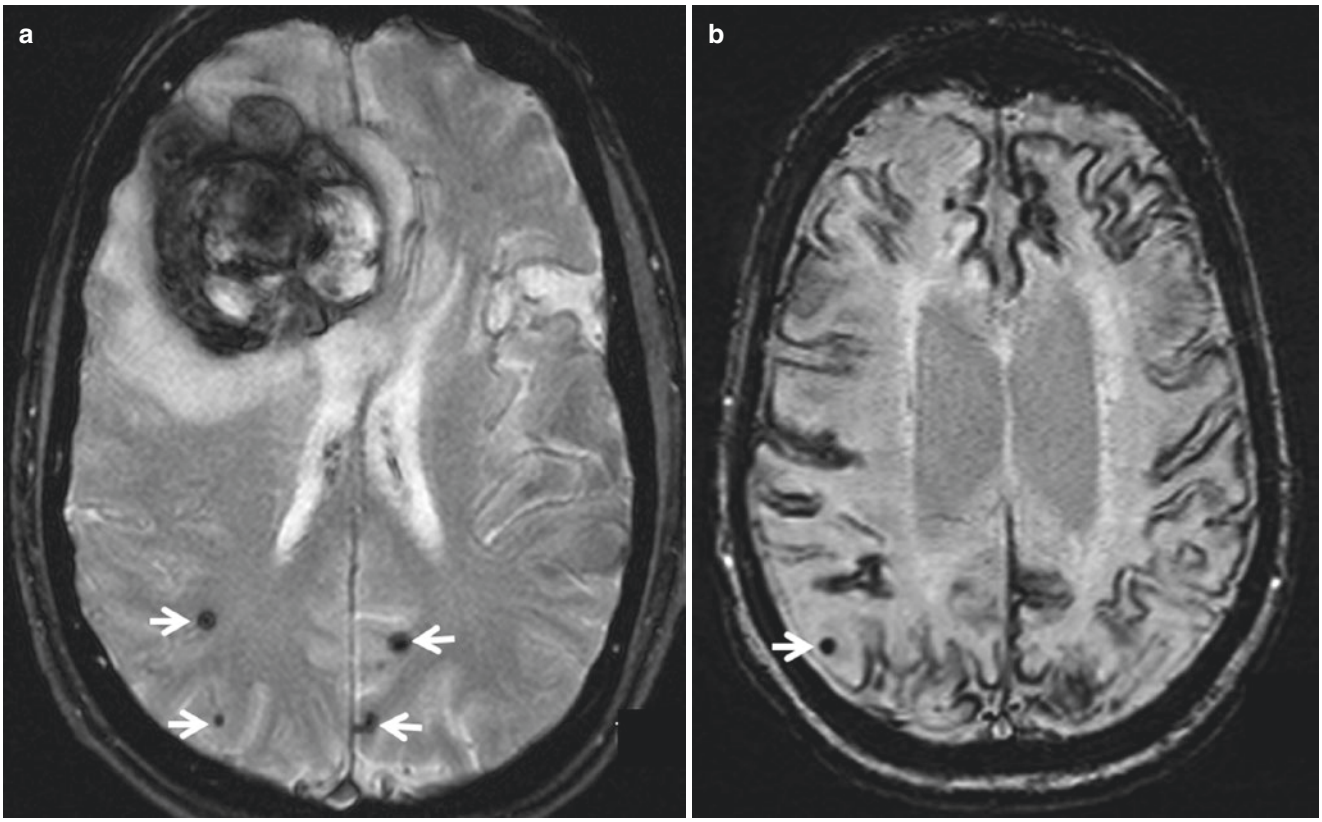

Fig. 6.7 Amyloid angiopathy. (**a**) Elderly patient presents with a large right frontal lobar hematoma seen on the GRE sequence. Several subcortical microhemorrhages in the bilateral occipital lobes (*arrows*) are consistent with amyloid deposition. (**b**) Patient with superficial siderosis from repeated subarachnoid hemorrhage on the SWI sequence. Note the additional subcortical amyloid deposition (*arrow*). Amyloid angiopathy is proven by biopsy

The sparing of deep gray matter and brain stem is the key differentiating feature from hypertensive hemorrhages. Besides CAA and hypertension, other common etiologies of intraparenchymal hemorrhage include vascular malformations (AVM, AVF, or cavernous malformation), underlying primary or metastatic tumors, coagulopathy, hemorrhagic transformation of ischemic infarction, cerebrovenous thrombosis, illicit drug use, etc. The differential diagnoses for multiple microhemorrhages include amyloid angiopathy, chronic hypertension, cavernous malformations, hemorrhagic metastasis, diffuse axonal injury, fat embolism, septic emboli, and vasculitis.

CAA is also a frequent cause of convexity subarachnoid hemorrhage and superficial siderosis in patients over 60 (Fig. 6.7b). Other etiologies for convexity SAH include trauma, cerebrovenous thrombosis, PRES, and RCVS.

CAA-related small vessel ischemic disease may cause progressive deep white matter FLAIR/T2 hyperintensity predominantly in the occipital lobes with sparing of subcortical U-fibers, as well as cortical microinfarcts [19].

CAA-related inflammation/angiitis occurs in many patients presenting with subacute cognitive impairment and seizure, due to immune response to the vascular deposits of amyloid. MRI shows a characteristic appearance of large, confluent, asymmetric T2 hyperintense lesions extending into the subcortical white and often the cortical gray matter in the pattern of vasogenic edema (Fig. 6.8). This can be confused with other entities such as encephalitis, neoplasm, or atypical PRES, though the presence of microhemorrhages within the area of edema is highly suggestive of CAA-related inflammation. This represents a treatable form of CAA as symptoms and edema are reversible after immunosuppressive therapy [20].

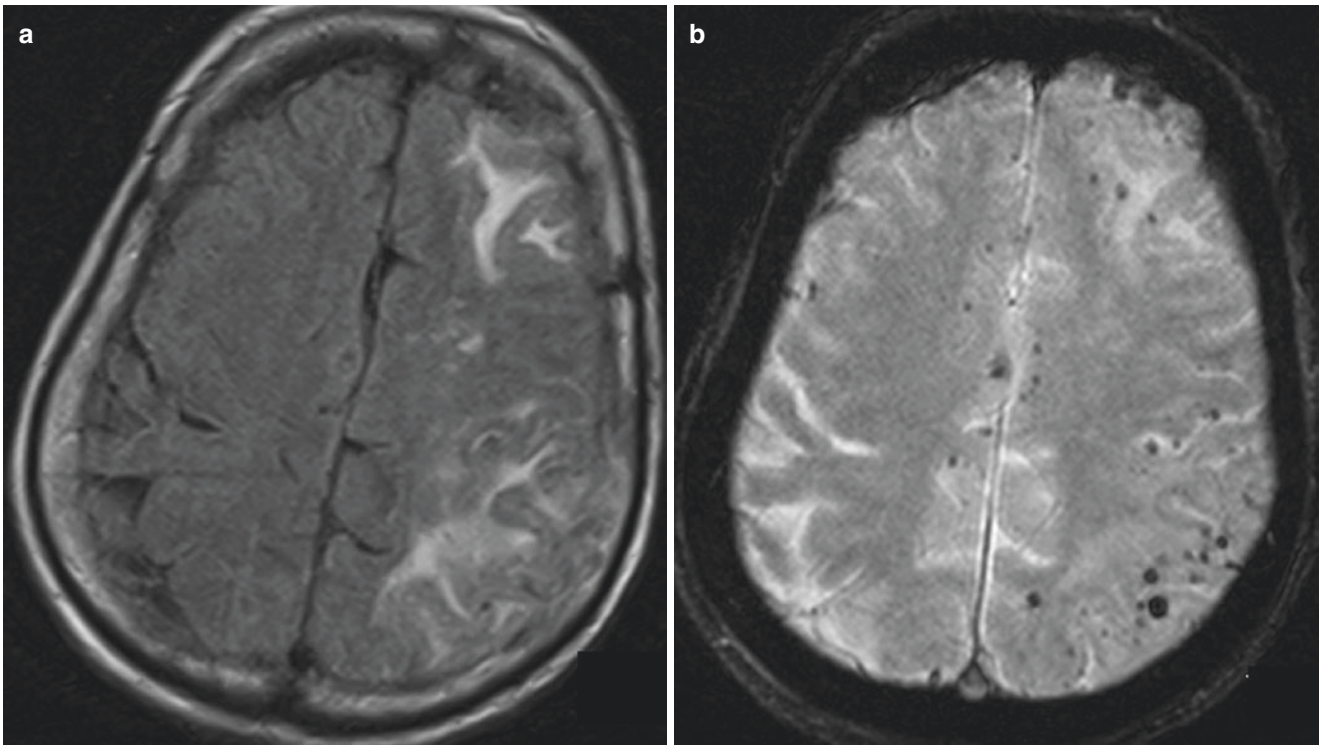

Fig. 6.8 CAA-related inflammation. Patient presents with altered mental status and seizure. (**a**) FLAIR shows asymmetric vasogenic edema of the left cerebral hemisphere. (**b**) GRE sequence shows multiple lobar microbleeds from amyloid deposition

References

1. Scott RM, Smith ER. Moyamoya disease and moyamoya syndrome. N Engl J Med. 2009;360:1226–37.
2. Fukui M, Kono S, Sueishi K, Ikezaki K. Moyamoya disease. Neuropathology. 2000;20:61–4.
3. Suzuki J, Takaku A. Cerebrovascular "moyamoya" disease: disease showing abnormal net-like vessels in base of brain. Arch Neurol. 1969;20:288–99.
4. Smith ER, Scott RM. Surgical management of moyamoya syndrome. Skull Base. 2005;15:15–26.
5. Murphy ES, Xie H, Merchant TE, Yu JS, Chao ST, Suh JH. Review of cranial radiotherapy-induced vasculopathy. J Neuro-Oncol. 2015;122:421–9.
6. Brant-Zawadzki M, Anderson M, DeArmond SJ, Conley FK, Jahnke RW. Radiation-induced large intracranial vessel occlusive vasculopathy. Am J Roentgenol. 1980;134:51–5.
7. McEvoy AW, Kitchen ND, Thomas DGT. Intracerebral haemorrhage and drug abuse in young adults. Br J Neurosurg. 2000;14:449–54.
8. Geibprasert S, Gallucci M, Krings T. Addictive illegal drugs: structural neuroimaging. Am J Neuroradiol. 2010;31:803–8.
9. Jordan LC, Hillis AE. Challenges in the diagnosis and treatment of pediatric stroke. Nat Rev Neurol. 2011;7:199–208.
10. Wintermark M, Hills NK, De Veber GA, et al. Clinical and imaging characteristics of arteriopathy subtypes in children with arterial ischemic stroke: results of the vips study. Am J Neuroradiol. 2017;38:2172–9.
11. Dlamini N, Yau I, Muthusami P, et al. Arterial wall imaging in pediatric stroke. Stroke. 2018;49:891–8.
12. Fearn ND, Mackay MT. Focal cerebral arteriopathy and childhood stroke. Curr Opin Neurol. 2019;1.
13. Engelter ST, Rueegg S, Kirsch EC, Fluri F, Probst A, Steck AJ, Lyrer PA. CADASIL mimicking primary angiitis of the central nervous system. Arch Neurol. 2002;59:1480–3.
14. Auer DP, Pütz B, Gössl C, Elbel GK, Gasser T, Dichgans M. Differential lesion patterns in CADASIL and sporadic subcortical arteriosclerotic encephalopathy: MR imaging study with statistical parametric group comparison. Radiology. 2001;218:443–51.
15. Yousry TA, Seelos K, Mayer M, Brüning R, Uttner I, Dichgans M, Mammi S, Straube A, Mai N, Filippi M. Characteristic MR lesion pattern and correlation of T1 and T2 lesion volume with neurologic and neuropsychological findings in cerebral autosomal dominant arteriopathy with subcortical infarcts and leukoencephalopathy (CADASIL). Am J Neuroradiol. 1999;20:91–100.
16. Dichgans M, Holtmannspötter M, Herzog J, Peters N, Bergmann M, Yousry TA. Cerebral microbleeds in CADASIL: a gradient-echo magnetic resonance imaging and autopsy study. Stroke. 2002;33:67–71.
17. Greenberg SM, William Rebeck G, Vonsattel JPG, Gomez-Isla T, Hyman BT. Apolipoprotein E ϵ4 and cerebral hemorrhage associated with amyloid angiopathy. Ann Neurol. 1995;38:254–9.
18. Linn J, Halpin A, Demaerel P, Ruhland J, Giese AD, Dichgans M, Van Buchem MA, Bruckmann H, Greenberg SM. Prevalence of superficial siderosis in patients with cerebral amyloid angiopathy. Neurology. 2010;74:1346–50.
19. Yamada M. Cerebral amyloid angiopathy: emerging concepts. J Stroke. 2015;17:17–30.
20. Kinnecom C, Lev MH, Wendell L, Smith EE, Rosand J, Frosch MP, Greenberg SM. Course of cerebral amyloid angiopathy-related inflammation. Neurology. 2007;68:1411–6.

Traumatic Neurovascular Injury

7

Yang Tang and Christopher Ovanez

Blunt cerebrovascular injury (BCVI) refers to blunt injury to carotid or vertebral arteries. It is associated with significant morbidity and mortality related to ischemic stroke. The reported incidence of BCVI has been variable in the literature, but with increased awareness and CTA screening, the incidence is now estimated to be 1–2.7% for patients admitted to trauma centers, higher in patients with risk factors and high injury severity scores [1].

7.1 Mechanism and Pathophysiology

BCVI is mostly associated with high-energy trauma mechanisms including high-speed motor vehicle collisions, fall, assaults, suicidal hanging, etc. Injury can occur to any segment of carotid or vertebral arteries. The most common sites of injury include the extracranial internal carotid arteries just below the skull base, vertebral arteries V2 segment within the transverse foramina, and V3 segment. Major mechanisms of injury include hyperextension with contralateral head rotation, direct blunt injury to the vessel, impingement or laceration from the adjacent fracture fragments, and direct intraoral trauma.

Intimal injury can cause subintimal dissection, intramural hematoma, luminal thrombosis, and arterial stenosis/occlusion, which eventually leads to cerebral ischemia due to hypoperfusion or embolic phenomenon. Adventitial injury can cause damage to the vasa vasorum and intramural hematoma without intimal injury. Pseudoaneurysms can form if the vascular rupture is contained by the adventitia or perivascular tissue. Transection represents the most severe form of arterial injury, typically manifests as rapid exsanguination, expanding neck hematoma and occasionally arteriovenous fistula.

7.2 Screening Criteria

A latent, asymptomatic period of 10–72 hours between injury and the onset of neurologic complication is commonly reported in BCVI. Early detection through screening and initiation of antithrombotic therapy can greatly reduce the incidence of ischemic stroke and improve outcome. Currently, there has been much debate regarding what patient population should be screened. Various screening criteria have been proposed including Denver, Memphis, and Boston criteria. The Modified Denver Criteria are the most studied and are endorsed by the Western and Eastern Trauma Associations [2, 3].

Clinical signs that should lead to emergent screening include:

- Arterial hemorrhage from the neck, mouth, nose, or ears
- Expanding cervical hematoma
- Cervical bruit in patient <50 years of age
- Any neurologic deficit inconsistent with imaging findings
- Stroke identified at secondary imaging

Radiological findings that should prompt urgent screening in asymptomatic patients:

- LeFort 2 or 3 facial fractures
- Skull base fracture with carotid canal involvement
- Cervical vertebral body or transverse foramen fracture, subluxation, or ligamentous injury
- Fracture of C1–C3
- Closed head injuries with diffuse axonal injury and Glasgow Coma Scale (GCS) <6
- Clothesline-type injury with associated swelling or pain
- Near-hanging with anoxia

CTA in patients selected by Denver screening criteria has been shown to be an optimal and cost-effective screening strategy [1]. However, approximately 30 to 37 percent of BCVI patients have none of the reported clinical or radiographic risk factors, and it has been suggested that more liberalized screening for BCVI should be performed in all trauma patients with sufficient injury mechanism [4].

© Springer Nature Switzerland AG 2020

Y. Tang, *Atlas of Emergency Neurovascular Imaging*, https://doi.org/10.1007/978-3-030-43654-4_7

7.3 Screening Modality

Multidetector CTA with 64 slice or higher is currently the imaging modality of choice for BCVI screening and has replaced DSA in most institutions. CTA is noninvasive, fast, and readily available in the emergency setting and has relatively high spatial resolution. It is worth noting that the diagnostic performance of CTA varies considerably among the published studies. Some early studies have shown that the sensitivity and specificity of CTA using 16-section or higher scanners approach 100% [5, 6], while other studies report lower sensitivity and specificity. For example, one study reported a sensitivity of 68% and a specificity of 92% for 64 slice CTA compared to DSA in 594 patients [7]. Another study reported a high false-positive rates of CTA up to 47.9% [8].

Trauma CTA protocol is variable among institutions. Traditionally, NCCT of the head and cervical spine are first performed. If radiological risk factors are identified based on the screening guideline, a dedicated CTA neck will be obtained to exclude or confirm vascular injuries. In recent years, many trauma centers have adopted universal BCVI screening to all trauma patients with sufficient mechanisms by integrating CTA neck into a whole body CT (WBCT) protocol [9]. In this protocol, NCCT of the head is first performed to evaluate intracranial injury. CT angiogram of the neck, chest, abdomen, and pelvis is performed immediately afterward following a single intravenous injection of contrast. Thin section axial source images, as well as multiplanar reconstructed (MPR) and volume-rendered images, are then reconstructed and reviewed. The WBCT protocol can be performed faster and with less contrast compared to the traditional segmental approach, and the accuracy has been shown to be comparable [10]. The protocol details are variable among different institutions. Some centers cover the entire head and neck CTA from the vertex to aortic arch, while others routinely scan the neck including the circle of Willis with the option of getting head CTA when significant intracranial injury is identified on head CT. Another variable is the arm position during the scan. Compared to "arm down" or "swimmer's," the "arm-up" position has been shown to generate the least amount of radiation, but the streak artifact from the elevated arm can compromise the quality of neck CTA [11]. For patients with high risk for BCVI but negative screening WBCT, dedicated neck CTA should be considered to more confidently exclude low-grade injuries [12].

There are several factors that can affect the quality and interpretation of CTA. Large body habitus and poor contrast bolus can greatly diminish the quality of the entire scan and render it non-diagnostic. Streak artifacts from the mandible and dental hardware can compromise the evaluation of distal ICAs near the skull base, which are the most vulnerable segment for injury, generating either false-positive or false-negative results. Opacification of venous plexuses and streak artifact from adjacent bony structures and fusion hardware can obscure the vertebral artery injury.

MRI/MRA is not routinely used as a screening modality given its limited availability, longer scanning time, lower spatial resolution, and the need of MR compatible life support/monitoring device required for the critically injured patients. However, MRI can be used as a complementary tool to CTA in selected cases to better characterize the intramural hematoma versus atherosclerotic plaques or other chronic changes.

DSA is still considered the reference standard for diagnosing BCVI given its superb spatial and temporal resolutions compared to CTA. Carotid/vertebral segments obscured by streak artifact on CTA can be better evaluated by DSA. Contrast injection can be repeated during DSA to overcome motion, which cannot be routinely done for CTA. However, DSA has several disadvantages that limit its use as a screening modality. It is an invasive technique that is labor-intensive and associated with a low but non-negligible rate of procedure-related complications, including groin hematoma, iatrogenic dissections, thromboembolism, etc. In addition, DSA provides no information about the vessel wall and limited in characterizing intramural hematoma. The current role of DSA is not well-defined. Some centers recommend DSA for patients with negative CTA findings but with persistent clinical concern for BCVI [8], while other centers only perform DSA as part of treatment planning in patients with high-grade injury identified on CTA.

7.4 BCVI Grading

The Biffl scale is widely used to grade BCVI, and the grading correlates with increasing risk of stroke and worse prognosis [13]. It was originally developed based on DSA findings of carotid injuries but has been adopted for CTA and MRA for both carotid and vertebral injuries.

- Grade I injury refers to mild vessel wall irregularity, dissection, or intramural hematoma with <25% stenosis (Figs. 7.1 and 7.2).

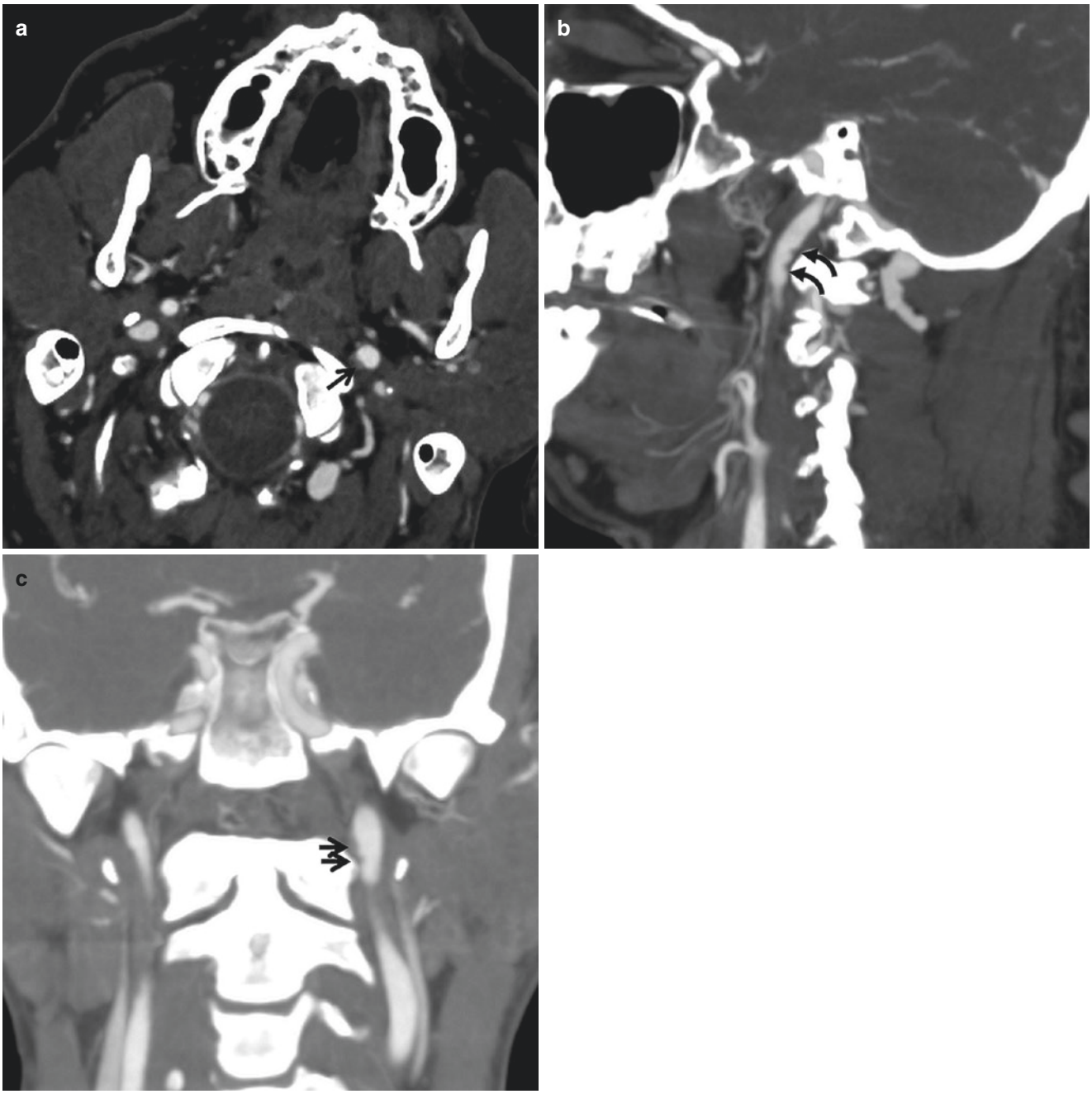

Fig. 7.1 Grade I ICA injury. Axial CTA of a patient with motor vehicle collision demonstrates minimal contour irregularity and wall thickening of left cervical ICA at the level of C1 (*arrow*) with less than 25% luminal stenosis, compatible with grade I injury (**a**). This is better seen on the sagittal (**b**) and coronal (**c**) reconstructed images

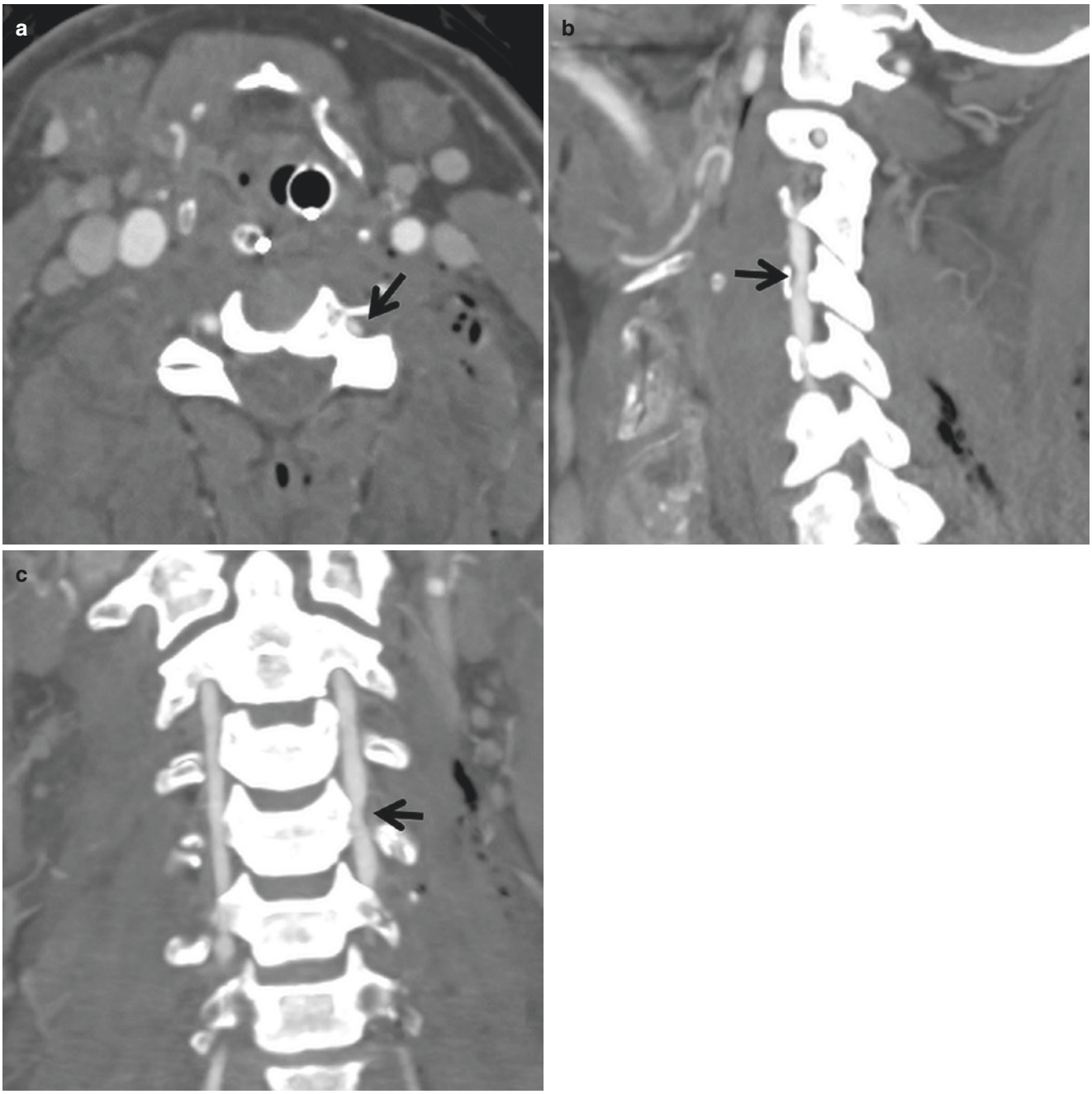

Fig. 7.2 Grade I vertebral artery injury. (**a**) Axial CTA of a patient with multiple cervical transverse process fractures demonstrate mild wall thickening and less than 25% stenosis of left vertebral artery (*arrow*), consistent with grade I injury. This is confirmed on the sagittal (**b**) and coronal (**c**) reconstructed images

- Grade II injury is defined as dissection or intramural hematoma with >25% stenosis. A visible intimal flap or intraluminal thrombus is also considered as grade II injury (Figs. 7.3, 7.4, and 7.5).
- Grade III injury refers to traumatic pseudoaneurysm (Fig. 7.6).
- Grade IV injury refers to complete traumatic arterial occlusion (Fig. 7.7).
- Grade V injury is transection with active hemorrhage or arteriovenous fistula (Fig. 7.8). It requires immediate attempts to control the bleeding and often lethal.

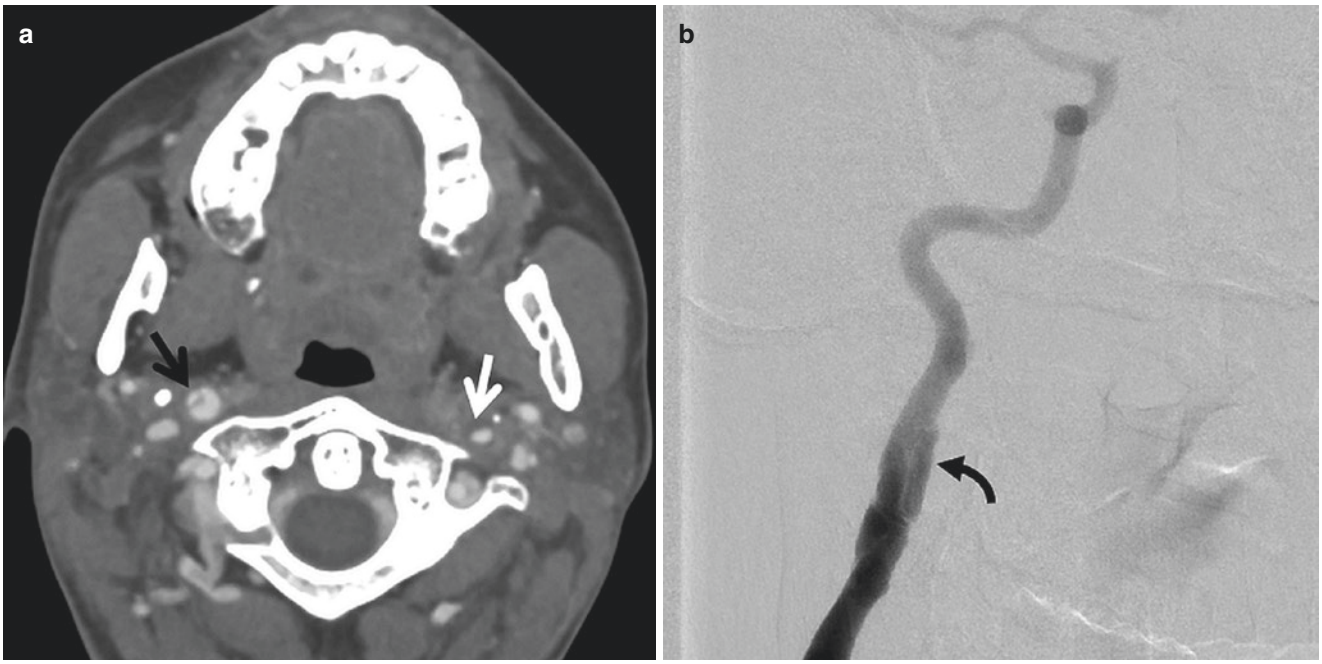

Fig. 7.3 Grade II ICA injury with intimal flap. (**a**) Axial CTA of a patient with high-speed motor vehicle collision demonstrates mild dilation of right ICA with an intimal flap at the level of C1 (*black arrow*). Note grade I injury of left ICA at the same level (*white arrow*). (**b**) Catheter angiogram of right ICA demonstrates the dissection and a false lumen (*curved arrow*)

7.5 Differential Diagnosis

It is important to differentiate BCVI from nontraumatic entities and anatomic variants. CTA is generally accurate in diagnosing high-grade injury (grades III, IV, and V) but lacks sensitivity and specificity for low-grade injury (grades I and II). A recent study compared the initial CTA diagnosis to an expert clinical consensus review and found that among 18 injuries suspected by CTAs, only 6 represented true BCVI, whereas 9 represented post-traumatic vasospasm, and 3 represented atherosclerotic disease [14].

Vasospasm is very common after traumatic injury and presents as mild vessel contour irregularity on luminal imaging. It is frequently impossible to differentiate it from low-grade injury on CTA. Vasospasm typically resolves on follow-up imaging, while low-grade injury persists or occasionally progresses into higher-grade injury on follow-up (Fig. 7.9).

Atherosclerotic disease is prevalent in elderly population with cardiovascular risk factors. It occurs more frequently in carotid bifurcations, carotid siphons, and vertebral artery origins and is associated with calcifications. Noncalcified fibrofatty plaques in atypical locations with wall thickening and luminal stenosis can be a diagnostic dilemma in trauma patients. High-resolution MRI with vessel wall imaging have shown promise in characterizing vessel wall pathology and can be a useful tool to differentiate intramural hematoma from atherosclerotic plaque [14].

Fibromuscular dysplasia is a non-atherosclerotic, non-inflammatory vascular disease that most commonly affects the renal and internal carotid arteries [15]. The pathological classification is based on the affect arterial layer: intima, media, or adventitia. Medial fibroplasia has the characteristic "string of beads" appearance on angiography and can mimic low-grade injury (Fig. 7.10). It is important to note that fibromuscular dysplasia is an important risk factor for dissection, and these two conditions can coexist.

A rare intimal variant of fibromuscular dysplasia is carotid web, which typically manifests as a thin shelflike filling defect arising from the dorsal wall of the carotid bulb. It is highly thrombogenic and felt to be an important cause for cryptogenic stroke especially in young African American females [16]. Although the imaging appearance is quite characteristic, it can mimic a dissection flap on vascular imaging for the inexperienced readers (Fig. 7.11).

Vascular tortuosity and looping are common variants and can mimic or obscure true injury. This is especially problematic for ICAs below the skull base and vertebral artery distal

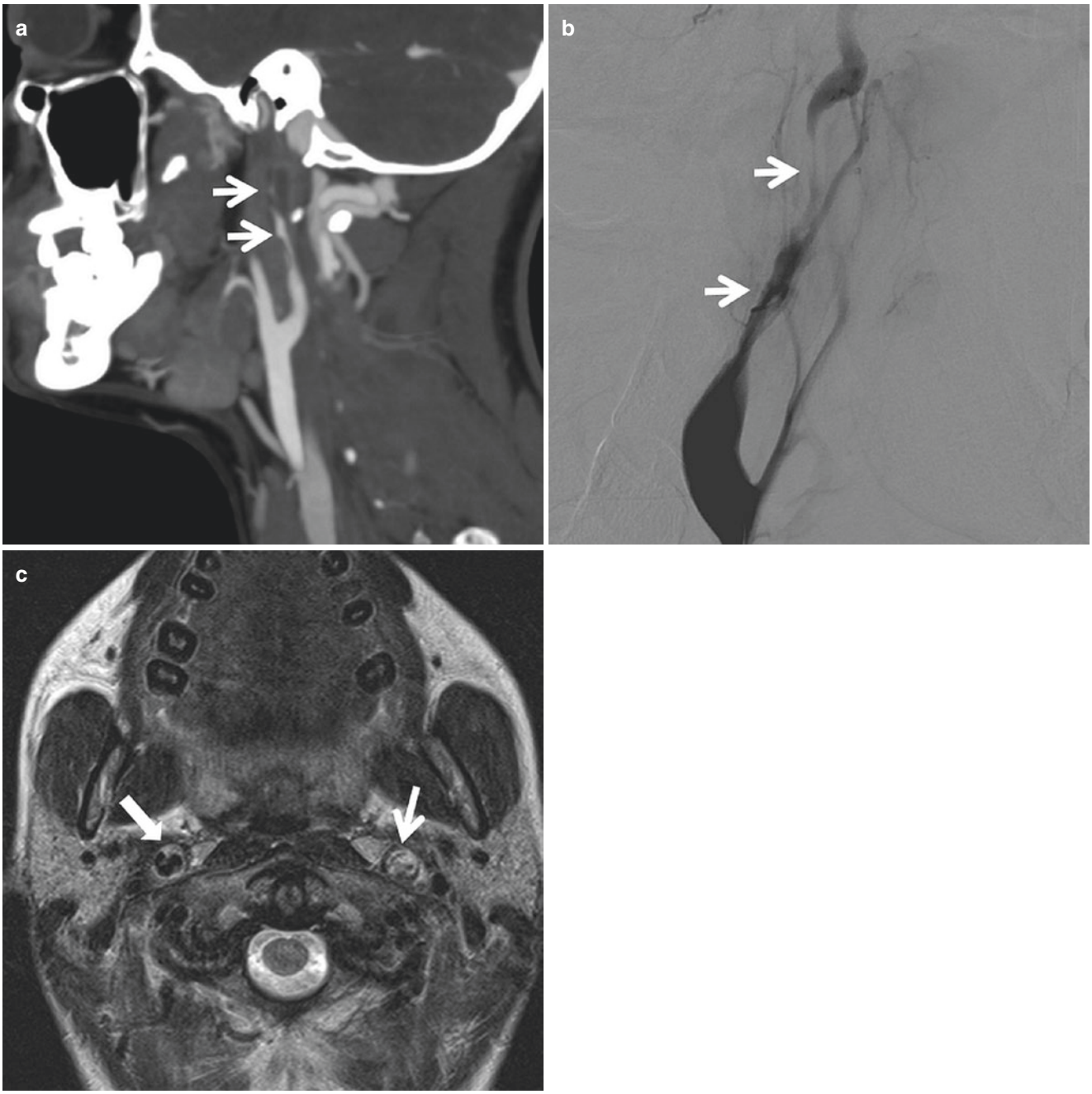

Fig. 7.4 Grade II ICA injury with intramural hematoma. Axial CTA (**a**) shows near-occlusive irregular luminal stenosis involves a long segment of left cervical ICA due to compression of an intramural hematoma (*arrow*), consistent with grade II injury. This is confirmed by catheter angiogram (**b**). (**c**) Axial T2 MRI shows loss of left ICA flow void (*arrow*). Also note mild narrowing of right ICA due to an intramural hematoma (*block arrow*), also consistent with grade II injury

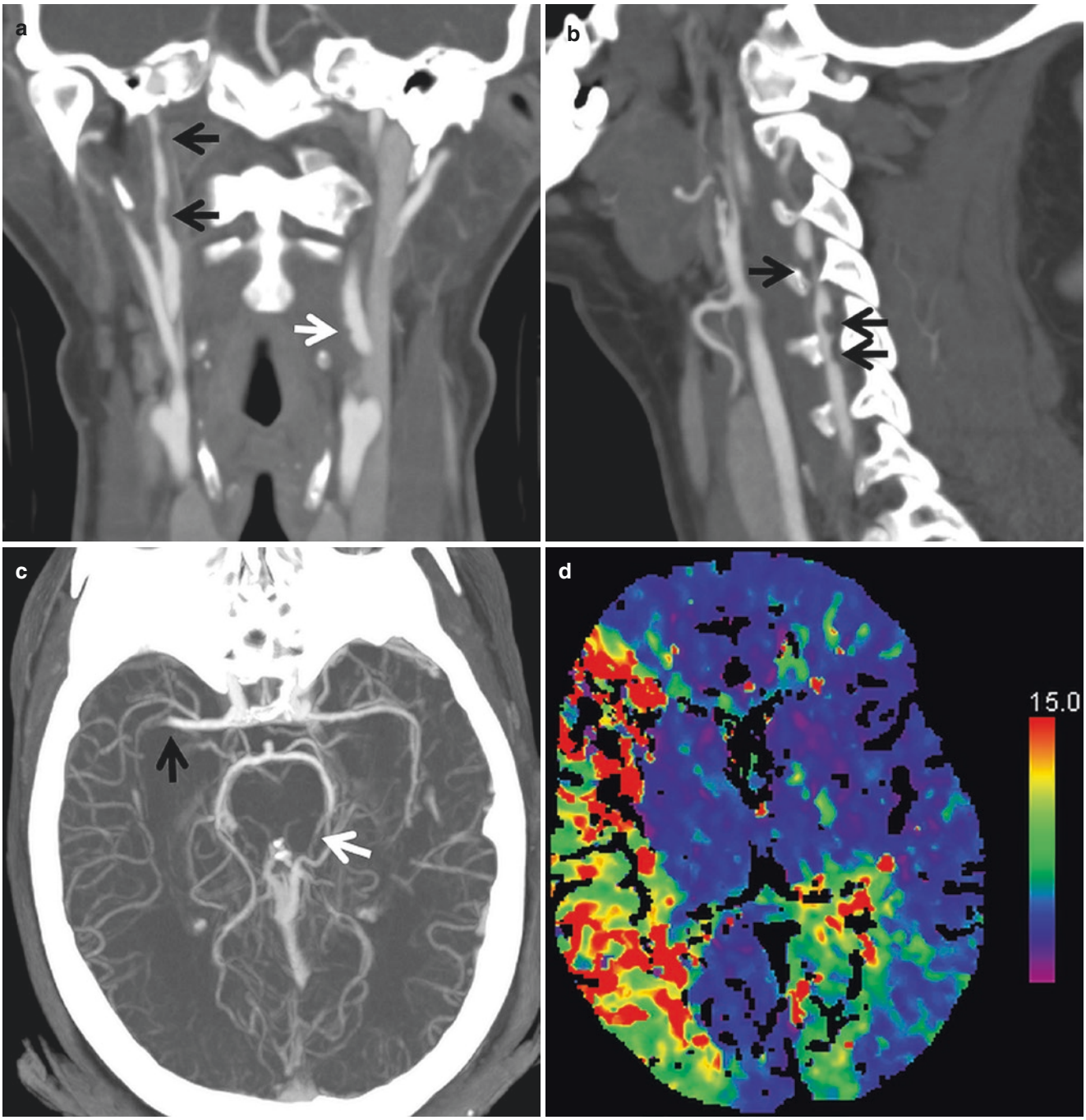

Fig. 7.5 Multivessel injury with intracranial embolization. (**a**) Coronal reconstructed CTA of patient with motor vehicle collision demonstrates grade II injury of right ICA (*black arrows*). Also note additional grade I injury of the left ICA (*white arrow*). (**b**) Multifocal grade II injury of left vertebral artery on the sagittal reconstructed image. (**c**) Intracranially, there is abrupt occlusion of right MCA (*black arrow*) and left PCA (*white arrow*) due to artery-to-artery embolization. (**d**) CT perfusion demonstrates prolongation of time of drain in the right MCA and left PCA territories. It is important to include intracranial arteries within the field of view as distal embolization is an indication for emergent endovascular treatment

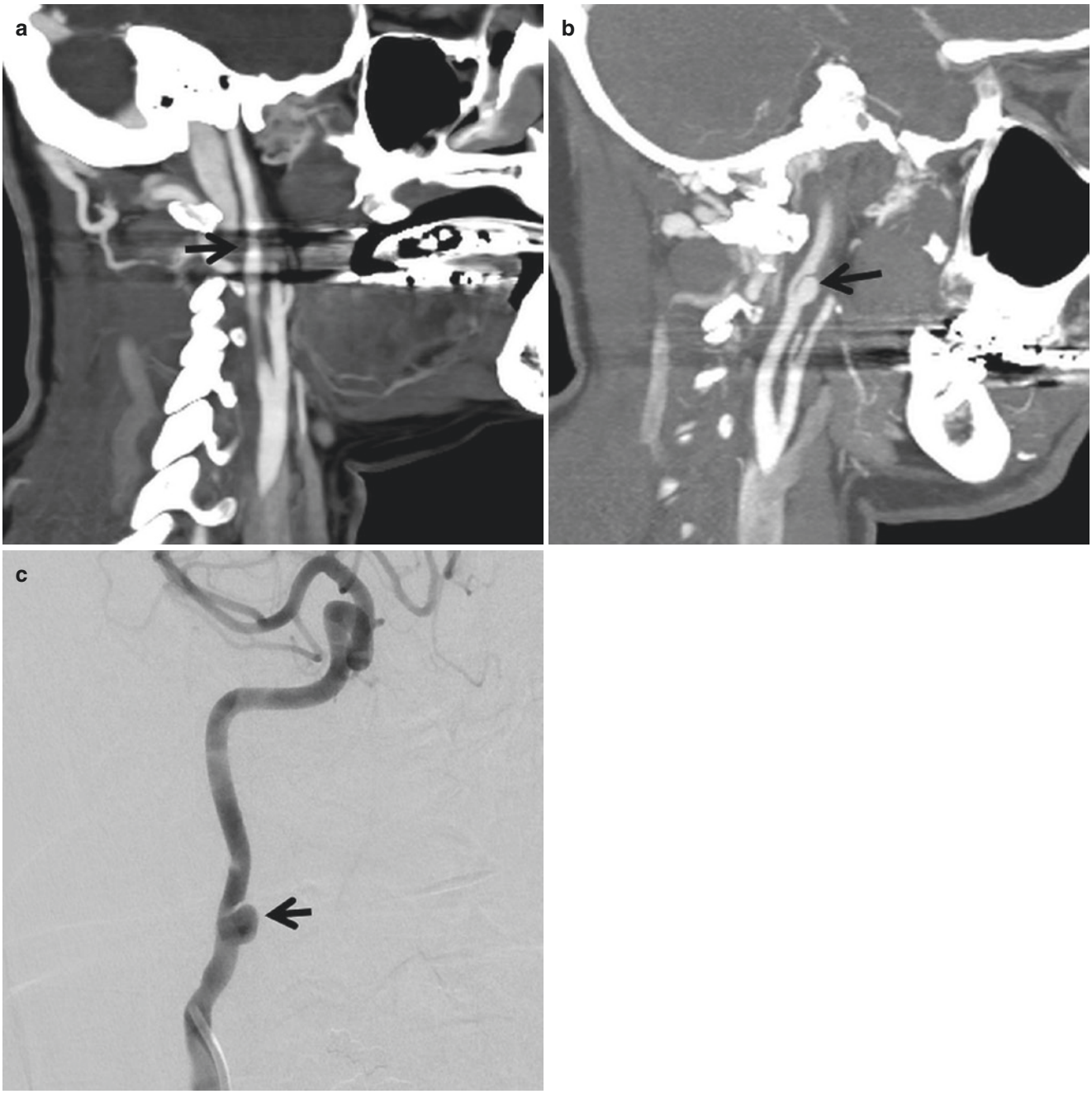

Fig. 7.6 Grade III ICA injury. (**a**) Sagittal reconstructed CTA following motor vehicle crash demonstrates grade II injury of right ICA with >25% stenosis, which is somewhat obscured by streak artifact from dental amalgam. (**b**) Three-month follow-up CTA shows progression of injury to grade III with development of a pseudoaneurysm (*arrow*). (**c**) This is confirmed by catheter angiogram and treated with endovascular stenting

Fig. 7.7 Grade IV ICA injury. Sagittal reconstructed CTA demonstrates tapered occlusion of ICA, consistent with grade IV injury (*arrow*). Note is made of a small intraluminal thrombus (*curved arrow*)

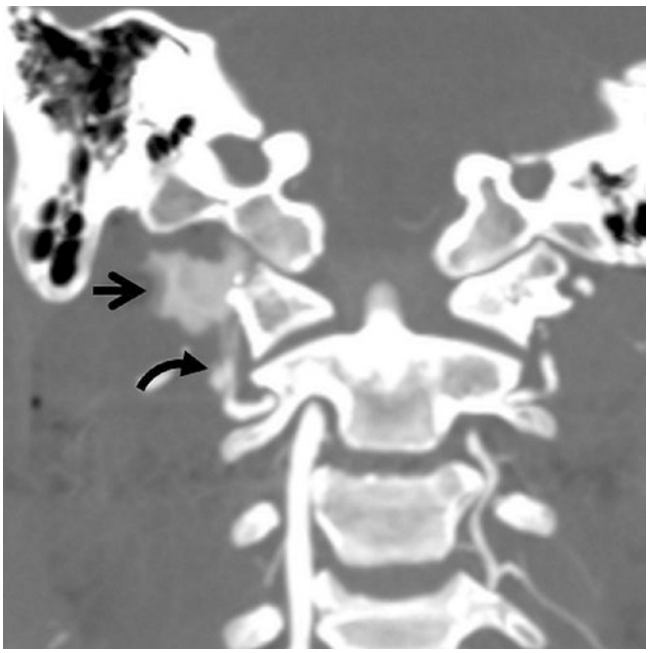

Fig. 7.8 Grade V vertebral artery injury. Coronal reconstructed CTA of patient with severe closed neck injury demonstrates transection of right vertebral artery (*curved arrow*) at C1–C2 with active contrast extravasation (*arrow*)

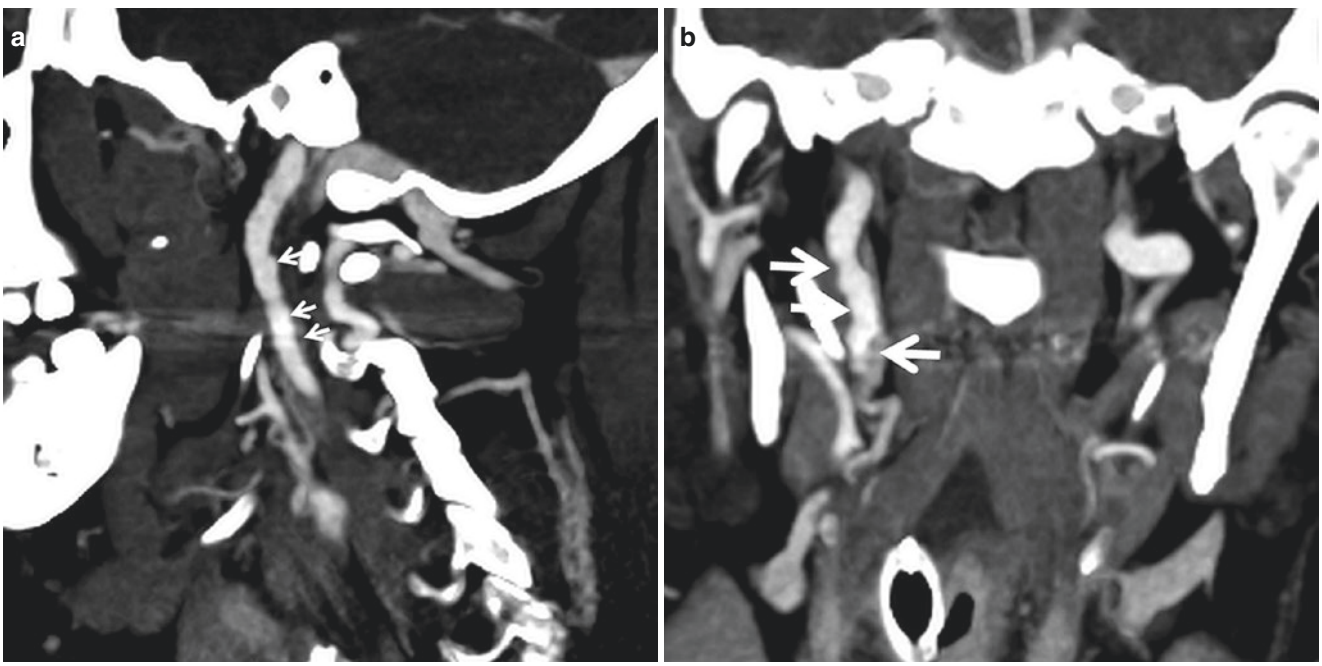

Fig. 7.9 Vasospasm mimicking grade I injury in a patient with motor vehicle crash. Sagittal (**a**) and coronal (**b**) CTA neck demonstrates contour irregularity of right cervical ICA, which resolves in the repeat CTA 24 hours later, and is consistent with vasospasm. It is frequently impossible to differentiate vasospasm from grade I injury without a follow-up study

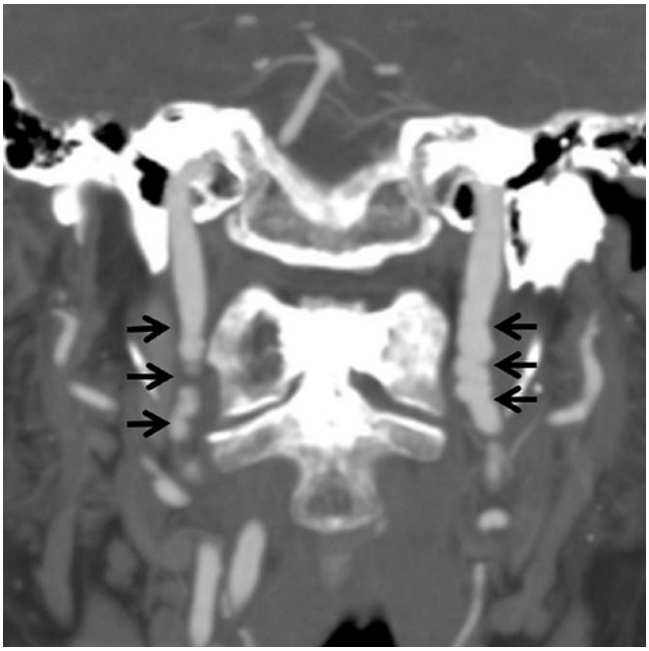

Fig. 7.10 Fibromuscular dysplasia mimicking grade I injury. Coronal CTA demonstrates contour irregularity of bilateral cervical ICAs with "string of beads" type of appearance, in a patient after motor vehicle crash. CTA of the abdomen shows similar appearance of renal arteries. This is most consistent with fibromuscular dysplasia. Follow-up CTA in 6 months does not show interval change

V2 and V3 segments, where injuries frequently occur. Careful examination of sagittal and coronal MPR images may help the distinction.

Congenital variants such as hypoplasia (Fig. 7.12) and fenestration can occasionally mimic arterial injury.

7.6 Treatment and Follow-Up Imaging

Patients with BCVI should be treated with antithrombotic (antiplatelet or anticoagulation) therapies unless there is a contraindication such as active hemorrhage. A study has shown that antithrombotic treatment is safe even in patients with traumatic brain injury or solid organ injury [17]. Antiplatelet therapy with aspirin is as efficacious as heparin for stroke prevention and with less bleeding complication [18].

CT angiography should be performed 7–10 days following initial identification of grades I–III BCVIs. If repeat imaging shows resolution of injury, the antithrombotic treatment may be discontinued. If abnormalities persist, antithrombotic treatment should be continued for 3–6 months, with re-imaging at follow-up to adjust the management. Injury progression is highly unlikely for grade I injuries. Progression is more common in grade II injuries, and endovascular management or surgical treatment should be

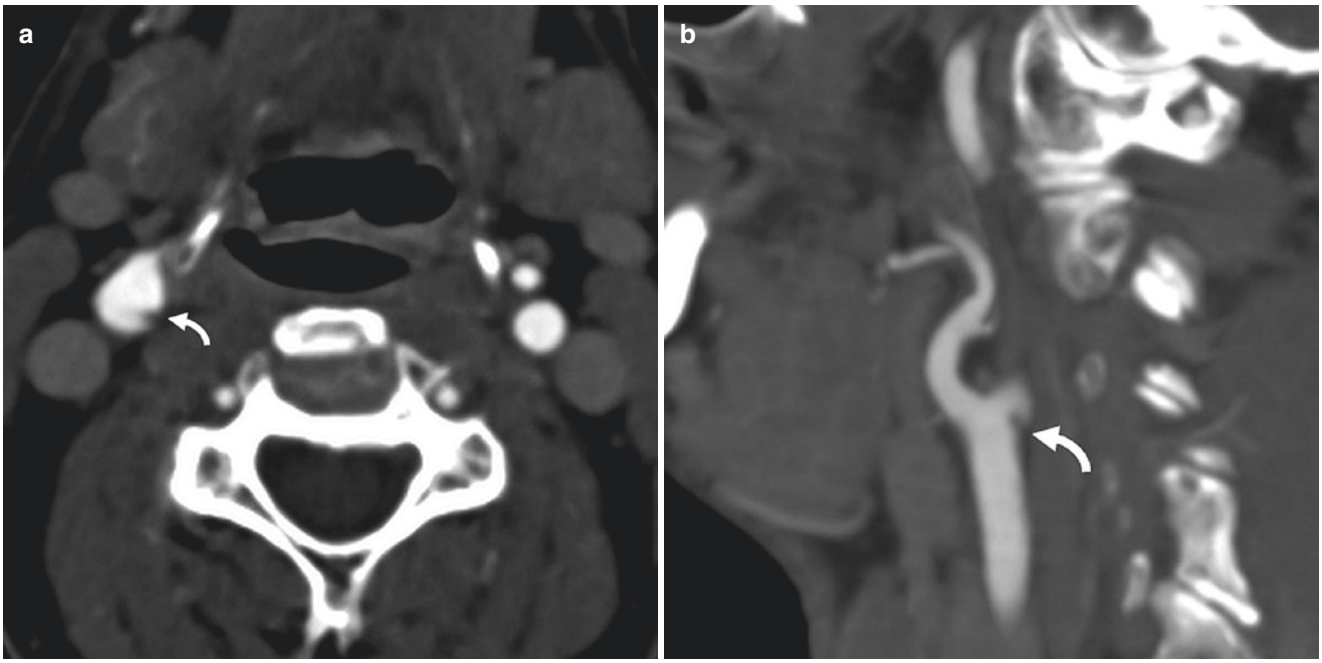

Fig. 7.11 Carotid web mimicking dissection flap. Axial (**a**) and sagittal (**b**) CTA shows a linear filling defect at the carotid bulb posteriorly consistent with carotid web

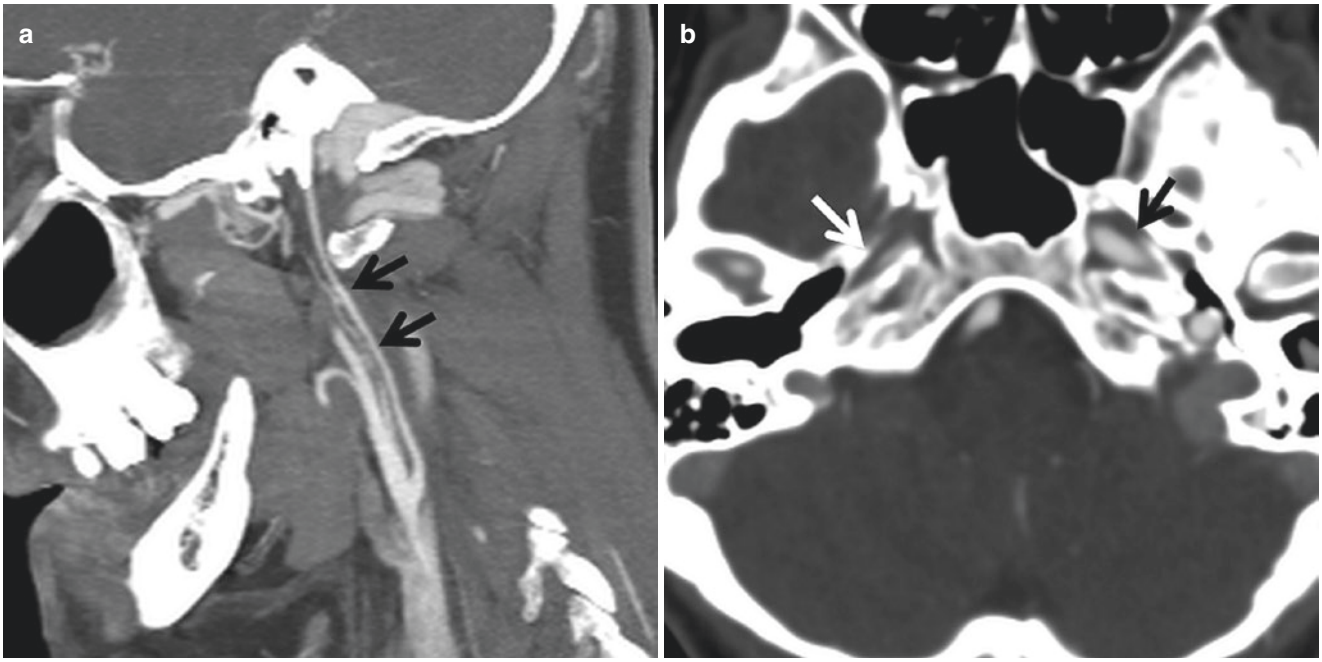

Fig. 7.12 Congenital ICA hypoplasia mimicking injury. (**a**) Sagittal CTA shows diffuse narrowing of right ICA. (**b**) Axial CTA shows small right petrous carotid canal (*white arrow*) compared to the left (*black arrow*), suggestive of congenital ICA hypoplasia rather than dissection

considered if there is progression at follow-up. Grade III injury or pseudoaneurysm can be treated endovascularly or repaired surgically, if the lesion becomes symptomatic despite optimal conservative management or if the pseudoaneurysm grows to 1.0–1.5 cm in diameter. For grade IV injury, surgical or endovascular intervention has not been shown to be beneficial, and these patients should remain on lifetime antiplatelet therapy [19, 20].

7.7 Spontaneous Dissection

In rare occasions, arterial dissection can occur following trivial injury such as chiropractor neck manipulation, athletic activities, rapid head movement, and daily activities such as sneezing, coughing, shaving, and nose-blowing or even occurs spontaneously without any inciting event. Underlying fibromuscular dysplasia or connective tissue disorders such as Marfan's syndrome, Ehlers–Danlos syndrome and cystic medial necrosis may play an important role in the pathogenesis of spontaneous dissection.

Dissection can occur in extracranial or intracranial arterial segments. Extracranial dissection is more common in the western countries and more frequently affects the anterior circulation. In comparison, intracranial dissection is more common in children or patients of Asian origin and more commonly involves the posterior circulation especially the vertebral V4 segment [21]. Intracranial dissection can lead to subarachnoid hemorrhage or cerebral ischemia.

The imaging findings of spontaneous dissection are similar to those of traumatic dissection and include intimal flap, double lumen, intramural hematoma, pseudoaneurysm, segmental stenosis, and tapered or abrupt occlusion. A fusiform or irregular intracranial aneurysm located at a non-branching site associated with segmental stenosis or rapid change in morphology is very suggestive of intracranial dissection (Figs. 7.13 and 7.14).

7.8 Traumatic Dural Sinus Injury

Dural venous sinus compromise after traumatic brain injury has been increasingly detected with the widespread use of CTA. Most cases are associated with skull fracture in the vicinity of a dural sinus (Fig. 7.15). Compared to other skull fractures, fractures of the petrous temporal bone have the highest chance of injury to the transverse/sigmoid sinuses and jugular bulbs.

The dural sinus compromise can take the forms of extrinsic compression, sinus thrombosis, or a combination of both [22]. Isolated sinus compression is more common than thrombosis and can be secondary to a depressed skull fracture, extra-axial hematoma, or pneumocephalus [22]. It is important to make the distinction as the treatment and prognosis are

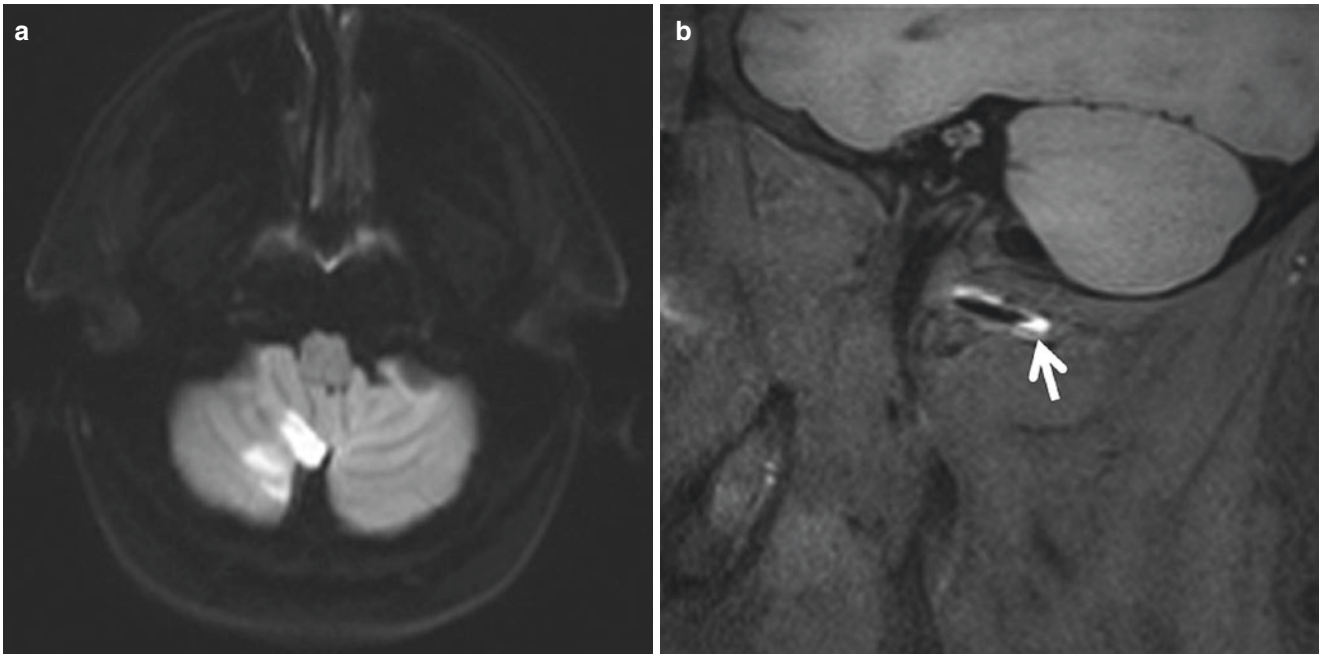

Fig. 7.13 Spontaneous dissection of cervical vertebral artery. Patient with no past medical history presents with sudden onset vertigo. (**a**) DWI MRI shows acute infarction of inferior right cerebellum in the PICA territory. (**b**) Sagittal T1 fat-saturated image demonstrates hyperintense signal (*arrow*) surrounding the right vertebral flow void, consistent with dissection with subacute intramural hematoma

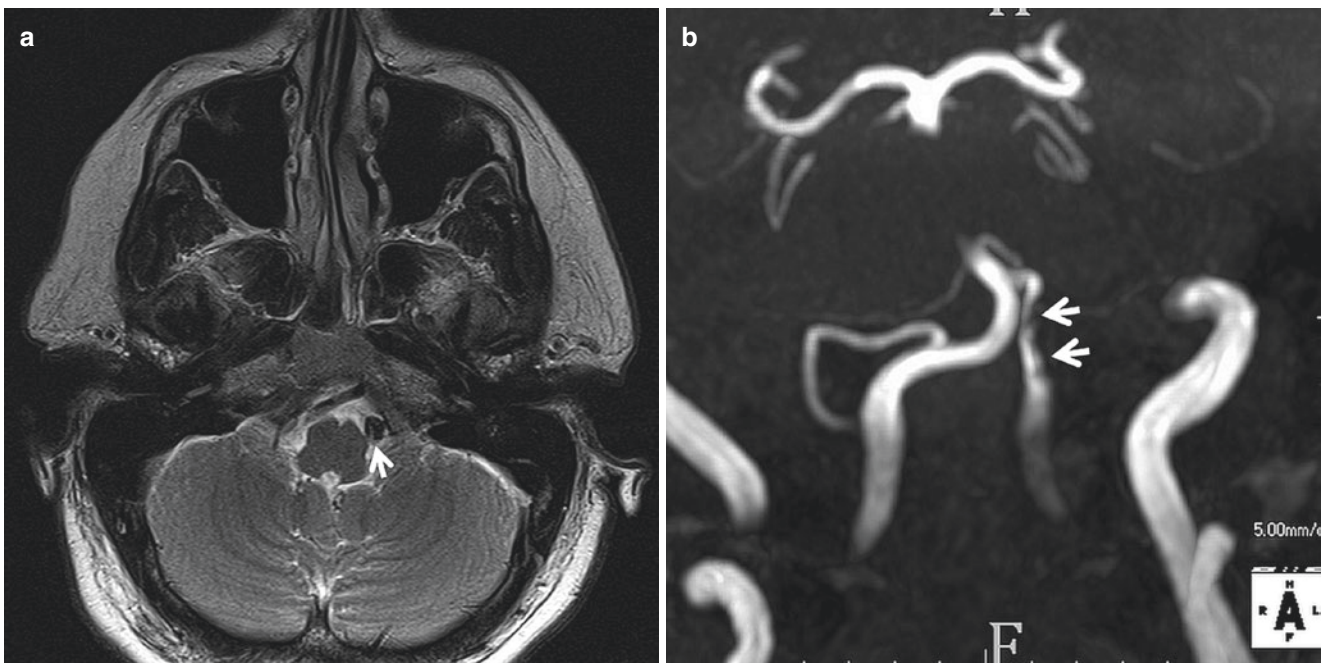

Fig. 7.14 Intracranial vertebral dissection. Patient presents with severe headache and diffuse subarachnoid hemorrhage on CT (not shown). (**a**) Axial T2 MRI shows a subtle dissection flap of the intracranial left vertebral artery. (**b**) TOF MRA demonstrates irregular luminal narrowing of left vertebral artery. (**c**) Catheter angiography confirms the dissection with double lumen (*arrow*)

Fig. 7.14 (continued)

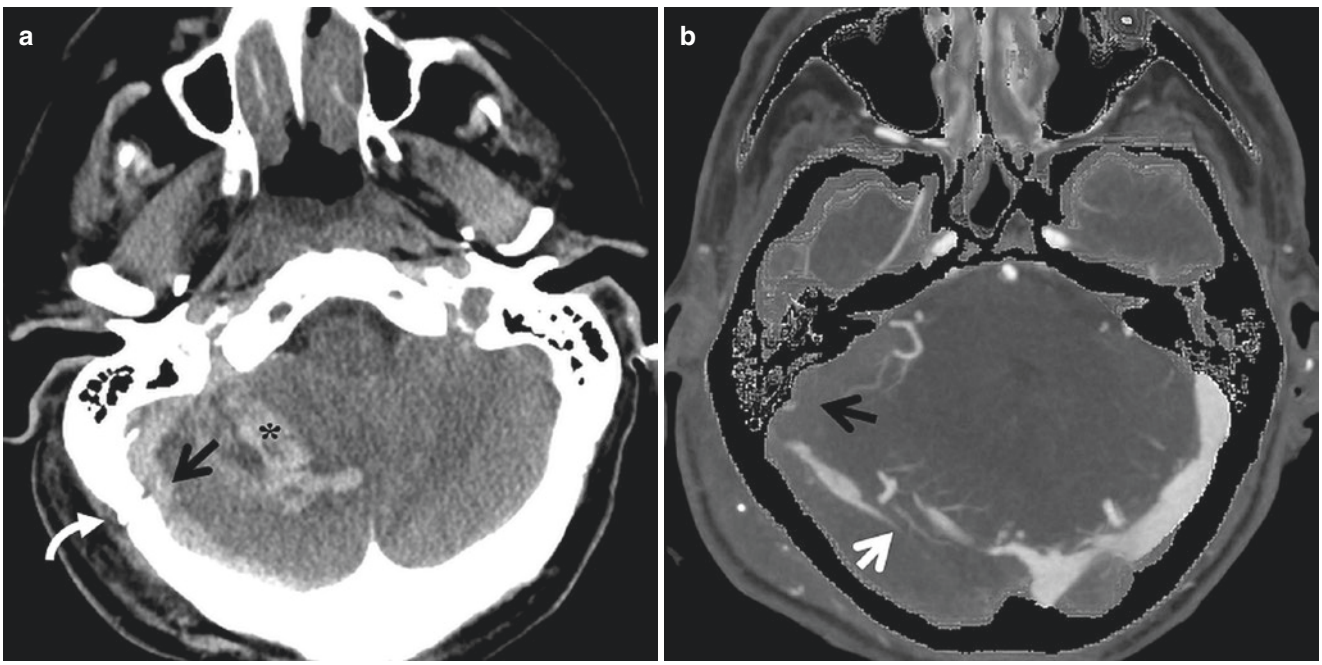

Fig. 7.15 Traumatic venous injury. (**a**) NCCT of a patient with closed head injury shows an epidural hematoma overlying the right cerebellum (*arrow*) and an intraparenchymal hematoma (∗). A fracture is noted in the right occipital bone (*curved arrow*). (**b**) Axial CTA demonstrates injury of right transverse sinus with irregular luminal narrowing (*white arrow*). The sigmoid sinus is thrombosed (*black arrow*)

different. Extrinsic sinus compression mostly follows a benign clinical course; however, dural sinus thrombosis can have major consequences including uncontrolled intracranial hypertension, venous infarcts, or hemorrhage [23].

The treatment of traumatic sinus thrombosis poses a major challenge when there are concurrent large intracranial hemorrhages or contusions [24]. The decision whether to anticoagulate and timing of such treatment need to be personalized depending on the risk of thrombosis progression and risk of exacerbation of hemorrhage. Endovascular mechanical thrombectomy is an option for patients with progressive sinus thrombosis and contraindication to anticoagulation.

References

1. Malhotra A, Wu X, Kalra VB, Schindler J, Matouk CC, Forman HP. Evaluation for blunt cerebrovascular injury: review of the literature and a cost-effectiveness analysis. Am J Neuroradiol. 2016;37:330–5.
2. Biffl WL, Cothren CC, Moore EE, Kozar R, Cocanour C, Davis JW, McIntyre RC, West MA, Moore FA. Western trauma association critical decisions in trauma: screening for and treatment of blunt cerebrovascular injuries. J Trauma – Inj Infect Crit Care. 2009;67:1150–3.
3. Bromberg WJ, Collier BC, Diebel LN, Dwyer KM, Holevar MR, Jacobs DG, Kurek SJ, Schreiber MA, Shapiro ML, Vogel TR. Blunt cerebrovascular injury practice management guidelines: the eastern association for the surgery of trauma. J Trauma – Inj Infect Crit Care. 2010;68:471–7.
4. Bruns BR, Tesoriero R, Kufera J, Sliker C, Laser A, Scalea TM, Stein DM. Blunt cerebrovascular injury screening guidelines: what are we willing to miss? J Trauma Acute Care Surg. 2014;76:691–5.
5. Eastman AL, Chason DP, Perez CL, McAnulty AL, Minei JP. Computed tomographic angiography for the diagnosis of blunt cervical vascular injury: is it ready for primetime? J Trauma. 2006;60:925–9.. discussion 929
6. Schneidereit NP, Simons R, Nicolaou S, Graeb D, Brown DR, Kirkpatrick A, Redekop G, McKevitt EC, Neyestani A. Utility of screening for blunt vascular neck injuries with computed tomographic angiography. J Trauma – Inj Infect Crit Care. 2006;60:209–15.
7. Roberts DJ, Chaubey VP, Zygun DA, Lorenzetti D, Faris PD, Ball CG, Kirkpatrick AW, James MT. Diagnostic accuracy of computed tomographic angiography for blunt cerebrovascular injury detection in trauma patients: a systematic review and meta-analysis. Ann Surg. 2013;257:621–32.
8. Shahan CP, Magnotti LJ, Stickley SM, Weinberg JA, Hendrick LE, Uhlmann RA, Schroeppel TJ, Hoit DA, Croce MA, Fabian TC. A safe and effective management strategy for blunt cerebrovascular injury: avoiding unnecessary anticoagulation and eliminating stroke. J Trauma Acute Care Surg. Lippincott Williams and Wilkins. 2016;76:915–22.
9. Dreizin D, Munera F. Blunt polytrauma: evaluation with 64-section whole-body CT angiography. Radiographics. 2012;32:609–32.
10. Sliker CW, Shanmuganathan K, Mirvis SE. Diagnosis of blunt cerebrovascular injuries with 16-MDCT: accuracy of whole-body MDCT compared with neck MDCT angiography. Am J Roentgenol. 2008;190:790–9.
11. Gunn ML, Kool DR, Lehnert BE. Improving outcomes in the patient with polytrauma: a review of the role of whole-body computed tomography. Radiol Clin N Am. 2015;53:639–56.
12. Laser A, Kufera JA, Bruns BR, Sliker CW, Tesoriero RB, Scalea TM, Stein DM. Initial screening test for blunt cerebrovascular injury: validity assessment of whole-body computed tomography. Surgery (United States). Mosby Inc. 2015;158:627–35.
13. Biffl WL, Moore EE, Offner PJ, Brega KE, Franciose RJ, Burch JM. Blunt carotid arterial injuries: implications of a new grading scale. J Trauma – Inj Infect Crit Care. Lippincott Williams and Wilkins. 1999;47:845–53.
14. Vranic JE, Huynh TJ, Fata P, et al. The ability of magnetic resonance black blood vessel wall imaging to evaluate blunt cerebrovascular injury following acute trauma. J Neuroradiol. 2019; https://doi.org/10.1016/j.neurad.2019.01.091.
15. Slovut DP, Olin JW. Fibromuscular Dysplasia. N Engl J Med. 2004;350:1862–71.
16. Choi PMC, Singh D, Trivedi A, Qazi E, George D, Wong J, Demchuk AM, Goyal M, Hill MD, Menon BK. Carotid webs and recurrent ischemic strokes in the era of CT angiography. Am J Neuroradiol. 2015;36:2134–9.
17. Shahan CP, Magnotti LJ, McBeth PB, Weinberg JA, Croce MA, Fabian TC. Early antithrombotic therapy is safe and effective in patients with blunt cerebrovascular injury and solid organ injury or traumatic brain injury. J Trauma Acute Care Surg. Lippincott Williams and Wilkins. 2016;81:173–7.
18. Wahl WL, Brandt M-M, Thompson BG, Taheri PA, Greenfield LJ. Antiplatelet therapy: an alternative to heparin for blunt carotid injury. J Trauma. 2002;52:896–901.
19. Nagpal P, Policeni BA, Bathla G, Khandelwal A, Derdeyn C, Skeete D. Blunt cerebrovascular injuries: advances in screening, imaging, and management trends. AJNR Am J Neuroradiol. 2017;39:406–14.
20. Rutman AM, Vranic JE, Mossa-Basha M. Imaging and management of blunt cerebrovascular injury. Radiographics. 2018;38:542–63.
21. Debette S, Compter A, Labeyrie MA, et al. Epidemiology, pathophysiology, diagnosis, and management of intracranial artery dissection. Lancet Neurol. 2015;14:640–54.
22. Rischall MA, Boegel KH, Palmer CS, Knoll B, McKinney AM. MDCT venographic patterns of dural venous sinus compromise after acute skull fracture. Am J Roentgenol. 2016;207:852–8.
23. Benifla M, Yoel U, Melamed I, Merkin V, Cohen A, Shelef I. Dural sinus obstruction following head injury: a diagnostic and clinical study. J Neurosurg Pediatr. 2016;18:253–62.
24. Afshari FT, Yakoub KM, Zisakis A, Thomas A, Ughratdar I, Sturman S, Belli A. Traumatic dural venous sinus thrombosis; a challenge in management of head injury patients. J Clin Neurosci. 2018;57:169–73.

Cerebral Aneurysm

8

Seyed Mohammad Gharavi and Yang Tang

8.1 Pathophysiology

A cerebral aneurysm is defined as an abnormal focal outpouching from the wall of cerebral arteries and is the most common cause of spontaneous cisternal subarachnoid hemorrhage (cSAH). The incidence of the intracranial aneurysm has been reported 1–5% among the adult population. The pathophysiology of the development of intracranial aneurysms is not completely clear. Altered hemodynamic factors and weakness of the vessel wall, particularly the tunica media, are significant factors in the formation of the aneurysm. It is believed that atherosclerosis and hypertension play important roles in aneurysm formation. Additional risk factors include infection, trauma, radiations, etc. Although aneurysms are considered acquired lesions, there are certain genetic disorders predisposing to the aneurysm formation, such as autosomal dominant polycystic kidney disease (ADPKD), Ehlers–Danlos syndrome, Loeys–Dietz syndrome, fibromuscular dysplasia, Marfan's syndrome, neurofibromatosis, etc. [1].

8.2 Classification

Cerebral aneurysms can be classified based on morphology, location, size, and etiology.

8.2.1 Saccular Aneurysms

Most aneurysms are saccular (berry aneurysms) and located at vascular branch points at the base of the brain. Saccular aneurysms can be round or lobulated, with regular or irregular surface. A surface bleb, sometimes referred to as "Murphy's tit," may indicate the point of rupture in case of subarachnoid hemorrhage.

Intracranial internal carotid artery (ICA) is collectively the most common location of cerebral aneurysms, which can be further divided into segments based on different schemes. For example, Shapiro et al. [2] have proposed a scheme to separate the ICA into seven segments based on the angiographic and cross-sectional database, which include cervical, petrous, cavernous, para-ophthalmic, posterior communicating, choroidal, and terminus segments.

Petrous ICA aneurysms are rare and may be traumatic or due to atherosclerosis. It can mimic other lytic lesions in the petrous apices on the cross-sectional imaging.

Cavernous aneurysms are also rare. Large cavernous aneurysm can cause compression of cranial nerves III, IV, V, and VI within the cavernous sinus (Fig. 8.1). Because of the extradural location, ruptured cavernous aneurysms cause carotid-cavernous fistula or epistaxis rather than SAH. However, more distally near the clinoid process, the distal dural ring is only loosely attached to the medial aspect

Fig. 8.1 Right cavernous ICA aneurysm. Patient presents with right VI nerve palsy. Axial T2 MRI demonstrates a large right cavernous ICA aneurysm with flow void (*arrow*)

© Springer Nature Switzerland AG 2020
Y. Tang, *Atlas of Emergency Neurovascular Imaging*, https://doi.org/10.1007/978-3-030-43654-4_8

of ICA creating a potential space called "carotid cave." Carotid cave aneurysm can be partially intradural and lead to SAH if ruptured [3].

The para-ophthalmic segment is intradural, extending from the distal border of cavernous segment to the orifice of P-comm. Ophthalmic artery (Fig. 8.2) and superior hypophyseal artery (Fig. 8.3) aneurysms arise from this segment. The superior hypophyseal aneurysm projects medially toward the sella. It can be obscured by the adjacent osseous structures on CTA and is frequently better depicted by MRA.

P-comm aneurysms are the most frequent ICA aneurysms and typically project posteriorly (Fig. 8.4). Large P-comm aneurysm may cause cranial nerve III palsy. More distally at the choroidal segment are the anterior choroidal artery aneu-

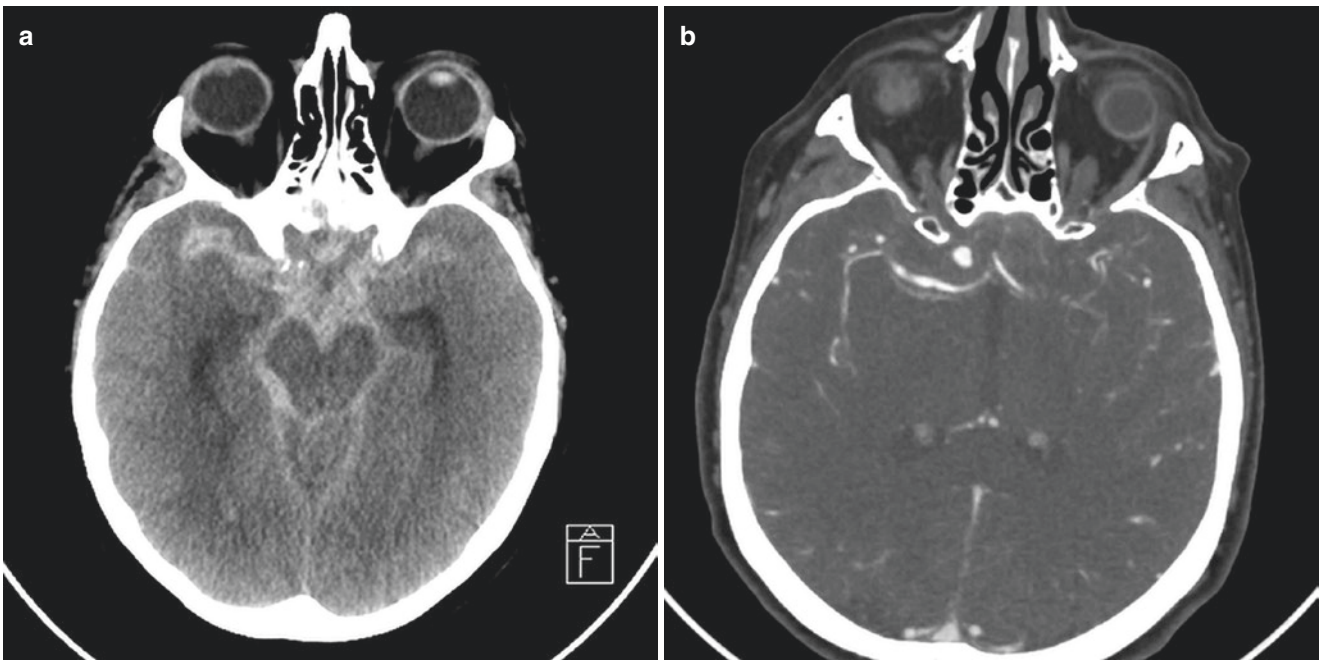

Fig. 8.2 Ophthalmic aneurysm. (**a**) NCCT shows diffuse subarachnoid hemorrhage within the basal cisterns and bilateral Sylvian fissures, typical for aneurysm rupture. (**b**) Axial CTA shows a saccular aneurysm at the ophthalmic segment of right supraclinoid ICA

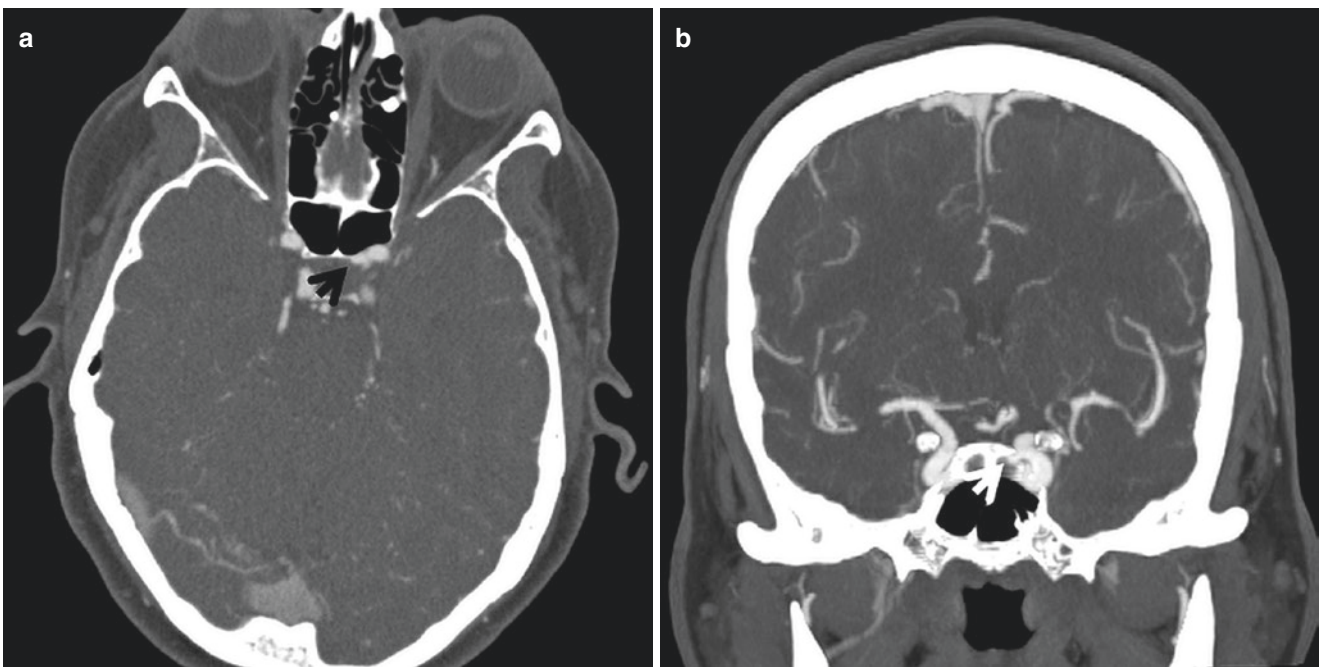

Fig. 8.3 Superior hypophyseal artery aneurysm. Axial (**a**) and coronal (**b**) CTA demonstrates an aneurysm from the para-ophthalmic left ICA projecting medially to the sella, consistent with a superior hypophyseal artery aneurysm

rysms, which are usually smaller than P-comm aneurysms and directed posteriorly and laterally (Fig. 8.5). Terminus aneurysm arises from the T-bifurcation of ICA (Fig. 8.6).

Most ACA aneurysms are located in the region of anterior communicating artery or A1–A2 junction (Fig. 8.7). A-comm aneurysms are the most commonly ruptured cerebral aneurysms. A less common location of ACA aneurysm is the pericallosal–callosomarginal artery junction (Fig. 8.8).

Most MCA aneurysms are located at bifurcation/trifurcation (Fig. 8.9). The superficial location allows relatively easy surgical access. In addition, MCA aneurysms are often wide-necked and incorporate the origin of M2 branches, which make it less favorable for endovascular coiling.

Posterior circulation aneurysms are less common and most frequently occur at the basilar tip (Fig. 8.10) and vertebral/PICA junction (Fig. 8.11).

8.2.2 Fusiform and Dissecting Aneurysms

Compared to saccular aneurysms, fusiform aneurysms are unrelated to vascular branching. They cause circumferential expansion of the vessel wall and do not have a recognizable neck. Fusiform aneurysms occur more commonly in the posterior circulation. While some fusiform aneurysms are likely related to atherosclerosis, many are dissecting aneurysms, especially in children and young non-atherosclerotic adults with underlying connective tissue diseases or vasculopathy.

Dissecting aneurysms can be acute or chronic [4]. Acute dissecting aneurysms are usually smaller in size and present with acute SAH. On angiography, they can appear as either fusiform or saccular. In addition, typical angiographic signs of dissection are usually observed in the parent arteries, including contour irregularity, stenosis, occlusion, and delayed and slow filling secondary to intramural hematoma (Fig. 8.12). The pathognomonic finding of a double lumen with visualization of both true and false channels is rarely seen in small intracranial arteries [4].

In comparison, chronic dissecting aneurysms are caused by silent or repeated dissections, with luminal thrombus formation and intramural hemorrhages. These aneurysms are usually large fusiform or serpentine lesions presenting with mass effect (Fig. 8.13). Ischemia and hydrocephalus can also occur, while hemorrhage is less common compared to acute dissecting aneurysms [4].

8.2.3 Dolichoectasia

Dolichoectasia is an arteriopathy characterized by abnormal elongation, tortuosity, and dilation of the cerebral arteries. It occurs more commonly in the vertebrobasilar

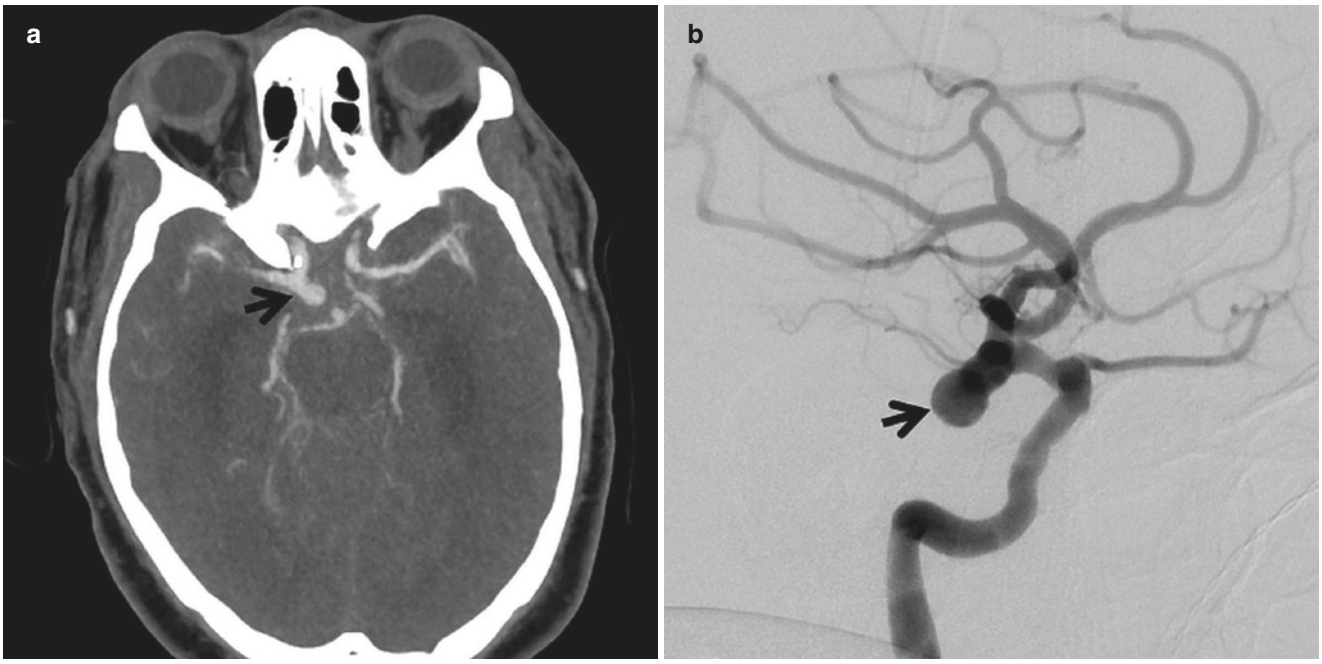

Fig. 8.4 P-comm aneurysm. (**a**) Axial CTA shows a lobulated aneurysm projecting posteriorly from the communicating segment of right supraclinoid ICA. (**b**) Lateral DSA from right ICA injection shows the P-comm aneurysm. The origin of the P-comm is obscured by the aneurysm on this projection

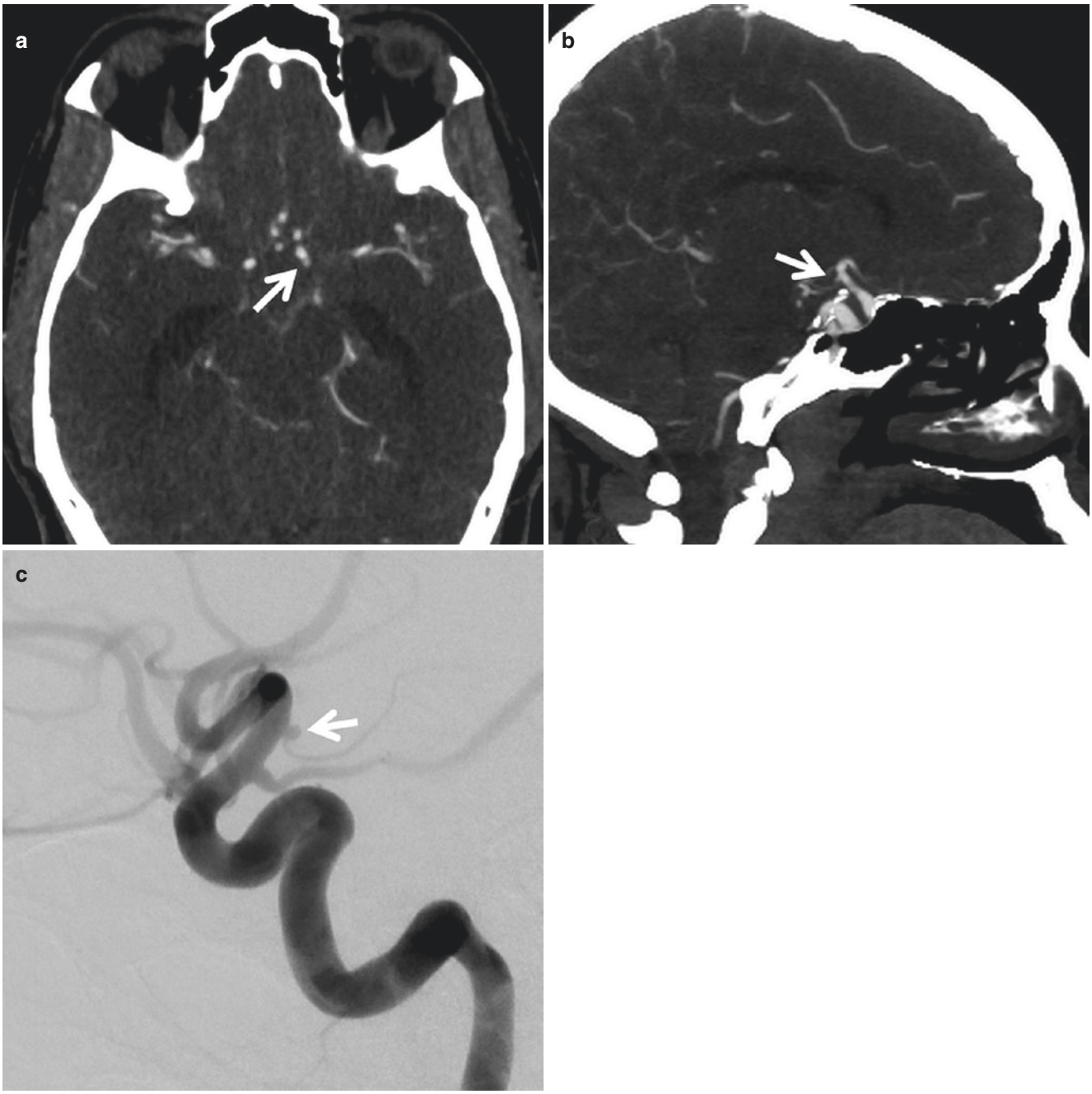

Fig. 8.5 Anterior choroidal artery aneurysm. Patient with acute SAH. Axial (**a**) and sagittal (**b**) CTA demonstrates a tiny posteriorly projecting aneurysm (*arrow*) at the origin of anterior choroidal artery, which is confirmed by DSA (**c**)

system although anterior circulation can also be involved (Fig. 8.14). Slow flow within the dolichoectatic arteries can predispose to thrombi formation, leading to embolic phenomenon or occlusion of small perforating arteries. Dilated vessel can also cause compression of adjacent structures such as brain stem and cranial nerves and cause hydrocephalus. Rarely, the affected vessel can rupture and cause catastrophic hemorrhage [5].

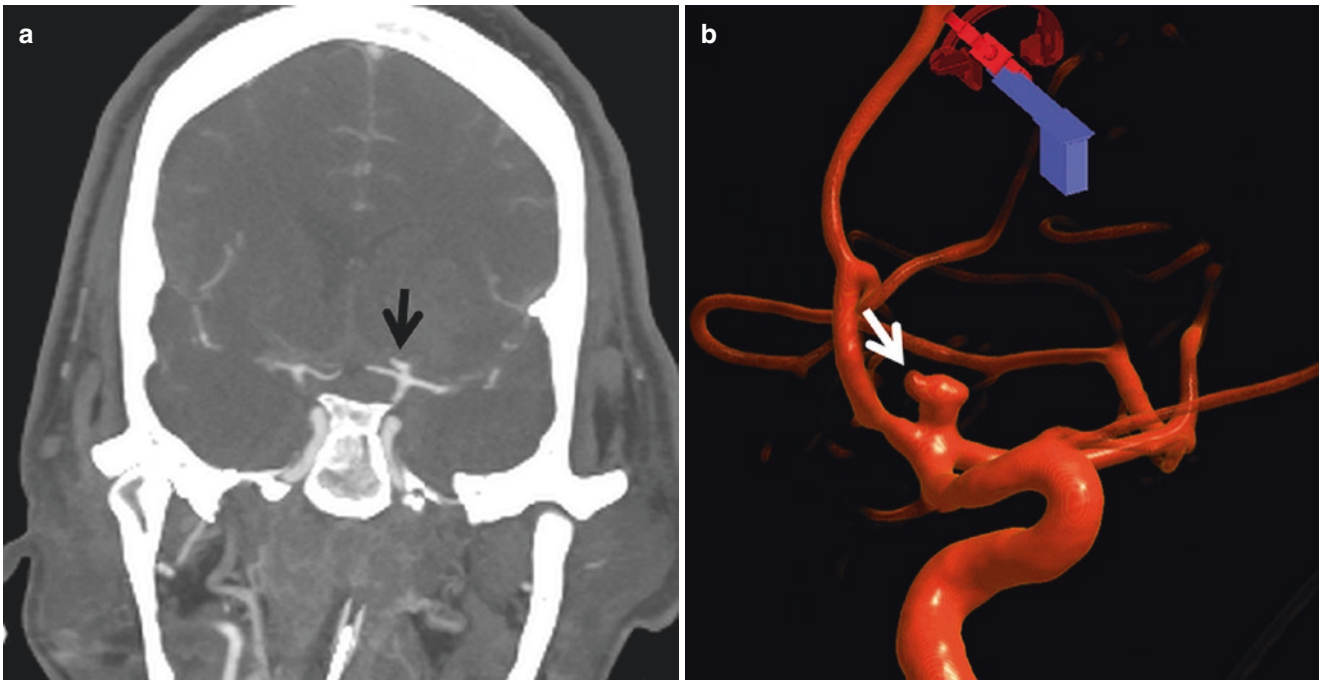

Fig. 8.6 ICA terminus aneurysm. (**a**) Coronal CTA demonstrates a superiorly projecting aneurysm from the ICA terminus. (**b**) 3-D rotational angiography confirms the aneurysm. Note the small lobule at the dome of the aneurysm, which is likely the point of rupture

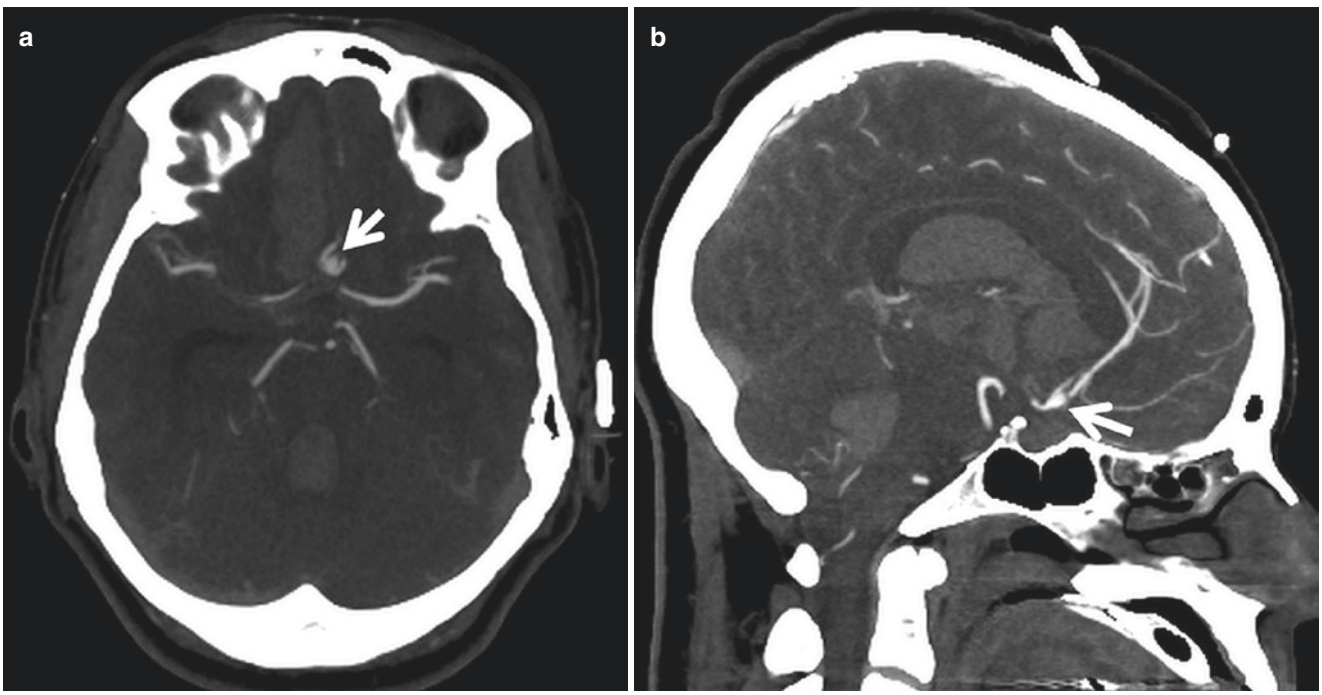

Fig. 8.7 A-comm aneurysm. Patient with acute subarachnoid, intraventricular, and right frontal parenchymal hemorrhage. Axial (**a**) and sagittal (**b**) CTA shows an anteriorly projecting aneurysm (*arrow*) arising from the anterior communicating artery

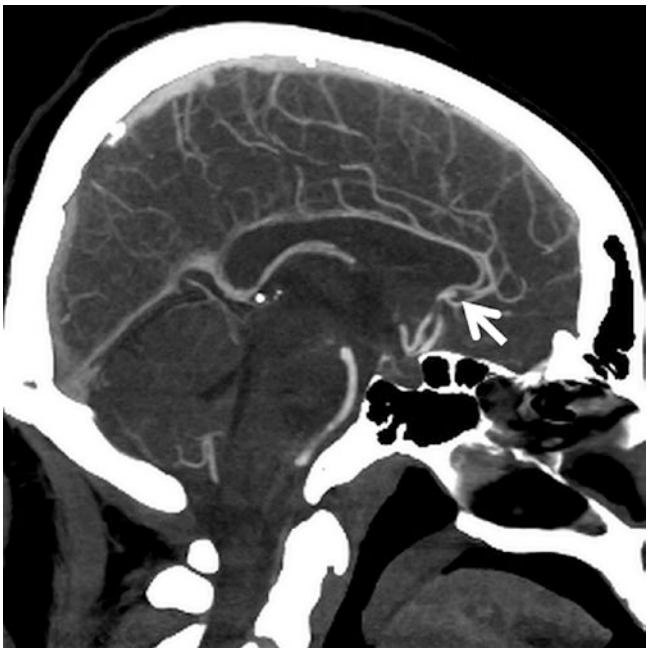

Fig. 8.8 Pericallosal aneurysm. Sagittal CTA shows an anteriorly projecting aneurysm at the junction of ACA pericallosal and callosomarginal arteries (*arrow*)

Fig. 8.10 Basilar tip aneurysm. Coronal CTA demonstrates a superiorly projecting aneurysm from the distal basilar artery. The neck is located between the origins of left posterior cerebral artery and superior cerebellar artery

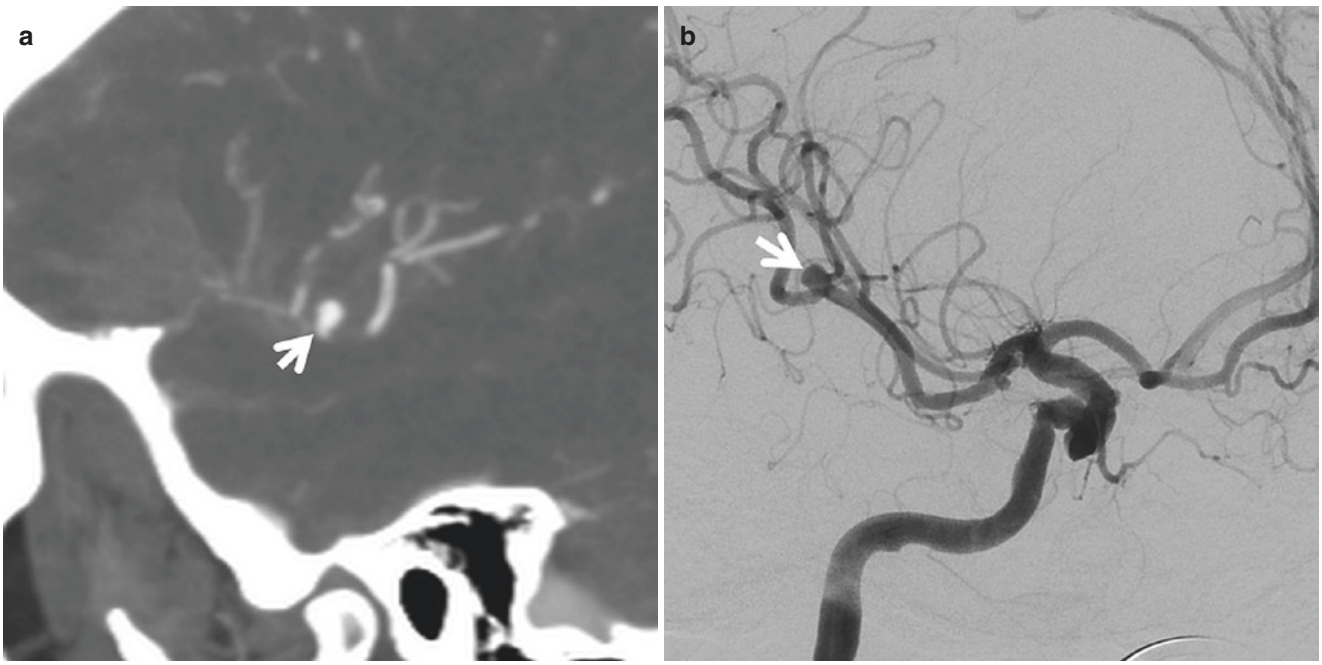

Fig. 8.9 MCA aneurysm. Sagittal CTA (**a**) shows a right MCA bifurcation aneurysm (*arrow*), confirmed by DSA (**b**). Note the origins of both M2 branches are incorporated into the neck of the aneurysm

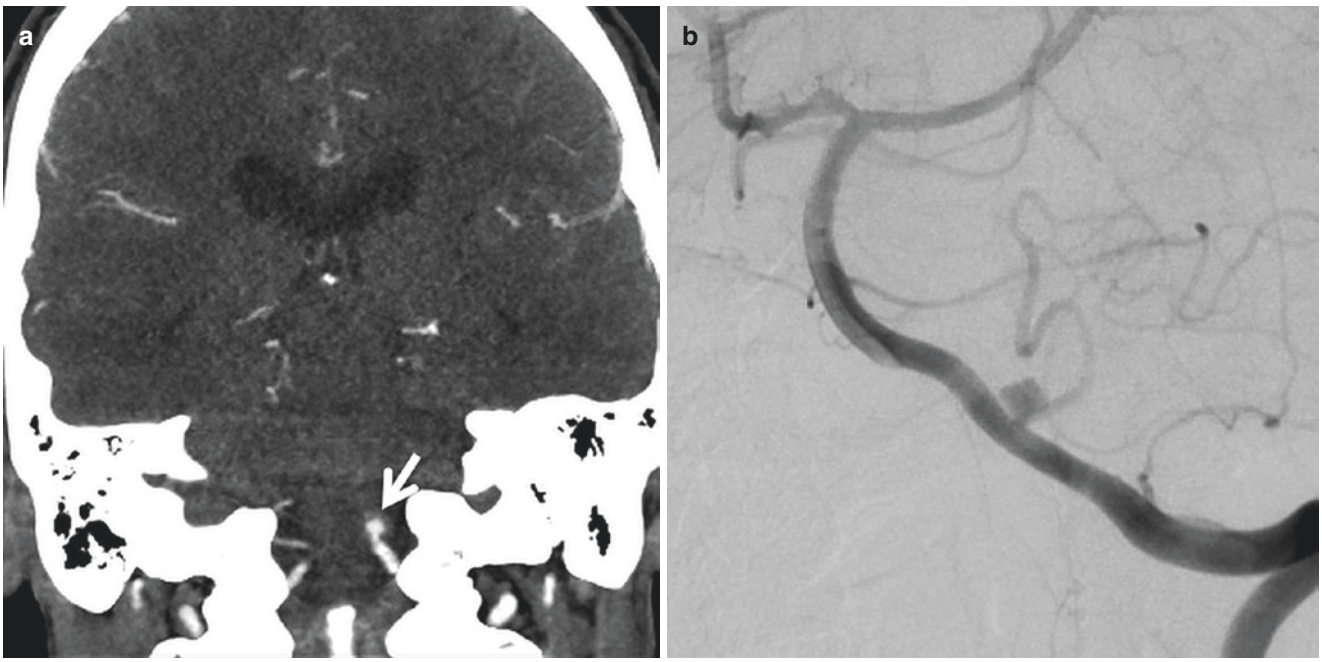

Fig. 8.11 PICA aneurysm. Coronal CTA (**a**) demonstrates an aneurysm at the left PICA origin, confirmed by DSA (**b**)

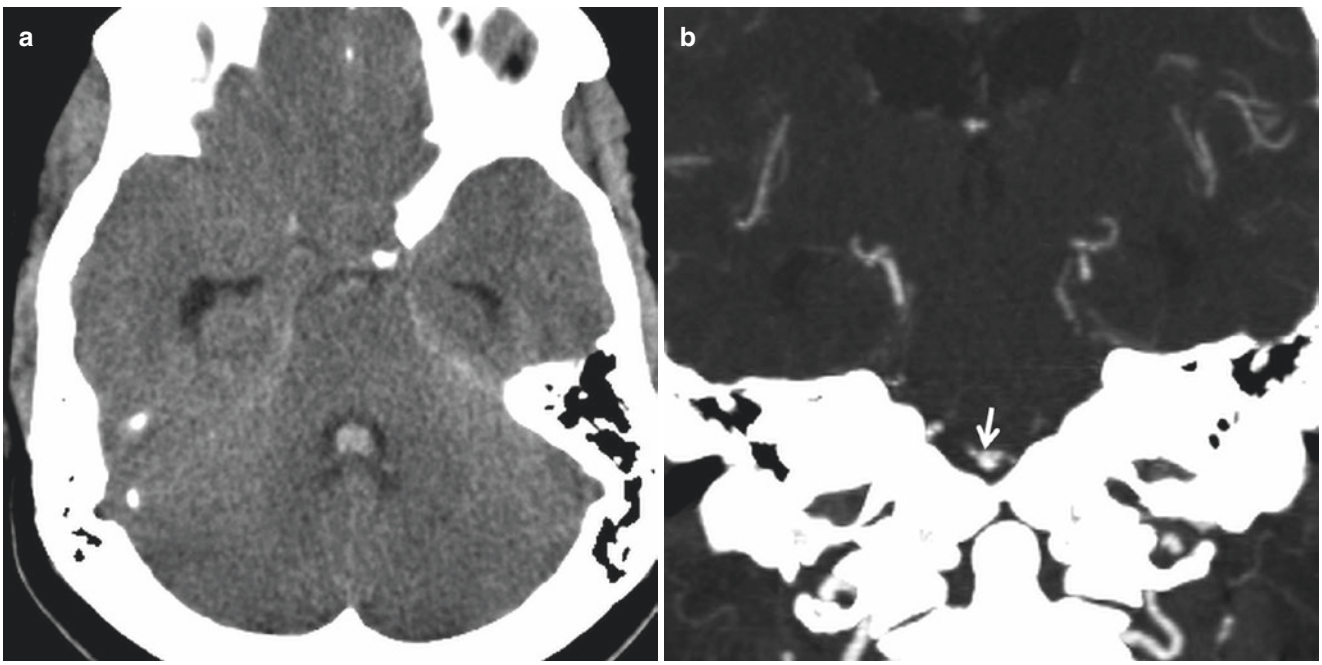

Fig. 8.12 Dissecting vertebral artery aneurysm. Young patient with acute headache. (**a**) NCCT shows a small amount of fourth ventricular hemorrhage and hydrocephalus. (**b**) Coronal CTA demonstrates a small aneurysm originating from left vertebral V4 segment (*arrow*). (**c**) 3D volume-rendered CTA reformation shows a fusiform aneurysm of V4 segment (*arrow*) with segmental narrowing of left vertebral artery proximal to the aneurysm, compatible with a dissection (*curved arrow*). (**d**) These findings are confirmed by DSA. Incidentally noted a fenestration of proximal basilar artery

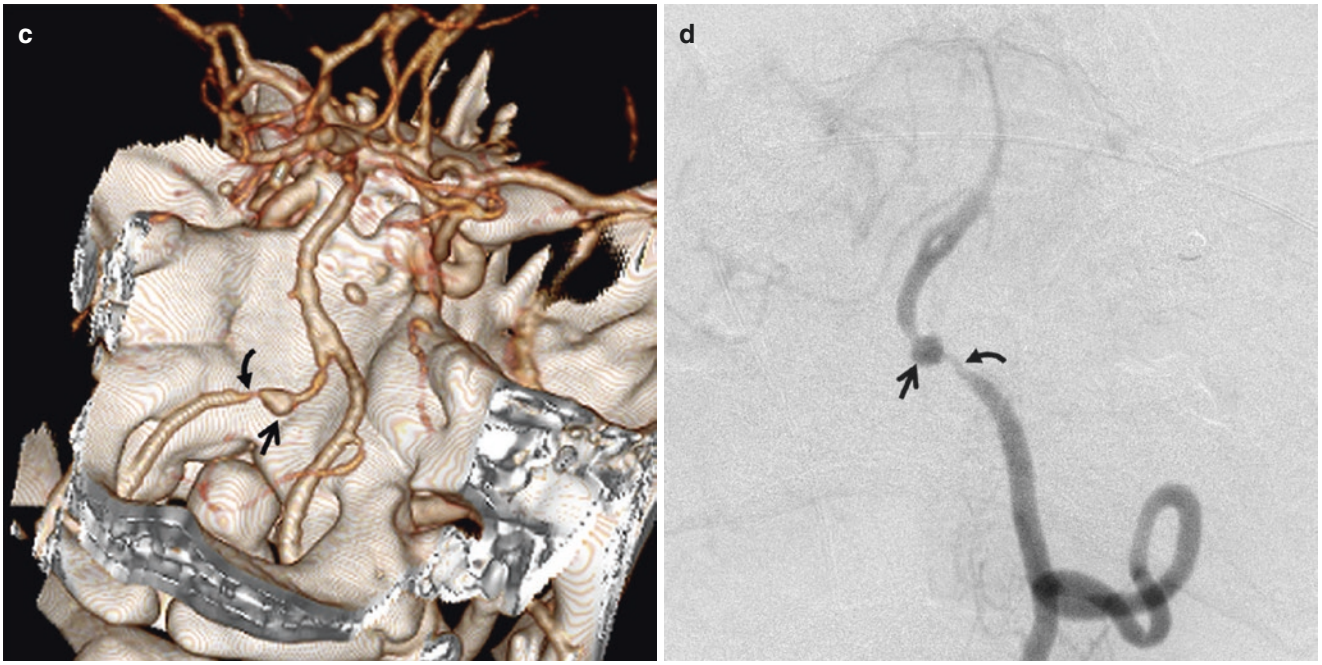

Fig. 8.12 (continued)

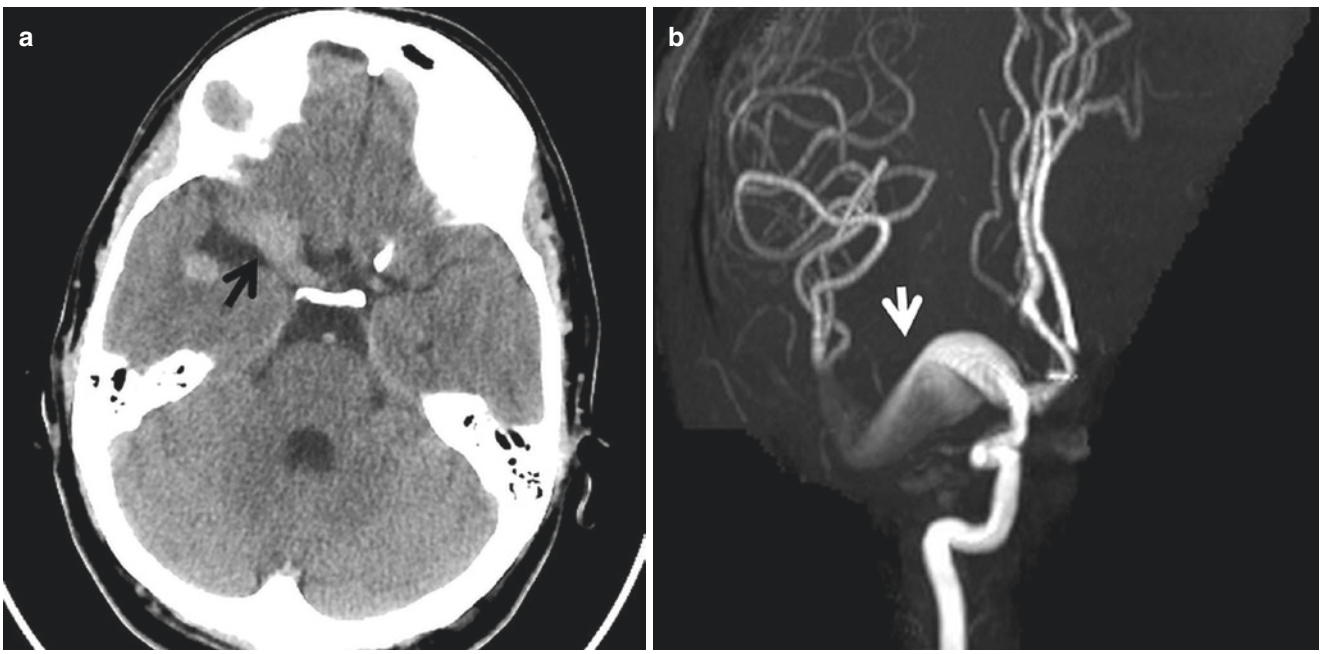

Fig. 8.13 Giant serpentine MCA aneurysm. Young patient presents with left-sided weakness and headache. (**a**) Axial NCCT shows hyperdense expansile appearance of the left MCA (*arrow*). (**b**) 3D TOF MRA demonstrates fusiform aneurysmal dilatation of the entire left MCA M1 and proximal M2 segment

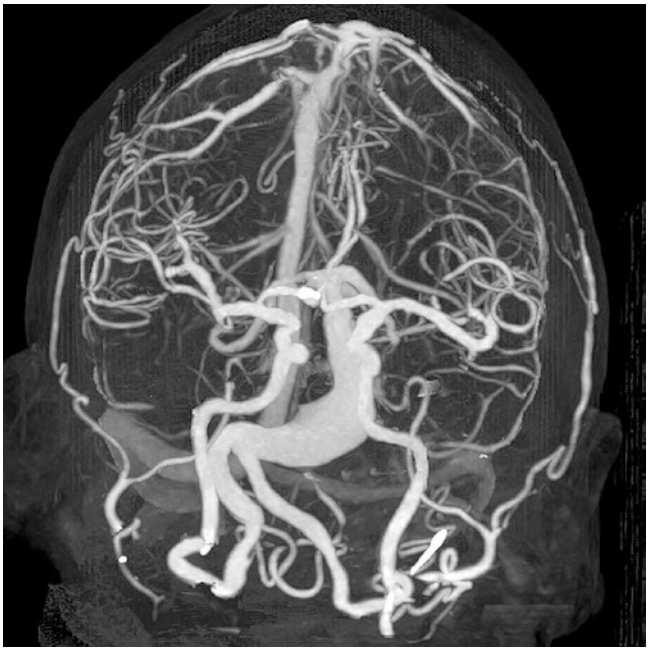

Fig. 8.14 Dolichoectasia. Patient with acute brain stem infarction. CTA shows marked fusiform aneurysmal dilatation of the basilar artery

8.2.4 Blood-Blister Aneurysm

Blood-blister aneurysms refer to small shallow wide-neck aneurysms, most commonly at the dorsal surface of supraclinoid ICAs. These aneurysms do not occur at the branch point and are likely related to focal dissections [6]. The wall is thin and covered almost entirely by adventitia and fibrous tissue. On angiography, they appear as small irregular bulges of the arterial wall (Fig. 8.15) [7]. Ruptured blister aneurysms have a high mortality rate and difficult to treat because they often lack a defined neck and has a very thin wall. Flow diversion is a promising treatment technique for these lesions [8].

8.2.5 Infectious Aneurysms

Most infectious or mycotic aneurysms occur secondary to septic emboli in patients with infectious endocarditis. They are often multiple and located in the distal arterial branches (Fig. 8.16). These aneurysms are fragile and usually rupture within the first weeks, with high morbidity and mortality [9, 10].

8.2.6 Size

Aneurysm can also be classified by its size. A commonly used scale is based on the maximum sac diameter: small (<10 mm), large (10–25 mm), and giant (>25 mm). Besides the maximal sac diameter, other parameters such as neck width or dome-to-neck ratio should be reported as wide-neck aneurysms are less likely to retain coils and may require adjunctive techniques such as neck remodeling, stent-assisted coiling, or flow diversion. The most commonly used definition for wide-neck aneurysm was a neck size of ≥4 mm and/or a dome-to-neck ratio of ≤2 [11].

8.3 Clinical Manifestations

A large, unruptured aneurysm can cause symptoms by exerting mass effect on the cranial nerves or other brain structures. For example, a large posterior communicating aneurysm can cause symptoms related to third nerve palsy.

Most commonly, patients with cerebral aneurysms become symptomatic when the aneurysms rupture and cause acute SAH. Most ruptured aneurysms are less than 10 mm. SAH can extend into the ventricles, brain parenchyma, or rarely subdural space. Nearly 10% of the patients with ruptured aneurysms die before reaching the hospital. Many patients present with coma or severe neurologic deficits. Others may present with an acute onset of severe headache, often described as the "worst headache of life." Some patients with "minor leak" may present with transient, less severe headache before the substantial SAH occurs [12]. Clinical grading scales such as the Hunt and Hess (Table 8.1) are used to describe the neurologic condition on admission and are considered good predictors of outcome [13].

CT is the modality of choice to evaluate suspected acute SAH. The four-point Fisher grading based on the amount of SAH on the non-contrast CT correlates with the chance of development of vasospasm (Table 8.2) [14]. Older studies showed that non-contrast CT might be negative in a small percentage of patients with SAH. However, more current studies have shown a significantly higher sensitivity of the non-contrast head CT in the detection of even a small amount of subarachnoid hemorrhage when performed within 6 hours from the headache onset [15]. With high clinical suspicion for SAH and negative CT, lumbar puncture should be performed. The bloody cerebrospinal fluid that fails to clear with a continued flow of cerebrospinal fluid should raise a suspicion of subarachnoid hemorrhage. The presence of xanthochromia, a yellowish discoloration of the cerebrospinal fluid representing bilirubin from the breakdown of hemoglobin, is even more definitive than a high red cell count in the cerebrospinal fluid [16].

Multiple complications can be seen in patients with SAH secondary to a ruptured aneurysm. Rebleeding is one of the most common complications with the incidence rate as high as 4% at 24 hours, 20% at 2 weeks, and 50% at 6 months among these patients [17]. Acute hydrocephalus can develop in up to 20% of patients who have aneurysmal SAH, requir-

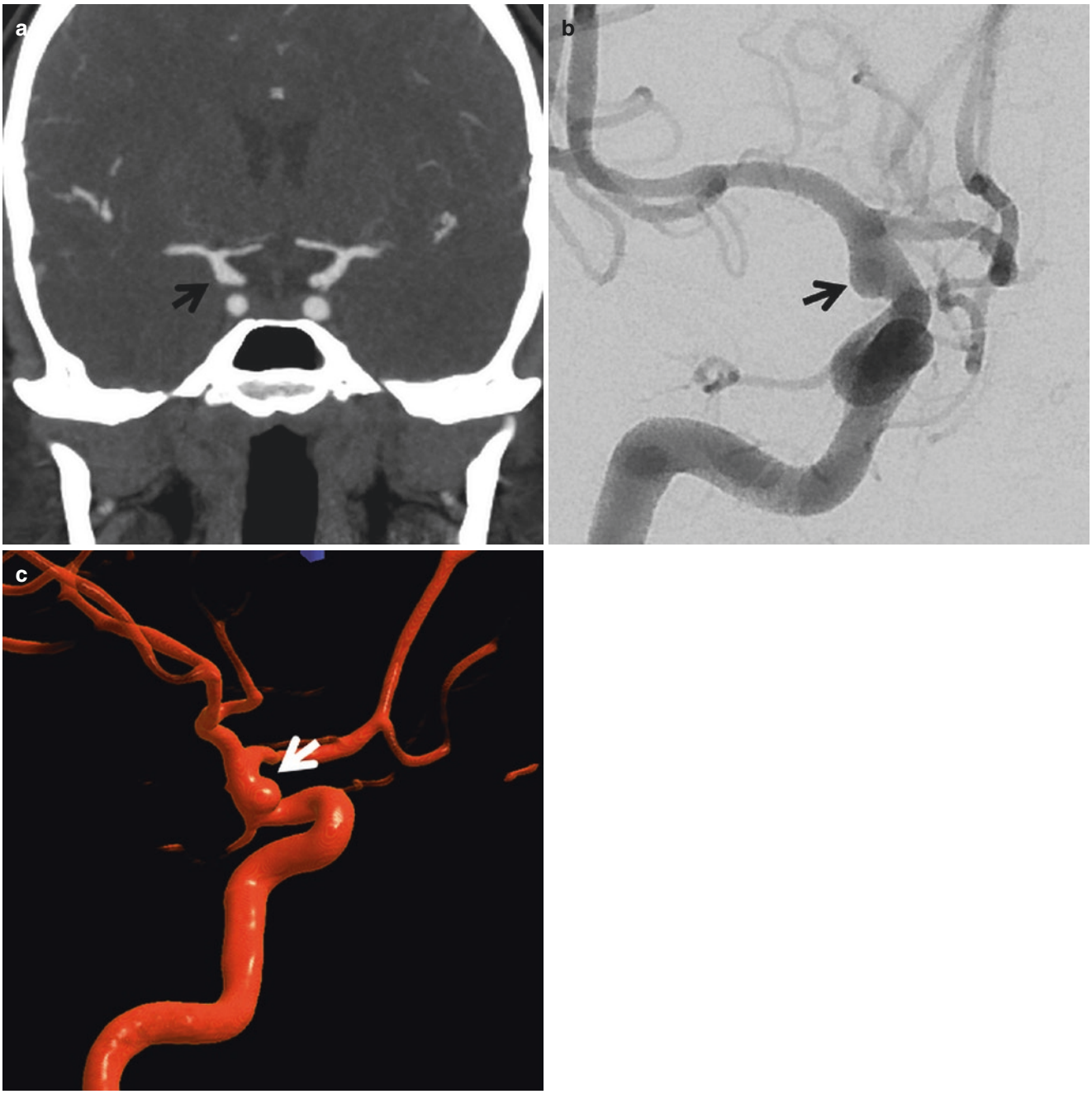

Fig. 8.15 Blood-blister aneurysm. (**a**) Coronal CTA shows a broad-based contour bulge of the right supraclinoid ICA (*arrow*). (**b**) AP DSA shows similar finding. (**c**) 3D rotational angiography better demonstrates the blister aneurysm at the superior surface of the right ICA

ing emergent ventriculostomy for drainage of CSF. Another known manifestation of SAH is "cardiac stun," likely caused by excessive catecholamine release in response to the intracranial hemorrhage. The presence of a markedly decreased ejection fraction with ventricular wall motion abnormalities that does not match the electrocardiographic vascular distribution of ischemia helps to make the diagnosis. Most cases of cardiac stun are temporary, and permanent injury is rare [18].

Cerebral vasospasm is a frequent complication of aneurysmal SAH associated with significant morbidity and mortality. Early vasospasm can occur immediately after aneurysm rupture due to a combination of the sudden rise in intracranial pressure, mechanical compression of arteries, and release of short-acting vasoconstrictors [19]. Delayed vasospasm and

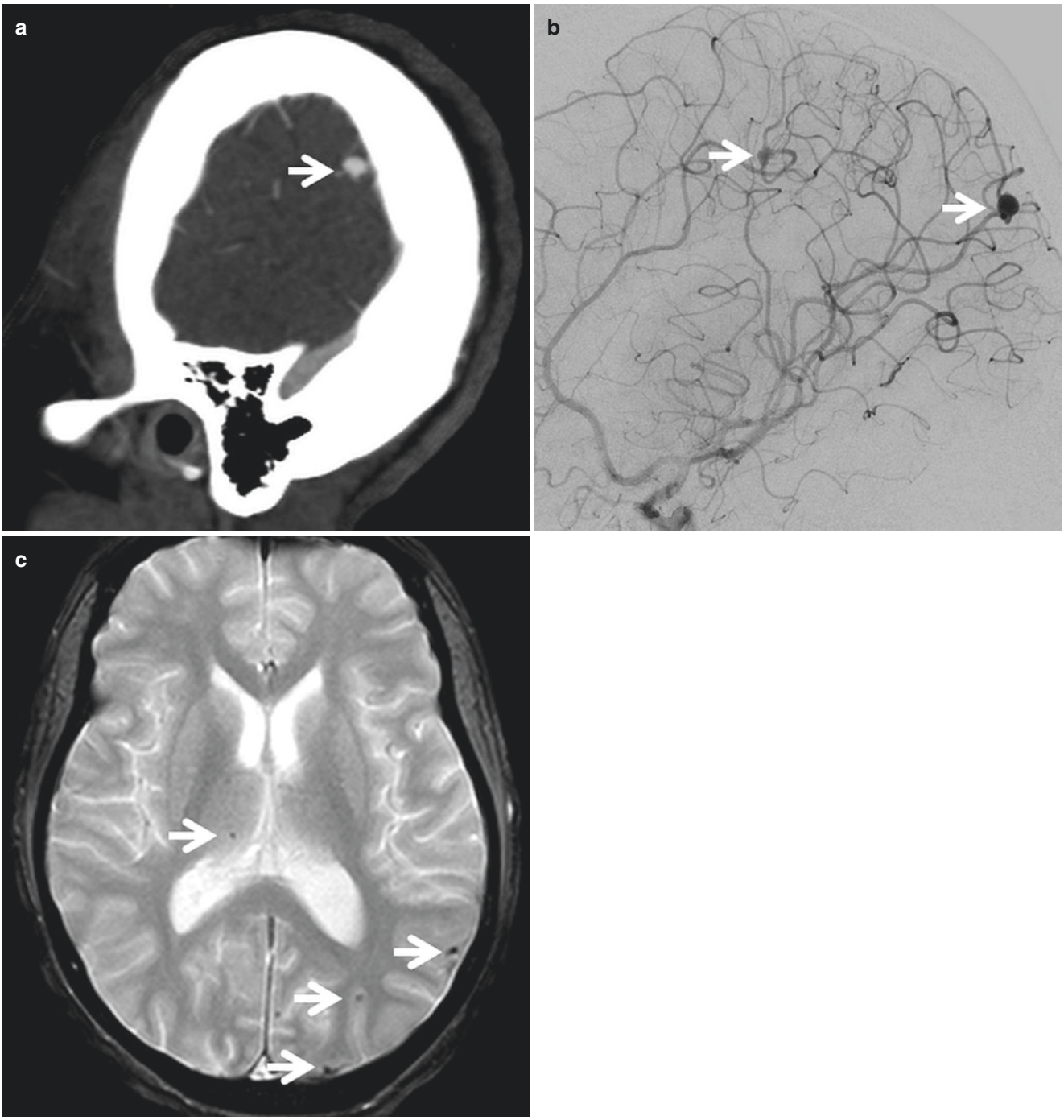

Fig. 8.16 Infectious aneurysm. Patient with history of IV drug abuse and endocarditis presents with left parietal parenchymal hemorrhage. (**a**) Sagittal CTA demonstrates an aneurysm in the left parietal region. (**b**) Lateral DSA from left ICA injection shows the aneurysm originating from a distal branch of left MCA (*arrow*). Additional aneurysm in the distal left ACA branch is also seen (*arrow*). The clinical history and distal location of the aneurysms are typical for infectious or mycotic aneurysms. (**c**) Axial GRE MRI shows multiple small foci of microhemorrhage, likely reflecting additional septic emboli

cerebral ischemia typically occur 3–14 days after SAH and can lead to stroke or death even with maximal treatment. It is likely caused by the exposure of cerebral arteries to the breakdown products of blood and subsequent changes in vascular smooth muscle function. Two-third of patients with SAH who undergo cerebral angiography exhibit evidence of vasospasm on imaging, known as angiographic vasospasm, and approximately one-third show clinical symptoms of vasospasm such

Table 8.1 Hunt and Hess grading scale for subarachnoid hemorrhage

Grade	Clinical description
1	Asymptomatic or minimal headache and slight nuchal rigidity
2	Moderate-to-severe headache, nuchal rigidity, and no neurologic deficit other than cranial nerve palsy
3	Drowsiness, confusion, or mild focal deficit
4	Stupor, moderate-to-severe hemiparesis, and possibly early decerebrate rigidity and vegetative disturbances
5	Deep coma, decerebrate rigidity, and moribund appearance

Table 8.2 Fisher scale system for quantification of SAH on CT

Grade	CT findings
1	No SAH or intraventricular hemorrhage (IVH) detected
2	Diffuse thin (<1 mm) SAH without clot
3	Localized clots and/or layers of blood >1 mm, no IVH
4	Diffuse SAH, presence of ICH or IVH

CT computed tomography, *ICH* intracerebral hemorrhage, *SAH* subarachnoid hemorrhage

as the development of new neurologic deficits. One-third of patients with clinical vasospasm die from cerebral infarction, and the other one-third live with significant neurologic sequelae [20].

All patients with SAH should be closely monitored for vasospasm clinically and by daily transcranial Doppler (TCD). When the TCD shows an increased velocity, CTA/CT perfusion should be considered (Fig. 8.17). Clinical deterioration that is not due to rebleeding or hydrocephalus can be a sign of vasospasm. Medical treatment of vasospasm consists of calcium antagonist and triple-H therapy (hypertension, hypervolemia, and hemodilution). In patients with severe persistent neurologic deficits, catheter angiography can confirm the presence of vasospasm, and treatment can be performed by either intra-arterial administration of vasodilators or balloon angioplasty.

8.4 Imaging Modality of Intracranial Aneurysms

CTA has become the modality of choice in the emergent evaluation of suspected cerebral aneurysms, due to the non-invasive nature, high spatial resolution, and fast acquisition. Although earlier studies on single-slice CT found sensitivity as low as 69%, more recent studies have reported higher sensitivity and specificity, ranging from 85.5% to 95% [21, 22]. When compared with digital subtraction angiography (DSA), CTA has an average specificity of 96–98%, sensitivity of 96–98%, and false-negative rate of 13% [23–25].

Catheter angiography is considered the reference standard for diagnosing cerebral angiogram and treatment planning. In particular, 3D rotational angiography can detect considerably more small (≤3 mm) aneurysms than DSA. In selected patients, accurate detection of these aneurysms may have consequences for the choice of treatment technique and for the frequency and duration of imaging follow-up [26].

3D time-of-flight (TOF) MR angiography (MRA) has been used for detection of aneurysms, usually in the non-acute setting. Patients with history of autosomal dominant polycystic kidney disease or family history of two immediate relatives with intracranial aneurysms require screening MRA for cerebral aneurysm. The main limitation of MRA is its sensitivity to motion, which makes it challenging to use in patients with SAH who cannot stay still. In addition, artifacts related to spin saturation and flow can mimic the aneurysm on this sequence. Finally, due to T1 characteristics of MRA, the substances causing T1-prolongation, such as hematoma, can also simulate cerebral aneurysms.

Angiogram-negative SAH accounts for 15% of spontaneous SAH. Non-aneurysmal peri-mesencephalic hemorrhage likely accounts for some of these cases, which is a diagnosis of exclusion. In other cases, ruptured aneurysms are either thrombosed or obscured by hemorrhage/vasospasm and become angiographically occult in the initial study but can be detected later (Fig. 8.18). Rare cases of intracranial dissection can cause subarachnoid hemorrhage, but not recognizable on the initial angiogram.

8.5 Management

Primary management options for intracranial aneurysms include craniotomy with clip ligation, endovascular treatment, and observation.

8.5.1 Ruptured Aneurysms

Patients with acute aneurysmal SAH need early treatment to secure the ruptured aneurysms. Endovascular coil embolization has substantially replaced neurosurgical clipping as the first-line treatment after the introduction of Guglielmi detachable coils in 1991 [27, 28]. The basic technique has evolved over the years with the introduction of improved coils, balloon-assisted and stent-assisted coiling. The advantage of coiling over clipping was first established by the International Subarachnoid Aneurysm Trial (ISAT) [29] and confirmed by subsequent randomized clinical trial [30]. The Barrow Ruptured Aneurysm Trial, although statistically underpowered, suggest little difference in outcome between coiling and clipping for anterior circulation aneurysms but a sustained advantage of coiling over clipping for the posterior circulation aneurysms [31].

Although endovascular treatment is the preferred method in patients with an aneurysm suitable for both techniques,

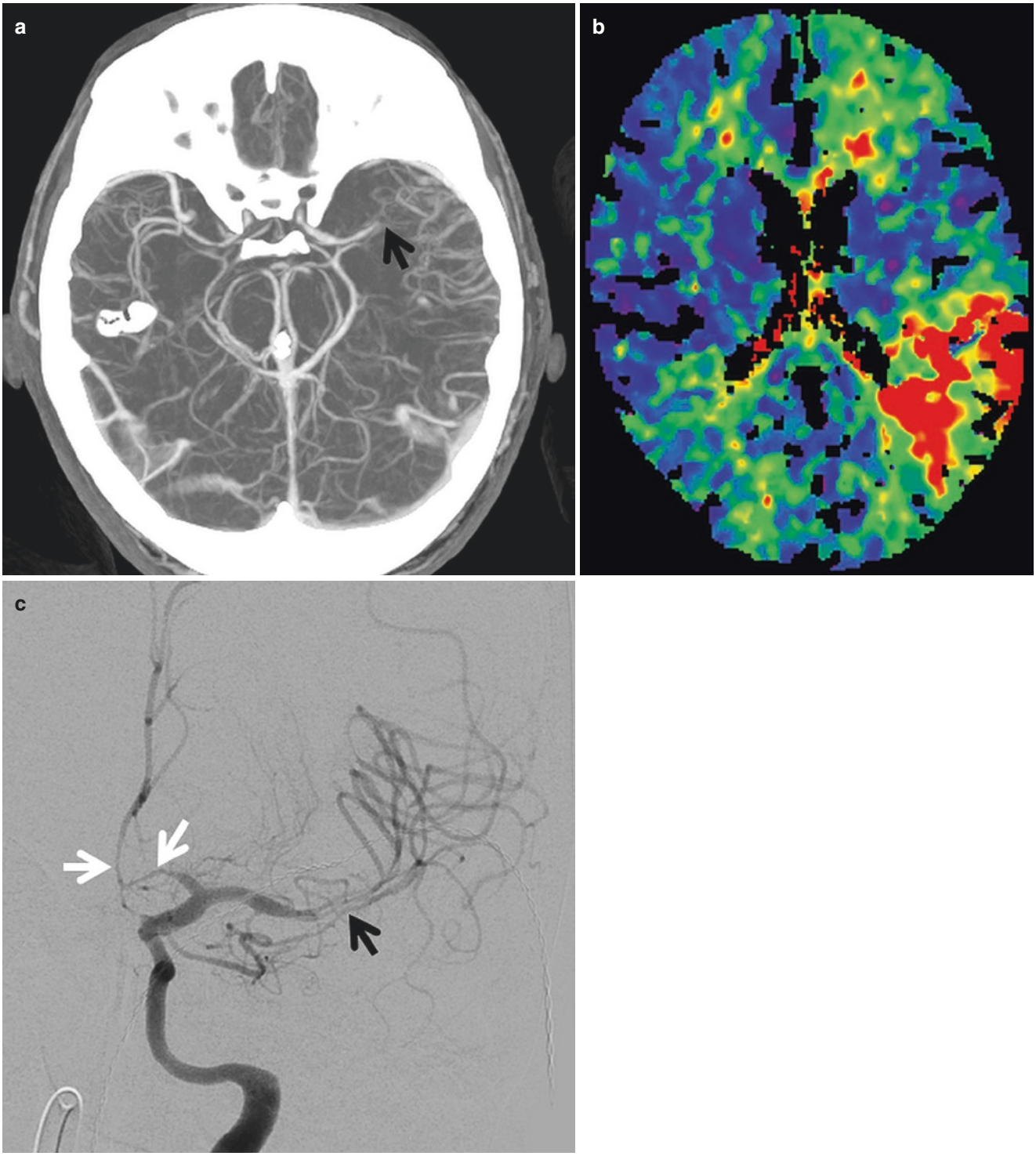

Fig. 8.17 Vasospasm and delayed cerebral ischemia. Patient with SAH developed progressive right-sided weakness and elevated velocity on the TCD. (**a**) Axial CTA shows diffuse vasospasm, most severe at the distal left M1 segment (*arrow*). (**b**) CT perfusion demonstrates markedly elevated time to drain in the left parietal/temporal region, corresponding to an infarction. (**c**) AP DSA from left ICA injection demonstrates severe vasospasm involving the distal left M1 (*black arrow*), left A1, and proximal A2 segments (*white arrows*)

aneurysm with a wide-neck or complex branch vessel anatomy might benefit from microsurgical clipping. In recent years, flow diversion has rapidly become an alternative option for many large or giant, wide-neck intracranial aneurysms with high cure rate and reasonably low complication rates [32]. Modern treatment of ruptured aneurysms should

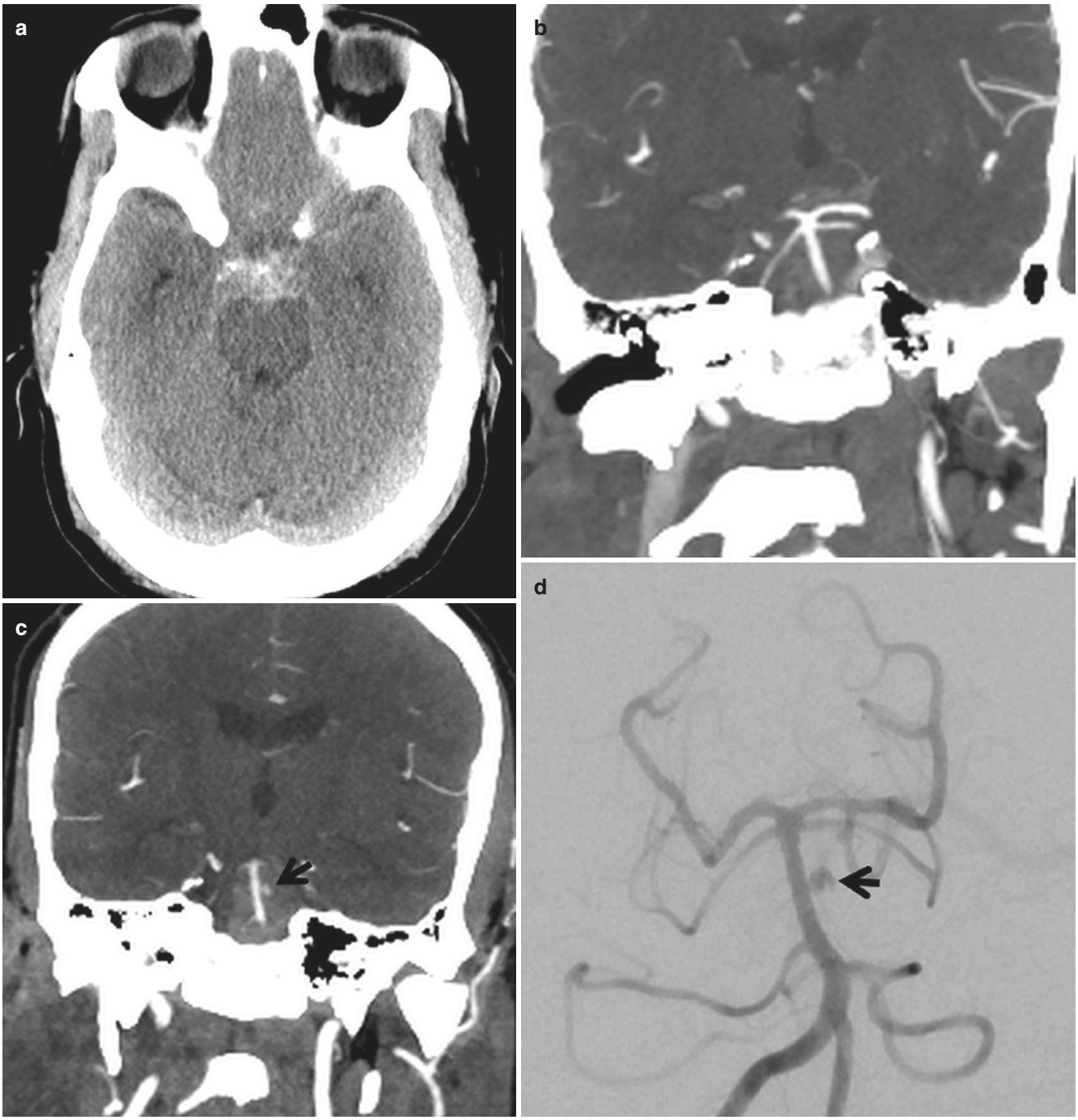

Fig. 8.18 Occult aneurysm. (**a**) NCCT shows a perimesencephalic SAH pattern. (**b**) Initial CTA is negative for aneurysm. DSA is also negative (not shown). (**c**) Follow-up CTA coronal image shows a blister type of aneurysm (*arrow*) arising from the left lateral aspect of the basilar artery, which is confirmed by DSA (**d**)

be individualized and ideally conducted in centers with endovascular and surgical expertise.

8.5.2 Unruptured Aneurysms

Increasing availability and sensitivity of noninvasive imaging has resulted in the detection of many incidental aneurysms. Majority of these aneurysms are small in size and never rupture. It is critical to identify and treat the high-risk aneurysms while avoiding overtreating those with low rup-

ture potential. The most important data in the natural history of the intracranial aneurysms comes from the International Study of Unruptured Intracranial Aneurysm (ISUIA), in which 1692 subjects were recruited. Of those, 1077 subjects belonged to group 1 without prior history of subarachnoid hemorrhage, and 615 belonged to group 2 with a history of prior subarachnoid hemorrhage from a separate aneurysm. The result of the study showed that the size and location of the aneurysm are predictors of future rupture. The 5-year cumulative risk of rupture in small aneurysms (<7 mm) of the anterior circulation was 0% and 1.5% in groups 1 and 2, respectively, whereas the risk of rupture in posterior circulation aneurysms was 2.5% and 3.4% in those groups [33].

8.6 Follow-Up After Treatment

Angiographic recurrence after endovascular treatment of the aneurysm is not infrequent, ranging from 14.7% to 33.6%, but usually not with severe clinical consequences [34]. The International Subarachnoid Aneurysm Trial (ISAT), for this purpose, showed a 0.2% yearly risk of rerupture with a mean follow-up of 4 years [29]. Coil embolization is associated with a higher rate of aneurysm recurrence than clipping. The best predictors of aneurysmal recurrence were aneurysmal anatomy (neck width > 4 mm and diameter > 10 mm) and the presence of a residual aneurysm after initial treatment [35].

Treated aneurysms can be graded with a three-point scale based on angiographic appearance [34, 36]. "Complete" refers to 100% obliteration of the aneurysm. "Residual neck or neck remnant" represents the persistence of any portion of original defect of arterial wall but without opacification of the aneurysmal sac. "Residual aneurysm or incomplete obliteration" refers to opacification of the aneurysm sac.

DSA has traditionally been the primary imaging modality in posttreatment follow-up in aneurysms, but because of the invasive nature and procedural risk, CTA and MRA have been increasingly used for this purpose. CTA is mostly used in the setting of rebleeding or other acute neurological presentations, but the sensitivity of detecting small recurrence is limited by the streak artifact from the coils or clips. MRA is the modality of choice for routine follow-up of the treated aneurysms in many practices. Contrast-enhanced (CE) MRA has been shown to be at least equivalent to DSA for characterization of aneurysmal remnants after coiling.

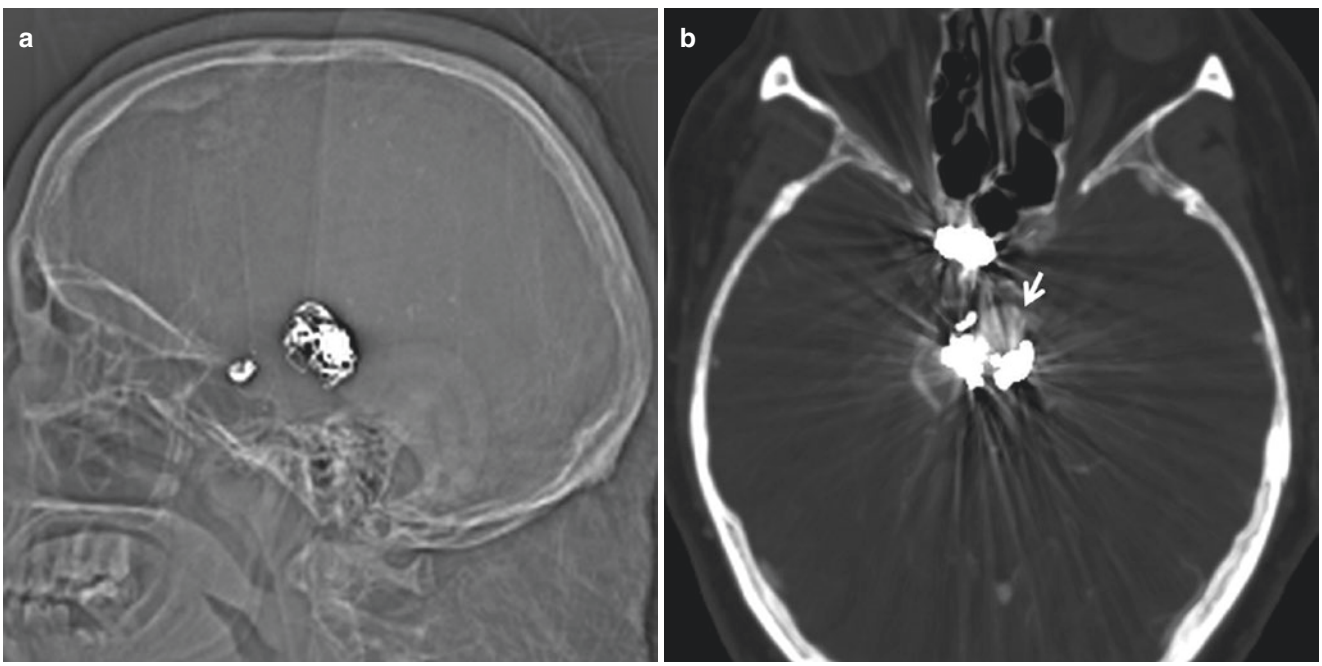

Fig. 8.19 Recurrent aneurysm after coiling. Patients with remote history of aneurysm coiling present with acute headache and weakness. (**a**) Lateral CT scout of the head reveals two coil masses in the expected regions of basilar artery and supraclinoid ICA, both of which show evidence of coil compaction. (**b**) Axial CTA with limited image quality shows recurrent aneurysmal sac filling in the basilar artery (*arrow*). (**c**) CE MRA more clearly shows the filling of the basilar aneurysm (*arrow*). There is also a recurrent right P-comm aneurysm (*curved arrow*), which is obscured on the CTA by the streak artifact. (**d**) DSA confirms the findings on the MRA

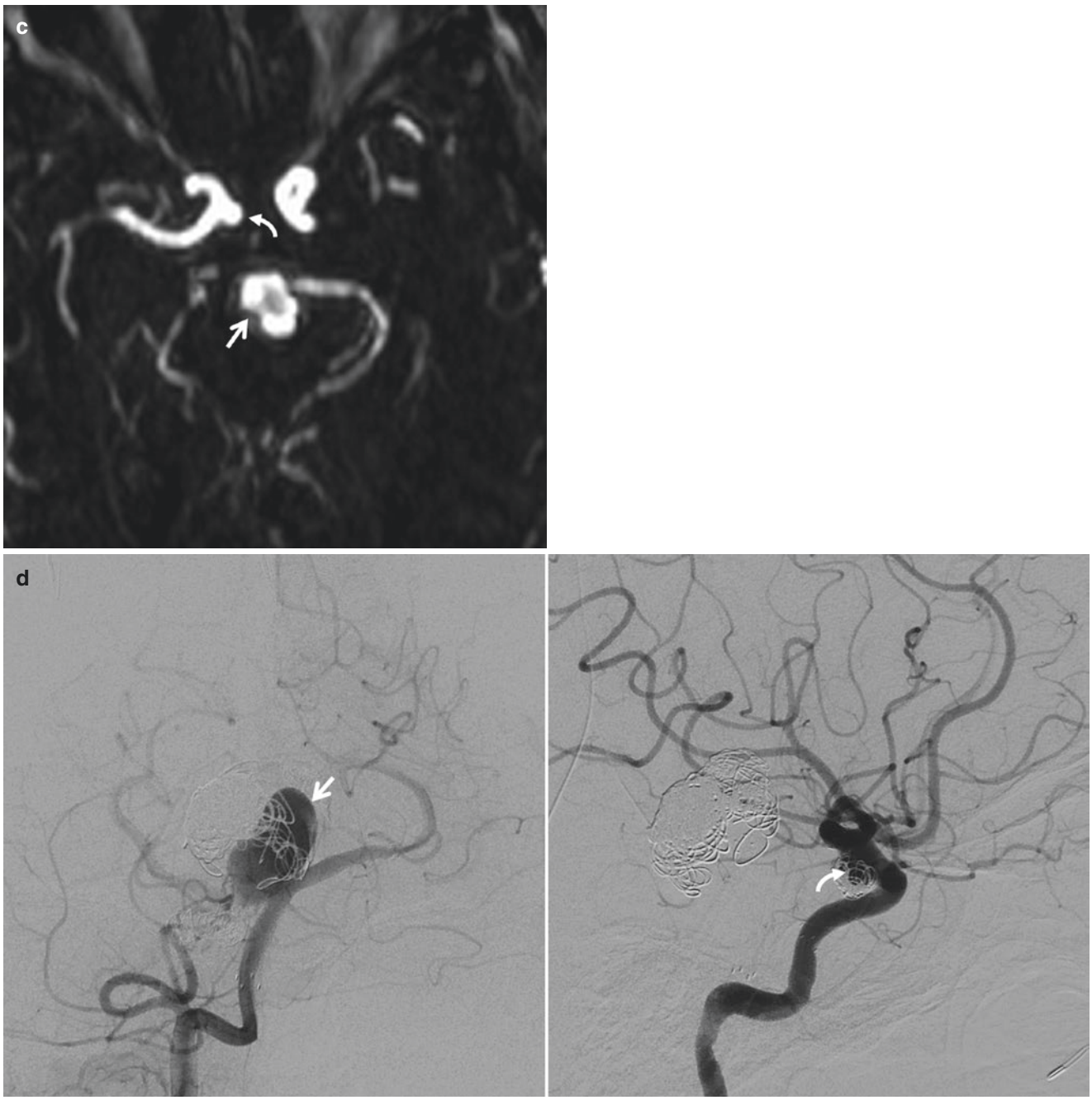

Fig. 8.19 (continued)

Contrast filling within the coil mass was more clearly seen with CE MRA than with DSA [37]. Unenhanced TOF and CE MRA sequences are similarly effective at classifying coiled aneurysms as occluded or residually patent. However, CE MRA is superior to TOF MRA for visualization of residual patency and is associated with fewer artifacts (Fig. 8.19) [38].

References

1. Brisman JL, Song JK, Newell DW. Cerebral aneurysms. N Engl J Med. 2006;355:928–39.
2. Shapiro M, Becske T, Riina HA, Raz E, Zumofen D, Jafar JJ, Huang PP, Nelson PK. Toward an endovascular internal carotid artery classification system. Am J Neuroradiol. 2014;35:230–6.
3. Kobayashi S, Kyoshima K, Gibo H, Hegde SA, Takemae T, Sugita K. Carotid cave aneurysms of the internal carotid artery. J Neurosurg. 1989;70:216–21.

4. Biondi A. Trunkal intracranial aneurysms: dissecting and fusiform aneurysms. https://doi.org/10.1016/j.nic.2006.05.006.
5. Del Brutto VJ, Ortiz JG, Biller J. Intracranial arterial dolichoectasia. Front Neurol. 2017;8 https://doi.org/10.3389/fneur.2017.00344.
6. Ogawa A, Suzuki M, Ogasawara K. Aneurysms at nonbranching sites in the supraclinoid portion of the internal carotid artery: internal carotid artery trunk aneurysms. Neurosurgery. 2000;47:578–86.
7. Gaughen JR, Raghavan P, Jensen ME, Hasan D, Pfeffer AN, Evans AJ. Utility of CT angiography in the identification and characterization of supraclinoid internal carotid. Am J Neuroradiol. 2010;31:640–4.
8. Rouchaud A, Brinjikji W, Cloft HJ, Kallmes DF. Endovascular treatment of ruptured blister-like aneurysms: a systematic review and meta-analysis with focus on deconstructive versus reconstructive and flow-diverter treatments. Am J Neuroradiol. 2015;36:2331–9.
9. Ducruet AF, Hickman ZL, Zacharia BE, Narula R, Grobelny BT, Gorski J, Connolly ES. Intracranial infectious aneurysms: a comprehensive review. Neurosurg Rev. 2010;33:37–45.
10. Bonneville F, Sourour N, Biondi A. Intracranial aneurysms: an overview. Neuroimaging Clin N Am. 2006;16:371–82.
11. Zhao B, Yin R, Lanzino G, Kallmes DF, Cloft HJ, Brinjikji W. Endovascular coiling of wide-neck and wide-neck bifurcation aneurysms: a systematic review and meta-analysis. Am J Neuroradiol. 2016;37:1700–5.
12. Juvela S. Minor leak before rupture of an intracranial aneurysm and subarachnoid hemorrhage of unknown etiology. Neurosurgery. 1992;30:7–11.
13. Hunt WE, Hess RM. Surgical risk as related to time of intervention in the repair of intracranial aneurysms. J Neurosurg. 1968;28:14–20.
14. Fisher CM, Kistler JP, Davis JM. Relation of cerebral vasospasm to subarachnoid hemorrhage visualized by computerized tomographic scanning. Neurosurgery. 1980;6:1–9.
15. Rabinstein AA, Lanzino G. Aneurysmal subarachnoid hemorrhage: unanswered questions. Neurosurg Clin N Am. 2018;29:255–62.
16. Edlow JA, Caplan LR. Avoiding pitfalls in the diagnosis of subarachnoid hemorrhage. N Engl J Med. 2000;342:29–36.
17. Eskesen V, Rosenørn J, Schmidt K. The impact of rebleeding on the life time probabilities of different outcomes in patients with ruptured intracranial aneurysms. A theoretical evaluation. Acta Neurochir (Wien). 1988;95:99–101.
18. Jain R, Deveikis J, Thompson BG. Management of patients with stunned myocardium associated with subarachnoid hemorrhage. AJNR Am J Neuroradiol. 2004;25:126–9.
19. Byrne JV. Tutorials in endovascular neurosurgery and interventional neuroradiology. Tutorials Endovasc Neurosurg Interv Neuroradiol. 2017; https://doi.org/10.1007/978-3-319-54835-7.
20. Achrol AS, Steinberg GK. Personalized medicine in cerebrovascular neurosurgery: precision neurosurgical management of cerebral aneurysms and subarachnoid hemorrhage. Front Surg. 2016;3 https://doi.org/10.3389/fsurg.2016.00034.
21. Wintermark M, Uske A, Chalaron M, Regli L, Maeder P, Meuli R, Schnyder P, Binaghi S. Multislice computerized tomography angiography in the evaluation of intracranial aneurysms: a comparison with intraarterial digital subtraction angiography. J Neurosurg. 2003;98:828–36.
22. Dammert S, Krings T, Ueffing E, Hans FJ, Willmes K, Mull M, Thron A. Detection of intracranial aneurysms with multislice CT: comparison with conventional angiography. Neuroradiology. 2004;46:427–34.
23. Mckinney AM, Palmer CS, Truwit CL, Karagulle A, Teksam M. Detection of aneurysms by 64-section multidetector CT angiography in patients acutely suspected of having an intracranial aneurysm and comparison with digital subtraction and 3D rotational angiography. Am J Neuroradiol. 2008;29:594–602.
24. Hacein-Bey L, Provenzale JM. Current imaging assessment and treatment of intracranial aneurysms. Am J Roentgenol. 2011;196:32–44.
25. Heit JJ, Pastena GT, Nogueira RG, Yoo AJ, Leslie-Mazwi TM, Hirsch JA, Rabinov JD. Cerebral angiography for evaluation of patients with CT angiogram-negative subarachnoid hemorrhage: an 11-year experience. Am J Neuroradiol. 2016;37:297–304.
26. Van Rooij WJ, Sprengers ME, De Gast AN, Peluso JPP, Sluzewski M. 3D rotational angiography: the new gold standard in the detection of additional intracranial aneurysms. In: Am J Neuroradiol; 2008. p. 976–9.
27. Guglielmi G, Vinuela F, Sepetka I, Macellari V. Electrothrombosis of saccular aneurysms via endovascular approach. Part 1: electrochemical basis, technique, and experimental results. J Neurosurg. 1991;75:1–7.
28. Guglielmi G, Vinuela F, Dion J, Duckwiler G. Electrothrombosis of saccular aneurysms via endovascular approach. Part 2: preliminary clinical experience. J Neurosurg. 1991;75:8–14.
29. Molyneux A, Kerr R, Stratton I, Sandercock P, Clarke M, Shrimpton J, Holman R. International Subarachnoid Aneurysm Trial (ISAT) of neurosurgical clipping versus endovascular coiling in 2143 patients with ruptured intracranial aneurysms: a randomised trial. Lancet. 2002;360:1267–74.
30. Cognard C, Pierot L, Anxionnat R, Ricolfi F. Results of embolization used as the first treatment choice in a consecutive nonselected population of ruptured aneurysms: clinical results of the clarity GDC study. Neurosurgery. 2011;69:837–42.
31. Spetzler RF, McDougall CG, Zabramski JM, Albuquerque FC, Hills NK, Russin JJ, Partovi S, Nakaji P, Wallace RC. The barrow ruptured aneurysm trial: 6-year results. J Neurosurg. 2015;123:609–17.
32. Dmytriw AA, Phan K, Moore JM, Pereira VM, Krings T, Thomas AJ. On flow diversion: the changing landscape of intracerebral aneurysm management. Am J Neuroradiol. 2019;40:591–600.
33. Wiebers DO. Unruptured intracranial aneurysms: natural history, clinical outcome, and risks of surgical and endovascular treatment. Lancet. 2003;362:103–10.
34. Raymond J, Guilbert F, Weill A, Georganos SA, Juravsky L, Lambert A, Lamoureux J, Chagnon M, Roy D. Long-term angiographic recurrences after selective endovascular treatment of aneurysms with detachable coils. Stroke. 2003;34:1398–403.
35. Ries T, Siemonsen S, Thomalla G, Grzyska U, Zeumer H, Fiehler J. Long-term follow-up of cerebral aneurysms after endovascular therapy-prediction and outcome of retreatment. Am J Neuroradiol. 2007;28:1755–61.
36. Murayama Y, Nien YL, Duckwiler G, Gobin YP, Jahan R, Frazee J, Martin N, Viñuela F. Guglielmi detachable coil embolization of cerebral aneurysms: 11 years' experience. J Neurosurg. 2003;98:959–66.
37. Agid R, Willinsky RA, Lee SK, TerBrugge KG, Farb RI. Characterization of aneurysm remnants after endovascular treatment: contrast-enhanced MR angiography versus catheter digital subtraction angiography. Am J Neuroradiol. 2008;29:1570–4.
38. Anzalone N, Scomazzoni F, Cirillo M, Righi C, Simionato F, Cadioli M, Iadanza A, Kirchin MA, Scotti G. Follow-up of coiled cerebral aneurysms at 3T: comparison of 3D time-of-flight MR angiography and contrast-enhanced MR angiography. Am J Neuroradiol. 2008;29:1530–6.

Cerebral Vascular Malformations

9

Seyed Mohammad Gharavi and Yang Tang

9.1 Arteriovenous Malformation (AVM)

9.1.1 Definition

Brain AVM or pial AVM is a tangle of abnormal vessels (nidus), directly connecting the arteries and veins without a regular intervening capillary bed. AVMs are likely congenital lesions, with the prevalence between 0.02% and 0.2%. Most AVMs are sporadic, although rare cases are associated with genetic syndromes such as hereditary hemorrhagic telangiectasia (Osler–Weber–Rendu) and Wyburn–Mason syndrome. The most common presentation of AVM is spontaneous intracranial hemorrhage (2–4% risk per year). Other clinical manifestations include epilepsy, headache, hydrocephalus, and focal or diffuse neurological deficits [1, 2]. The diagnostic criteria of AVM include the presence of a nidus that can be either compact or diffuse and arteriovenous shunting or early venous drainage seen during the arterial phase of angiography [1].

9.1.2 Feeding Artery and Draining Vein

For superficial or cortical AVMs, the arterial feeders are usually derived from pial arteries (branches of anterior, middle, and posterior cerebral arteries), and the draining veins are through the cortical veins. For deep and ventricular AVMs, the arterial feeders usually arise from perforators (lenticulostriate and thalamoperforators) or choroidal (anterior, medial and lateral posterior) arteries, and the venous drainage is through the deep venous system (internal cerebral veins, basal veins of Rosenthal, and straight sinus). Meningeal arterial recruitment can be seen in larger lesions.

9.1.3 Associated Aneurysms

Aneurysms are frequently seen in patients with AVMs. Aneurysms can arise from the nidus (nidal) or the feeding arterial pedicle (prenidal). These are usually the primary sites of hemorrhage and are treated by embolization or surgical ligation before treatment of AVM itself. Pseudoaneurysm can also develop at the site of rupture. On angiography, pseudoaneurysm can be identified as irregular outpouching at the margin of the acute hematoma. Other aneurysms located on the supplying arteries distant from the nidus are thought to be related to the increased vascular flow. These flow-related aneurysms can decrease in size or even resolve after the AVM is obliterated [3].

9.1.4 Grading

Spetzler–Martin (SM) grading system has been developed to predict the risk of surgical intervention of AVMs, based on the points assigned to each of the three following features: size of nidus: 1–3 cm (1), 3–6 cm (2), and > 6 cm (3); location, eloquent (1) versus non-eloquent (0); and venous drainage, deep (1) versus superficial (0). Based on the sum of score from the grading system, AVMs can be classified into low-grade (grades I and II), intermediate (grade III), and high-grade (grades IV, V, and VI) lesions, correlating with surgical risk. Grade VI lesions are essentially inoperable [4].

9.1.5 Imaging Evaluation

Non-contrast CT (NCCT) is the first modality in the emergency setting to evaluate the acute intracranial hemorrhage from AVM. Occasionally, the tortuous vessels or speckled

© Springer Nature Switzerland AG 2020
Y. Tang, *Atlas of Emergency Neurovascular Imaging*, https://doi.org/10.1007/978-3-030-43654-4_9

calcifications in the nidus are visible on NCCT. AVM usually does not cause mass effect unless it bleeds; in fact, it may cause volume loss in the adjacent brain parenchyma due to gliosis or hemosiderosis. Hemorrhage is mostly intraparenchymal and less frequently subarachnoid or intraventricular.

CTA is the diagnostic modality of choice for cerebral vascular malformation in the emergency setting. The characteristic features of the AVM, such as enlarged feeding arteries, nidus, flow-related or nidal aneurysms, draining vein, and venous varix, can be identified by CTA (Figs. 9.1 and 9.2). Certain angiographic features are suggestive of high risk of bleeding, such as evidence of previous bleeding, presence of nidal aneurysms, venous stenosis or ectasia, deep venous drainage, single venous drainage, and deep or posterior fossa location [1].

Micro-AVMs and subtle AV shunting can be difficult to detect on CTA. In the presence of hemorrhage, the nidus can be compressed by the hematoma, limiting the detection of a small underlying lesion. Catheter angiography remains essential in the characterization of detailed AVM angioarchitecture and for interventional planning (Fig. 9.3).

MRI/MRA is an excellent modality for screening or follow-up of AVMs, although not routinely used in the emergency setting. MRI can detect blood products in different stages. For example, hemosiderin from a chronic hematoma can easily be seen on the gradient recall echo (GRE) sequence. The gliosis in the adjacent parenchyma secondary to the steal phenomenon or sump effect of AVM is also better seen on MRI than CT. The abnormal vessels manifest as tangles or clusters of flow voids on T2 sequence and show enhancement on the postcontrast sequence (Fig. 9.4). In addition, MRI is more accurate in delineating the location of nidus in relation to the adjacent brain structures. Time-resolved contrast-enhanced MRA correlates well with DSA in terms of nidus size and location, arterial feeders, venous drainage pattern, and AVM grading [5]. MRI/MRA is frequently used to evaluate the residual AVM after radiosurgery, although DSA is still considered the reference standard to confirm the obliteration. The residual nidus is seen as residual flow voids, with persistent feeding arteries and draining veins. Contrast enhancement is, however, not specific, as radiation-induced parenchymal scarring also enhances.

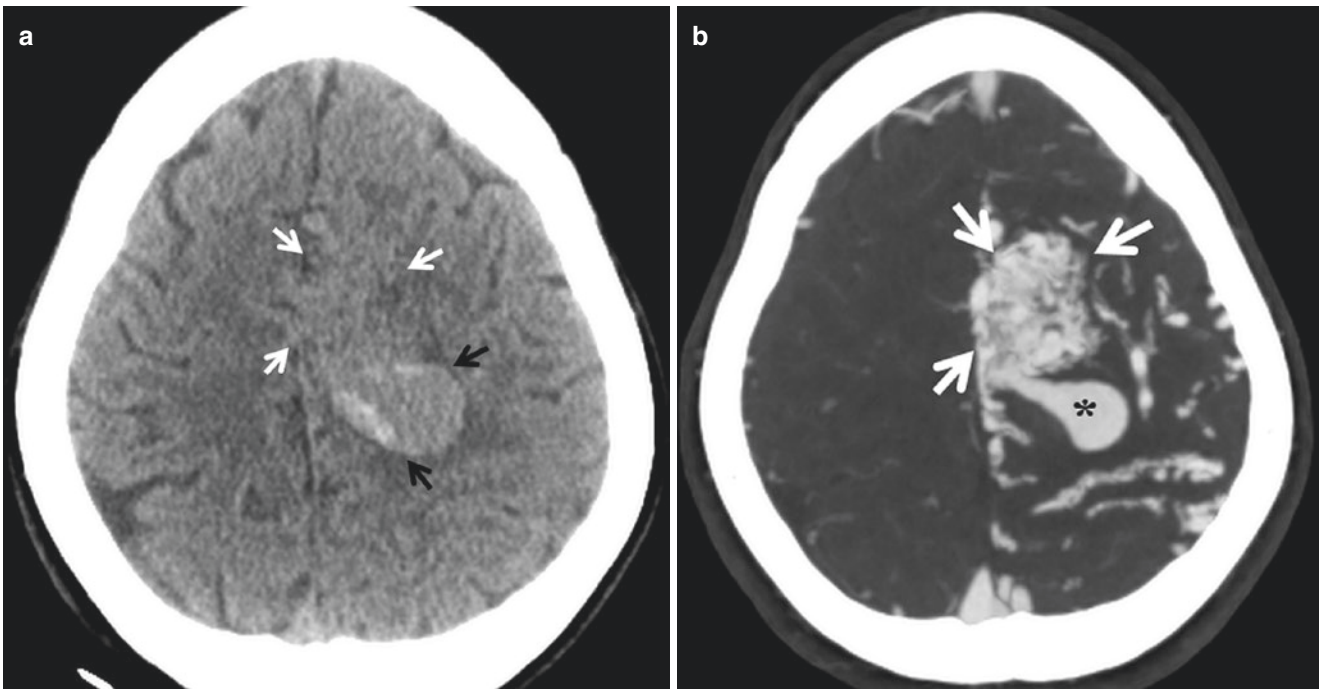

Fig. 9.1 Unruptured AVM. A 19-year-old presents with headache and weakness. (**a**) NCCT shows a mixed density oval structure (*black arrow*) in the deep posterior left frontal lobe. Note serpiginous structures anteriorly (*white arrows*), suspicious for an underlying vascular malformation. (**b**) CT angiography demonstrates an AVM nidus (*arrow*). The contrast-filled sac posteriorly (∗) represents a large nidal aneurysm, corresponding to the oval structure seen on the NCCT. (**c**) 3D reconstructed CTA with bone subtraction demonstrates hypertrophied arterial feeders from ACA (*arrow*) and MCA (*curved arrow*). (**d**) AP view from catheter angiogram in early arterial phase demonstrates a diffuse AVM nidus in the left cerebral hemisphere, supplied by ACA (*arrow*) and MCA (*curved arrows*). (**e**) Lateral view in the venous phase more clearly shows the large nidal aneurysm (∗). The venous drainage is mostly to the superior sagittal sinus (*arrow*), also to the vein of Labbe (*curved arrow*). No definite deep drainage is detected. Spetzler–Martin score is 3, given the size of nidus (3–6 cm), involvement of eloquent cortex, and lack of deep venous drainage. The nidal aneurysm is treated emergently with Onyx embolization, and AVM is later treated with radiation therapy

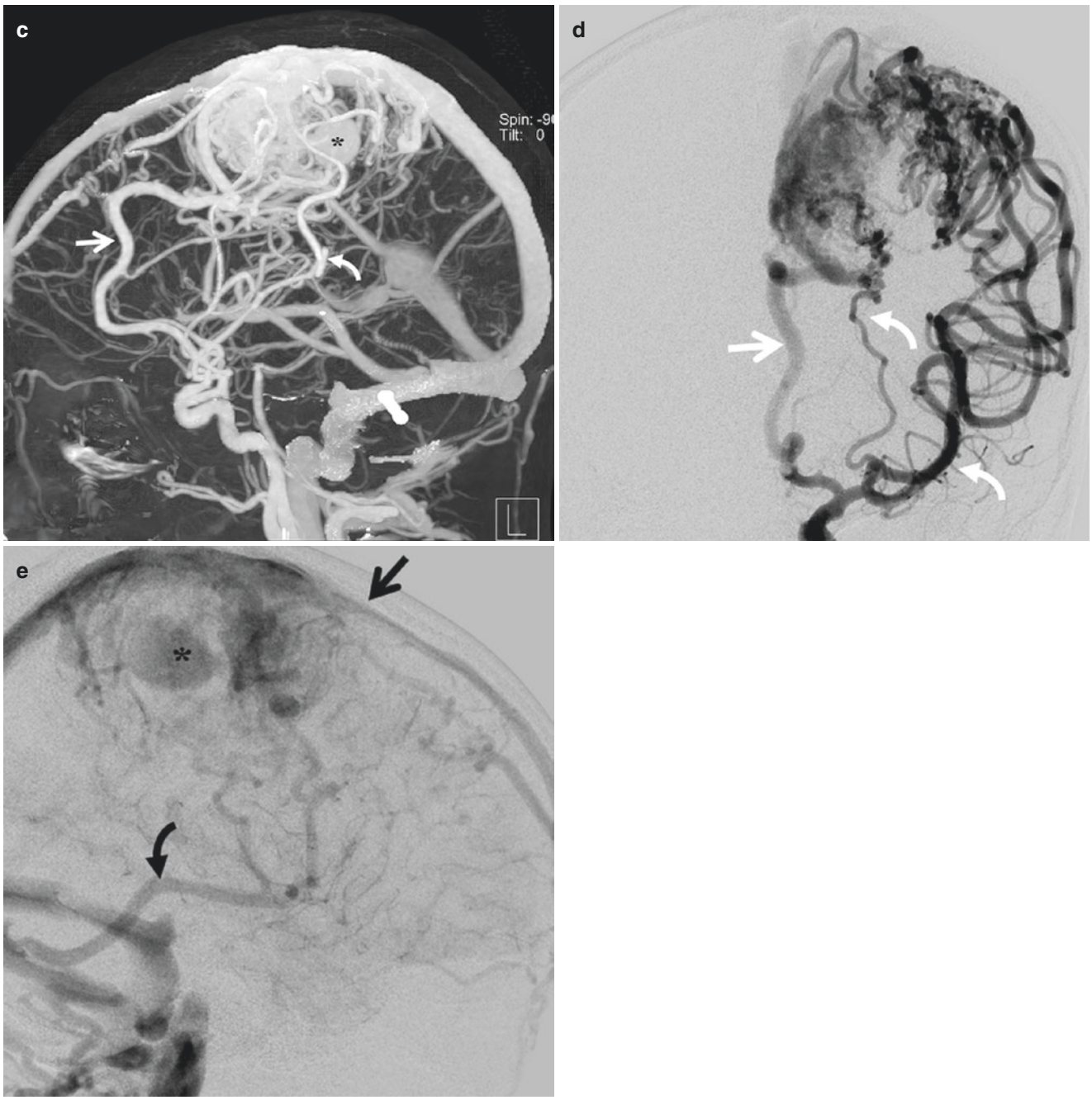

Fig. 9.1 (continued)

9.1.6 Treatment

AVMs with a high risk of hemorrhage should be considered for treatment. The main treatment options include surgical excision and stereotactic radiosurgery. Endovascular embolization is an effective adjunct to surgery and radiosurgery, though complete obliteration following embolization alone is unusual [6, 7].

The main advantages of surgical excision are high success rate, complete nidus obliteration, and immediate elimination of hemorrhage risk. Older patients with other medical comorbidities and high SM scores are poor candidates for surgical intervention. Even with intracranial hemorrhage, the surgical resection of AVM tends to be performed in a delayed fashion, unless the source of bleeding is an associated aneurysm. In that case, emergent microsurgical or endovascular treatment of the aneurysm is required to prevent future rupture secondary to increased pressure.

Stereotactic radiation surgery (SRS) is a method of choice in surgically challenging, small, or moderate-size AVMs.

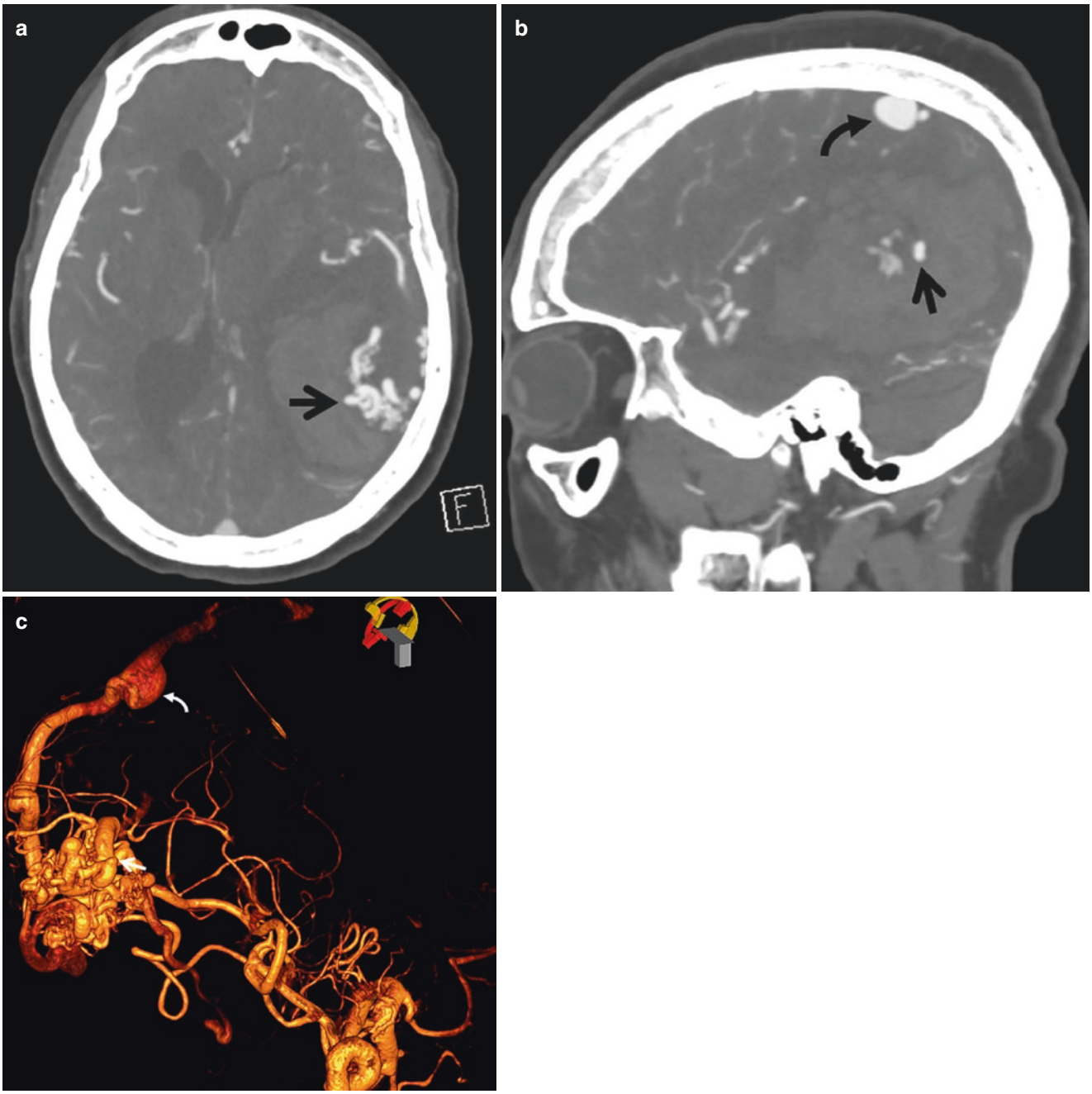

Fig. 9.2 Ruptured AVM. Patient with left intracerebral hemorrhage. (**a**) CTA axial image shows a ruptured AVM with an intranidal aneurysm (*arrow*). (**b**) Sagittal MIP again demonstrates an intranidal aneurysm as the source of hemorrhage. Note a venous pouch superiorly adjacent to the superior sagittal sinus (*curved arrow*). (**c**) 3D rotational angiography demonstrates AVM supplied mostly by the left MCA with superficial drainage to superior sagittal sinus. Note the intranidal aneurysm (*arrow*), multifocal stenosis of draining vein with associated venous pouch (*curved arrow*)

More recently, SRS is used in the treatment of AVMs with high SM scores. The major disadvantage of SRS is that it takes a latency period (several months to a few years) after radiation before the nidus obliterates, during which the patient is still at risk for bleeding. Radiation therapy is also less effective for AVMs with diffuse nidus. Radiation-induced injury can occur as a complication and may progress to radiation necrosis and cyst formation.

Conservative therapy is a reasonable option for patients with unruptured brain AVMs and no additional angiographic risk factors. The Randomised trial of Unruptured Brain Arteriovenous malformations (ARUBA) showed

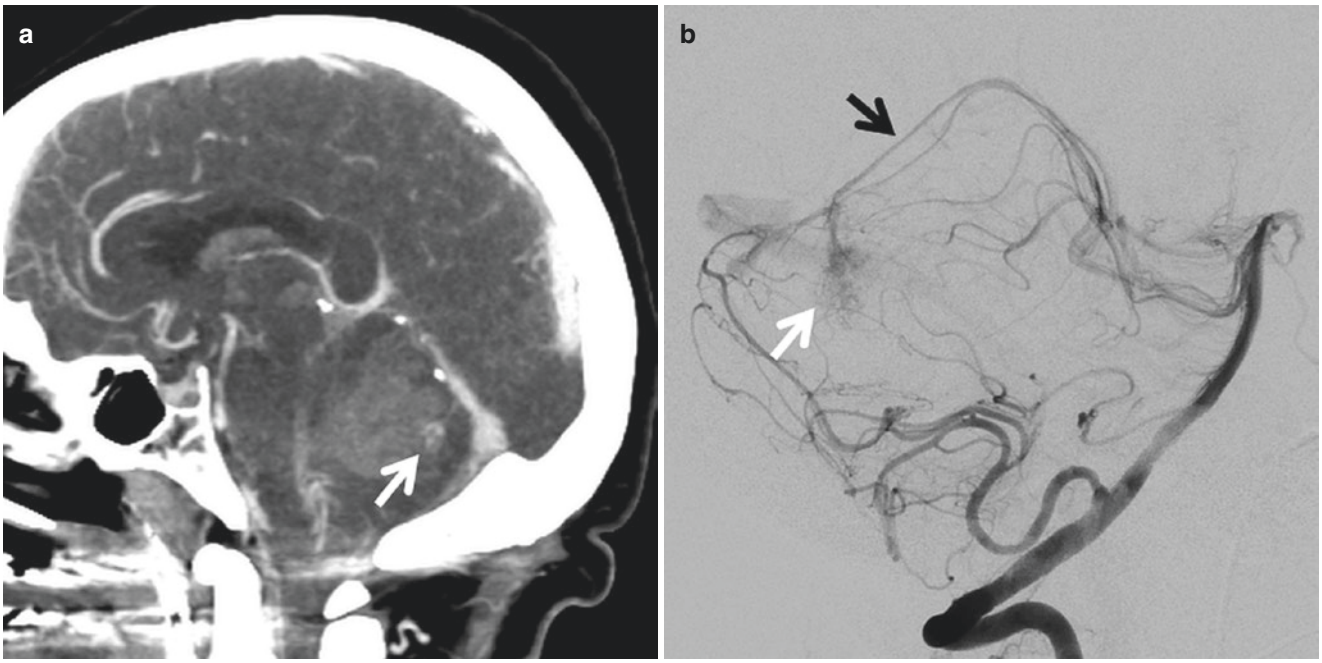

Fig. 9.3 Subtle vermian AVM. Patient presents with cerebellar hemorrhage. (**a**) Sagittal CTA demonstrates a subtle cluster of abnormal vessels in the vermis (*arrow*). (**b**) Catheter angiogram lateral view from right vertebral injection demonstrates a small nidus (*white arrow*) supplied by the superior cerebellar artery (*white arrow*)

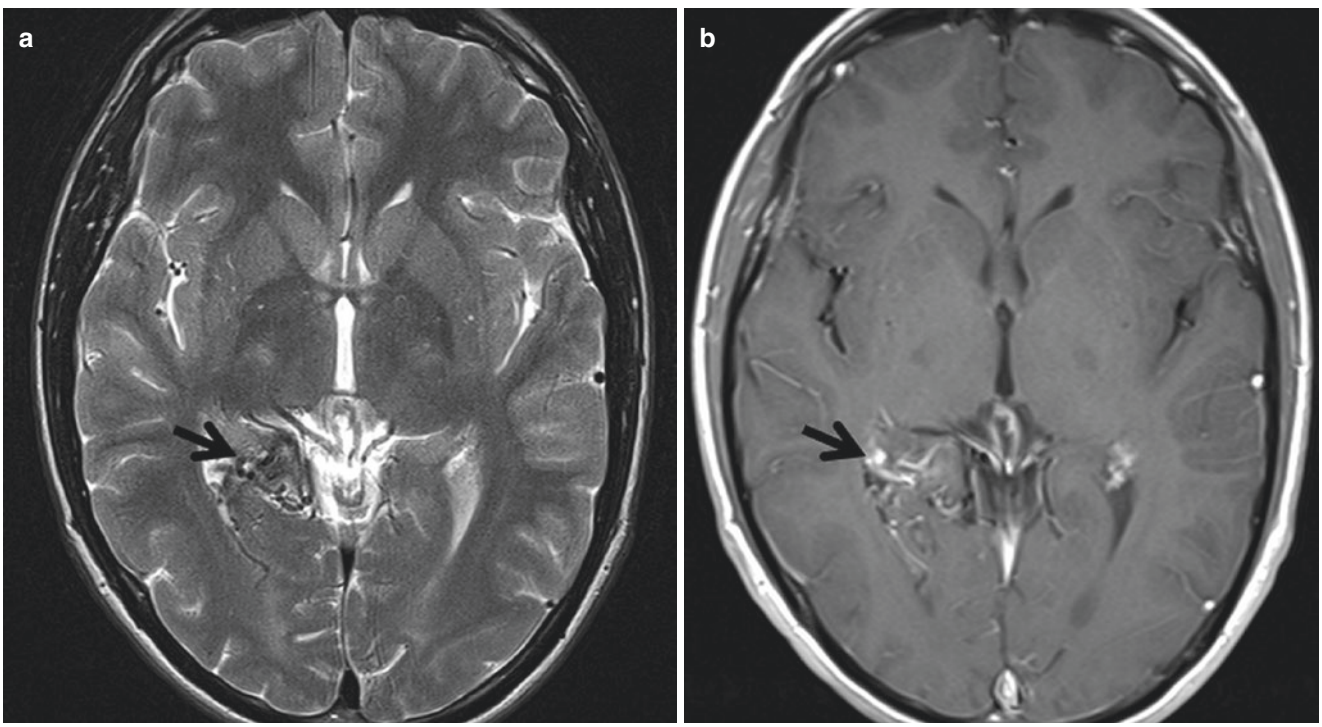

Fig. 9.4 MRI of AVM. Patient presents with seizure. (**a**) Axial T2 MRI image demonstrates a cluster of abnormal flow void (*arrow*) in the right hippocampal tail, which shows serpiginous enhancement on the postcontrast T1 image (**b**)

that medical management alone is superior to medical management with interventional therapy for the prevention of death or stroke in patients with unruptured brain arteriovenous malformations, although the results are highly controversial [8].

9.1.7 Differential Diagnosis

The differential diagnosis for AVM is limited and includes other vascular malformations such as arteriovenous fistula (AVF), developmental venous anomaly (DVA), or rarely cerebral proliferative angiopathy. AVF and DVA will be discussed in the following sections. Cerebral proliferative angiopathy is a rare form of vascular malformation distinct from the classic AVMs. The typical imaging findings include a proliferative type nidus in which normal brain parenchyma is interspersed between the abnormal vessels. Often, an entire lobe or even a hemisphere is affected. At cerebral angiography, the arterial feeder vessels tend to be of normal size or only mildly enlarged. Lack of clear early venous drainage on dynamic images is the key to differentiating it from classic brain AVM [1].

An intra-axial tumor especially GBM can demonstrate hypervascularity, AV shunting, and tumor hemorrhage. Occasionally, it can difficult to differentiate it from an occult AVM especially if MRI is not performed (Fig. 9.5) [9].

9.2 Dural Arteriovenous Fistula (DAVF)

9.2.1 Definition

DAVFs are pathological shunts between the dural arteries and dural venous sinuses, meningeal veins, or cortical veins. They are considered acquired lesions and are often associated with history of prior head trauma, cranial surgery, dural sinus or cortical venous thrombosis, infection, hypercoagulable states, and tumors. DAVFs are distinguished from pial AVMs by the lack of nidus and presence of the dural arterial supply. They can present with a wide spectrum of symptomatology including intracranial hemorrhage (more common in high-grade lesions) as well as non-hemorrhagic manifestations such as seizure, dementia, cranial nerve abnormalities, pulsatile tinnitus (transverse and sigmoid sinuses), ophthalmoplegia, proptosis, chemosis, retroorbital pain, or decreased vision (cavernous sinus) [2, 10] .

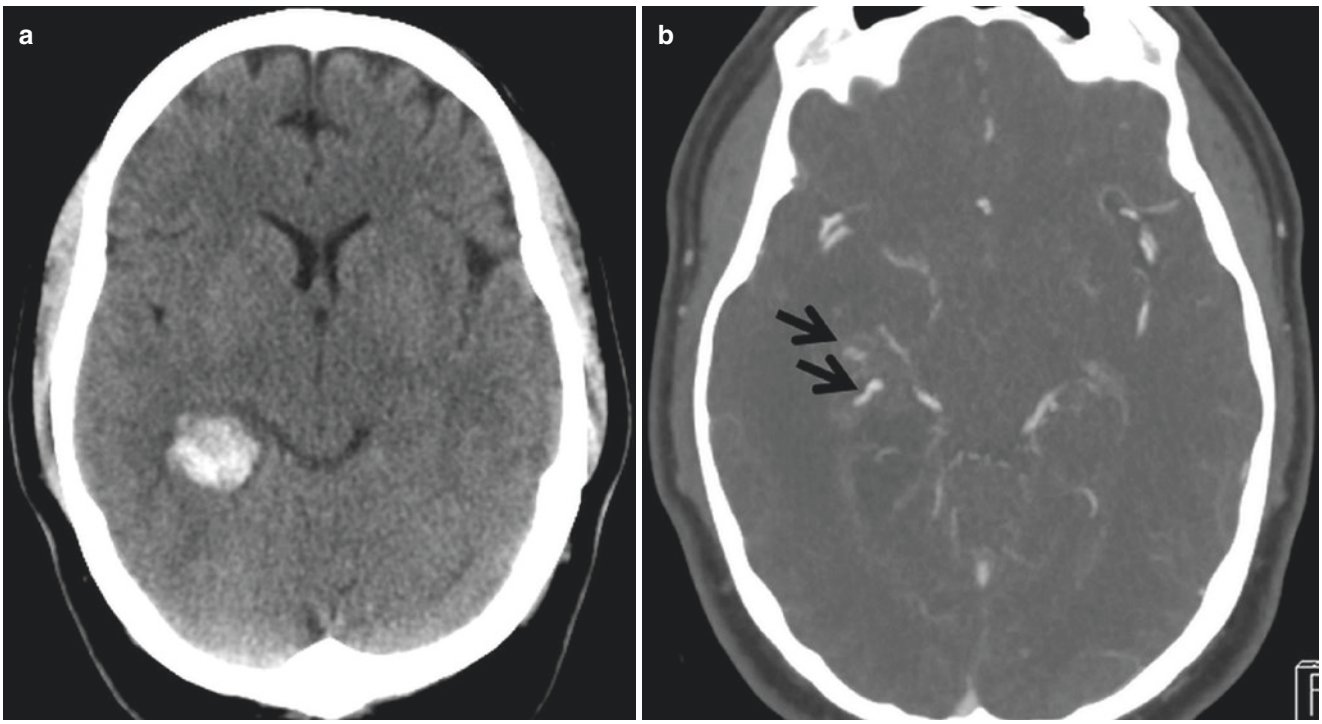

Fig. 9.5 GBM mimicking AVM. (**a**) Patient presents with acute right temporal intraparenchymal hemorrhage. (**b**) Axial CTA shows a cluster of abnormal vessels adjacent to the hemorrhage (*arrow*) suspicious for a small AVM, although catheter angiogram does not confirm the presumed diagnosis. (**c**) Three-month follow-up NCCT demonstrates a mass-like lesion in the right temporal lobe with surrounding edema. The acute hemorrhage has resolved. This is surgically proven to be a GBM. In retrospect, the abnormal vasculature represented tumor vascularity, while the mass lesion was obscured by the acute hemorrhage on the initial study and progressed in the next few months

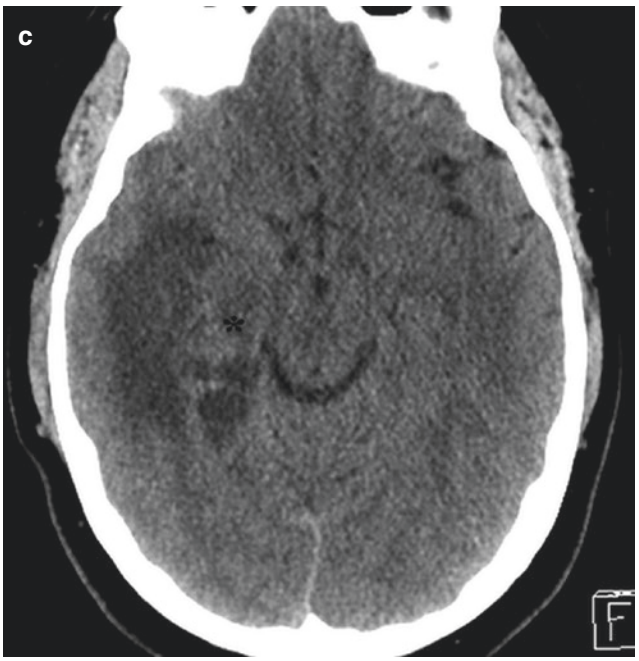

Fig. 9.5 (continued)

Table 9.1 Cognard classification system

Type	Definition
I	Confined to the dural venous sinus wall Normal antegrade venous drainage
IIA, IIB	Confined to the dural venous sinus Venous drainage directly into the dural venous sinus with retrograde reflux into the sinus/cortical vein
III	Venous drainage directly into the cortical vein without ectasia
IV	Venous drainage directly into the cortical vein with ectasia
V	spinal perimedullary drainage (strongly associated with progressive myelopathy)

Table 9.2 Borden classification system

Type	Definition
I	(Benign): drainage into dural sinuses without cortical vein drainage
II	(Aggressive): drainage into the dural sinuses and then to the cortical veins
III	(Aggressive): direct drainage into the cortical veins

9.2.2 Classifications

The symptoms of DAVF are predominantly related to disturbance of normal cerebral venous drainage and venous hypertension. In this regard, DAVF can be classified according to Cognard [11] and Borden [12] classifications (Tables 9.1 and 9.2). DAVFs with lack of cortical venous drainage (CVD) and lower scores in these classifications are considered more benign with low risk of bleeding, and the ones with CVD and higher scores are considered more aggressive with increased risk of bleeding [10].

DAVFs can also be classified based on the shunt location. Transverse/sigmoid sinus is the most commonly affected area, followed by cavernous sinus, superior sagittal sinus, tentorium, and anterior cranial fossa/ethmoidal and foramen magnum.

9.2.3 Imaging

CTA is the most frequently used modality for detection of DAVF in the acute setting. Common findings on CTA include asymmetrical dural sinus enhancement, engorged feeding arteries, draining veins, transcalvarial venous channels, abnormal size, and number of cortical veins [13] .

On MRI, findings of DAVF include abnormal flow void near the affected dural sinus, engorged ophthalmic vein/proptosis, dilated cortical or medullary vessels, abnormal vascular enhancement, venous pouch, as well as brain parenchymal changes secondary to venous hypertension such as edema or hemorrhage [14]. Time-of-flight MRA has limited value in the evaluation of AVFs but may show evidence of arterialized flow in the sinus or cortical veins. Contrast-enhanced, time-resolved MRA can provide dynamic information and reveal the retrograde venous drainage or arteriovenous shunt. DSA continues to be the gold standard modality for the characterization of suspected DAVFs (Figs. 9.6, 9.7, and 9.8).

9.2.4 Treatment

The risk of treatment should always be weighed against the natural history and expected clinical course of the lesion. High-grade lesions need to be treated early to avoid bleeding. Low-grade lesions can be treated conservatively unless they cause debilitating symptoms.

The main treatment method for DAVFs is endovascular embolization which can be performed in transarterial, transvenous, or combined approach. Coil in combination with liquid embolic agents such as Onyx or nBCA is used for DAVF embolization. Surgery is indicated when endovascular approaches have failed or are not feasible. Options include direct intraoperative embolization of meningeal arteries or veins, resection of abnormal dura, packing of the diseased sinus, disconnection of the retrograde leptomeningeal venous drainage, and skeletonization of the dural sinus with disconnection of the dural arterial supply. Presurgical arterial embolization can reduce the risk of surgical complications.

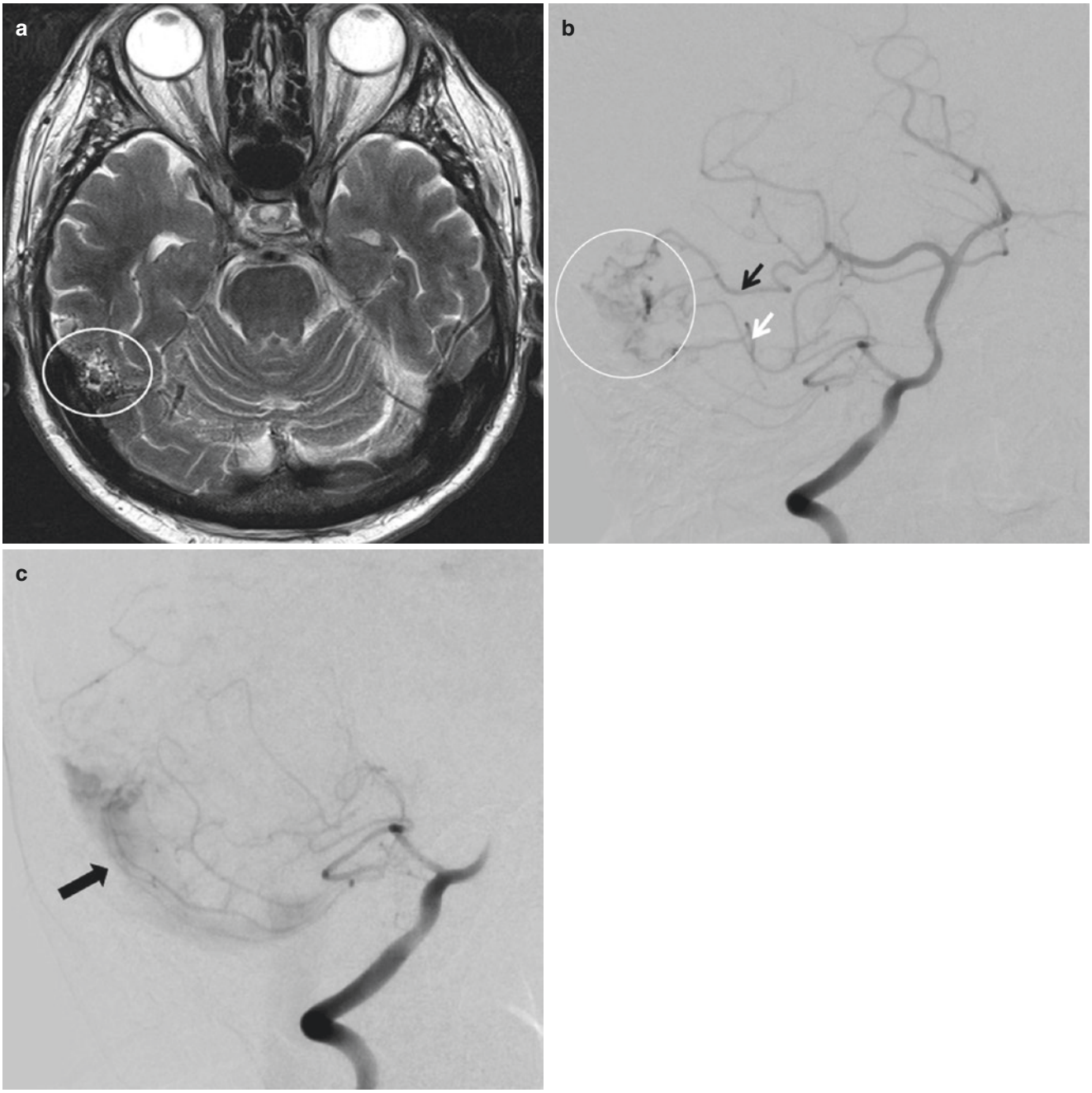

Fig. 9.6 Borden type I sigmoid sinus DAVF. Patient with headache and tinnitus presents to ER. (**a**) Axial T2 MRI shows a cluster of abnormal flow void in the right temporal lobe, suspicious for a vascular malformation. (**b**) Oblique view of catheter angiogram during arterial phase of right vertebral injection shows an AV fistula supplied by the distal right PCA (*black arrow*) and SCA (*white arrow*) branches. (**c**) The venous phase image demonstrates antegrade flow to the sigmoid sinus. No retrograde venous drainage is seen. This is consistent with a Borden type I lesion

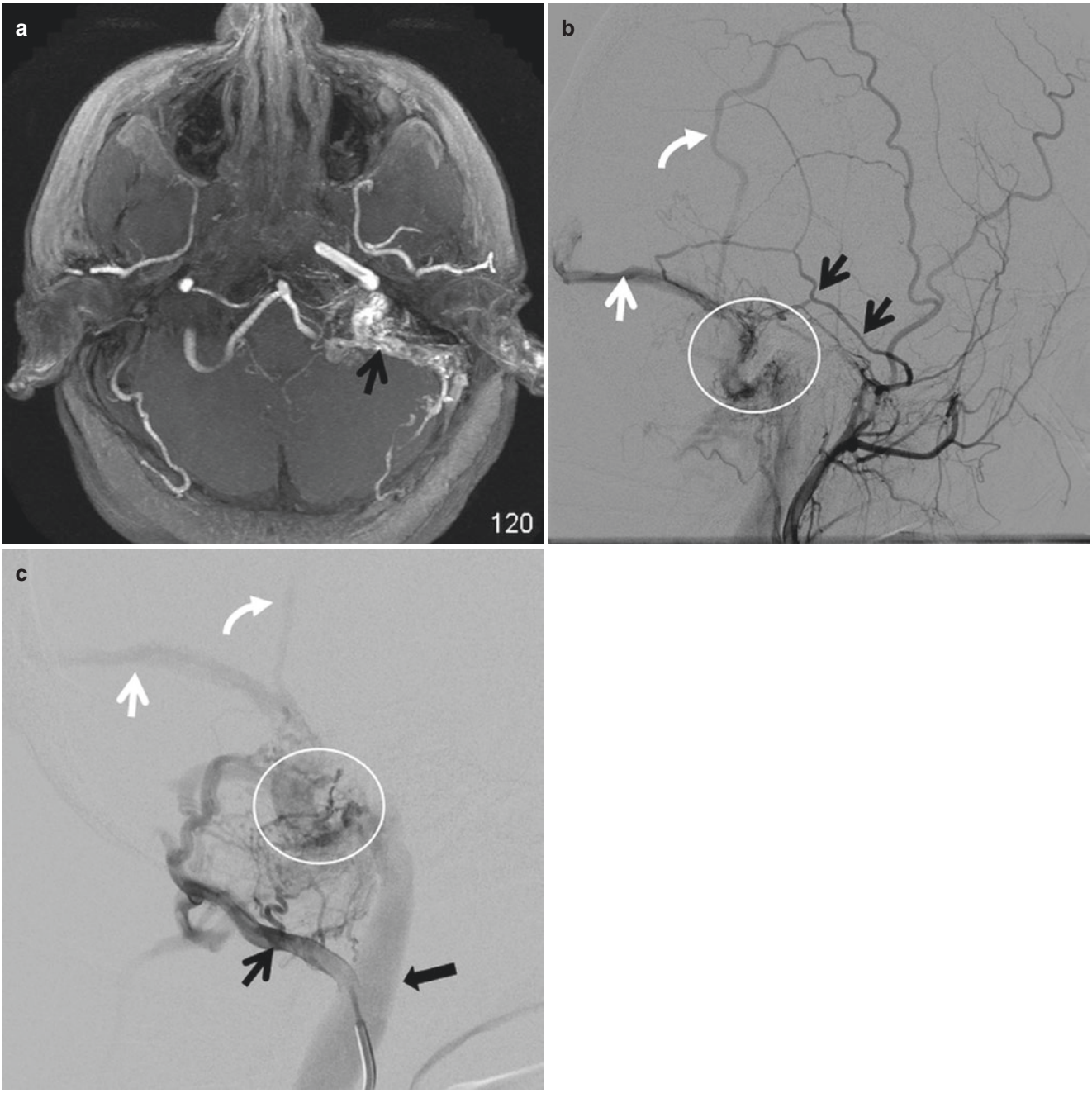

Fig. 9.7 Borden type II sigmoid sinus DAVF. Patient with pulsatile tinnitus. (**a**) Axial thick slab TOF MRA demonstrate abnormal flow-related enhancement of left sigmoid sinus and jugular bulb, suspicious for a DAVF. (**b**) Lateral angiogram with injection of left ECA demonstrates a DAVF at the left sigmoid sinus and proximal jugular vein (*circle*), with robust arterial supply from middle meningeal artery (*arrow*). There is retrograde filling of the left transverse sinus (*white arrow*) and a large cortical vein (*curved arrow*). (**c**) Selective injection of the hypertrophic left occipital artery (*black arrow*) again demonstrates the fistula at left sigmoid sinus (*circle*), with retrograde filling of left transverse sinus (*white arrow*) and cortical vein (*white curved arrow*). Antegrade venous drainage through the internal jugular vein (*black block arrow*). Additional arterial supplies from the muscular branches of left vertebral artery and meningohypophyseal trunk of left ICA are also present (not shown). This is consistent with Borden type II DAVF with presence of cortical venous drainage

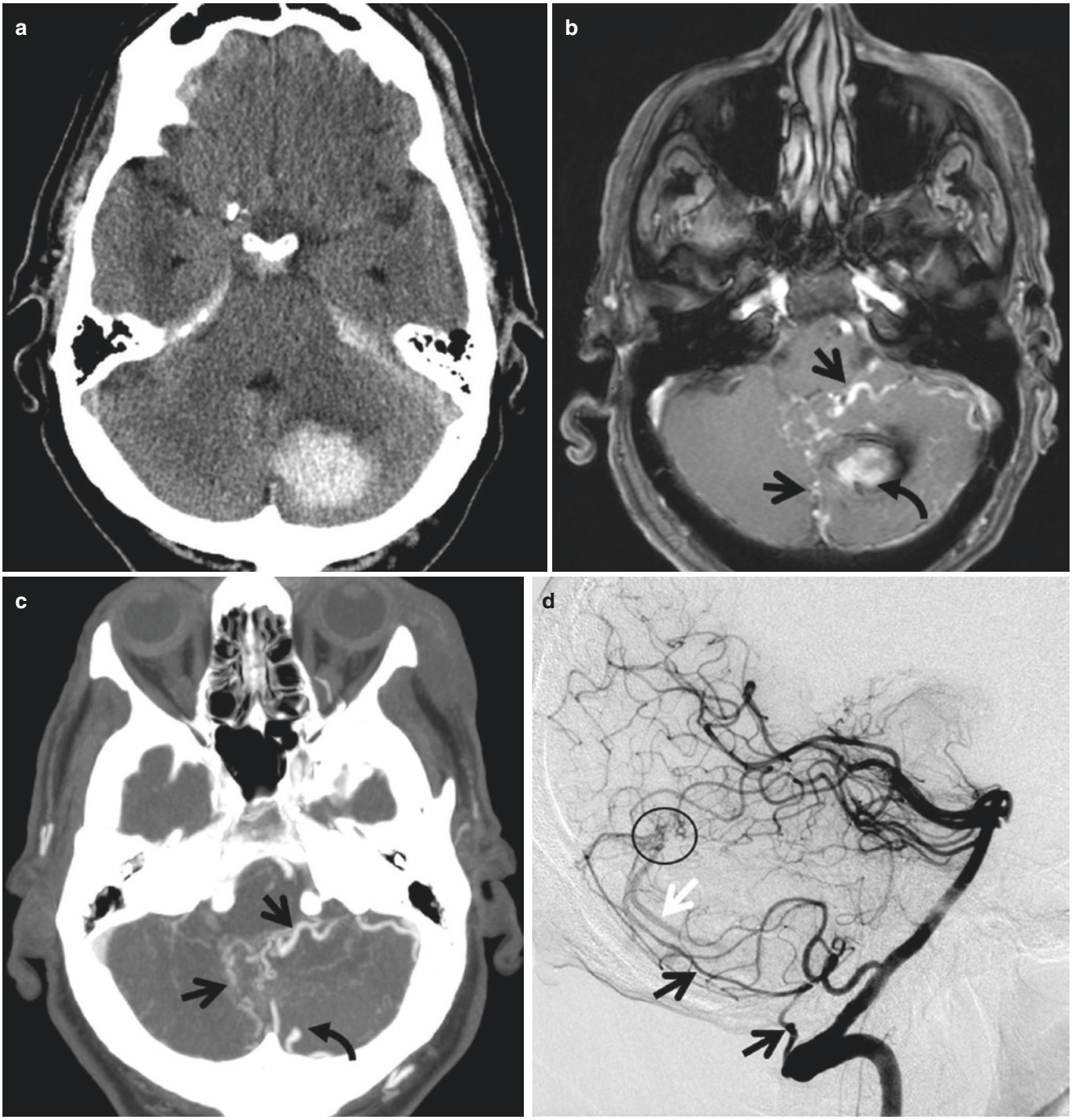

Fig. 9.8 Cerebellar DAVF. (**a**) NCCT shows acute left cerebellar hemorrhage. (**b**) Postcontrast axial T1 MRI demonstrates multiple enhancing vessels (*arrows*) in the left cerebellum surrounding the hematoma (*curved arrow*), suspicious for an underlying high-flow vascular malformation. (**c**) Axial CTA again demonstrates multiple abnormal vasculature in the left cerebellum (*arrows*). A discrete nidus is not seen but a small aneurysm is identified (*curved arrow*). (**d**) Lateral view of catheter angiogram right vertebral injection arterial phase shows an extracranial muscular branch from the right vertebral artery (*black arrows*) supplying a DAVF at the torcula (*circle*) with an early draining vein (*white arrow*). (**e**) AP view in the parenchymal phase demonstrates cortical draining vein (*white arrows*) from the torcula to the left cerebellum. Note is made of a venous aneurysm (*curved arrow*) as seen in the prior CTA. This is consistent with a Borden type II DAVF

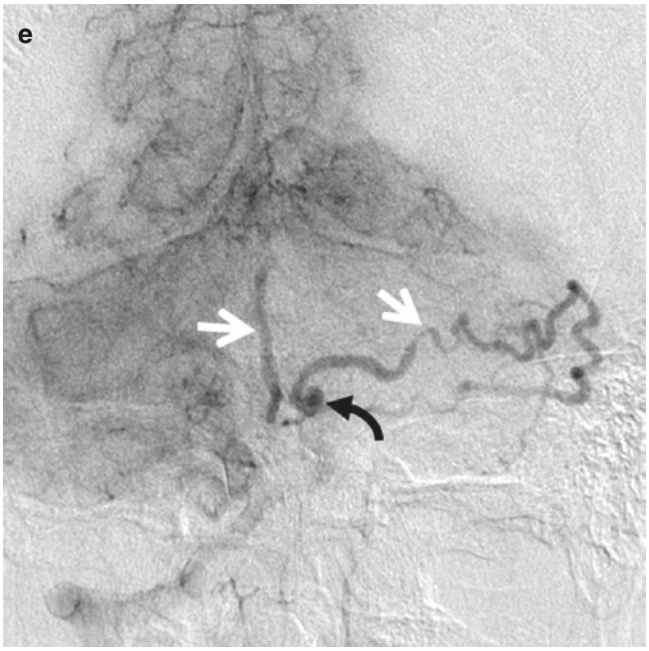

Fig. 9.8 (continued)

SRS is reserved for failed surgical and endovascular cases. Radiation causes thrombosis and closure of the fistula after a latent period that may take several months to a few years; therefore, for aggressive lesions with higher risk of bleeding, SRS as an only method of treatment is contraindicated [15].

9.3 Vein of Galen Aneurysmal Malformation (VGAM)

VGAM is a rare direct arteriovenous fistula between the intracranial arteries and a midline venous sac, which represents the embryonic prosencephalic vein of Markowski [16]. The primary arterial feeders include the anterior and posterior choroidal arteries as well as the pericallosal branches of ACAs. Thalamoperforators and distal cortical branches of the PCAs are common secondary feeders. The vein of Galen aneurysm lies between the foramina of Monro anteriorly and the confluence of the free margin of the falx and tentorium and is typically drained by the straight sinus and/or a persistent falcine sinus. VGAM can be classified into choroidal and mural types. Choroidal type is more common (>90%) and frequently present with high-output cardiac failure in the neonate due to multiple high-flow fistula [17].

On ultrasound, VGAM can be seen as a hypoechoic or anechoic midline structure with turbulent Doppler flow. It can be seen as a hyperdense structure in the quadrigeminal cistern on non-contrast CT. On CTA, MRI, MRA, and catheter angiography, it manifests as a midline venous varix connected to the dilated straight sinus or fetal falcine sinus, with multiple arterial feeders in the ambient and quadrigeminal cisterns (Fig. 9.9). MRI and CT are also helpful in delineating the associated hydrocephalus, hemorrhage, infarction, and other brain parenchymal abnormalities. Staged embolization of the fistula site is the standard treatment for VGAM.

9.4 Cavernous Malformation (CM)

CMs are angiographically occult, low-flow vascular malformations comprised of variable sized sinusoid and cavernous spaces without intervening brain tissue. It can occur anywhere in the brain or spinal cord and is the second most common vascular malformation after developmental venous anomaly [18]. They are sporadic lesions but can be multiple in patients with familial multiple cavernous malformation syndrome (Fig. 9.10). These lesions are usually asymptomatic but can occasionally cause hemorrhage or seizure.

CMs can be classified into four types based on the age of hemorrhage and MRI presentation [19]. Type I has subacute blood products which are T1 and T2 hyperintense; Type 2 has varying age blood products that is mixed T1 and T2 signal with T2 hypointense rim and classic "popcorn" appearance (Fig. 9.11). Lesions with recent acute or subacute hemorrhage may demonstrate perilesional edema and incomplete hemosiderin ring. The T1 hyperintensity from internal blood products can persist for years, unlike in regular parenchymal hematomas; Type 3 has chronic blood products and is T1 and T2 hypointense on MRI. Type 4 are small lesions that appear as punctate microhemorrhages on T2∗/GRE sequence. The large lesions may avidly enhance or show fluid–fluid levels. SWI or GRE sequence may reveal extensive regional hemosiderosis related to leaking into the adjacent tissue. Multiplicity, history of prior radiation, and presence of a developmental venous anomaly in the vicinity are helpful clues in differentiating cavernous malformations from mimicking lesions.

9.5 Developmental Venous Anomaly (DVA)

DVA consists of a cluster of radially oriented converging medullary veins that drains centripetally into a collector. It is hypothesized that these lesions are formed during fetal life

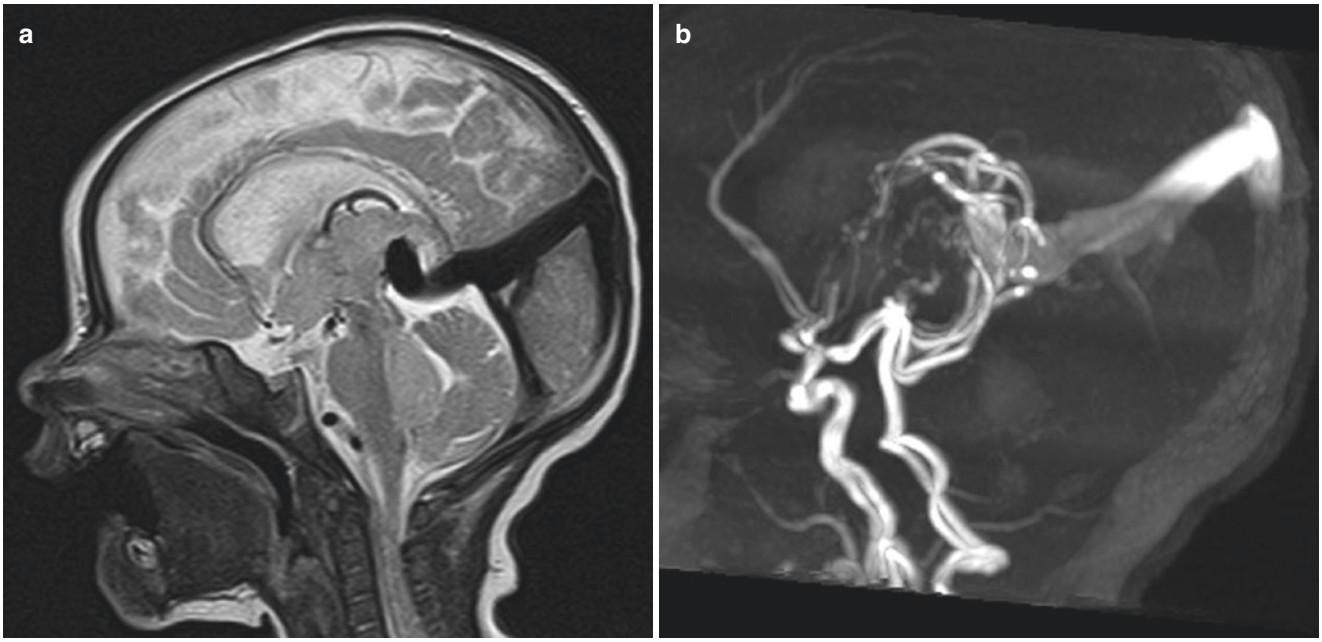

Fig. 9.9 Vein of Galen aneurysmal malformation. (**a**) Sagittal T2 image shows the prominent VGAM draining into the persistent fetal falcine sinus. (**b**) 3D thick slab TOF MRA shows the VGAM supplied by the thalamoperforators and posterior choroidal artery branches and drain into the fetal falcine sinus

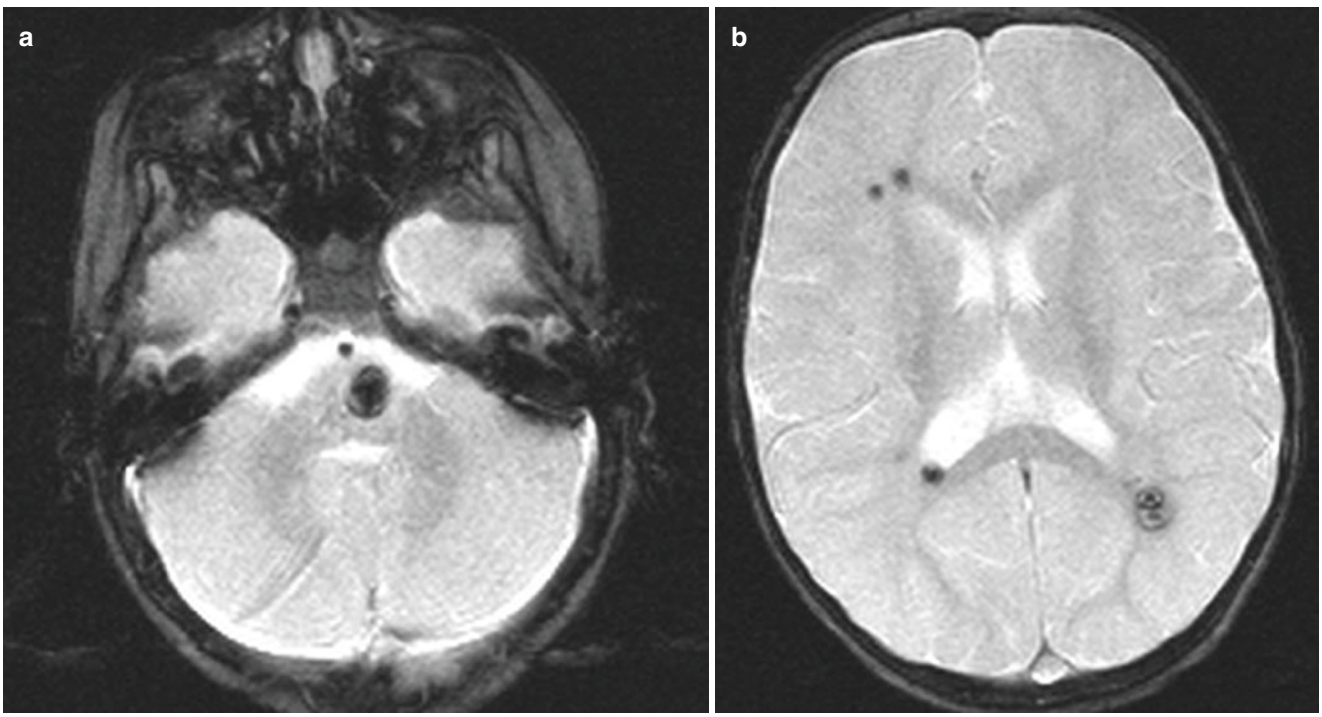

Fig. 9.10 Familial cavernomatosis. A 2-year-old patient with pontine hemorrhage. (**a**) Axial GRE shows a hemorrhagic lesion in the pons. (**b**) Axial GRE at the level of lateral ventricle demonstrates multiple additional foci of microhemorrhages, consistent with familial cavernomatosis

before the development of normal deep or superficial veins. They are usually associated with other vascular malformations, especially cavernous malformations.

DVA is often an incidentally finding on imaging. CTA, post-contrast MRI, or conventional angiography typically demonstrates a characteristic "caput medusa" or "reverse umbrella" sign, which represents medullary venous radicles draining into a collector vein. On the conventional angiography, DVAs are seen in the venous phase, with no arterial phase enhancement [20].

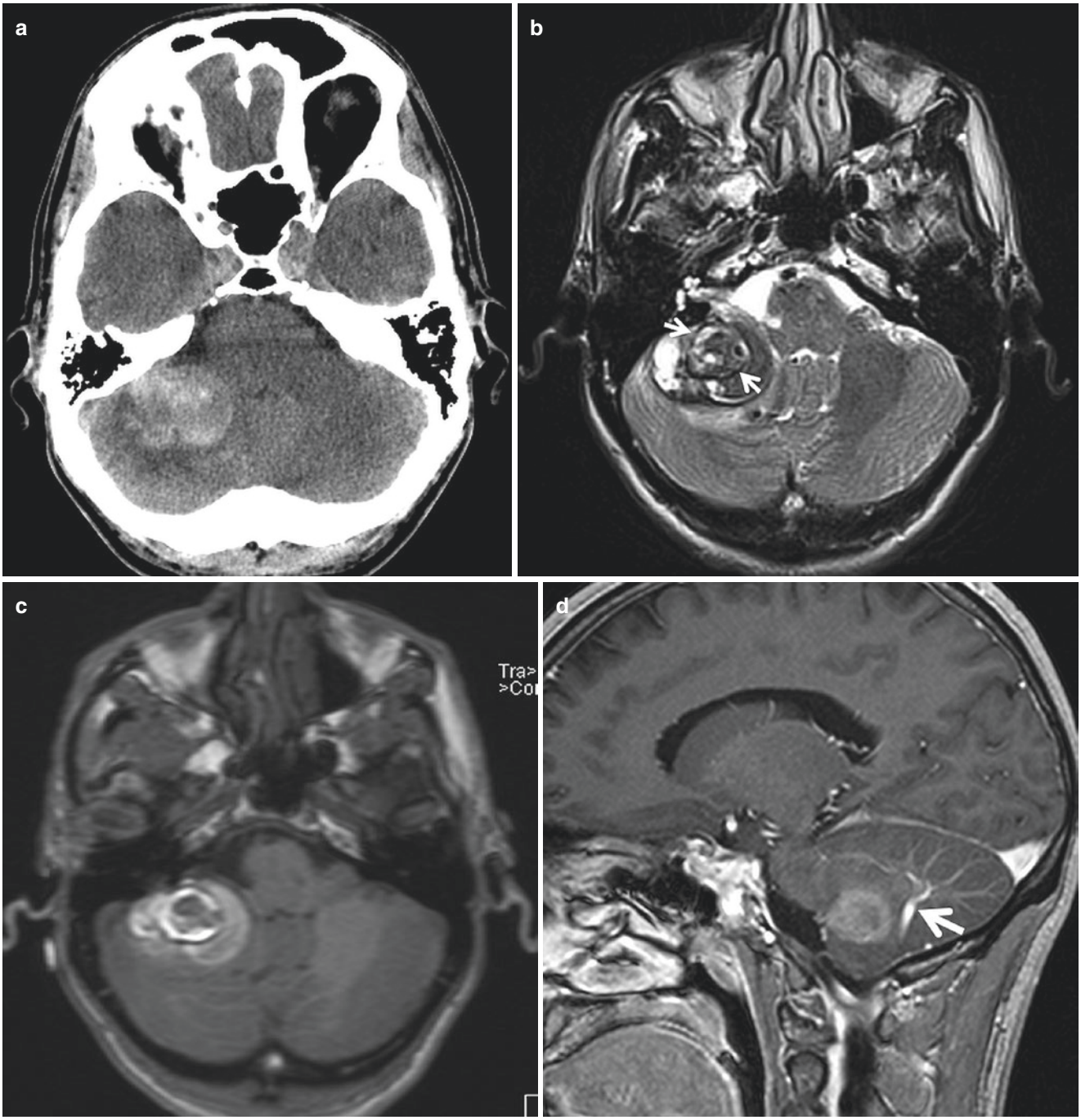

Fig. 9.11 Cavernous malformation with associated DVA. (**a**) NCCT shows right cerebellar hemorrhage. Axial T2 (**b**) and T1 (**c**) MRI demonstrates a right cerebellar intraparenchymal hematoma with heterogeneous T2 and T1 signal. Note an ovoid lesion with a hemosiderin ring (*arrow*) within the hematoma, suggestive of a cavernous malformation as the source of hemorrhage. (**d**) Postcontrast sagittal MPRAGE shows a developmental venous anomaly posterior to the hematoma (*arrow*)

DVA itself is seldom symptomatic. If DVA is seen adjacent to a hematoma, an associated cavernous malformation is usually the source of hemorrhage and should be sought after (Fig. 9.11). Occasionally, a thrombosed DAV can cause venous infarction (Fig. 9.12). No treatment is required for DVAs and resection should be avoided.

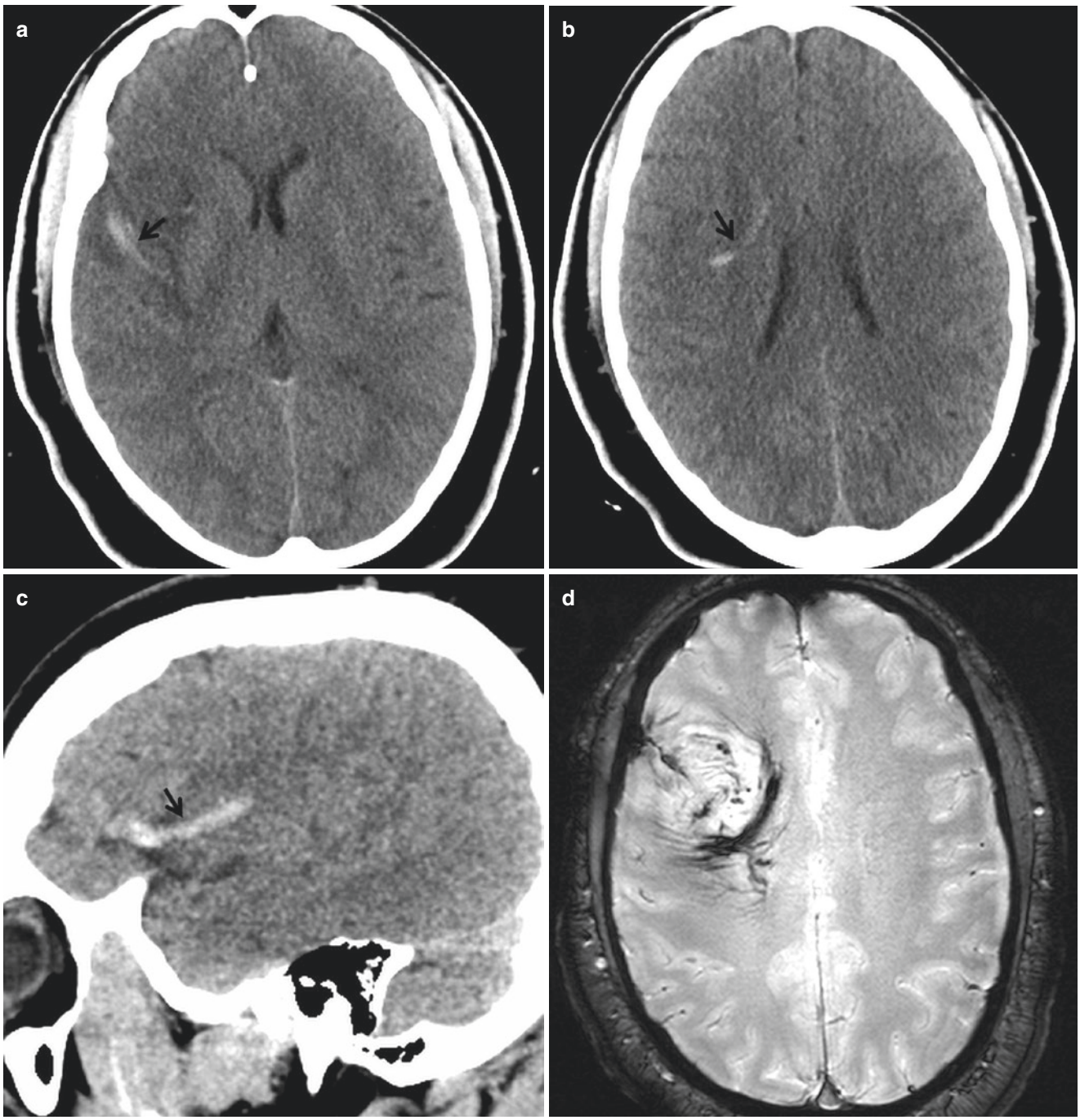

Fig. 9.12 Thrombosed DVA. Patient presents with seizure. (**a**) NCCT demonstrates edema in the right frontal lobe and insula. Note a hyperdense tubular structure with the area of edema. More superior axial (**b**) and sagittal (**c**) NCCT images better demonstrates the course of this structure (*arrow*), which likely represents a thrombosed transcortical DVA collector that anastomoses between the superficial middle cerebral vein and deep venous system. (**d**) Axial GRE sequence shows multiple dilated medullary tributary veins in the area of edema/venous infarction

References

1. Geibprasert S, Pongpech S, Jiarakongmun P, Shroff MM, Armstrong DC, Krings T. Radiologic assessment of brain arteriovenous malformations: what clinicians need to know. Radiographics. 2010;30:483–501.
2. Mossa-Basha M, Chen J, Gandhi D. Imaging of cerebral arteriovenous malformations and dural arteriovenous fistulas. Neurosurg Clin N Am. 2012;23:27–42.
3. Bradac GB. Cerebral angiography: normal anatomy and vascular pathology: Berlin, Heidelberg: Springer-Verlag; 2011.
4. Spetzler RF, Martin NA. A proposed grading system for arteriovenous malformations. J Neurosurg. 1986;65:476–83.
5. Taschner CA, Gieseke J, Le Thuc V, Rachdi H, Reyns N, Gauvrit JY, Leclerc X. Intracranial arteriovenous malformation: time-resolved contrast-enhanced MR angiography with combination of parallel imaging, keyhole acquisition, and k-space sampling techniques at 1.5 T. Radiology. 2008;246:871–9.
6. Brain arteriovenous malformations – UpToDate. Accessed 31 Jan 2020.
7. Kalani MYS, Albuquerque FC, Fiorella D, McDougall CG. Endovascular treatment of cerebral arteriovenous malformations. Neuroimaging Clin N Am. 2013;23:605–24.
8. Mohr JP, Parides MK, Stapf C, et al. Medical management with or without interventional therapy for unruptured brain arteriovenous malformations (ARUBA): a multicentre, non-blinded, randomised trial. Lancet. 2014;383:614–21.
9. Khanna A, Venteicher AS, Walcott BP, Kahle KT, Mordes DA, William CM, Ghogawala Z, Ogilvy CS. Glioblastoma mimicking an arteriovenous malformation. Front Neurol. 2013;4 https://doi.org/10.3389/fneur.2013.00144.
10. Gandhi D, Chen J, Pearl M, Huang J, Gemmete JJ, Kathuria S. Intracranial dural arteriovenous fistulas: classification, imaging findings, and treatment. Am J Neuroradiol. 2012;33:1007–13.
11. Cognard C, Gobin YP, Pierot L, Bailly AL, Houdart E, Casasco A, Chiras J, Merland JJ. Cerebral dural arteriovenous fistulas: clinical and angiographic correlation with a revised classification of venous drainage. Radiology. 1995;194:671–80.
12. Borden JA, Wu JK, Shucart WA. A proposed classification for spinal and cranial dural arteriovenous fistulous malformations and implications for treatment. J Neurosurg. 1995;82:166–79.
13. Narvid J, Do HM, Blevins NH, Fischbein NJ. CT angiography as a screening tool for dural arteriovenous fistula in patients with pulsatile tinnitus: feasibility and test characteristics. Am J Neuroradiol. 2011;32:446–53.
14. Kwon BJ, Han MH, Kang H-S, Chang K-H. MR imaging findings of intracranial dural arteriovenous fistulas: relations with venous drainage patterns. AJNR Am J Neuroradiol. 2005;26:2500–7.
15. Jabbour P, Tjoumakaris S, Chalouhi N, Randazzo C, Gonzalez LF, Dumont A, Rosenwasser R. Endovascular treatment of cerebral dural and pial arteriovenous fistulas. Neuroimaging Clin N Am. 2013;23:625–36.
16. Raybaud CA, Strother CM, Hald JK. Aneurysms of the vein of Galen: embryonic considerations and anatomical features relating to the pathogenesis of the malformation. Neuroradiology. 1989;31:109–28.
17. Bukhari S, AlSugair F, Bhattacharya J, Nicolas-Jilwan M. Vein of Galen aneurysmal malformations: an overview for the diagnostic neuroradiologist. Neurographics. 2019;9:264–72.
18. Batra S, Lin D, Recinos PF, Zhang J, Rigamonti D. Cavernous malformations: natural history, diagnosis and treatment. Nat Rev Neurol. 2009;5:659–70.
19. Zabramski JM, Wascher TM, Spetzler RF, Johnson B, Golfinos J, Drayer BP, Brown B, Rigamonti D, Brown G. The natural history of familial cavernous malformations: results of an ongoing study. J Neurosurg. 1994;80:422–32.
20. Lee M, Kim MS. Image findings in brain developmental venous anomalies. J Cerebrovasc Endovasc Neurosurg. 2012;14:37.

Vascular Emergency of the Head and Neck

10

Yang Tang

10.1 Traumatic Injury to External Carotid Artery

Injury to the external carotid artery (ECA) and its branches can occur following blunt or penetrating facial or neck trauma. Although not associated with stroke, injury to the ECA can lead to life-threatening rapid exsanguination, hypovolemic shock, and airway compromise. ECA injuries are frequently overlooked as the attention is mostly paid to the ICAs and vertebral arteries on the trauma screening CTAs. A high index of suspicion for ECA injury should be maintained, and familiarity of the ECA anatomy is needed in cases of traumatic head and neck injury. Similar to ICA injury, the findings of ECA injury include contour irregularity, dissection, pseudoaneurysm, occlusion, transection, and AV fistula, which are usually well demonstrated on a high-quality CTA (Figs. 10.1 and 10.2). Acquisition of venous phase images is beneficial for detection of active bleeding, as active contrast extravasation typically becomes more obvious on the delayed images. Trans-arterial embolization is the treatment of choice to control the bleeding.

Fig. 10.1 Traumatic pseudoaneurysm of superficial temporal artery. Patient with blunt facial injury presents with an expanding left scalp hematoma. Axial CTA demonstrates a focal pseudoaneurysm of left superficial temporal artery (*arrow*)

10.2 Iatrogenic Vascular Injury

Intraoperative vascular injury is a feared complication of head and neck surgeries.

For example, injuries to the lingual and facial arteries can occur after tonsillectomy (Fig. 10.3). Bleeding after functional endoscopic sinus surgery is frequently associated with injuries to the sphenopalatine artery or anterior ethmoidal artery. The sphenopalatine artery is the terminal branch of the internal maxillary artery entering the sphenopalatine foramen and supplying the nasal septum, turbinates, and lateral wall of the nasal cavity. Injury to the this artery can result in massive epistasis (Fig. 10.4) [1]. The anterior ethmoidal artery is a branch of the ophthalmic artery that supplies portions of the paranasal sinuses and nasal cavity. Inadvertent injury of the anterior ethmoidal artery can result in a rapidly enlarging orbital hematoma due to retraction of the transected vessel into the orbit, which frequently requires repair from an external approach [1].

© Springer Nature Switzerland AG 2020
Y. Tang, *Atlas of Emergency Neurovascular Imaging*, https://doi.org/10.1007/978-3-030-43654-4_10

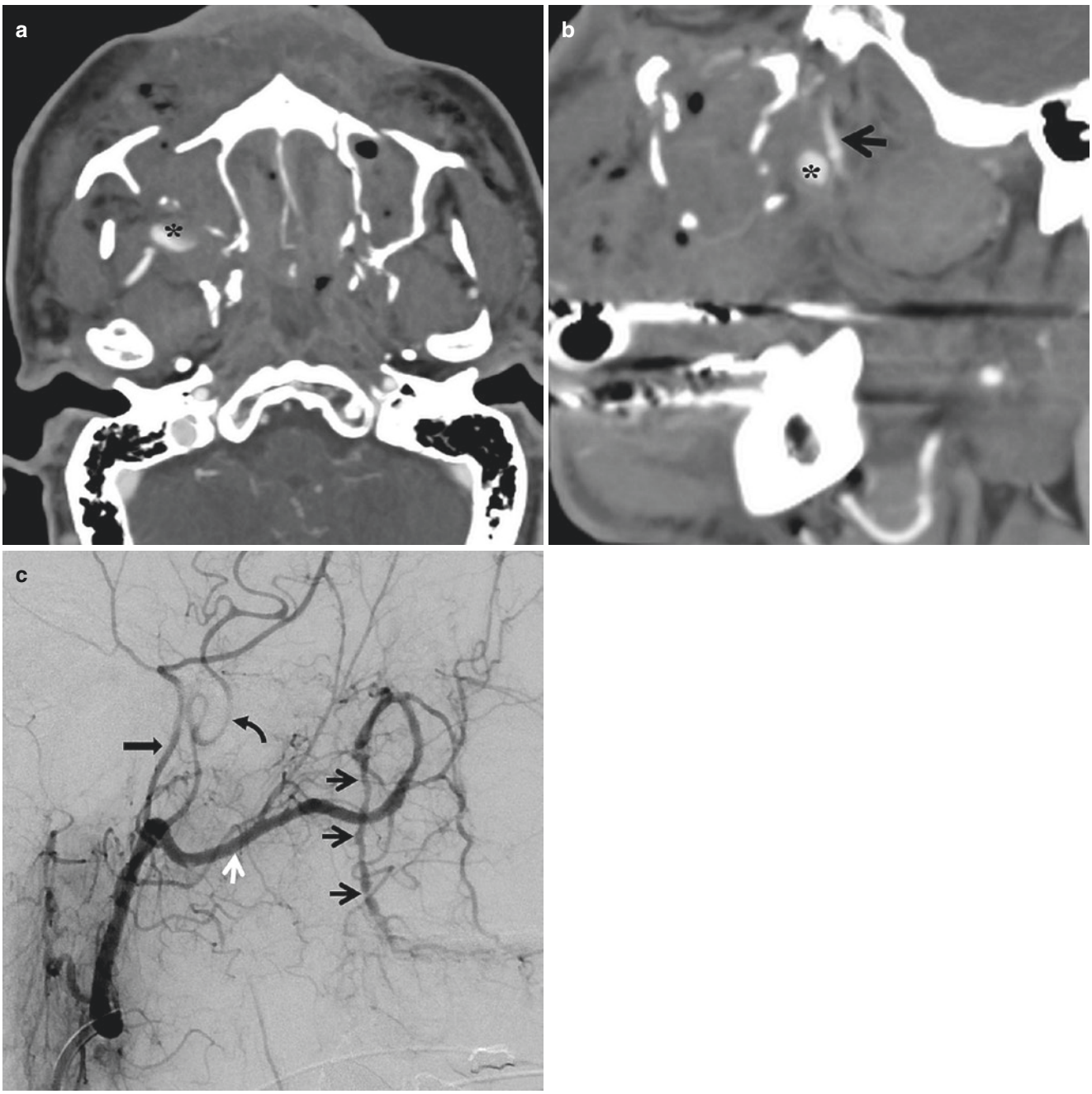

Fig. 10.2 Traumatic injury of internal maxillary artery. Trauma patient with bilateral LeFort 3 fractures and uncontrollable epistaxis. (**a**) Axial CTA demonstrates active extravasation (∗) posterior to the fractured right maxillary sinus. (**b**) Sagittal CTA shows the hemorrhage is adjacent to the descending palatine artery (*arrow*), a distal branch of internal maxillary artery. (**c**) Selective injection of external carotid artery demonstrates marked contour irregularity and multifocal stenosis of descending palatine artery (*arrow*), consistent with traumatic injury. This patient is successfully treated with embolization. Internal maxillary artery (*white arrow*), middle meningeal artery (*black arrow*), and superficial temporal artery (*curved arrow*)

Injury to the internal carotid artery is a rare but most catastrophic complication during transsphenoidal pituitary surgery, trans-nasal endoscopic skull surgery, and rarely functional endoscopic sinus surgery, which can lead to rapid exsanguination, cerebral ischemia, and death.

It should be noted that some developmental variants of paranasal sinus and skull base can place patients at higher risk of vascular injury and should be described in the preoperative imaging. For example, pneumatization of supraorbital ethmoid air cells above the anterior ethmoidal notch places the anterior ethmoidal artery at risk of surgical injury as the artery travels freely within the ethmoid sinus. Dehiscence of bony covering the carotid canal, attachment of deviated sphenoid sinus septum to the carotid canal, as well as extensive lateral

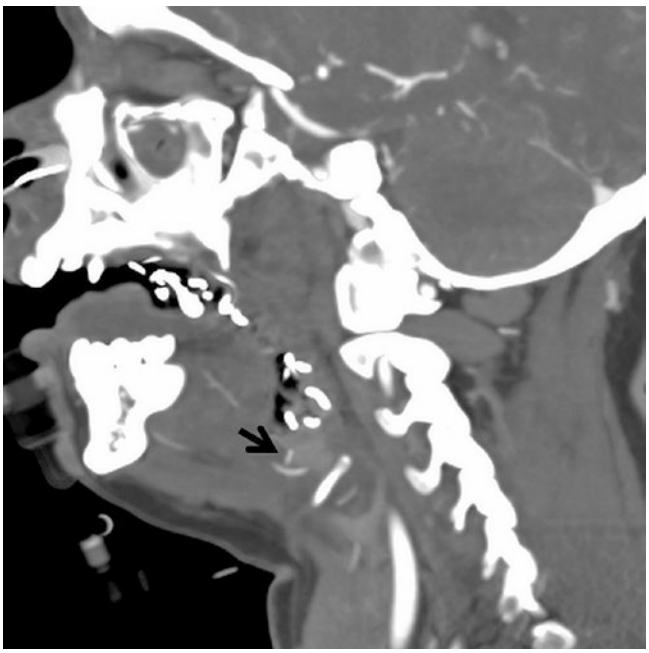

Fig. 10.3 Injury to the lingual artery. Patient with oropharyngeal bleeding after tonsillectomy. CTA demonstrates a focus of active extravasation (*arrow*) adjacent to the lingual artery. Note the hemorrhage and packing material within the oropharynx

Fig. 10.4 Injury to the sphenopalatine artery. Patient presents with epistaxis after endoscopic polypectomy. CTA demonstrates a focus of active extravasation medial to the sphenopalatine foramen (*arrow*), consistent with injury to sphenopalatine artery

pneumatization of the sphenoid sinus increase the risk of iatrogenic injury to internal carotid artery [2].

Vascular injury can cause immediate or delayed postsurgical hemorrhage. In cases that cannot be controlled with packing or cauterization, or recurrent immediate bleeding, emergency catheter angiography and endovascular treatment should be performed. Cross-sectional imaging may delay lifesaving treatment and is not indicated. In cases of less severe or delayed postsurgical hemorrhage, CTA can be performed to evaluate the site and extent of injury and provide a roadmap for endovascular or surgical intervention.

10.3 Vascular Complication of Head and Neck Infections

Head and neck infections such as tonsillitis, rhinosinusitis, and otogenic and odontogenic infections are among the common causes of emergency visits, though most of which follow a benign course. Occasionally, severe infections can become refractory to treatment and lead to vascular, intracranial, or systemic complications.

Acute angioinvasive fungal sinusitis is the most lethal form of head and neck infection. It can affect poorly controlled diabetics (zygomycosis), or immunocompromised patients with severe neutropenia, such as patients with hematological malignancy, systemic chemotherapy, or bone marrow transplant (aspergillosis). Fungi can rapidly spread along and invade the skull base and vasculature leading to cavernous ICA narrowing, occlusion, mycotic pseudoaneurysm, and thrombophlebitis of cavernous sinus (Fig. 10.5).

Poorly controlled otogenic infections such as coalescent mastoiditis or petrous apicitis can also spread to the adjacent vasculature causing compromise of petrous ICA and transverse/sigmoid sinus thrombosis (Fig. 10.6).

Occasionally, oropharyngeal infections can cause septic thrombophlebitis of internal jugular vein and its tributaries leading to systemic septic emboli (Lemierre syndrome) (Fig. 10.7).

10.4 Vascular Complications of Head and Neck Tumors

Advanced head and neck malignancies can compress or encase adjacent vasculature. Ischemic stroke can occasionally be the initial presentation for these patients (Fig. 10.8).

The most feared and life-threatening complication of head and neck cancers is the so-called carotid blowout syndrome. It can involve common, internal, or external carotid arteries and its branches (Figs. 10.9 and 10.10). Major risk factors include extensive surgery, radiation, recurrent tumor, wound breakdown or pharyngocutanous fistula with infection, and exposed artery. It is classified into threatened, impending, and active stages. Vascular imaging can reveal luminal irregularity, pseudoaneurysm, active contrast extrav-

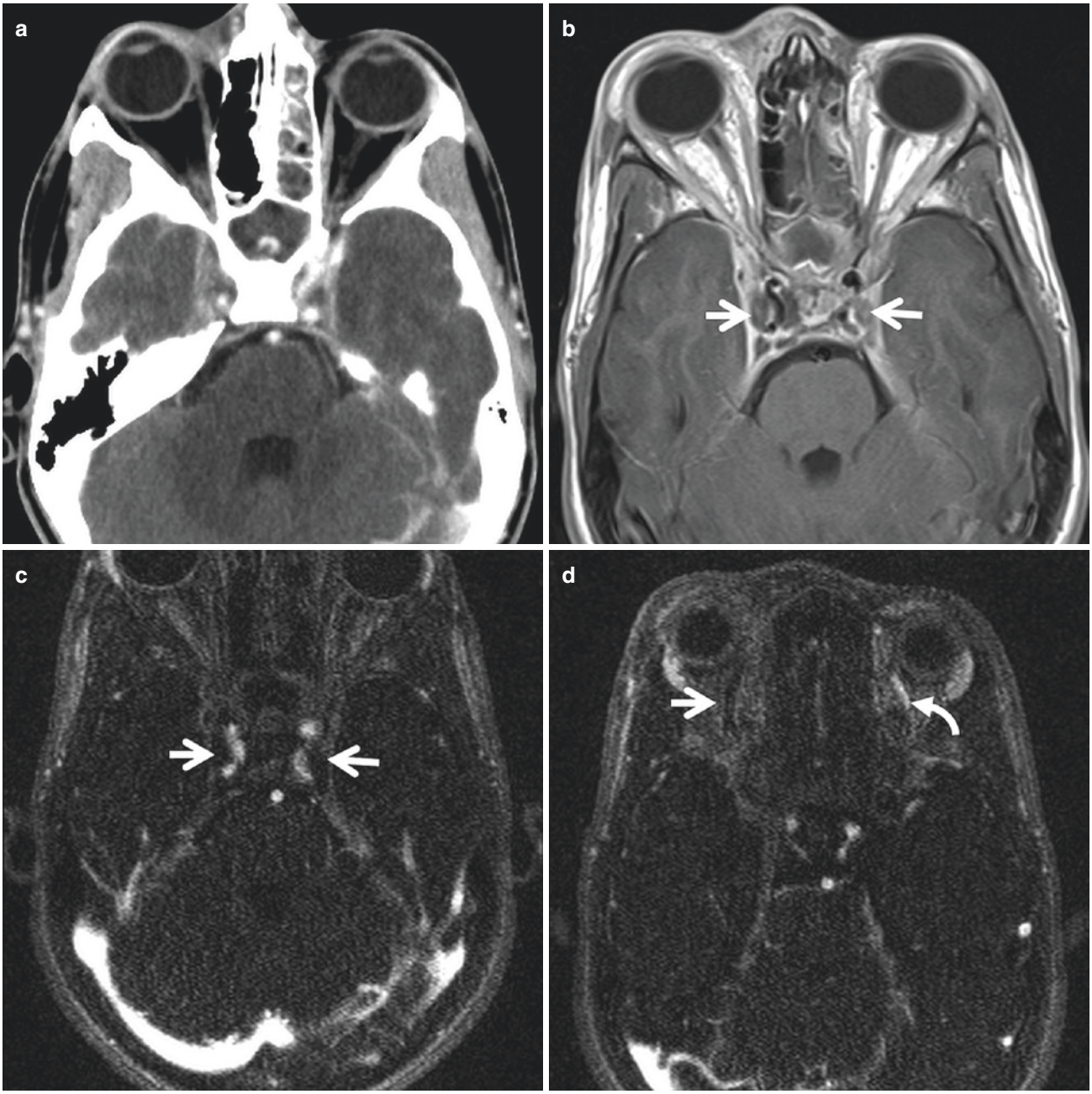

Fig. 10.5 Cavernous sinus and superior ophthalmic vein (SOV) thrombosis due to sinusitis. Child with leukemia on chemotherapy presents with headache and right eye swelling. (**a**) Postcontrast CT demonstrates fluid opacification of sphenoid sinuses and left ethmoid air cells consistent with acute sinusitis. The bilateral cavernous sinuses are expanded and non-enhancing, suggestive of thrombosis. (**b**) Postcontrast T1 MRI demonstrates filling defects within the bilateral cavernous sinuses (*arrows*). (**c**) 3D contrast-enhanced MRV demonstrate no enhancement of cavernous sinuses (*arrows*). (**d**) Non-enhancement of right SOV (*arrow*) consistent with thrombosis, compared to the normally enhancing left SOV (*curved arrow*)

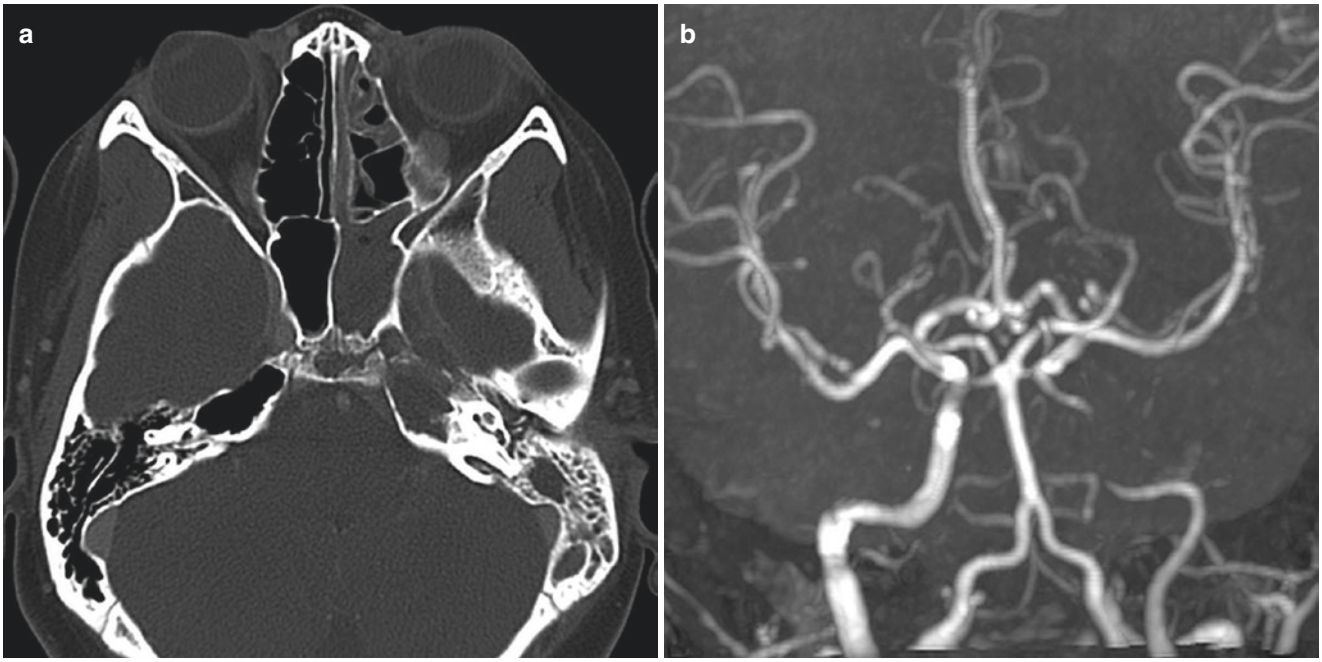

Fig. 10.6 ICA stenosis due to petrous apicitis: a 10-year-old with fever, ear pain, and ophthalmoplegia. (**a**) Postcontrast CT demonstrates opacification of the left mastoid, tympanic cavity, and petrous apex, consistent with acute otomastoiditis and petrous apicitis. Bulging contour of left cavernous sinus is noted suggestive of thrombosis. (**b**) 3D TOF MRA shows severe narrowing of the left ICA with decreased flow-related enhancement

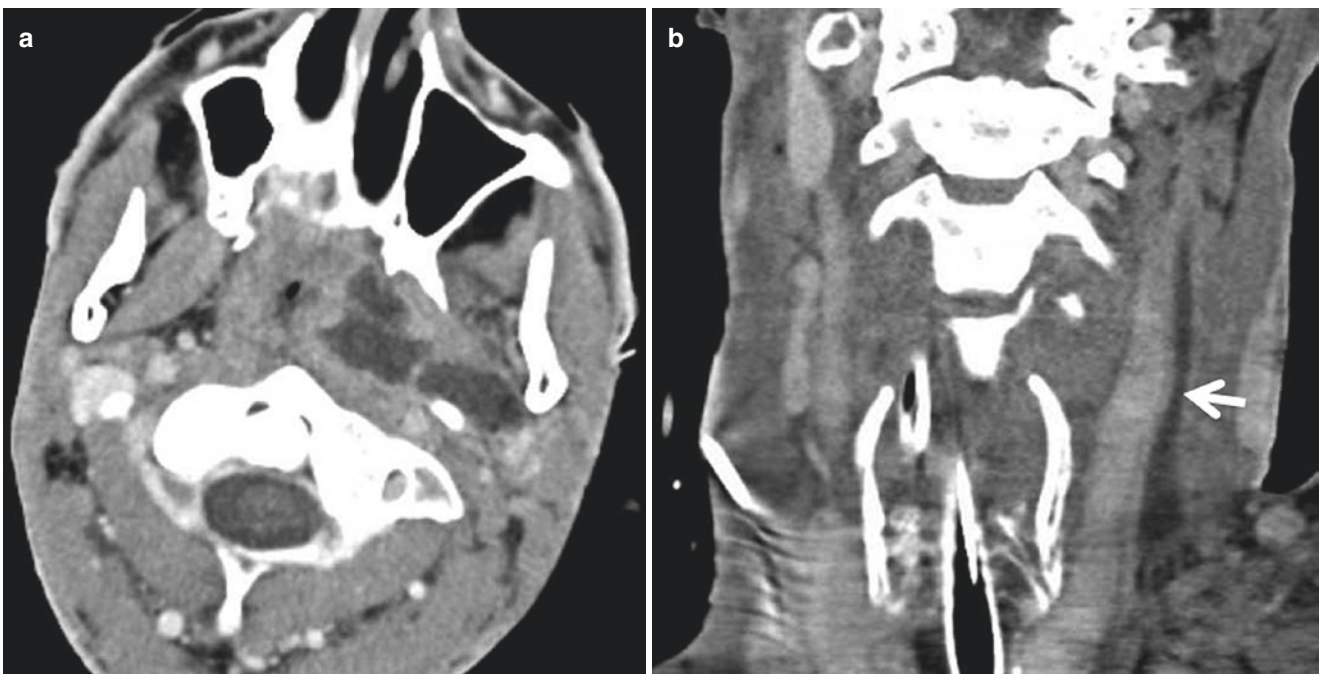

Fig. 10.7 Lemierre syndrome. HIV+ patient with throat pain and fever. (**a**) Axial contrast-enhanced neck CT demonstrates left tonsillar and parapharyngeal abscess. (**b**) Coronal image reveals thrombosis of left internal jugular vein (*arrow*). (**c**) Axial image through the lung apices demonstrates multifocal nodular opacities/consolidations and left pleural effusion, suggestive of septic embolism from thrombophlebitis of left internal jugular vein

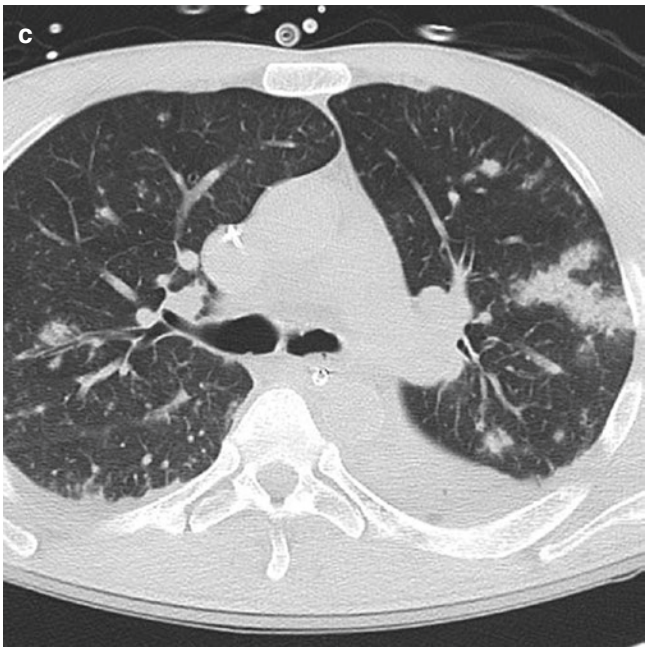

Fig. 10.7 (continued)

asation, or arteriovenous fistula. CTA is typically the imaging modality of choice in hemodynamically stable patients. It provides information on both vascular abnormalities and extraluminal soft tissue pathology and facilitates treatment planning. DSA is the reference standard of imaging, while endovascular embolization or stenting can be performed at the same time [3].

Compared to head and neck malignancies, benign entities such as paragangliomas rarely present with emergent symptoms, although they are sometimes identified for the evaluation of neck mass or discovered incidentally. Juvenile nasopharyngeal angiofibroma (JNA) is a rare benign tumor found nearly exclusively in young males, who typically present with epistaxis and nasal obstruction. It originates at the sphenopalatine foramen usually extending to the pterygopalatine fossa, infratemporal masticator space, nasal cavity, and nasopharynx and sometimes intracranially to the cavernous sinus and middle cranial fossa (Fig. 10.11). Due to the hypervascularity, preoperative embolization is usually required for these tumors to reduce blood loss during surgical resection.

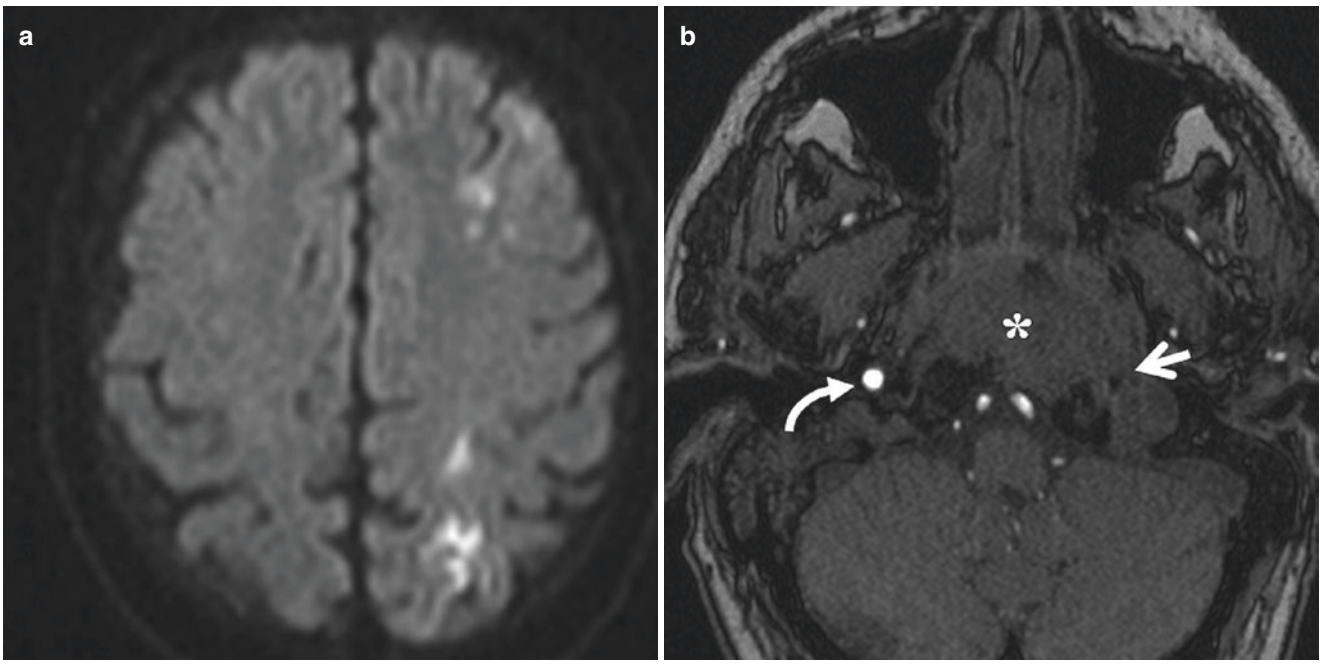

Fig. 10.8 Nasopharyngeal carcinoma with occlusion of left ICA. Patient with acute left-sided weakness. (**a**) DWI MRI shows acute infarction of left cerebral hemisphere in a watershed distribution. (**b**) Axial source image from 3D TOF MRA demonstrates absence of flow-related enhancement of left ICA (*arrow*), compared to the normal right ICA (*curved arrow*). Note a mass lesion in the nasopharynx (∗) with invasion of skull base, which is later biopsy-proven to be a nasopharyngeal carcinoma

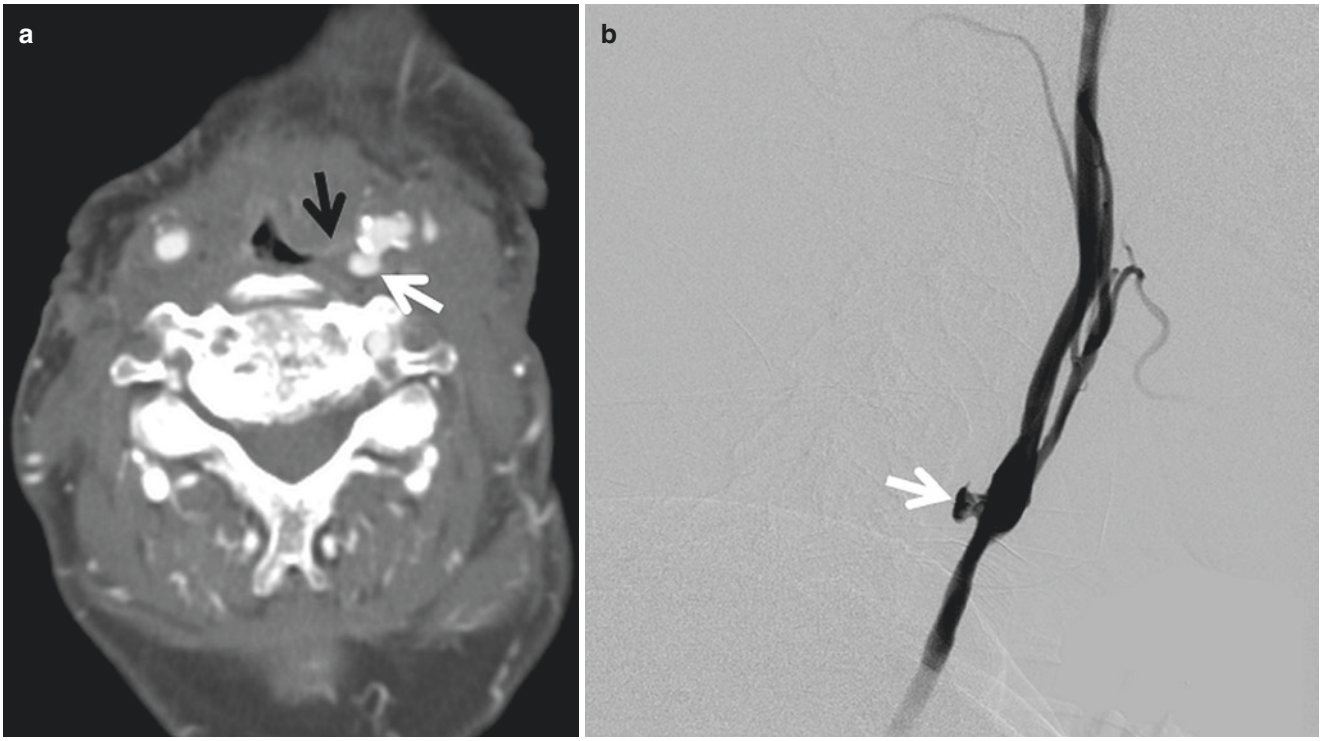

Fig. 10.9 Carotid blowout syndrome with an ICA pseudoaneurysm. Patient with history of laryngeal cancer status post chemoradiation, total laryngectomy, and bilateral neck dissection presents with large volume of hematemesis. (**a**) CTA neck demonstrates a dorsally projecting pseudoaneurysm (*white arrow*) from the origin of left ICA, adjacent to a pharyngocutaneous fistula (*black arrow*). (**b**) Lateral DSA of left ICA confirms the pseudoaneurysm (*white arrow*), which is subsequently occluded with a stent

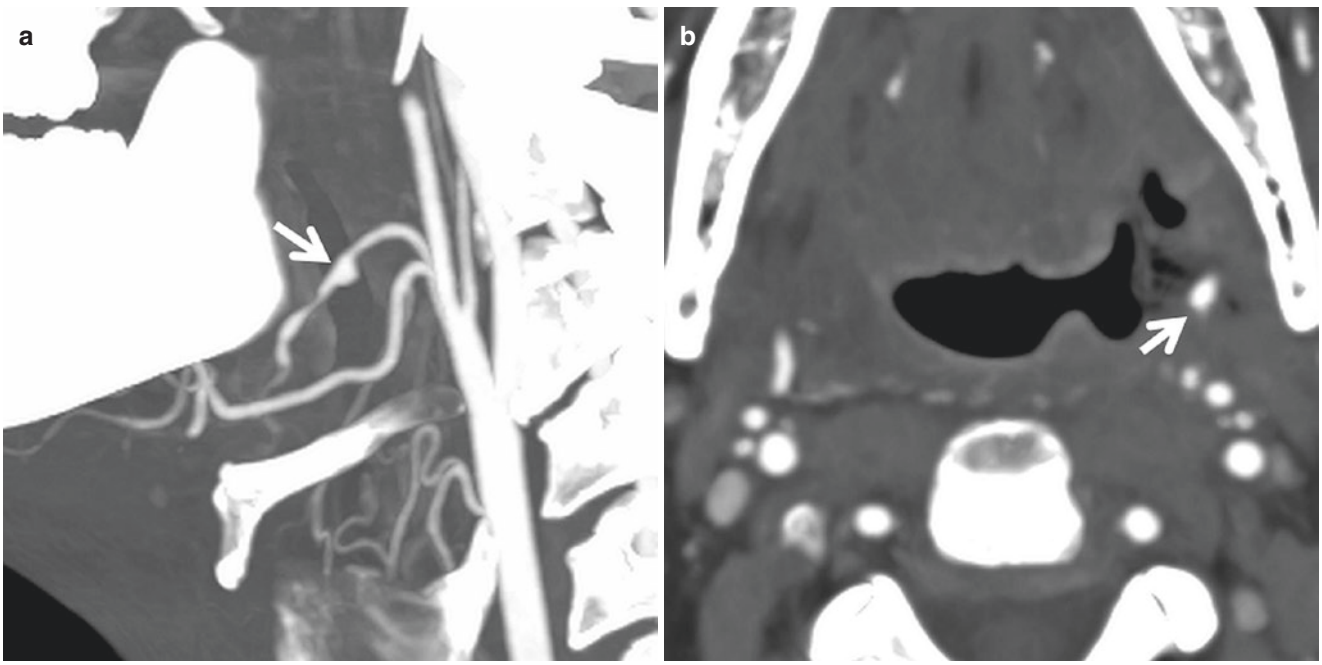

Fig. 10.10 Carotid blowout syndrome from ECA branches. Patient with history of left base of tongue cancer status post radiation presents with hematemesis. (**a**) Sagittal CTA MIP image shows a pseudoaneurysm of left facial artery (*arrow*). (**b**) Axial CTA MIP shows the pseudoaneurysm (*arrow*) is within the treated lesion of left base of the tongue surrounded by debris. (**c**) Lateral DSA of selective left facial artery injection shows active contrast extravasation (**d**) Lateral DSA of left ECA after coil embolization of left facial artery (*black arrow*) demonstrates multifocal contour irregularity of left lingual artery (*black arrow*) with a fusiform pseudoaneurysm (*white arrow*). It is later treated with coil embolization as well

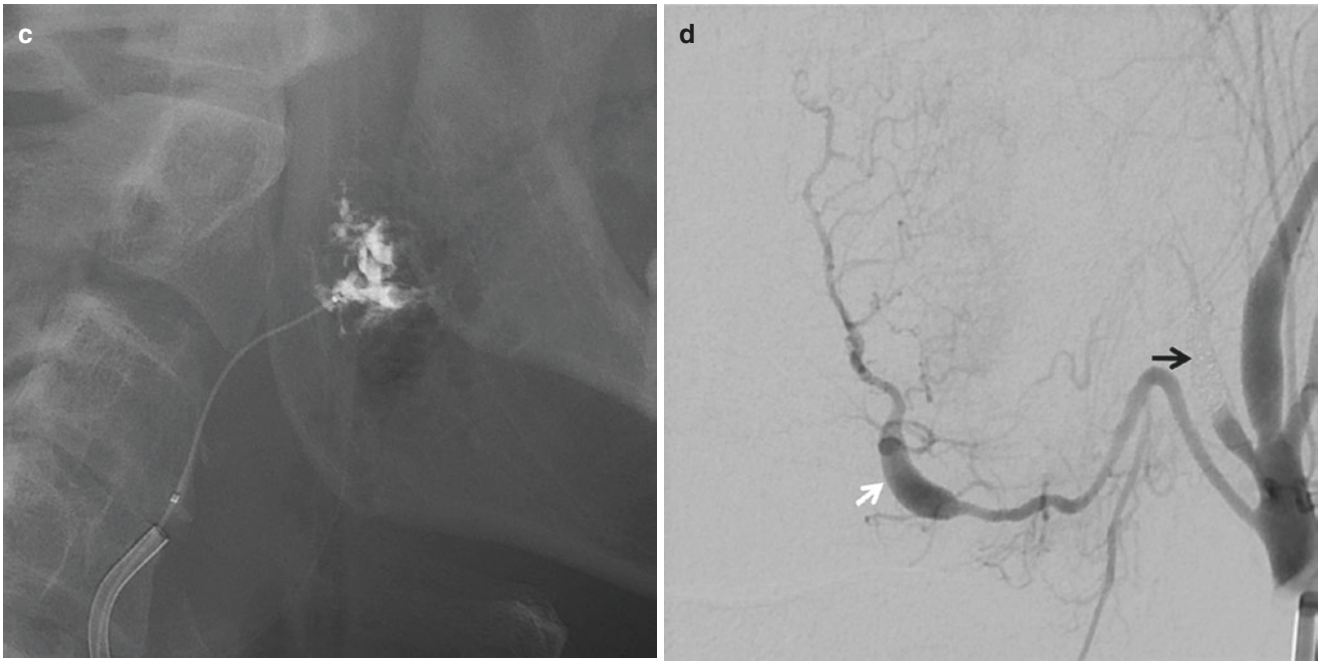

Fig. 10.10 (continued)

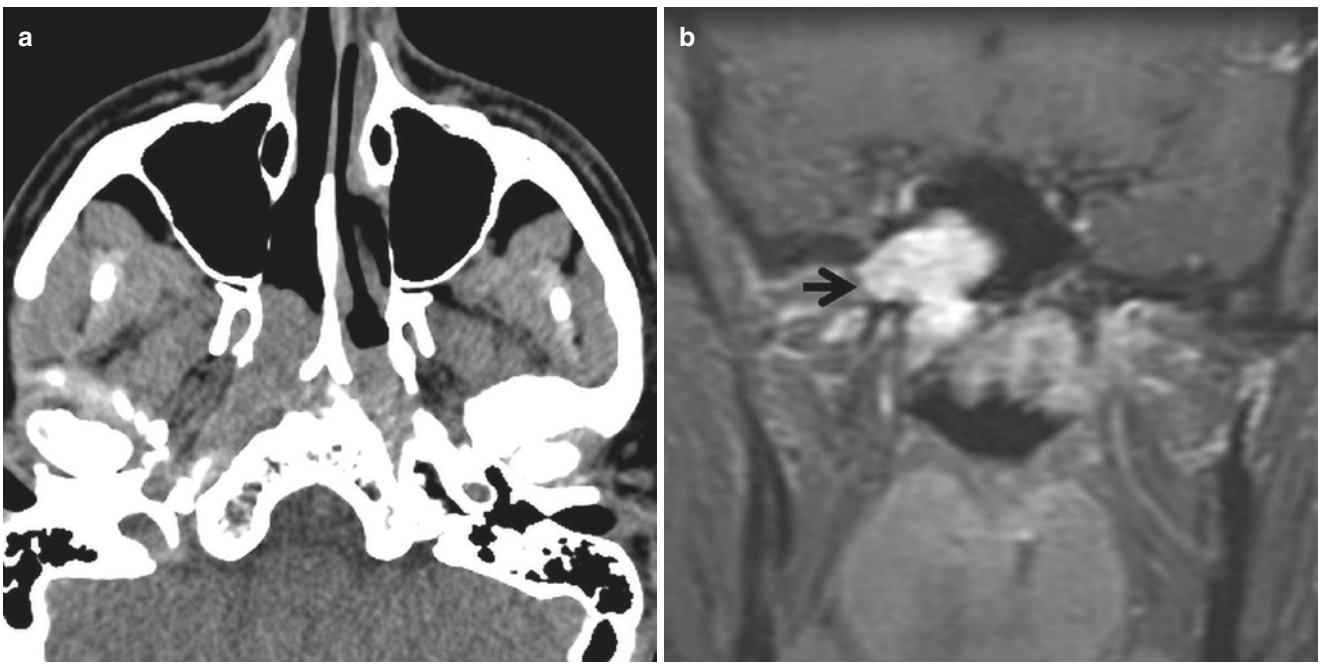

Fig. 10.11 Juvenile nasopharyngeal angiofibroma. A 9-year-old with recurrent epistaxis. (**a**) Axial CT shows a soft tissue mass in the right nasopharynx. (**b**) Postcontrast coronal MRI demonstrates an avidly enhancing mass in the right sphenoid sinus and nasopharynx extending through the sphenopalatine foramen to the pterygopalatine fossa (*arrow*). (**c**) AP projection of DSA of right ECA injection demonstrates the hypervascular mass lesion mostly supplied by the distal branches of internal maxillary artery

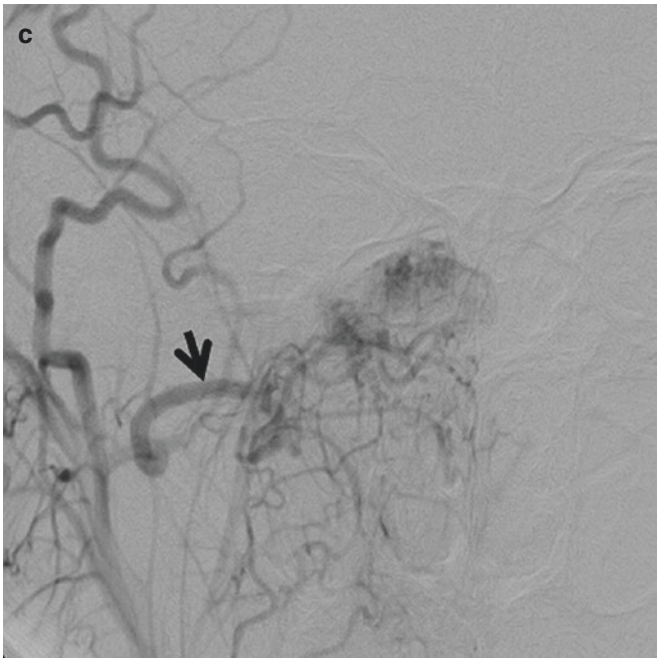

Fig. 10.11 (continued)

10.5 Vascular Malformation

10.5.1 Carotid-Cavernous Fistula

A carotid-cavernous fistula (CCF) is an abnormal communication between the carotid artery and cavernous sinus. It is classified into four subtypes (Barrow et al. [4]):

- Type A: direction communications between the ICA and cavernous sinus
- Type B: indirect fistula between meningeal branches of the ICA and cavernous sinus
- Type C: indirect fistula between the meningeal branches of the ECA and cavernous sinus
- Type D: indirect fistula between the meningeal branches of both ICA and ECA and cavernous sinus

Traumatic CCF is a direct type A high-flow shunt due to injury of cavernous ICA, typically due to severe head/facial injury and skull base fractures (Fig. 10.12). The shunting results in venous hypertension and reversed flow in the cavernous sinuses and its major tributaries including superior/inferior ophthalmic veins, sphenoparietal sinus, basal vein of Rosenthal, superior/inferior petrosal sinuses, and pterygoid and clival venous plexuses. Common symptoms include subjective bruit, blurred vision, headache, diplopia, ocular pain, proptosis, chemosis, etc. Occasionally, cerebral hemorrhage or infarction can occur. CTA is the initial modality of choice in the acute trauma setting, and DSA is the gold standard for diagnosis and treatment planning. Imaging findings of traumatic CCF include direct evidence of ICA injuries such as dissection, transection or pseudoaneurysm, visualization of the fistula, abnormal bulging appearance of the cavernous sinuses, dilatation of superior/inferior ophthalmic veins or facial veins, engorgement of cortical or deep drainage veins, etc.

In comparison, the majority of the indirect CCFs (types B, C, and D) are low-flow, often spontaneous, shunts that occur more frequently in middle-aged women. The symptoms often present more insidiously and are less severe than direct CCFs. The clinical presentations include diplopia, chemosis, proptosis, dilated episcleral veins, diminished vision, cranial nerve IV and III paresis, etc. MRI and MRA are frequently performed for these patients, which may show engorgement and abnormal flow voids of superior ophthalmic vein and cavernous sinus, but findings are frequently subtle (Fig. 10.13). CCFs can be treated endovascularly with trans-arterial or transvenous approaches.

10.5.2 Low-Flow Orbital Vascular Lesions

Venous varix is a low-flow orbital vascular lesion that can present emergently. Varices are the most common cause of spontaneous orbital hemorrhage. They typically manifest in the second or third decade of life and affect males and females equally. Most varices have communication with the venous system and distend during maneuvers that increase venous pressure [5]. Patients with thrombosed orbital varix typically present with acute retroorbital pain and proptosis. CT demonstrates a hyperdense orbital mass. MRI findings are characteristic and demonstrate a hemorrhagic orbital mass with variable T1 and T2 signal intensity corresponding to the age of blood products and peripheral enhancement after contrast [6]. Connection to the ophthalmic veins and cavernous sinus is sometimes identified (Fig. 10.14).

The major differential diagnosis is orbital lymphatic malformation with recent hemorrhage, which can also cause acute proptosis. MRI shows a multicompartmental orbital mass often with both intraconal and extraconal components. Fluid–fluid levels produced by hemorrhages of various ages within multiple cysts are almost pathognomonic [5].

10.5.3 Mandibular AVM

Arteriovenous malformation (AVM) of the mandible is a rarely encountered entity, which can present with life-threatening hemorrhage during a dental procedure. The panoramic radiograph and CT typically demonstrate a nonspecific unilocular or multilocular osteolytic lesion, which may be mistaken for other more common mandibular

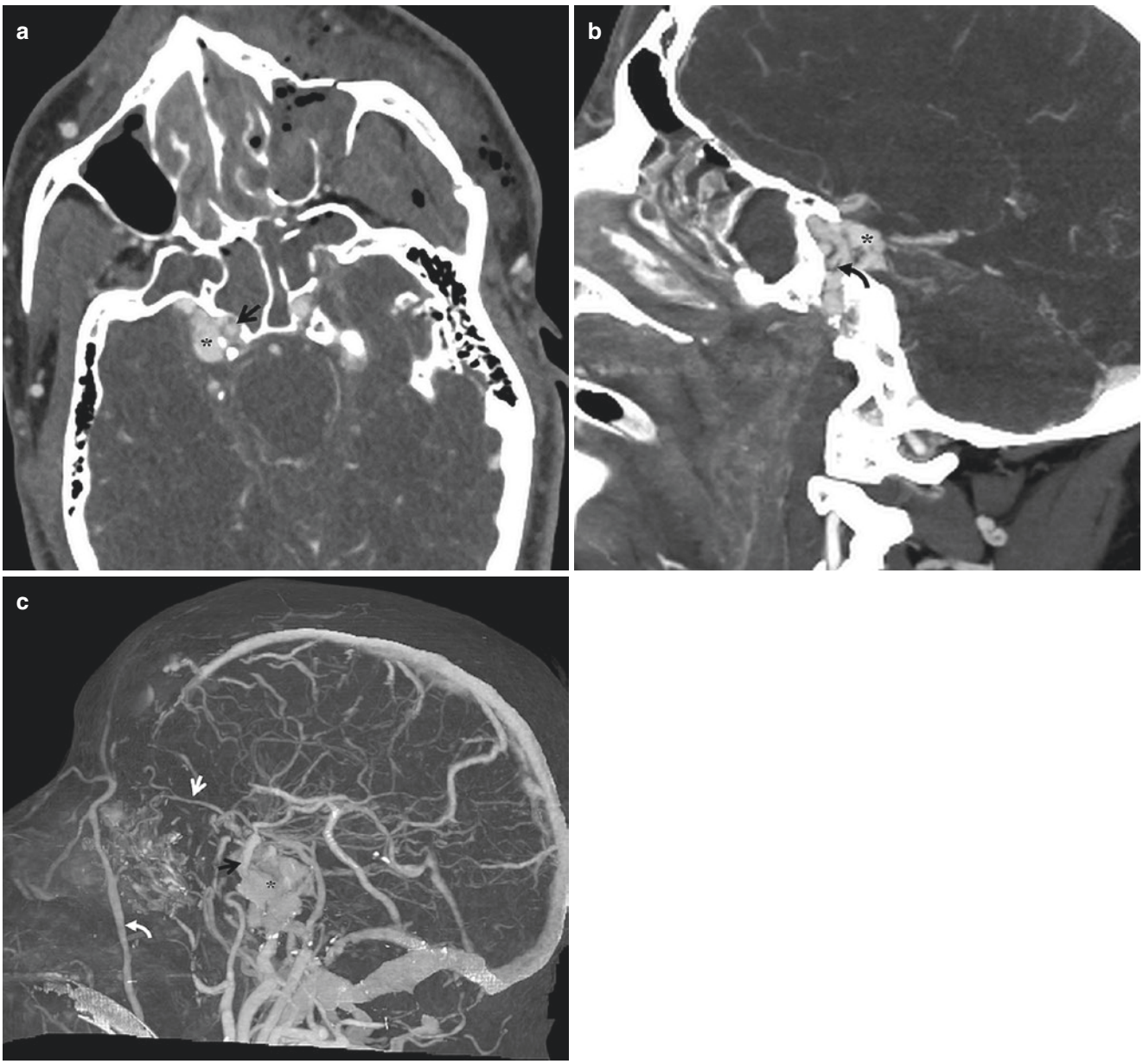

Fig. 10.12 Direct carotid-cavernous fistula. Trauma patient with multiple facial and skull base fractures. (**a**) Axial CTA shows narrowing of the right ICA cavernous segment (*black arrow*) and asymmetric bulging of right cavernous sinus (∗) compared to the left, consistent with carotid-cavernous fistula. (**b**) Sagittal CTA shows a direct communication of ICA and cavernous sinus (*curved arrow*). (**c**) 3D volume-rendered reconstruction with bone subtraction shows contour irregularity of right ICA (*black arrow*), enhancement of right cavernous sinus (∗), and engorgement of egress veins including superior ophthalmic vein (*white arrow*) and angular facial vein (*white curved arrow*)

cystic lesions such as ameloblastoma, odontogenic keratocyst, aneurysmal bone cyst, etc. CTA or DSA will make the diagnosis and provide crucial information on treatment planning including feeding arteries, draining vein, flow rate, and collaterals (Fig. 10.15). Treatment includes trans-arterial or direct puncture embolization and surgical resection [7].

10.6 Carotidynia

Carotidynia is an idiopathic neck pain syndrome associated with tenderness to palpation over the carotid bifurcation. It is a relatively rare entity, with the incidence of approximately 2.8% among patients with acute neck pain reported

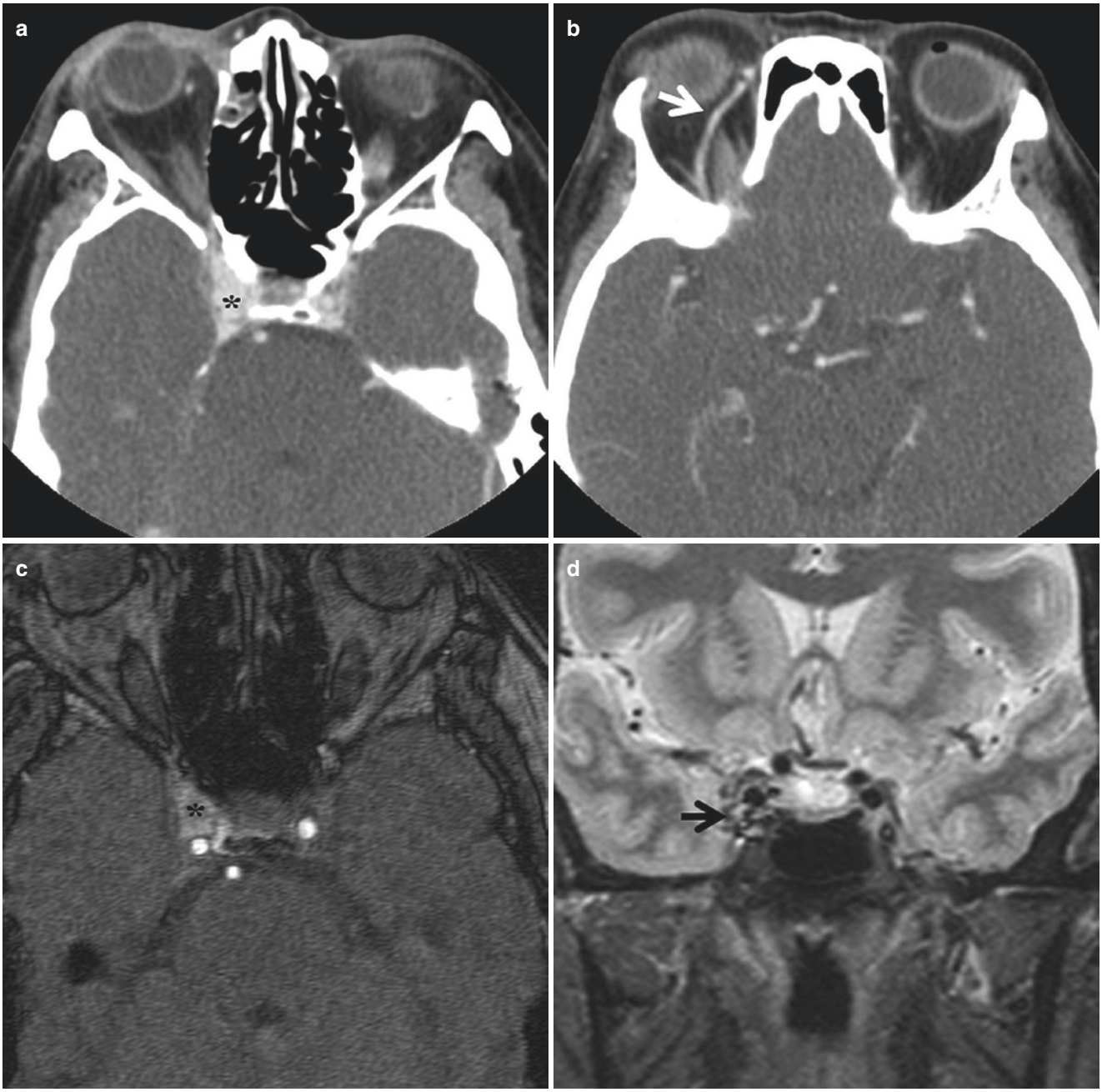

Fig. 10.13 Indirect carotid-cavernous fistula. A 59-year-old with right orbital swelling and blurred vision. (**a**, **b**) Postcontrast orbital CT demonstrates asymmetric enhancement of right cavernous sinus (∗) (**a**) and superior ophthalmic vein (*arrow*) (**b**). (**c**) 3D TOF MRA shows arterialized flow within the right cavernous sinus, consistent with carotid-cavernous fistula. (**d**) Coronal T2 MRI shows several flow voids within the right cavernous sinus. (**e**) DSA with right ICA injection confirms right CC fistula with feeders from the meningohypophyseal trunk of right ICA (*white arrow*), with early filling of cavernous sinus (∗) and superior ophthalmic vein (*black arrow*)

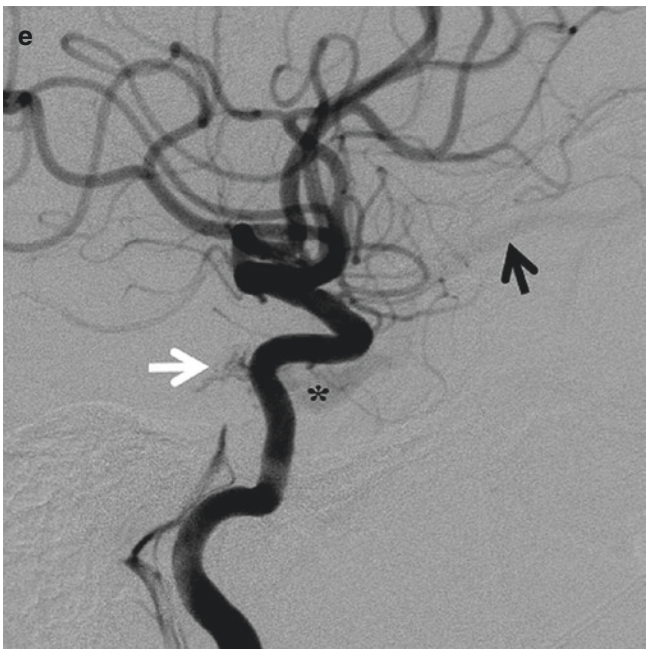

Fig. 10.13 (continued)

in one center although this may be underestimated [8]. It is a clinical diagnosis of exclusion, but imaging studies including CT, MRI, and ultrasound in recent years have shown a consistent pattern of abnormal perivascular inflammatory tissue surrounding the symptomatic carotid artery centered at the level of the distal common carotid and carotid bifurcation. On MRI, the abnormal tissue shows iso- or hypointensity on T1, hyperintensity on T2, and marked enhancement after gadolinium (Fig. 10.16) [9]. Some patients have mild associated luminal narrowing, though most patients have no luminal change. The remaining portions of the carotid artery are normal. The major differential considerations include inflammatory vasculitis, carotid dissection, or early atherosclerotic changes. Recently, a discrete clinico-radiological entity named transient perivascular inflammation of the carotid artery syndrome (TIPIC syndrome) has been proposed to replace the name carotidynia [8]. The treatment consists of nonsteroidal anti-inflammatory agents.

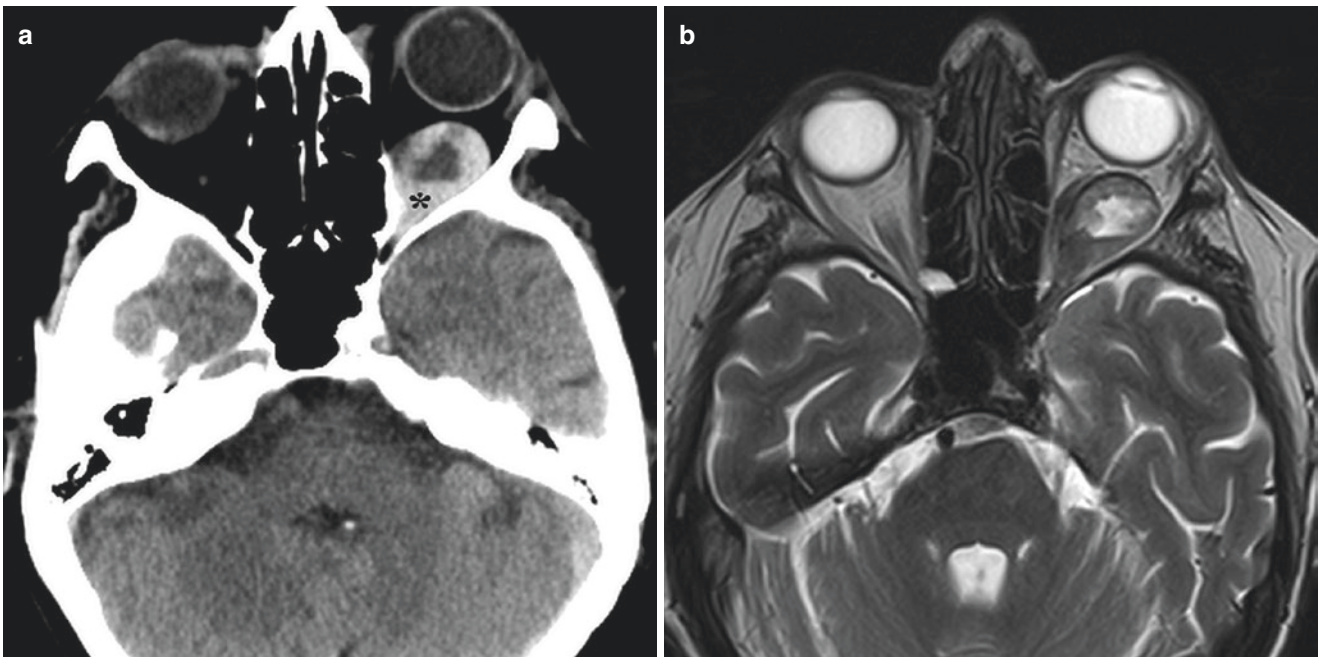

Fig. 10.14 Thrombosed orbital varix. A 79-year-old with sudden onset of diplopia and proptosis. (**a**) NCCT demonstrates an intraconal left orbital mass causing deviation of optic nerve. The mass has peripheral hyperdensity with attenuation measuring 70–80 Hounsfield unit consistent with acute thrombus. Note a hematocrit level within the mass. (**b**) The axial T2 MRI shows hypointensity along the periphery of the lesion consistent with thrombus, and a hematocrit level, confirming the CT findings. (**c**) Axial T1 postcontrast shows no enhancement, thus excluding neoplasm or cavernous hemangioma. (**d**) CTA shows no evidence of arteriovenous malformation or aneurysm. A pedicle is noted extending toward the left cavernous sinus. This appearance is most compatible with a venous varix with hemorrhage and partial thrombosis. Note a small enhancing varix in the right orbit

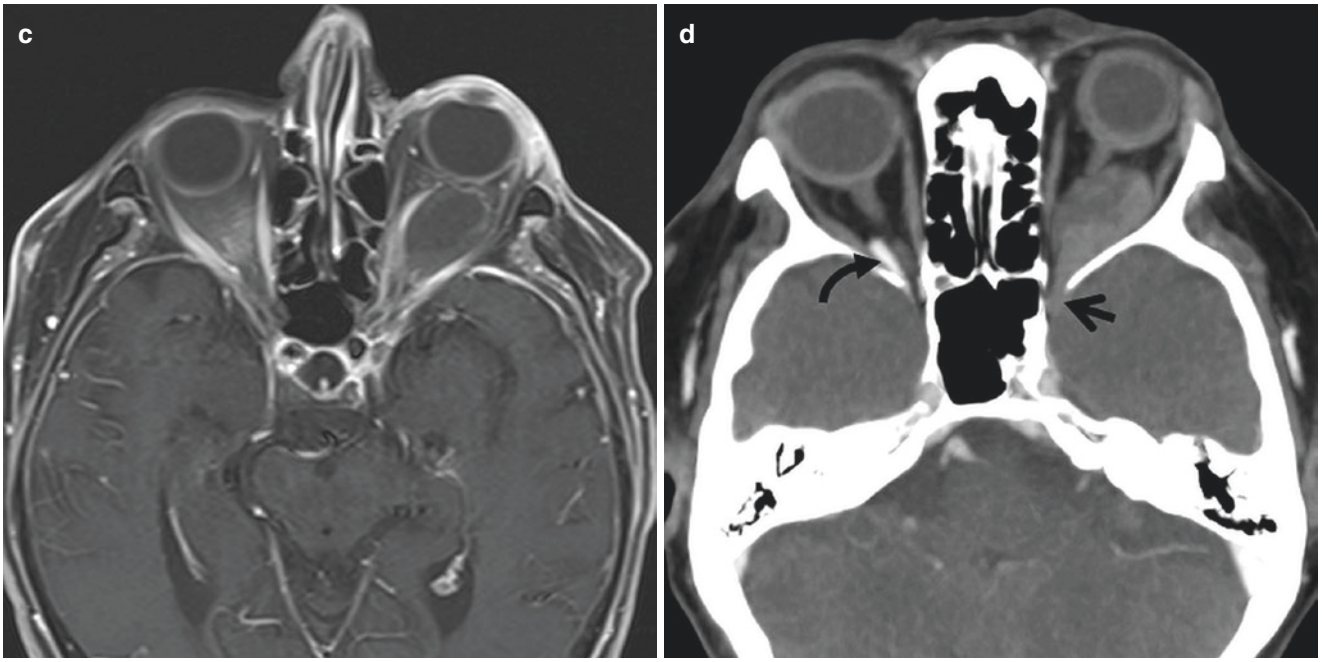

Fig. 10.14 (continued)

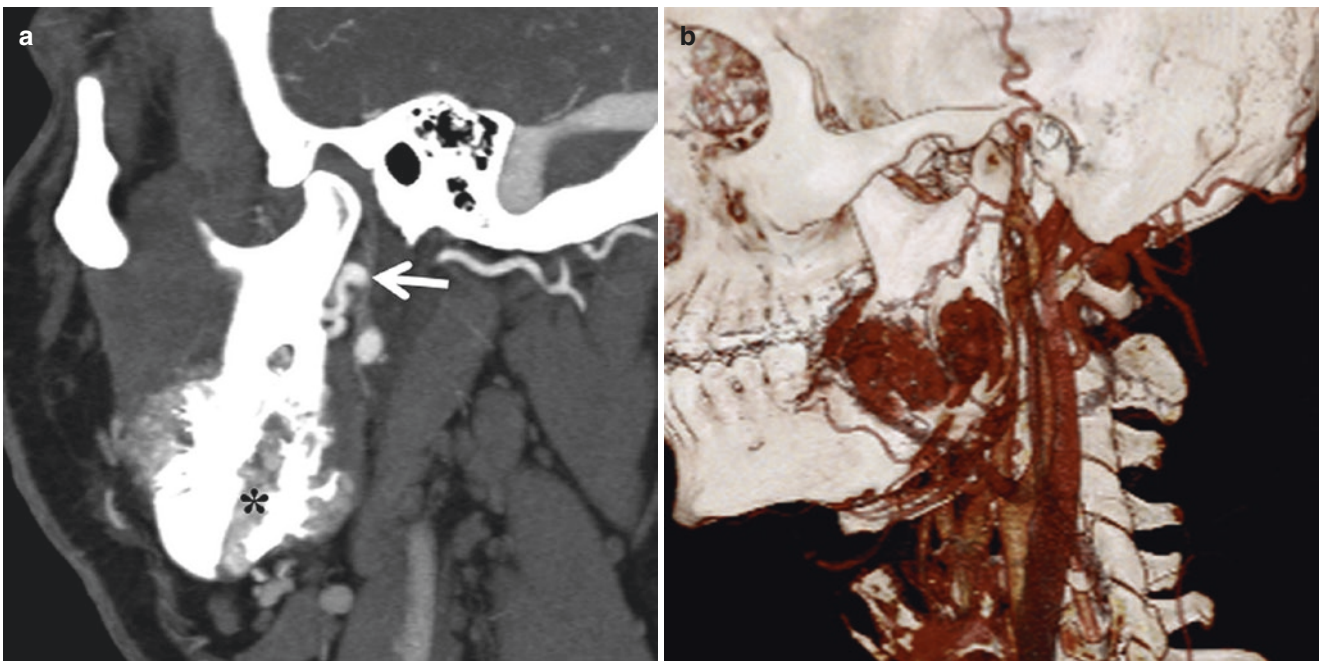

Fig. 10.15 Mandibular AVM. A 31-year-old presents with hemorrhage after a dental procedure. (**a**) Sagittal MIP CTA demonstrates a lytic hypervascular mass in the left mandibular ramus (∗), mostly supplied by the inferior alveolar branch of internal maxillary artery. (**b**) 3D volume-rendered reconstructed CTA image confirms AVM

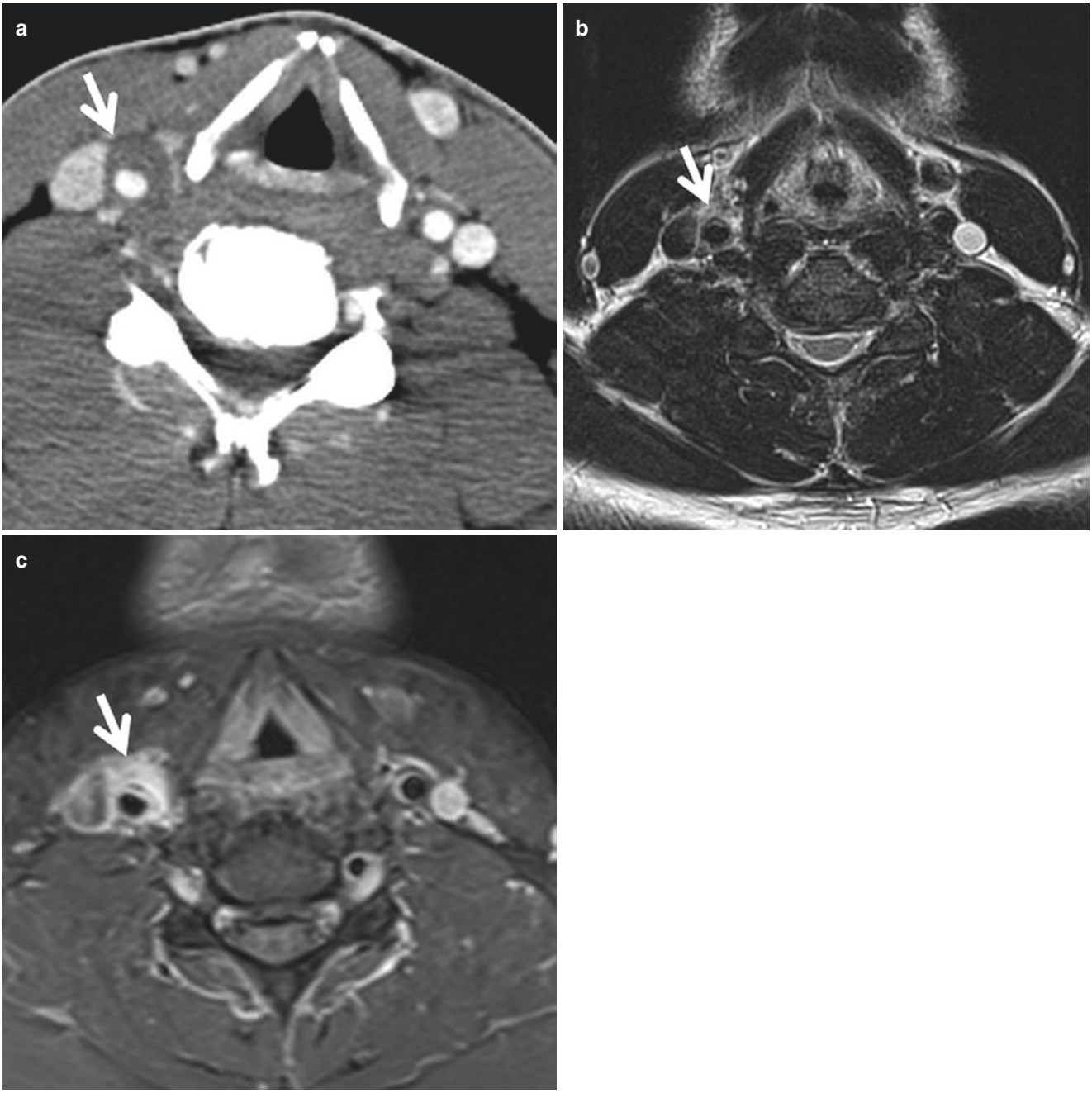

Fig. 10.16 Carotidynia. A 30-year-old with right neck pain. (**a**) Axial CECT of the neck shows circumferential low-density soft tissue surrounding right common carotid artery near the bifurcation. (**b**, **c**) MRI of the neck. This tissue is T2 hyperintense (**b**) and demonstrates avid, homogenous enhancement on the fat-saturated T1 postcontrast image (**c**). Note the caliber of the right common carotid artery is well preserved

References

1. Campbell RG. Sphenopalatine artery pseudoaneurysm after endoscopic sinus surgery: a case report and literature review. Ear Nose Throat J. 2012;91:E4. https://doi.org/10.1177/014556131209100215.
2. Labruzzo SV, Aygun N, Zinreich SJ. Imaging of the paranasal sinuses: mitigation, identification, and workup of functional endoscopic surgery complications. Otolaryngol Clin N Am. 2015;48:805–15.
3. Mazumdar A, Derdeyn CP, Holloway W, Moran CJ, Cross DWT. Update on endovascular management of the Carotid Blowout Syndrome. Neuroimaging Clin N Am. 2009;19:271–81.
4. Barrow DL, Spector RH, Braun IF. Classification and treatment of spontaneous carotid-cavernous sinus fistulas. J Neurosurg. 1985;62(2):248–56.

5. Smoker WRK, Gentry LR, Yee NK, Reede DL, Nerad JA. Vascular lesions of the orbit: more than meets the eye. Radiographics. 2008;28:185–204.
6. Thrombosed orbital varix|Radiology Case|Radiopaedia.org. https://radiopaedia.org/cases/thrombosed-orbital-varix-2. Accessed 21 Dec 2019.
7. Fan XD, Su LX, Zheng JW, Zheng LZ, Zhang ZY. Ethanol embolization of arteriovenous malformations of the mandible. Am J Neuroradiol. 2009;30:1178–83.
8. Lecler A, Obadia M, Savatovsky J, et al. TIPIC syndrome: beyond the myth of carotidynia, a new distinct unclassified entity. Am J Neuroradiol. 2017;38:1391–8.
9. Burton BS, Syms MJ, Petermann GW, Burgess LPA. MR imaging of patients with carotidynia. Am J Neuroradiol. 2000;21:766–9.

Spinal Vascular Diseases

11

Yang Tang

11.1 Vascular Anatomy

An in-depth knowledge of spinal vascular anatomy is essential to the understanding of the pathophysiology and imaging appearance of spinal vascular disease. The chapter will start with a brief introduction to the spinal vascular anatomy. The detailed discussion is beyond the scope of this chapter and can be found in many other excellent sources.

11.1.1 Arterial System

The anterior spinal artery (ASA) is formed by the descending branches of the intracranial vertebral arteries. The two posterior spinal arteries (PSA) also originate from the ipsilateral vertebral artery or posterior inferior cerebellar arteries. The ASA and PSAs descend along the cord and are reinforced by multiple segmental arteries at variable cervical, thoracic, and lumbar levels.

Each segmental artery gives off a radicular branch to supply the nerve root. Branches of the radicular arteries that supply the ASA are termed radiculomedullary arteries, while those supplying the PSAs are termed radiculopial arteries. The levels at which the radiculomedullary and radiculopial arteries originate are highly variable among different individuals. The dominant radiculomedullary artery feeding the ASA at the thoracolumbar region is named the artery of Adamkiewicz (AKA), which typically arises between T8 and L3, more frequently on the left [1].

Coursing through the ventral sulcus of the spinal cord, the ASA gives off a number of sulcocomissural arteries that penetrate the central gray matter and branch outward toward the white matter in a centrifugal pattern, supplying anterior two-thirds of the spinal cord including the anterior horns, the spinothalamic and corticospinal tracts. The PSAs are paired arteries that descend along the dorsal sulci of the cord and give off many perforators that supply the posterior third of the spinal cord, including the dorsal columns, dorsal gray matter, and superficial dorsal aspect of the lateral columns of the spinal cord in a centripetal manner [2].

11.1.2 Venous System

The venous drainage of the spinal cord is complex. Briefly, the intrinsic veins of the spinal cord are directed peripherally toward the superficial extrinsic system, which consists of longitudinally oriented anterior median spinal vein and posterior spinal veins as well as an anastomotic coronal venous plexus network [3]. Unlike the arteries, there is no predominant pattern in terms of anterior and posterior venous drainage of the spinal cord. The superficial veins drain into the radiculomedullary veins at variable levels and eventually into the epidural venous plexus. Of note, the great anterior radiculomedullary vein (GARV), the largest vein draining the anterior thoracolumbar spinal cord, can be easily mistaken for the AKA during the venous phase [2], a potential pitfall especially when interpreting the noninvasive spinal vascular imaging.

11.2 Diagnostic Modality

Catheter spinal angiography (DSA) is the gold standard for the study of spinal vascular anatomy and remains the most accurate modality for the diagnosis of spinal vascular malformation and localization of the AKA for presurgical planning. However, it is an invasive and lengthy procedure, requires selective catheterization of all the arteries supplying the spinal cord, and carries a small risk of complications.

MRI has been widely used to evaluate patients with myelopathy of various etiologies including suspected spinal cord infarction or vascular abnormalities due to its superb soft tissue characterization. Traditionally, the MRI diagnosis

© Springer Nature Switzerland AG 2020

Y. Tang, *Atlas of Emergency Neurovascular Imaging*, https://doi.org/10.1007/978-3-030-43654-4_11

was predominantly based on the signal changes of the cord but not on direct visualization of abnormal vasculature. Advances in MR technologies in recent years have enabled direct visualization of spinal vascular lesions in a noninvasive manner. Multiple sequences have been investigated including contrast-enhanced MRA techniques with 3D TOF acquisition [4], elliptic-centric contrast-enhanced MRA [5], time-resolved imaging of contrast kinetics (TRICKS) [6], and 3D high-resolution T2 sequence [7]. MRI/MRA can provide important diagnostic information about the location of the spinal vascular lesions to guide the DSA. Multiplanar reformation (MPR), curved planar reformation (CPR), and maximum-intensity projection (MIP) images are crucial for the detection and analysis of the feeding artery, venous drainage, location of AKA, etc.

CTA has also been used for evaluation of spinal vascular disease [8, 9]. It has spatial resolution superior to MRA. Presenting vascular malformation together with the adjacent bone and soft tissue may provide additional advantage in treatment planning. However, CT requires the use of iodinated contrast and high dose of radiation. It is also very limited in evaluating the spinal cord and other neural structures, therefore unlikely to replace MRA as the primary noninvasive modality for spinal vascular imaging.

11.3 Cord Infarction

Spinal cord infarction (SCI) is a devastating neurological disorder and is one of the important differential considerations for patients presenting with acute onset myelopathy. Although with limited treatment options, it is critical to differentiate it from other treatable causes.

SCI is associated with a number of risk factors. Many of these cases occur in the postprocedural setting, most notably after repair of thoracoabdominal aortic aneurysm or dissection. Other procedures include cardiac surgery, spinal decompression, epidural injection, angiography, nerve block, embolization, other vascular surgery, and thoracic surgery [10]. Additional risk factors include arteriosclerosis, systemic hypotension/hypoperfusion, vasculitis, cardioembolism, and fibrocartilaginous emboli from herniated discs. Some cases have no identifiable causes.

The most common clinical presentation of SCI is anterior spinal artery (ASA) syndrome. Patients typically present with rapidly progressive paraparesis or quadriparesis peaked within 12–24 hours. A small portion of patients can have more gradual symptoms that peak in a few days. Other symptoms include temperature and sensory loss, severe back/limb pain, and bowel or bladder dysfunction [10].

MRI is the imaging modality of choice. Early infarction may show diffusion restriction on DWI sequence, which is more sensitive than T2. Involvement can be either patchy/noncontinuous or longitudinally extensive. A variety of patterns on T2 sequence have been described, including "owl eyes," "pencillike hyperintensity," hologrey, holocord, anteromedial spot, and anterior U/V. Postcontrast enhancement can be seen in the area of infarction, particularly a linear craniocaudal strip along the gray matter [11]. It is worth mentioning that the above findings including diffusion restriction are not entirely specific for cord infarction and can be seen in other causes of acute myelopathy, such as idiopathic transverse myelitis, demyelinating disease (multiple sclerosis, ADEM, or NMO), or other inflammatory/vasculitic processes, as well as spinal vascular malformations. Adjacent vertebral body infarction can be seen in a small percentage of SCI patients and is a more specific finding if present. MRA or other vascular imaging may demonstrate thoracoabdominal aneurysm/dissection, vertebral dissection/occlusion, aortoiliac occlusion, other vascular pathologies that may contribute to cord infarction (Fig. 11.1) [11].

11.4 Spinal Vascular Malformation

A number of classification systems exist for spinal arteriovenous malformations [12]. One of the most widely used systems includes four categories [13]:

- Type I: Spinal dural AVF
- Type II: Intramedullary AVM (glomus AVM with nidus)
- Type III: Intradural and extradural, metameric or juvenile AVM
- Type IV: Intradural perimedullary AVF

Additional spinal vascular lesions include spinal artery aneurysm, vascular tumor, and cavernous malformation.

11.4.1 Type I Spinal Dural AV Fistula (SDAVF)

SDAVF is the most common spinal vascular malformation and is an important differential consideration when evaluating adults with progressively worsening myelopathy. It typically affects older patients with male predominance. Most patients present with progressive paraparesis, back pain, and bowel and bladder dysfunction.

The fistulas are located near the nerve roots between the outer and inner dural layers, supplied by the dural branch of radicular artery with drainage into the radiculomedullary vein. The arteriovenous shunting results in arterialization of the radiculomedullary vein, which in turn transmits the pressure to the coronal venous plexus, causing venous hypertension, congestive myelopathy, and eventually cord infarction. It can be further categorized into type A (single arterial feeder) or type B (multiple arterial feeders).

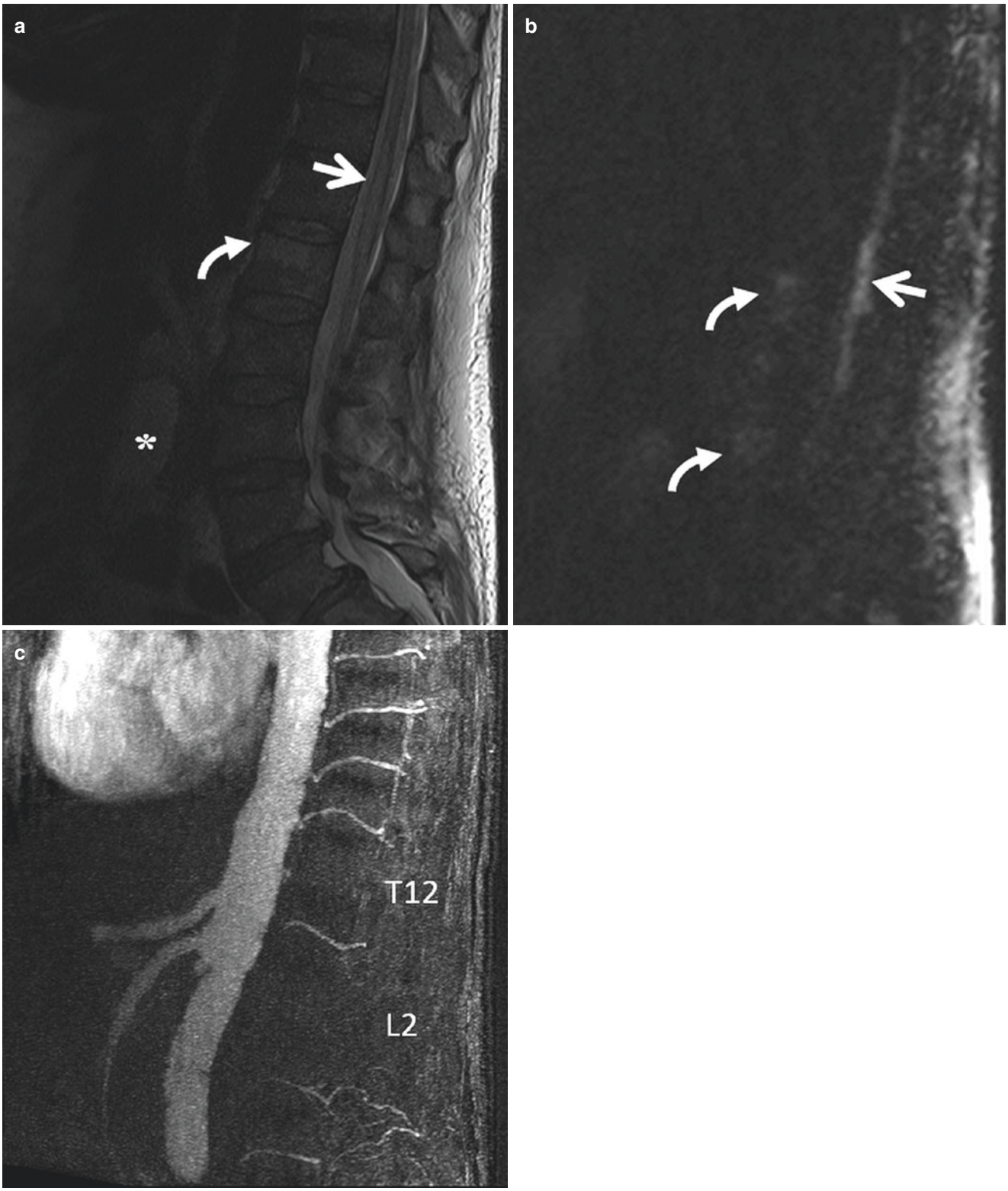

Fig. 11.1 Cord infarction. A 61-year-old with lower extremity weakness after surgical repair of abdominal aortic aneurysm. (**a**) Sagittal T2 MRI shows hyperintensity and mild expansion of conus from T11 to L1 (*arrow*). Abnormal bone marrow signal of L1 vertebral body, suggestive of bone infarction (*curved arrow*). Note abdominal aortic aneurysm (∗). (**b**) Sagittal DWI shows corresponding diffusion restriction (*arrow*), consistent with cord infarction. Abnormal signal of several vertebral bodies is also noted. (**c**) Sagittal thick slab MIP of contrast-enhanced MRA shows absence of the subcostal artery at T12 and the lumbar artery at L2

MRI can demonstrate cord edema and expansion on T2 sequence. Dilated veins are usually evident in the subarachnoid space. Following gadolinium injection, enhancement can be seen in the area of cord infarction, which is an indicator for poor prognosis. Dilated perimedullary veins and coronal plexus also enhance. Contrast-enhanced and time-resolved MR angiography may predict the level of fistula before the definite diagnosis of DSA (Fig. 11.2).

Fig. 11.2 Type I spinal dural AV fistula. A 70-year-old presents with neurogenic claudication for 6 months. (**a**) Sagittal T2 lumbar spine MRI shows edema and expansion of the conus medullaris. Note multilevel severe spondylosis. (**b**) Sagittal MIP of 3D contrast-enhanced MRA shows engorged venous plexus along the surface of the cord (*curved arrow*). Note a small focus of abnormal enhancement at the left L3 neural foramen suspicious for a dural AV fistula (*arrow*). (**c**) Axial MIP of MRA again shows the abnormal focus of enhancement at the left L3–L4 neural foramen (*arrow*). (**d**) Spinal DSA with injection of left L3 lumbar artery shows a dural AV fistula supplied by the left L3 radicular artery at the L3–L4 nerve root sleeve (*arrow*). Note the enlarged draining vein (*curved arrow*)

11.4.2 Type II Intramedullary AVM

Type II intramedullary AVM is the second most common spinal vascular malformations. Similar to brain AVMs, intramedullary AVMs are high-flow lesions and consist of a nidus supplied by anterior or posterior spinal arteries and drain through the dilated spinal veins. Many have associated flow-related aneurysms and venous varices. These are congenital lesions and sometimes associated with Klippel–Trenaunay–Weber or Osler–Weber–Rendu syndromes. Most patients present before the age of 40 with acute myelopathy secondary to intramedullary or subarachnoid hemorrhage. Small portion of patients have gradual onset of symptoms due to congestive myelopathy and vascular steal phenomenon. MRI is the best modality to identify these lesions, which typically manifest as conglomerates of abnormal intramedullary and perimedullary flow voids with associated cord edema and hemorrhage. Catheter angiography is best for characterizing the feeding artery and draining veins for treatment planning (Fig. 11.3).

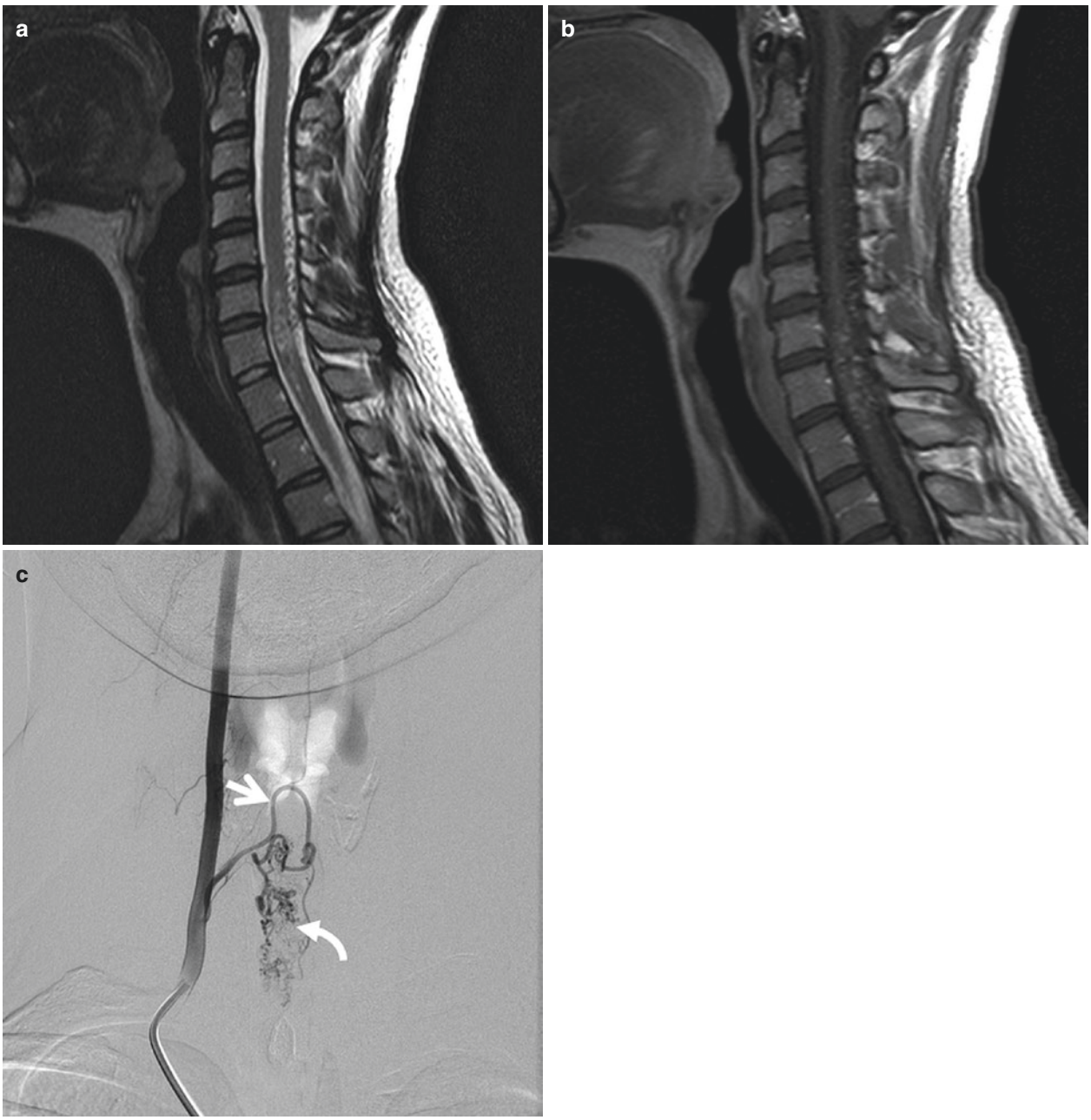

Fig. 11.3 Type II intramedullary AVM. A 30-year-old with progressive left trunk and leg weakness. (**a**) Sagittal T2 of cervical spine demonstrates cord edema at C6 and C7. Note abnormal vascular flow voids along the posterior spinal canal. (**b**) Postcontrast T1 demonstrates intramedullary vascular enhancement at C6 and C7. (**c**) DSA of right vertebral artery demonstrates a very prominent artery of cervical enlargement with a characteristic hairpin turn (*arrow*) supplying an intramedullary nidus (*curved arrow*), consistent with type II spinal AVM

11.4.3 Type III Intradural and Extradural AVM

Type III intradural and extradural AVM (aka juvenile or metameric AVM) is a rare congenital vascular malformation involving the spinal cord, dura, vertebra, musculature and skin at the same segmental metamere. If all these layers are involved, it is termed Cobb syndrome. On MRI, these lesions involve both intradural and extradural compartments.

11.4.4 Type IV Intradural Perimedullary AVF

Type IV intradural perimedullary AVF represents direct fistulous connection outside the cord between a pial artery (anterior or posterior spinal artery) and a corresponding draining vein. It is further classified into three subtypes (A, B, and C) based on the size and shunt flow. Compared to type I dural AVFs, patients with perimedullary AVFs usually present early before the age of 40 with acute onset of hemorrhage, or insidious myelopathy in a minority of patients. Like other types of spinal vascular malformations, MRI will show cord edema and/or hemorrhage. Serpentine intradural vascular flow voids can be seen, representing dilated feeding arteries and draining veins, sometimes causing deformity of the cord.

11.5 Spinal Cavernous Malformation

Cavernous malformation can rarely occur in the spinal cord. It can cause sudden onset of neurological deficit due to acute macrohemorrhage, or slowly progressive neurological decline secondary to repetitive intralesional microhemorrhage. It consists of closely packed dysplastic vessels without interposition of cord parenchyma, surrounded by hemosiderin and gliosis. Similar to its brain counterpart, spinal cavernous malformation is angiographically occult. The MRI appearance is characterized by a well-circumscribed lesion with blooming artifact on gradient echo sequence, as well as heterogeneous signal on T1 and T2 sequences reflecting blood products of different ages. The lesion can enhance to a variable degree on the postcontrast sequence. A peripheral hemosiderin ring is usually present. Incomplete hemosiderin ring and surrounding edema may indicate recent hemorrhage (Fig. 11.4).

11.6 Spinal Hemangioblastoma

Hemangioblastomas can be sporadic or associated with von Hippel–Lindau (VHL) syndrome. It most commonly occurs intracranially in the posterior fossa, with a small percentage occurring in the spinal cord. MRI is the best diagnostic modality. The key finding is a T2 hyperintense, avidly enhancing nodule in the spinal canal typically along the pial surface of the cord. Multiple serpentine flow voids can be seen associated with the lesion reflecting the tumor hypervascularity. It is frequently associated with a syrinx. Angiography typically shows a hypervascular mass supplied by medullary arteries, which can mimic a glomus AVM (Fig. 11.5).

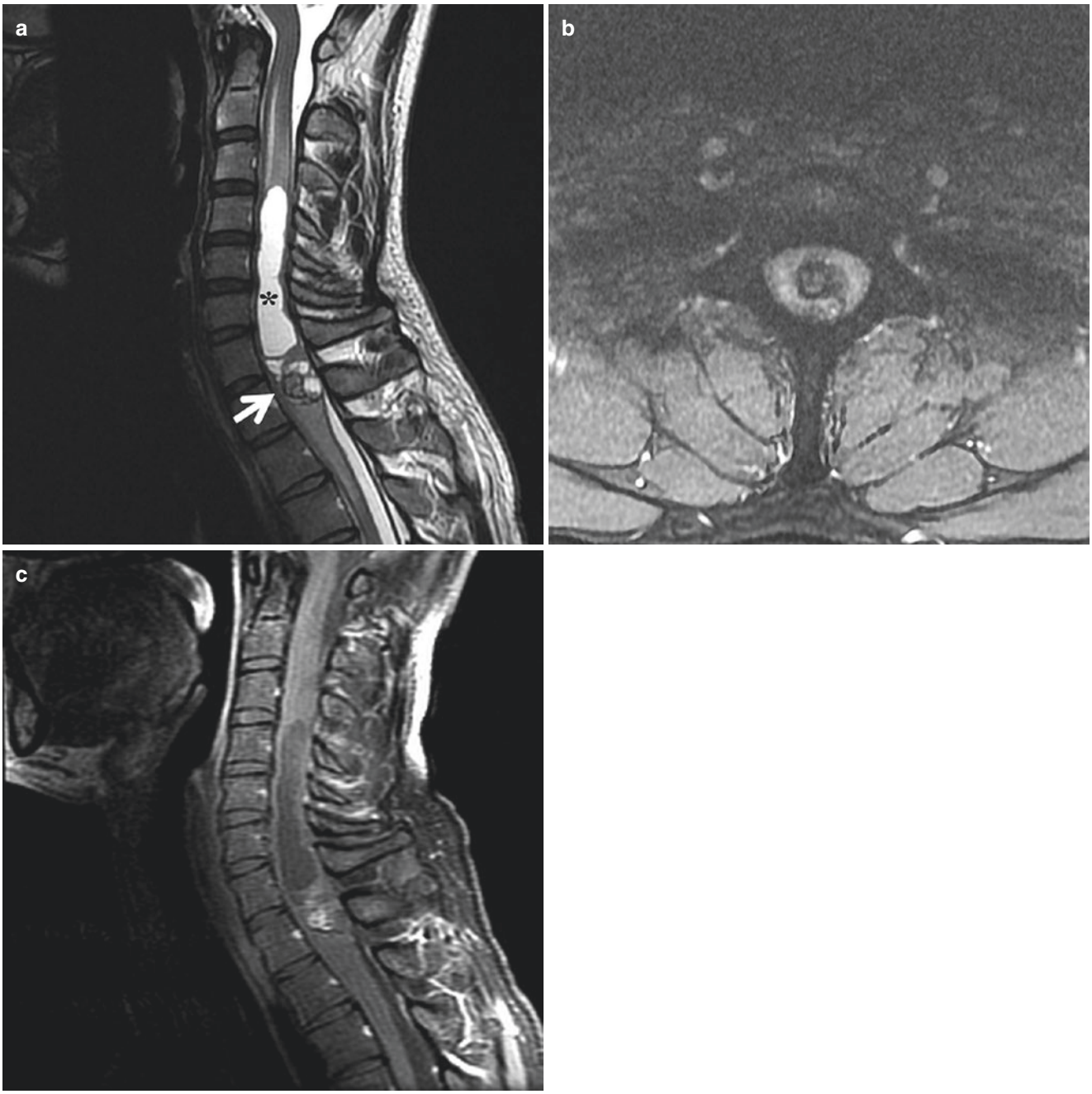

Fig. 11.4 Spinal cavernoma. A 34-year-old with bilateral arm weakness and paresthesia. (**a**) Sagittal T2 shows a multiloculated partially cystic intramedullary mass at the C7 and T1. There is extensive cervical syrinx proximal to the lesion. (**b**) Axial GRE shows a hemorrhagic ring along the periphery of the lesion. (**c**) Postcontrast T1 shows partial enhancement of this lesion

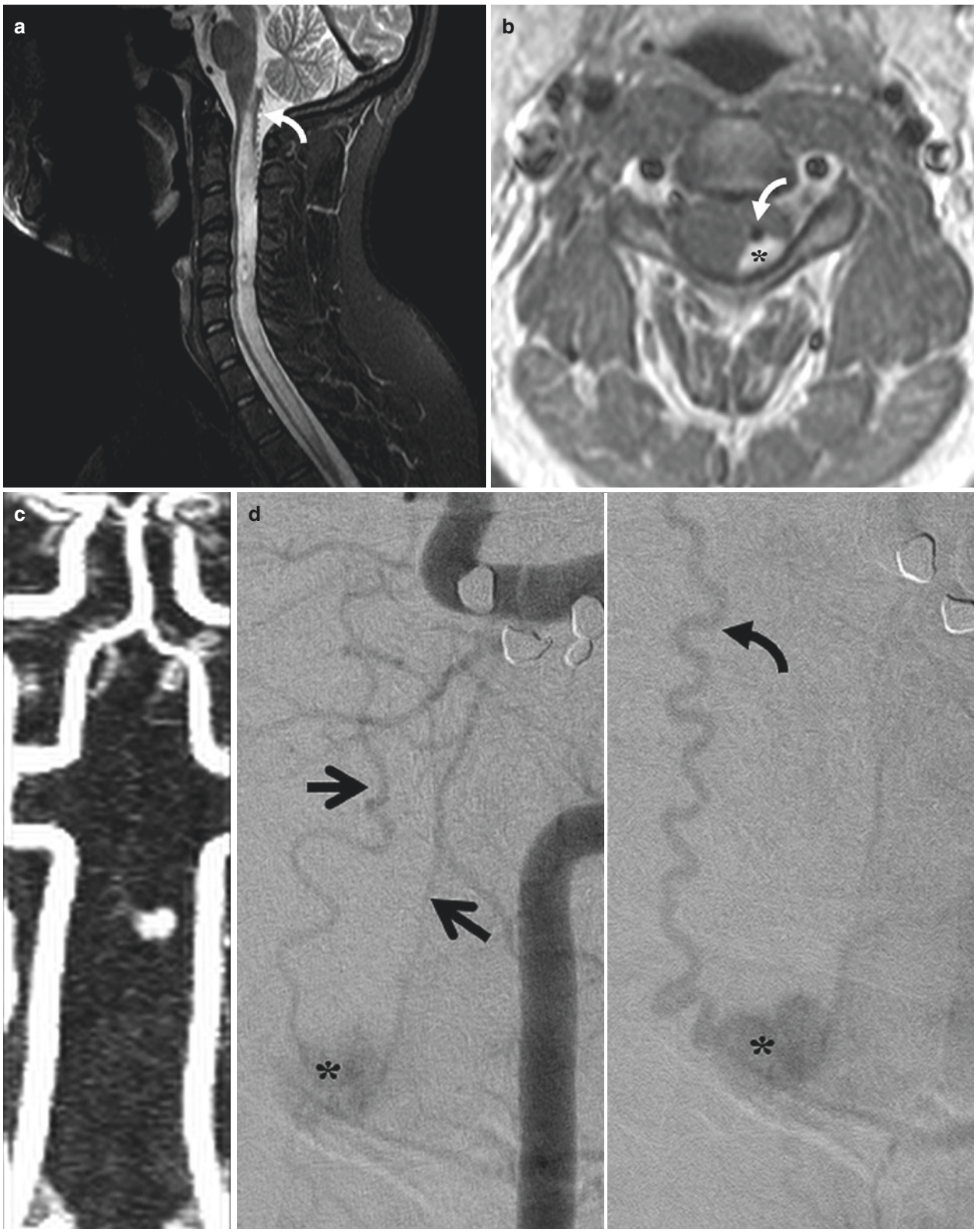

Fig. 11.5 Spinal hemangioblastoma. A 24-year-old presents with weakness. (**a**) Sagittal T2 shows extensive cord edema/syrinx. Note prominent vascular flow void along the dorsal surface of the cord (*curved arrow*). (**b**) Axial postcontrast T1 shows an avidly enhancing nodule (∗) along the left dorsal pial surface of the cord at C3, along with a prominent vessel (*curved arrow*). (**c**) Coronal MIP of contrast-enhanced MRA shows arterial phase enhancement of this lesion. (**d**) AP DSA of left vertebral injection during arterial phase (left panel) and venous phase (right panel) show a hypervascular mass (∗) with arterial supply from posterior spinal arteries (*arrows*) and venous drainage extending intracranially (*curved arrow*)

References

1. Charles YP, Barbe B, Beaujeux R, Boujan F, Steib JP. Relevance of the anatomical location of the Adamkiewicz artery in spine surgery. Surg Radiol Anat. 2011;33:3–9.
2. Byrne JV, Byrne JV. Spinal vascular anatomy. Tutorials Endovasc Neurosurg Interv Neuroradiol. Springer International Publishing. 2017:77–89.
3. Miyasaka K, Asano T, Ushikoshi S, Hida K, Koyanagi I. Vascular anatomy of the spinal cord and classification of spinal arteriovenous malformations. Interv Neuroradiol. 2000;6:195–8.
4. Saraf-Lavi E, Bowen BC, Quencer RM, Sklar EML, Holz A, Falcone S, Latchaw RE, Duncan R, Wakhloo A. Detection of spinal dural arteriovenous fistulae with MR imaging and contrast-enhanced MR angiography: sensitivity, specificity, and prediction of vertebral level. Am J Neuroradiol. 2002;23(5):858–67.
5. Luetmer PH, Lane JI, Gilbertson JR, Bernstein MA, Huston J, Atkinson JLD. Preangiographic evaluation of spinal dural arteriovenous fistulas with elliptic centric contrast-enhanced MR angiography and effect on radiation dose and volume of iodinated contrast material. Am J Neuroradiol. 2005;26(4):711–8.
6. Amarouche M, Hart JL, Siddiqui A, Hampton T, Walsh DC. Time-resolved contrast-enhanced MR angiography of spinal vascular malformations. Am J Neuroradiol. 2015;36:417–22.
7. Kralik SF, Murph D, Mehta P, O'Neill DP. Diagnosis of spinal dural arteriovenous fistula using 3D T2-weighted imaging. Neuroradiology. 2017;59:997–1002.
8. Multidetector CT. Angiography in diagnosing type I and type IVA spinal vascular malformations|American Journal of Neuroradiology. http://www.ajnr.org/content/27/4/813.full. Accessed 26 Dec 2019.
9. Boll DT, Bulow H, Blackham KA, Aschoff AJ, Schmitz BL. MDCT angiography of the spinal vasculature and the artery of Adamkiewicz. Am J Roentgenol. 2006;187:1054–60.
10. Zalewski NL, Rabinstein AA, Krecke KN, Brown RD, Wijdicks EFM, Weinshenker BG, Doolittle DA, Flanagan EP. Spinal cord infarction: clinical and imaging insights from the periprocedural setting. J Neurol Sci. 2018;388:162–7.
11. Zalewski NL, Rabinstein AA, Krecke KN, et al. Characteristics of spontaneous spinal cord infarction and proposed diagnostic criteria. JAMA Neurol. 2019;76:56–63.
12. Takai K. Spinal arteriovenous shunts: Angioarchitecture and historical changes in classification. Neurol Med Chir (Tokyo). 2017;57:356–65.
13. Rosenblum B, Oldfield EH, Doppman JL, Di Chiro G. Spinal arteriovenous malformations: a comparison of dural arteriovenous fistulas and intradural AVM's in 81 patients. J Neurosurg. 1987;67:795–802.

Index

A
Alberta Stroke Program Early CT Score (ASPECTS), 3
Angioinvasive fungal sinusitis, 129
Anterior cerebral artery (ACA), 23–25
Anterior circulation
  ACA, 23–25
  ICA, 21, 22
  MCA, 21–23
Anterior inferior cerebellar artery (AICA), 26
Anterior spinal artery (ASA), 143
Arteriopathy, 72–74
Arteriovenous malformation (AVM), 135, 136, 139
  definition, 111
  differential diagnosis, 116
  feeding artery, 111
  imaging evaluation, 111, 112, 114, 115
  pseudoaneurysm, 111
  SM grading system, 111
  treatment, 113, 114, 116
  venous drainage, 111

B
Blunt cerebrovascular injury (BCVI)
  Biffl scale, 80
  differential diagnosis, 83, 87–89
  grade I injury, 80–82
  grade II injury, 82–85
  grade III injury, 82, 86
  grade IV injury, 82, 87
  grade V injury, 82, 87
  mechanism and pathophysiology, 79
  screening criteria, 79
  screening modality, 80
  spontaneous dissection, 89, 90
  traumatic sinus thrombosis, 89, 91, 92
  treatment and follow-up, 88, 89

C
Carotid blowout syndrome, 129, 132–134
Carotid-cavernous fistula (CCF), 135–137
Carotidynia, 136, 138, 140
Catheter spinal angiography (DSA), 143, 144
Cavernoma, 148, 149
Cavernous malformation (CM), 121–123
Cerebral amyloid angiopathy (CAA), 74–77
Cerebral aneurysms
  blood-blister aneurysms, 101, 102
  clinical manifestations, 101–105
  dissecting aneurysms, 95, 99, 100
  dolichoectasia, 95, 96, 101
  follow-up, 107
  fusiform aneurysms, 95
  imaging modality, 104, 106
  infectious/mycotic aneurysms, 101, 103
  pathophysiology, 93
  primary management
    ruptured aneurysms, 104, 105
    unruptured aneurysms, 106, 107
  saccular aneurysms, 93–95
    A-comm aneurysm, 97
    anterior choroidal artery, 96
    basilar tip aneurysm, 98
    MCA, 98
    ophthalmic aneurysm, 94
    P-comm aneurysm, 95
    pericallosal aneurysm, 98
    PICA aneurysm, 99
    right cavernous aneurysm, 93
    superior hypophyseal artery, 94
    terminus aneurysm, 97
  size, 101
Cerebral autosomal dominant arteriopathy with subcortical infarcts and leukoencephalopathy (CADASIL), 74, 75
Cerebral blood flow (CBF), 33
Cerebral blood volume (CBV), 33
Cerebral fat embolism (CFE), 46
Cerebrovenous thrombosis (CVT)
  CTV, 54
  diagnosis, 49
  MRI, 54–57
  MRV, 57
  NCCT, 49, 50, 52, 54
  parenchymal changes, 49–51, 53
  treatment, 57
Childhood stroke, 72–74
Creutzfeldt-Jakob disease (CJD), 36, 41
CT angiography (CTA), 4, 5
CT perfusion (CTP), 5–7, 9, 11, 12, 14, 17
CT venogram (CTV), 54
Curved planar reformation (CPR), 144

D
Delayed post hypoxic leukoencephalopathy (DPHL), 41
Developmental venous anomaly (DVA), 116, 121–124
Digital subtraction angiography (DSA), 104
Drug-induced cerebral vasculopathy, 72, 73
Dural arteriovenous fistula (DAVF)
  classifications, 117
  definition, 116
  imaging, 117–120
  treatment, 117, 121

© Springer Nature Switzerland AG 2020

Y. Tang, *Atlas of Emergency Neurovascular Imaging*, https://doi.org/10.1007/978-3-030-43654-4

E
Encephaloduroarteriosynangiosis (EDAS), 69
Encephalomyoarteriosynangiosis (EMAS), 69
External carotid artery (ECA), 127, 128

F
Fluid-attenuated inversion-recovery (FLAIR), 18

G
Gradient recall echo (GRE), 18
Great anterior radiculomedullary vein (GARV), 143

H
Head and neck cancers, 129, 132–134
Head and neck infections, 129–131
Hemangioblastoma, 148, 150
Herpes encephalitis, 40
Hypoxic ischemic encephalopathy (HIE), 41, 42

I
Iatrogenic vascular injury, 127–129
Internal carotid artery (ICA), 21, 22
Intracranial dissection (FCA-d), 74
Intracranial internal carotid artery (ICA), 93, 94

J
Juvenile nasopharyngeal angiofibroma, 134

L
Large vessel occlusion (LVO)
  benign oligemia, 1
  collateral assessment, 5
  CTA, 4, 5
  CTP, 5–7, 9, 11, 12, 14, 17
  goal of imaging, 1, 2
  ischemic core and penumbra, 1
  MRI-based imaging protocols, 11, 18, 19
  NCCT, 2–4
Lemierre syndrome, 131
Low-flow orbital vascular lesion, 135, 138

M
Maximum-intensity projection (MIP), 144
Middle cerebral artery (MCA), 21–23, 98
Mitochondrial myopathy, encephalopathy with lactic acidosis, and stroke-like episodes (MELAS), 35, 36, 40
Modified Denver Criteria, 79
Moyamoya vasculopathy, 69, 70
MR venogram (MRV), 57
MRI vessel wall imaging (VWI), 65
Multiplanar reformation (MPR), 144

N
Nasopharyngeal carcinoma, 132
Non-contrast CT (NCCT), 2–4, 49, 50, 52, 54

O
Osmotic demyelination syndrome (ODS), 45
Otogenic infections, 129

P
Pial synangiosis, 69
PICA aneurysm, 99
Posterior cerebral artery (PCA), 28–30
Posterior circulation
  AICA, 26
  basilar artery, 24, 26–28
  border zone infarction, 30, 31
  PCA, 28–30
  SCA, 28
  vertebral artery, 23, 26
Posterior inferior cerebellar artery (PICA), 23
Posterior reversible encephalopathy syndrome (PRES), 65, 66
Posterior spinal arteries (PSA), 143
Primary angiitis of CNS (PACNS), 61–63

R
Radiation-induced vasculopathy, 70, 71
Recurrent artery of Heubner (RAH), 23
Reversible vasoconstriction syndrome (RCVS)
  clinical presentation, 63
  conventional imaging, 63–65
  definition, 63
  treatment, 65
  VWI, 65

S
Saccular aneurysms, 93–95
  A-comm aneurysm, 97
  anterior choroidal artery, 96
  basilar tip aneurysm, 98
  MCA, 98
  ophthalmic aneurysm, 94
  P-comm aneurysm, 95
  pericallosal aneurysm, 98
  PICA aneurysm, 99
  right cavernous aneurysm, 93
  superior hypophyseal artery, 94
  terminus aneurysm, 97
Spetzler–Martin (SM) grading system, 111
Spinal arteriovenous malformations, 144
Spinal cavernous malformation, 148
Spinal cord infarction (SCI), 144, 145
Stereotactic radiation surgery (SRS), 113
Stroke mimics
  brain tumor, 33, 37, 38
  CFE, 46
  CJD, 36, 41
  drug toxicity, 46
  HIE, 41, 42
  hyperammonemic/hepatic encephalopathy, 41–43
  hypoglycemic encephalopathy, 41
  infection and inflammation, 33, 35, 40
  MELAS, 35, 36, 40
  migraine, 33, 36
  ODS, 45

seizure, 33–35
Wernicke's encephalopathy, 42, 43
Subarachnoid hemorrhage (SAH), 63
Superior cerebellar artery (SCA), 28
Superior ophthalmic vein (SOV), 130
Susceptibility weighted (SWI), 54

T
Time to drain (TTD), 33
Time-resolved imaging of contrast kinetics (TRICKS), 144
2D time-of-flight (2D TOF), 57
Type I spinal dural AV fistula (SDAVF), 144, 146
Type II intramedullary AVM, 147
Type III intradural and extradural AVM, 148
Type IV intradural perimedullary AVF, 148

V
Vasculopathy
CNS vasculitis
imaging modality, 60, 61
PACNS, 61–63
secondary vasculitis, 59, 60
diagnostic and therapeutic challenges, 59
PRES, 65, 66
RCVS
clinical presentation, 63
conventional imaging, 63–65
definition, 63
treatment, 65
VWI, 65
Vein of Galen aneurysmal malformation (VGAM), 121, 122
Venous system, 143
von Hippel–Lindau (VHL) syndrome, 148

W
Wallenberg syndrome, 23
Wernicke's encephalopathy, 42, 43